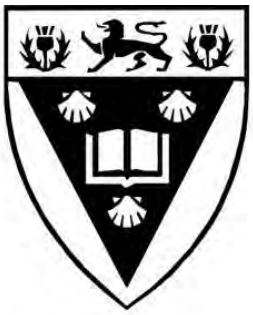

RHODES UNIVERSITY

Where Leaders Learn

Petrogenesis of the Bysteek and Koenap Formation Migmatites, Central Namaqualand

By

Jason A. Moodley

August 2012

Thesis submitted in fulfilment of the requirements for degree of Master of Science in the Department of Geology, Rhodes University.

DECLARATION

I declare that this thesis is my own work, and information from other publications is adequately referenced. It is being submitted in fulfilment for the Master of Sciences degree in the Department of Geology, Rhodes University.

_____ _____

Name of candidate Signature

signed on _____ day of _____ 2012.

Acknowledgments

1) First and foremost, thank you God.

2) My deepest gratitude is extended to my supervisor Steffen Büttner for his continuous, guidance, encouragement, respect and above all his patience. Many thanks is made to the countless hours Steffen spent editing my drafts, teaching me, training me, helping me in all aspects with this project and for his unwavering support. I could not have asked for a better supervisor. Thanks Steffen.

3) A great deal of gratitude is extended toward my co-supervisor Gelu 'Gabi' Costin for assisting me in the many aspects of my research, particularly petrography, EPMA and EDS mineral chemistry analyses, thermobarometry and phase equilibria.

4) Steve Prevec, our head of department, for helping me put things into perspective and for frequently providing me with sound scientific advice.

5) John Hepple and staff for assisting in sample and thin section preparation, and for always being willing to help with any technical problem.

6) Goonie Marsh is thanked for producing the XRF whole rock chemical data and for assisting in the interpretation of these results.

7) Rhodes University and NRF for providing funding for my MSc.

8) My lovely mother and sisters, of which without their perpetual love, support, encouragement and understanding, I would not be where I am.

9) My dearest friend Henusha Jhundoo for always being at my side when things took a rough turn, always providing me with strong support to keep my head above water and for being a great teacher to me. Thank you.

10) I sincerely thank the Naran family in Grahamstown, Roger Bills, Daksha Naran, Tony Coopasamy, Mike Naidoo and Sonal Patel for always accommodating me, especially when I needed it most. A sentence cannot describe how appreciative I am.

Abstract

The Mesoproterozoic rocks of the Bysteek and Koenap Formations of the Arribees Group are exposed within a NW-SE striking antiformal structure comprised of mafic granulites and metapelitic diatexites, and a number of marble and calc-silicate rock layers.

The mafic granulites of the Bysteek Formation show a typological variety of anatectic features, including nebulitic, stromatitic mesosomes, melanosomes, quartz syenitic leucocratic vein networks and syenitic pools. Melanosomes consist of hedenbergitic to diopside-rich clinopyroxene (X_{Mg}: 0.40), anorthitic plagioclase (An90), with some quartz, minor apatite and titanite. Anatexis was caused by biotite dehydration melting and formed a melt of probably granitic composition. The leucosome composition ranges from either alkali-feldspar-granitic to plagioclase rich or granitic. This variation is interpreted as a result of variable extraction of melt from the source to granitic pools.

The diatexites of the Koenap Formation are most likely of metapelitic or meta-greywacke origin. They are texturally variable but always contain high modal contents of alkali feldspar and quartz which generally form magmatic textures. Almandine-rich garnet (X_{Mg}: 0.18-0.25), cordierite (X_{Mg}: 0.71) form secondary biotite, sillimanite and magnetite during retrograde breakdown. Thermodynamic modelling of mafic granulite compositions suggests peak *P-T* conditions of ~865 °C and 8.6 kbar. Occasionally, garnet rich in ferric iron (X_{Adr}: 0.55) forms by plagioclase-clinopyroxene breakdown under oxidising conditions at ~6 kilobar and ~ 800 °C. At the same stage amphibole forms in some melanosomes.

P-T estimations for the diatexites based on thermodynamic modelling suggest the equilibration of the assemblage garnet, cordierite, alkali feldspar and melt at ~860 °C and 5.5 kbar. Conditions comparable to the peak pressure in the mafic granulites could not be established. However, since the diatexites and the mafic granulites are closely related in the field and no evidence of juxtaposition after the thermal peak exists, the *P-T* record of the diatexites might be incomplete.

Keywords: anatexis, mafic granulite, diatexite, leucosome, melanosome, thermobarometry, thermodynamic modelling

List of terms

1) Migmatite: These are rocks formed via partial melting, exhibiting hetergenous features between light- and dark-coloured domains on a mesoscopic to microscopic scale. Migmatites are typically associated with medium- to high-grade metamorphic areas (Brown, 1994).

2) Melanosomes: Domains which are characterised by dark coloured layers, often consisting of iron-magnesium-rich phases such as pyroxene, garnet, biotite or amphibole. They represent the solid fraction left behind after the extraction of anatectic melt (Mehnert, 1968). These domains may also be termed 'residuum' (Sawyer, 1998).

3) Leucosome: Light coloured domains rich in felsic phases are termed 'leucosomes' (Kenah and Hollister, 1983). These domains are comprised almost entirely of feldspar or quartz. The leucocratic domains represent the melt fraction that has been separated from the original protolith after partial melting had taken place. In addition, the leucosome melt may be mobile due to its lower density and viscosity (Sawyer, 1998).

4) Neosome: The neosome refers to recently formed portions of the migmatites which have been generated via anatexis (Sawyer, 2008). Neosomes may exhibit mixed proportions of solid residue and melt which may or may not have migrated or been isolated. As the neosome is a product of partial melting, it implies that the protolith will not be present as a domain within the neosome (Brown, 1994).

5) Mesosome: These are domains within migmatites that range in colour between melanocratic and leucocratic layers (Sawyer, 2008). Mesosomes frequently occur within the neosomes and are in their chemical composition similar to the protolith (Wimmernauer and Bryhni, 2007). They exhibit variable grain size and structures such as metamorphic layering, foliations and folds (Didier, 1968). Mesosomes are often described as 'nebulitic' since dark and light coloured phases have not separated into discrete domains (Brown, 1994).

6) *In-situ* leucosomes: These are leucosomes which have been separated from the residue but are however immobile and remain as distinct leucocratic domains within the neosome (Mehnert 1968). These are often adjacent and in direct contact to melanosome layers. A diffuse relationship is often maintained between the leucosome and neighbouring restite layers.

7) Melt pockets and pools: These are leucocratic domains which have completely segregated from their respective melanocratic residue, migrated away in the form of fracture networks and

accumulated into larger pools and pockets (Winter, 2001).These domains often exhibit well defined feldspar or quartz phenocrysts that are relatively undeformed and magmatic.

8) Diatexite: Brown (1973) has defined diatexites as migmatites in which partial melting has destroyed any pre-anatectic features and which are characterised by homogenous grain coarsening textures with leucocratic domains being pervasively distributed in the neosomes.

9) Kinzigite: These are rocks consisting of a quartz-K-feldspar-plagioclase-rich groundmass with less abundant garnet (almandine/pyrope), cordierite, biotite, sillimanite (Mehnert, 1968).

Table of Contents

List of Figures

Chapter 6:

Chapter 7:

List of Tables

Chapter 3:

Chapter 4:

Chapter 5:

Chapter 6:

1. Introduction

1.1 Regional and local geology

The Namaqua-Natal Metamorphic Province belongs to the global network of Grenvillian-aged orogenic belts that have formed during the assembly of Rodinia between ~1000-1200 Ma (Thomas *et al*., 1994). In southern Africa the Namaqua-Natal belt forms a >~ 400 km wide belt along the margin of the Kaapvaal Craton, extending over ~ 2000 km from central Namibia to Kwa-Zulu Natal in south-eastern South Africa. Large parts are covered by Phanerozoic sedimentary rocks of the Cape and Karoo Supergroups. Rocks and structures of the Neoproterozoic Damara Belt overprinted the western and northern margins of the Namaqua basement in South Africa and Namibia (Figure 1.1a, Thomas *et al*., 1994).

The study area is located on farm 'Oup 80', ca. situated 30 km east of Onseepkans or 90 km west of Kakamas in the Northern Cape Province (Figure 1.1b). The regional geology of the Onseepkans area is relatively unexplored with little publication history but has been documented in a general sense. Work on the regional geological evolution and has been published from the 1980s on by Joubert (1986), Stowe (1986), Thomas *et al*. (1993; 1994), and, more recently Cornell *et al*. (2006). Lithostratigraphic mapping at a regional scale was undertaken by a group based in Bloemfontein (Colliston and Schoch, 1998; 2002; 2003; 2006) Particularly important for this study was a geological map published in 2007 by the Council for Geosciences (sheet 2818 Onseepkans) and the map explanation by Moen and Toogood (2007).

The existing literature offers a plethora of tectono-stratigraphic units and boundaries, including the proposition of numerous terranes. Their boundaries, positions and existence are matter of controversial debate and often the proposed terranes overlap in position, as most recently described in Moen and Toogood (2007). It is not the purpose of this study to evaluate the propositions made for the nomenclature, subdivision and interpretation of the regional geology at the scale of the Namaqua Belt. Since much reference is made to the local geology mapped and described by Moen and Toogood (2007), this study also has adopted their classifications and, to a large extent, their nomenclature of lithological units.

According to Moen and Toogood (2007), the study area is part of the Grünau Terrane which separated from the Pofadder Terrane (Colliston and Schoch, 1998) or Bushmanland Subprovince by the Onseepkans Thrust. The Onseepkans Thrust, located about 30 km west of the study area, separates granulite facies metamorphic and granitic Grünau Terrane basement in

the east from amphibolite facies rocks in the west. The Bushmanland Subprovince shows gradually lower grade metamorphic rocks and pre-Namaquan basement in its western continuation, particularly in the Richtersveld.

The rocks exposed in the study area belong to the Mesoproterozoic Arribees Group (Cornell *et al*., 2006; Moen and Toogood, 2007), which consists of calc-silicate rocks and mafic granulites of the Bysteek Formation, metapelitic rocks in the Koenap Formation, and, as mapped by Moen and Toogood (2007), enderbitic plutons, such as the Swartoup Enderbite. The classification of this rock type as enderbite has been challenged in recent studies (Kanime, 2011; Sithole, 2011) which propose alkali-syenitic composition of the pluton. The youngest pluton in the study area is the Polisiehoek Gneiss, an intrusive granite with some gneissic domains. Dykes that can be related to this granite crosscut the meta-sedimentary country rocks of the Koenap and Bysteek Formations and also the Swartoup Enderbite/alkali-syenite (Kanime, 2011). Pegmatites of the late-Namaquan regional pegmatite belt are abundant in the area. Their age of ~ 950 Ma postdates the regional high-temperature events which occurred in two peaks at about 1200 and 1100 Ma (Eglington, 2006).

The Hartebees River shear zone, by some authors referred to as Hartbees River Thrust, transects the Arribees Group along the eastern border of the study area (Figure 1.1b-c). This shear zone is about 50 to 100 m thick and of a regional extent. It has been proposed as boundary of the Kakamas Terrane (Thomas *et al*., 1994; Cornell *et al*., 2006). However, Moen and Toogood's (2007) new mapping demonstrates that this shear zone is discontinuous and therefore cannot be interpreted as a terrane boundary.

The tectonic history has been subdivided in four stages. The earliest stage (D_1) of deformation, according to Du Plessis (1979, not seen, as cited in Moen and Toogood, 2007), is preserved only as intrafolial folds developed in layered metasedimentary rocks and migmatites. This stage was followed by non-cylindrical isoclinal folding and thrusting (D_2). Moen and Toogood (2007) suggest that the first two deformation episodes are related to southwest-directing nappe tectonics following the collision of the Namaqua continental plate with the Kaapvaal Craton. A product of this event is that of the Hartbees River Shear Zone. Regional anti- and synformal, often doubly plunging folds (D_3) are superimposed D_2 folds. According to Moen and Toogood (2007) the kilometre-scale antiform in the study area was formed during D3. The final deformation episode (D_4) is defined by north-east trending shear zones with variable kinematic

history ranging from strike-slip to dip-slip, such as the Oup fault, which intersects and displaces the Hartbeest River Shear Zone.

The study focuses on the south-western limb of a kilometre-sized D3 antiform. The limbs of the antiform are formed, from outside to inside, by Polisiehoek Gneiss and Koenap Formation kinzigites, mafic granulites and calc-silicate rocks of the Bysteek Formation, a K-feldspar-rich plutonic layer, mapped as Swartoup Enderbite, and a second layer of Polisiehoek Gneiss in its core (Figures 1.1b-d). The north-east verging fold plunges moderately north-west (Kanime 2011, Sithole 2011).

1.1.1 Bysteek Formation

The Bysteek Formation has been described (Moen and Toogood, 2007) as sequences of calcic metasediments intercalated with dolomitic marbles. While these rock types are indeed present, the study shows a significant proportion of clinopyroxene-rich mafic granulites, locally anatectic, as part of the Bysteek Formation. These mafic rocks are not described in Moen and Toogood (2007).

Marble and calc-silicate bands show gradual transitions with one another and with the mafic granulites. The calc-silicate rocks are often banded, dark-grey, and range in thickness from 2 to 20m. Calcite dissolution commonly forms cellular karst features in calcite bearing calc-silicate rocks. In more massive marbles no such features exist but thin garnet layers may be present. Thin section study of the calc-silicate rocks shows quartz, green hornblende, microcline and some titanite. Other constituents include calcic plagioclase, diopside, grossularite, epidote and opaques. More detailed petrography of the Bysteek Formation is presented in chapter 3.

1.1.2 Koenap Formation

Moen and Toogood (2007) describe the Koenap Formation as sequence of metapelitic rocks which are massive and dark grey to black in colour, and display gneissic to migmatitic textures. They consist of quartz, alkali feldspar, almandine garnet, biotite, ±sillimanite, ±cordierite and accessory minerals. Rocks exhibiting these properties have been classified as ‘kinzigites’ (Didier, 1963). Kinzigites are defined as migmatites produced via the anatexis of quartz and feldspar components of a protolith generating a restite comprised of biotite, garnet, cordierite and sillimanite (Mehnert, 1968).

1.1.3 Swartoup Enderbite

According to Moen and Toogood (2007) the Swartoup Enderbite is a coarse- to fine-grained rock that is dark grey in colour displaying schlieren textures and containing stretched inclusions of semi-pelite. The assemblage is quartz, plagioclase, orthopyroxene, clinopyroxene and biotite, with minor quantities of alkali feldspar and hornblende. The enderbites grade from a dark grey coarse grained augite granodiorite to megacrystic quartz-feldspar-biotite-hornblende gneiss whereby the latter is located adjacent to the Polisiehoek Gneiss. Recent studies (Kanime, 2011; Sithole, 2011) challenge the description and lithological classification of the Swartoup Enderbite and re-classify it as alkali feldspar syenite.

1.1.4 Polisiehoek Gneiss

Moen and Toogood (2007) describe the Polisiehoek Gneiss as orange-brown fine-grained gneiss with augen structures and a continuous foliation, which applies to the rocks in the immediate study area. However, in its vicinity the Polisiehoek Gneiss is often undeformed and granitic. The modal composition of the Polisiehoek Gneiss, based on three samples, is 42 vol% quartz, 37 vol% alkali feldspar (micro-perthite and microcline), 18 vol% plagioclase and minor biotite (< 3%). Accessory fine-grained garnet, and sillimanite are occasionally present (Moen and Toogood, 2007).

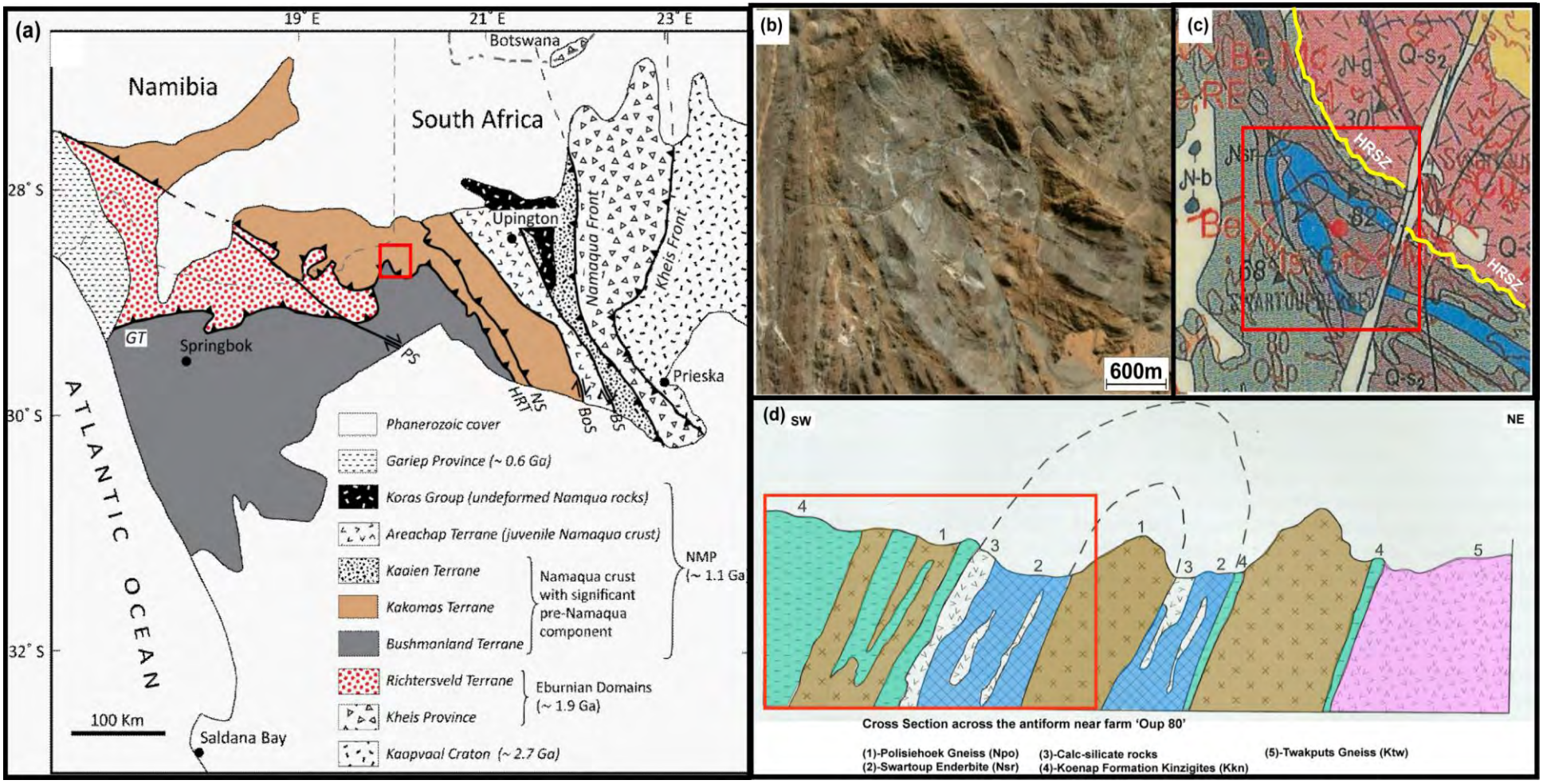

Figure 1.1. Geological locations of the study area (a) Geologic map outlining the tectonic subdivisions of the Namaqua terranes after Thomas *et al.* (1994). The red square indicates position of the study area. (b) Satellite image of the study area. (c-d) Outlined geologic map and cross-section of the study area modified after Moen and Toogood (2007). The Hartbeest River Shear Zone (HRSZ) is indicated in yellow. The study area lies on the SW limb of the fold (outlined as red rectangle). The colours of the units coincide with the geologic units outlined in (c).

1.2 Aims and objectives

The study area is relatively unexplored and previous research does not investigate the metamorphic history of this high-grade metamorphic section of the Namaqua belt. Therefore the purpose of this study is to provide (i) a description of the mesoscopic field appearance of the Bysteek and Koenap Formations in the study area (ii) documentation of the field relationships between the various lithologies; (iii) microscopic descriptions and modal analysis; (iv) classification of relevant rock types on the basis of whole rock compositions and mineral modes (v) investigation of the pressure-temperature conditions of the regional metamorphism using thermodymamic modelling and conventional geothermobarometric techniques.

1.3 Methodology

1.3.1 Field relationships and mesoscopic observations

During ten days of fieldwork in March 2010 and April 2011, mesoscopic structures of lithologies were documented, the nature of contacts and transitions between various rocks investigated, and documented via photography and field sketches. The set of rock specimens taken during field work includes 8 samples from the mafic granulites of the Bysteek Formation and 4 samples from the related calc-silicate domains, and 11 samples from the Koenap Formation diatexites.

1.3.2 Petrography

Petrographic analysis was conducted with the intention to understanding the textural relationships of phases, determination of modal quantities, detailed description of specimens on a microscopic level, and for microchemical mineral analysis. Thin sections were prepared at the Department of Geology, Rhodes University. Their position on the hand specimens is marked indicated on hand specimens shown in several figures in Chapter 2. All mineral abbreviations follow the nomenclature outlined after Kretz (1983).

1.3.3 Mineral chemistry

The chemical mineral composition was determined using both Electron Probe Micro Analysis (EPMA) and Energy Dispersive Spectrometry (EDS). EPMA analysis was done at the Department of Geology, Rhodes University, using a JEOL JXA-8230 Superprobe with four WD spectrometers. A standard deviation of analytical measurement error confirms the accuracy of individual EPMA analysis. The standard deviation of analytical error lies in range of 0.02-0.14% error per individual phase. EDS were conducted utilizing the SEM-based EDS at Rhodes University's Electronic Microscopy Unit. The Unit is equipped with a TESCAN Vega TS 5136LM SEM and an Oxford Instruments INCA PentaFET-x3 Si(Li) EDS Detector. The

analytical conditions for mineral analyses are outlined in the mineral chemistry chapter (Chapter 4).

1.3.4 Whole rock chemistry

Representative major oxide whole rock chemical analysis was performed from selected hand specimen domains using three methods: (i) X-ray fluorescence (XRF), utilizing the fusion technique of Norrish and Hutton (1969) (ii) Electron Dispersive Spectrometry (EDS) area scans and (iii) whole rock chemical calculations based on modal abundances and mineral compositions using the 'Rock-Maker' spreadsheet (Büttner, 2012). The XRF analysis was performed at the Department of Geology, Rhodes University using a Philips PW 1480 automatic wave-length dispersive X-ray spectrometer. The loss of ignition (LOI) was determined gravimetrically during the preparation of the XRF fusion discs. Other analytical constraints are outlined in the whole rock chemistry chapter (Chapter 5).

2. Field Observations and Hand Specimen Descriptions

This chapter describes the most important varieties of rocks in the study area. The chapter is subdivided in sections describing individual rock types or features separately. However, since such features often do not occur in isolated form it is necessary to describe the relationships to related rocks and features. This may require to refer to other sections or to present material that is not necessarily covered by individual section headings. Although this chapter essentially deals with macroscopic features is also refers to the mineral content of rocks and domains. The minerals were usually identified or confirmed under the microscope. More detailed information obtained from microscopic observation is presented in Chapter 3.

The field relationships of various lithologies in the Bysteek and Koenap Formations were investigated by field mapping and representative sample collection in an area of approximately one square kilometre. The area comprises of a mafic unit, marbles and calc-silicates in the Bysteek Formation and migmatitic metapelites in the Koenap Formation (Figure 2.1), the latter being classified as kinzigites by Moen and Toogood (2007). The mafic suite of the Bysteek Formation displays heterogeneous migmatitic textures and for descriptive purposes are referred to as 'mafic granulites'. Alkali feldspar granites and the partly gneissic or mylonitic Polisiehoek Granite intrude the metamorphic rocks of the Bysteek and Koenap Formation.

The Bysteek Formation mafic granulites show variable migmatitic structures that range from nebulitic (Figure 2.2 a-b) and stromatitic mesosomes (Figures 2.3 a-b and 2.4) to *in-situ* leucosomes, leucocratic networks (Figure 2.7), and leucosome pools (Figure 2.10). Often the original relationship between melanosome and leucosome is preserved. 10 mafic granulite samples were analysed. The neighbouring calc-silicate and marble domains show a diffuse gradational relationship to the mafic granulite sequence. The Koenap Formation rocks (Moen and Toogood's (2007) kinzigites), show a mineral assemblage of quartz, alkali feldspar, almandine-rich garnet, biotite, ±sillimanite, ±cordierite. However field and mesoscopic observations show heterogeneity in appearance. Hence, in this study this litho-type will be referred to as diatexites instead of kinzigite. Based on 11 hand specimens the diatexites have been categorised into four types: (i) leucocratic diatexites; (ii) nebulitic diatexites; (iii) banded diatexites; (iv) melanocratic domains. A sample and location map is shown in Figure 2.1.

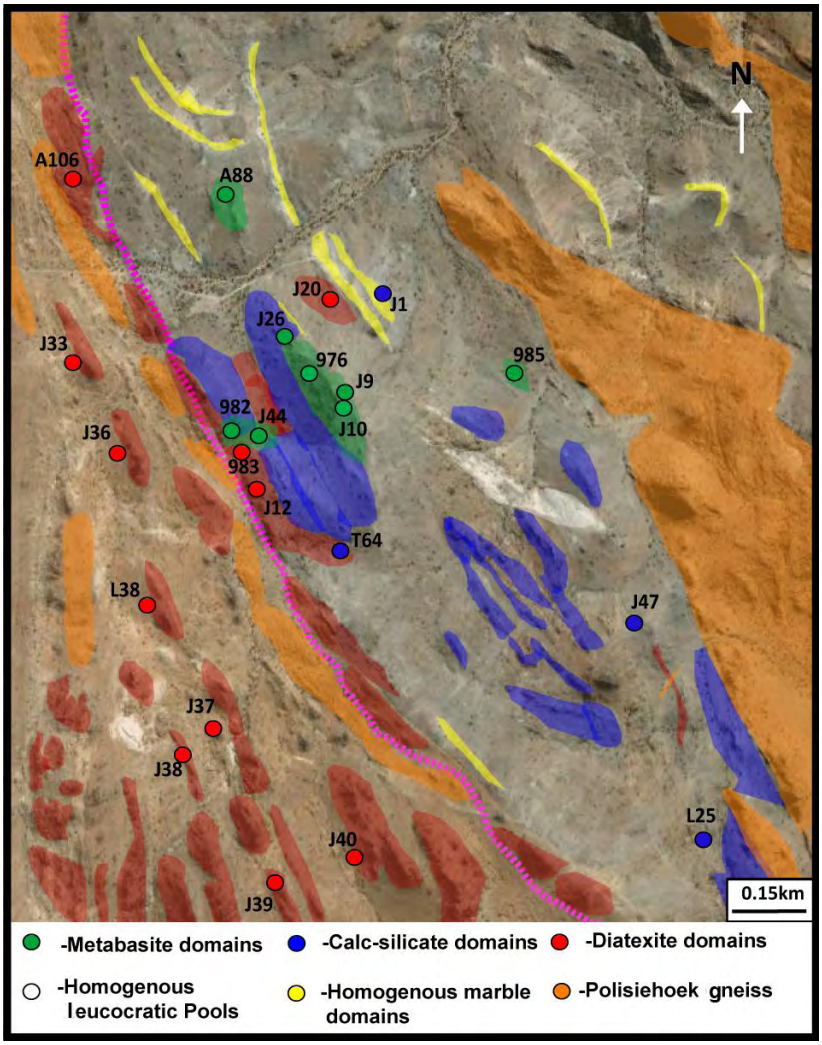

Figure 2.1. Field map of lithological units and sample locations. 23 specimens were sampled, eight from the Bysteek Formation mafic granulite unit (green spots), four calc-silicate domains (blue spots) and eleven samples from the diatexite domains of the Koenap Formation (red spots). The orange domains are those areas covered by the Polisiehoek Gneiss, whereas yellow domains represent homogenous marble units. The pink dashed line outlines the sharp boundary between mafic granulite and diatexite domains.

2.1 Mafic granulites and associated leucocratic domains

The field appearance of mafic granulites of the Bysteek Formation is highly variable. Based on proportions and textural variations of leuco- and melanocratic components the most common varieties have been subdivided in ten domain types which are described in the following sections.

2.1.1 Mesosomes and in-situ leucosome domains

The observed mesosomes consist of either melanocratic residue interlayered with leucosome, forming the stromatitic type (Figures 2.3 and 2.4), or of intermingled leucosome and melanosome, forming nebulitic leucosomes (Figure 2.2). The mesosomes vary in grain size and

may or may not show structures such as metamorphic layering, foliations and folds. The observed mesosomes often are nebulitic as it is almost impossible to distinguish dark and light coloured phases macroscopically. Based on these criteria, the mesosome domains are categorised into two divisions, stromatitic and nebulitic mesosomes.

2.1.1.1 Nebulitic mesosomes:

Nebulitic mesosome domains are defined by small-scale unsegregated leucosome and melanosome domains whereby no discrimination between mafic and felsic phases can be made macroscopically in the field or in cut hand specimens (Mehnert, 1968). Nebulitic mesosome domains from three samples (samples 976A, 976B and 982E) have been analysed. On an outcrop scale the mesosomes belonging to sample 976A (Figure 2.2a) are adjacent to thick melanocratic schlieren layers, they are medium-grained and light grey on the surface. The hand specimen however shows both medium and coarse-grained neosome domains with a massive non-layered structure. Individual plagioclase and clinopyroxene grains are easily recognisable due to their coarse grain size (>0.5-1mm) and distinctive colour (light grey and dark green respectively). In the outcrop and hand-specimen the mesosomes from mafic granulite 976B (Figure 2.2b-domain 2) occur as patchy light green and garnet free domains adjacent to the melanosome patches and dark brown garnetiferous melanosome domains (Figure 2.2-domain 3). They are fine-grained (~0.5mm grain size) and consist of clinopyroxene, plagioclase and quartz.

The mesosomes occurring in specimen 982E (Figure 2.4) reside in the interstices between several stretched elongated mafic fragments. They grade from the adjacent stromatitic leucosome veinlets and melanosome layers to small melanocratic patches and leucocratic networks. Mesosomes occur as medium-grained (~0.5-0.8mm sized) patches comprised of detached clinopyroxene, plagioclase, quartz and alkali feldspar grains. The size of these fragments varies between 1.5-5 cm.

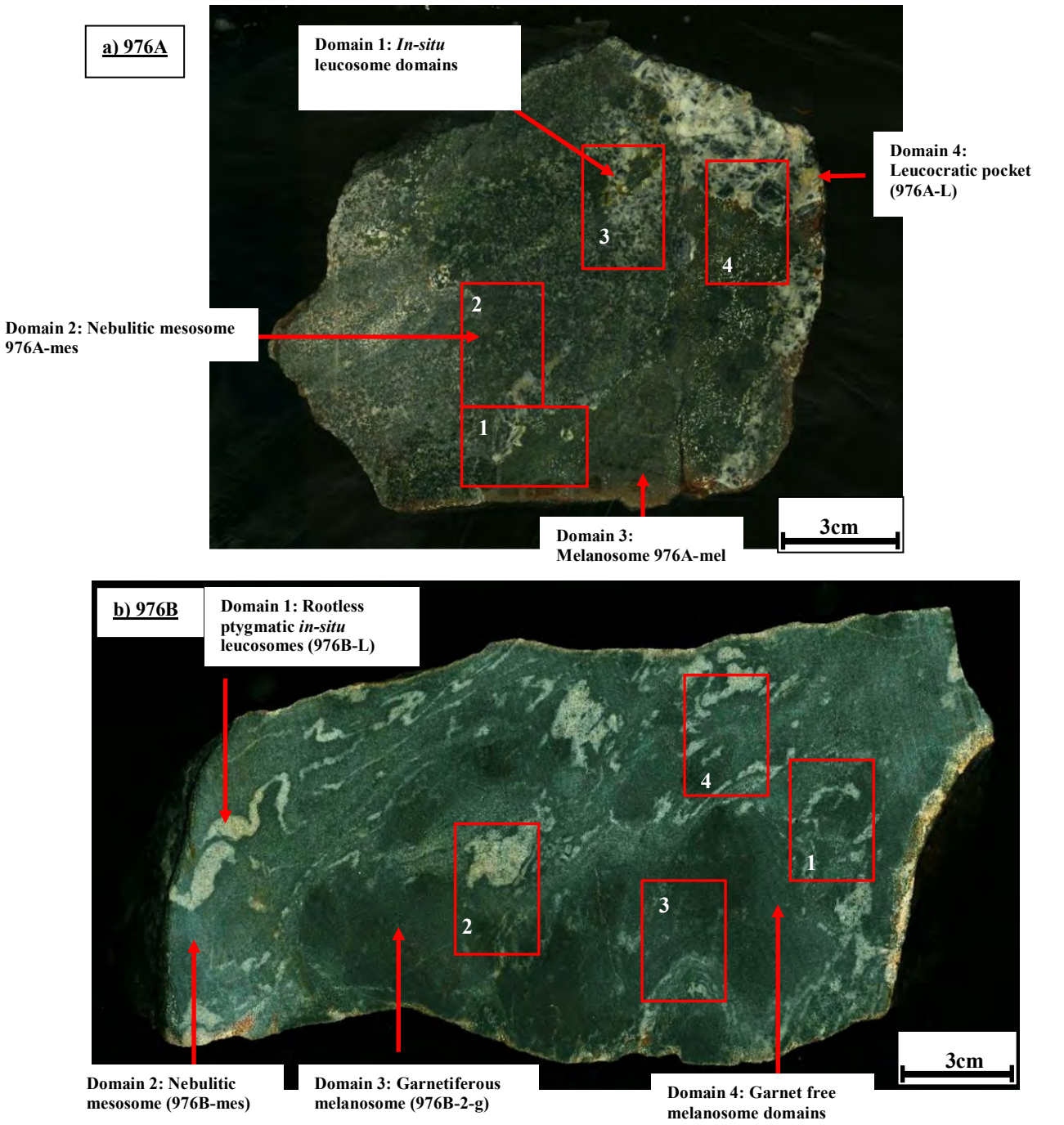

Figure 2.2. (a) Scanned offcut of hand specimen 976A showing melanosomes (976A-mel: domain 3), nebulitic mesosomes (976A-mes: domain 2), *in-situ* leucosome domains and leucocratic pockets (976A-L: domains 3 and 4).The pockets are comprised of dark-grey plagioclase phenocrysts that are tabular and range in grain size between 1 and 2.5 cm. The nebulitic mesosomes are medium-grained (~0.5 mm) (b) Scanned offcut from sample 976B showing garnet poor (976B-mel: domain 4) and garnetiferous melanosomes (976B-2-g: domain 3), nebulitic mesosomes (976B-mes: domain 2) and *in-situ* leucosome domains (976B-L: domain 1). The mesosomes are light grey fine-grained (<1mm) patches neighbouring the melanosomes and *in-situ* leucosomes. The *in-situ* leucosome domains are rootless and ptygmatic in shape. This provides the leucosome domains with a 'blob-like' appearance. The numbered red rectangles indicate the sites for thin section observations (sections 3.1.1; 3.1.2 and 3.1.4).

2.1.1.2 Stromatitic mesosomes

Stromatic mesosomes (Figures 2.3 and 2.4) are characterised by successive alternating leucosome and melanosome bands. The bands are laterally continuous and boundaries often diffuse. The thickness of the stromatitic layers varies from millimetre scale (sample 982E; Figure 2.4; domain 5) to a few centimetres (sample 976A; Figure 2.3a, sample J9A;domain 1).

Sample 982E exhibits thin layers of clinopyroxene dominated melanosome layers alternating with successive, thin (0.1-0.5 mm in width), diffuse K-feldspar-quartz veinlets. The layer thickness in thinly layered stromatitic mesosomes ranges from 0.3 to 0.7cm. Some of the leucocratic veins join at interstitial spaces between the mafic enclaves hereby producing small centimetre sized pockets (Figure 2.4; domain 4). Additionally, leucocratic dykes cut the stromatitic mesosomes along sharp contacts (Figure 2.4; domain 3).

The thinly veined successive leucocratic layers of the stromatitic domain appear to grade from the fine-grained (<0.5mm sized) stromatite, into the nebulitic domains comprised of clinopyroxene fragments, plagioclase, quartz and alkali feldspar aggregates. These nebulites eventually form small centimetre scale leucocratic networks comprised of alkali feldspar and quartz (Figure 2.4; domain 1).

The thicker leucosome layers (sample J10, Figure 2.6b) are milky white in colour, comprised of K-feldspar and quartz, frequently containing prismatic clinopyroxene grains aligned parallel to the foliated planes. The planar leucocratic layers are often sharply bound, concordant to melanocratic layers, and continuous with little gradation into the adjacent melanocratic layers. Some of the thicker melanocratic layers often contain few leucocratic grains incorporated into its groundmass. Other layers exhibit a good proportion of both dark and light coloured phases.

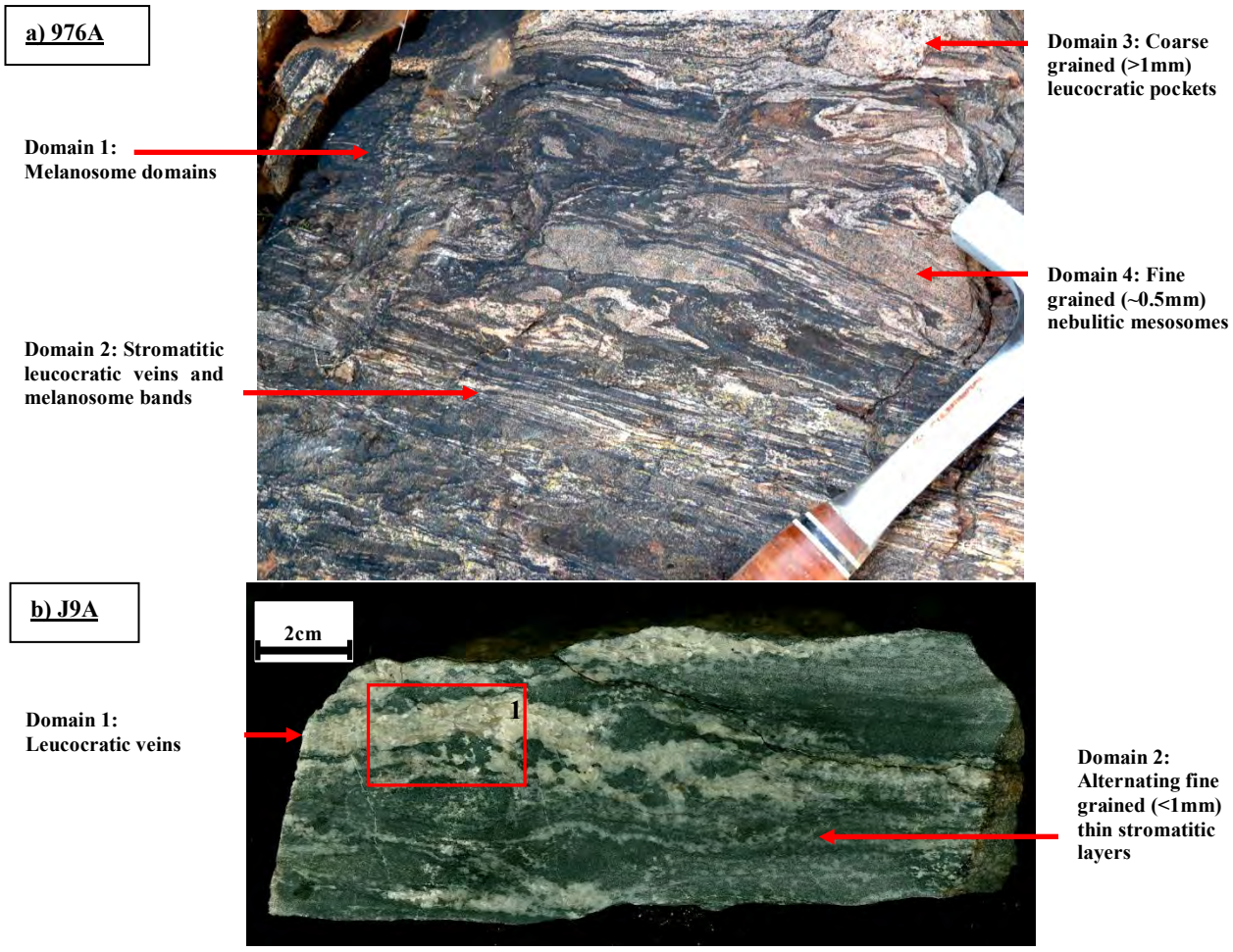

Figure 2.3. (a) Location 976 displays small fine-grained (<0.5mm) nebulitic mesosomes (domain 4) surrounded by stromatically interlayered melanosome bands and leucocratic veins (domain 2). The leucosome veins appear to accumulate and coalesce into small melt pockets (domain 3). (b) Sample J9A displays thick (0.75-1 cm) leucocratic veins showing a sharp boundary to finer-grained (<1mm sized) dark green stromatitic mesosomes. The numbered red rectangle indicates the sites for thin section observations (sample J9A-L; section 3.1.4).

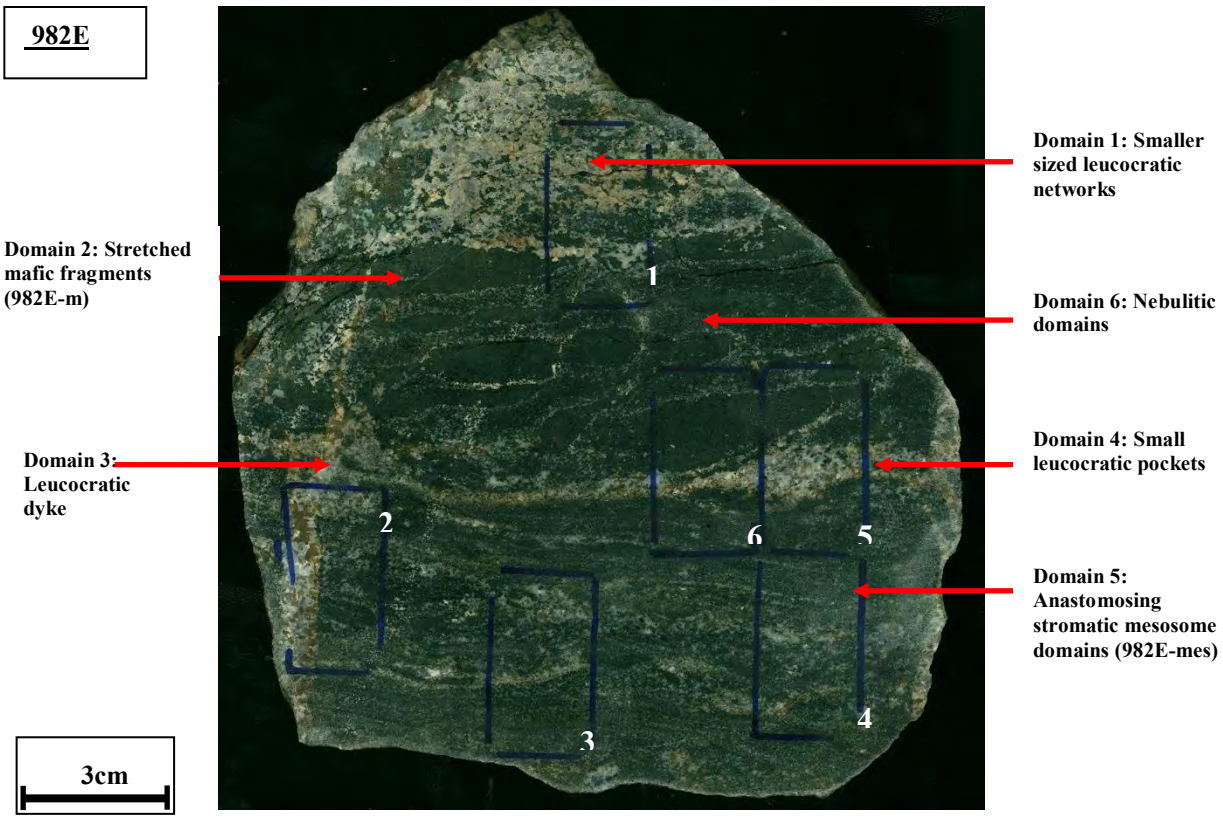

Figure 2.4. Off-cut illustrating the leucocratic network pattern from 982E. The nebulitic domains (domain 6) occur within interstitial spaces between stretched-shaped mafic fragments (domain 2). Small leucocratic pockets (domain 4) also reside within the spaces of larger stretched mafic fragments. The specimen diffusely grades from anastomosing stromatitic layers (domain 5) into nebulitic mesosome domains hosting stretched mafic fragments (domain 2), and then further grading into parts of a larger leucocratic network (domain 1). Highlighted rectangles indicate the sites for thin section observations (thin sections 982E 1-6; sections 3.1.1, 3.1.2, 3.1.3 and 3.1.4).

2.1.2 Melanosomes

Melanosomes have been defined as any mafic domain with no alkali feldspar and low modal abundance of quartz (<5%) (Sawyer, 2008). Melanocratic domains occurring in hand specimen 976A (Figure 2.2a-domain 3) occurs as coarse-grained concentrations of dark green subhedral clusters of clinopyroxene. The clinopyroxene appear segregated from the massive nebulitic mesosome associated with plagioclase into domains comprised entirely of dark green clinopyroxene.

The melanosomes associated with specimen 976B (Figure 2.2b-domains 3 and 4) are comprised of mineral assemblages either Grt-Cpx-Pl-Qtz or Cpx-Pl-Qtz (garnet free domains). The garnet free melanosomes frequently exist as thin (0.5-1.5 mm sized) rims surrounding the ptygmatic folded *in-situ* leucosomes of the mafic granulite or they reside as dark-green fine-grained (<0.5mm) patches neighbouring the pale green-grey nebulitic mesosomes of the host rock. The garnetiferous melanosomes are distinct in the hand specimen by their noticeable dark-brown

colour and fine grain size (~<0.5mm) frequently grading from the patchy dark green garnet free Cpx-Pl-Qtz melanosomes.

Sample J44 (Figure 2.5b) is a mafic granofels largely comprised of homogenous fine-grained (<0.5mm) clinopyroxene, plagioclase, biotite and amphibole. Its texture is entirely massive with no banding, layering or foliation, neither are there any associated *in-situ* leucocratic domains related to the melanosome.

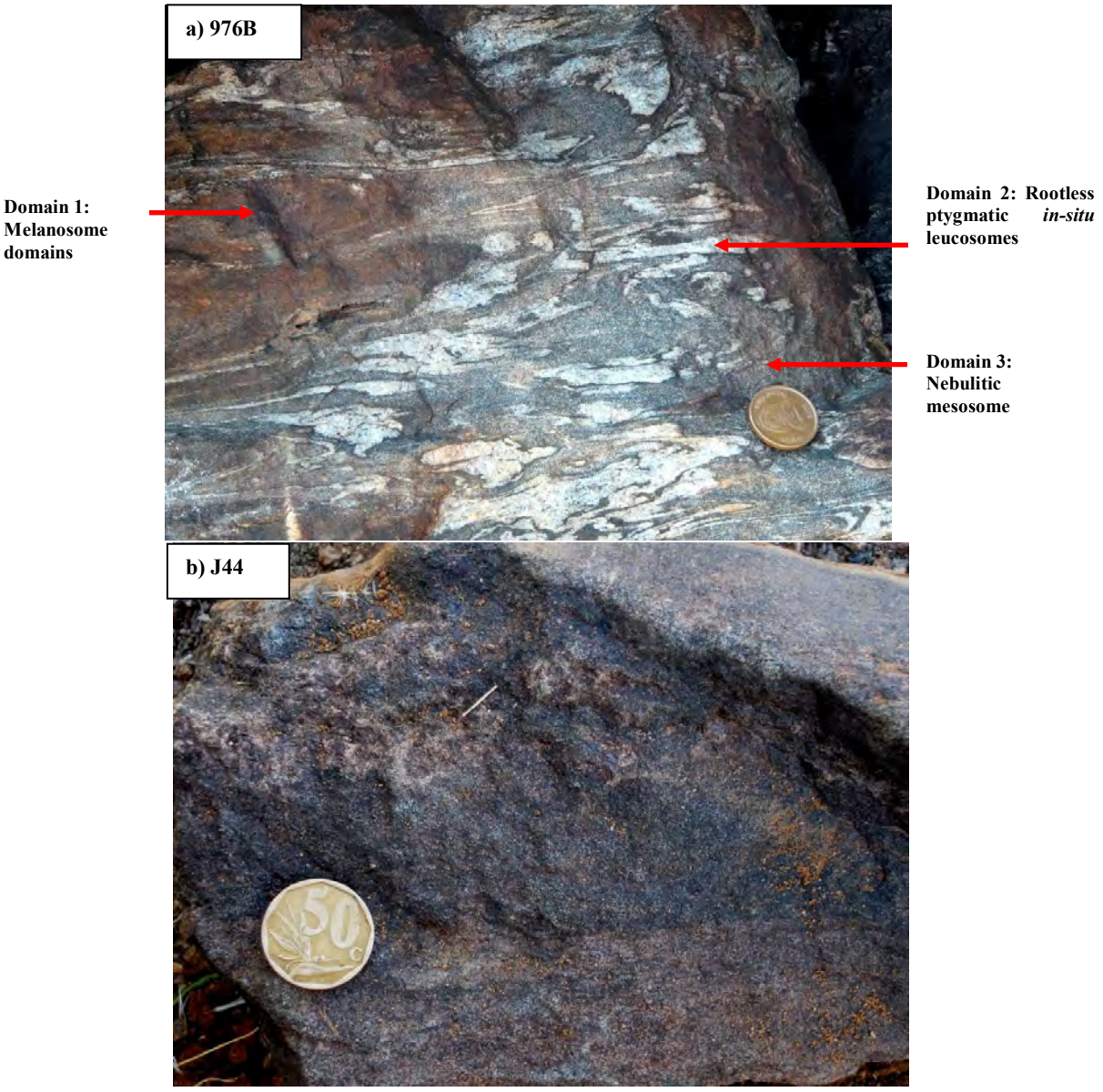

Figure 2.5. (a) In the field mafic granulite 976B shows discrete rootless ptygmatic leucosome folds (domain 2) located within nebulitic Cpx-Pl-Qtz mesosomes (domain 3). The leucocratic boundaries exhibit thinly-rimmed restitic layers. The dark brown patches show segregated clinopyroxene, andradite, plagioclase and quartz domains (domain 1). (b) Location J44 displays a fine-grained melanosome that is homogenous in colour and grain size (<0.5mm) that is devoid of any leucosome domains.

2.1.3 Leucocratic domains

The leucocratic domains consist almost entirely of alkali feldspar, quartz and minor plagioclase. They represent the melt fraction that has been separated from the original protolith after partial melting has taken place. The leucocratic features associated with the mafic granulites exhibit various mesoscopic textures and can be further be divided into (i) *in-situ* leucosomes (ii) leucocratic veins (iii) leucocratic pockets (iv) leucocratic networks, and (v) leucocratic pools.

2.1.3.1 In-situ leucosomes and leucocratic veins

In-situ leucosomes are those leucocratic domains that remained close to their source and form lenses or pockets within nebulitic of stromatitic neosomes. The mesosomes of mafic granulite 976A (Figure 2.2a) is characterised by fine- to medium-grained domains of dark green clinopyroxene fragments and dark grey plagioclase grains. However, the nebulitic neosome contains small centimetre scale concentrations of light grey coarse-grained (<0.5 cm) leucocratic domains within the mesosome.

The *in-situ* leucosome domains of mafic granulite 976B (Figure 2.2b) consist of fine-grained (<0.5mm) alkali feldspar and quartz. These domains are easily recognisable due to the light colour of the leucosome as it provides a stark colour contrast to the dark grey-green mesosomes. Where *in-situ* leucosomes formed planar geometries, they are often ptygmatic folded and may be contracted to a 'blob-like' geometry. The boundaries of these *in-situ* rootless leucocratic folds show melanocratic rims comprised of fine grained (<0.5mm) clinopyroxene.

2.1.3.2 Leucocratic pockets:

The leucosome veinlets and dykes join and accumulate in pockets located in between larger-sized and stretched mafic fragments and magmatic breccias of the mafic granulite unit (Figure 2.7). Sample A88-L (Figure 2.6a) shows a coarse-grained (>0.5mm) milky white syenitic domain and a light grey granitic domain separated by a distinct sharp boundary. Leucocratic pockets residing in sample 976A (Figure 2.2a-domain 1) show dark grey tabular equidimensional magmatic plagioclase phenocrysts (0.5-2 cm sized) located adjacent fine grained (<0.5mm) nebulitic mesosomes. However leucocratic pocket J10B-L differs as it exhibits stromatitic features whereby dark green melanocratic and white leucocratic layers are oriented parallel to another (Figure 2.6b).

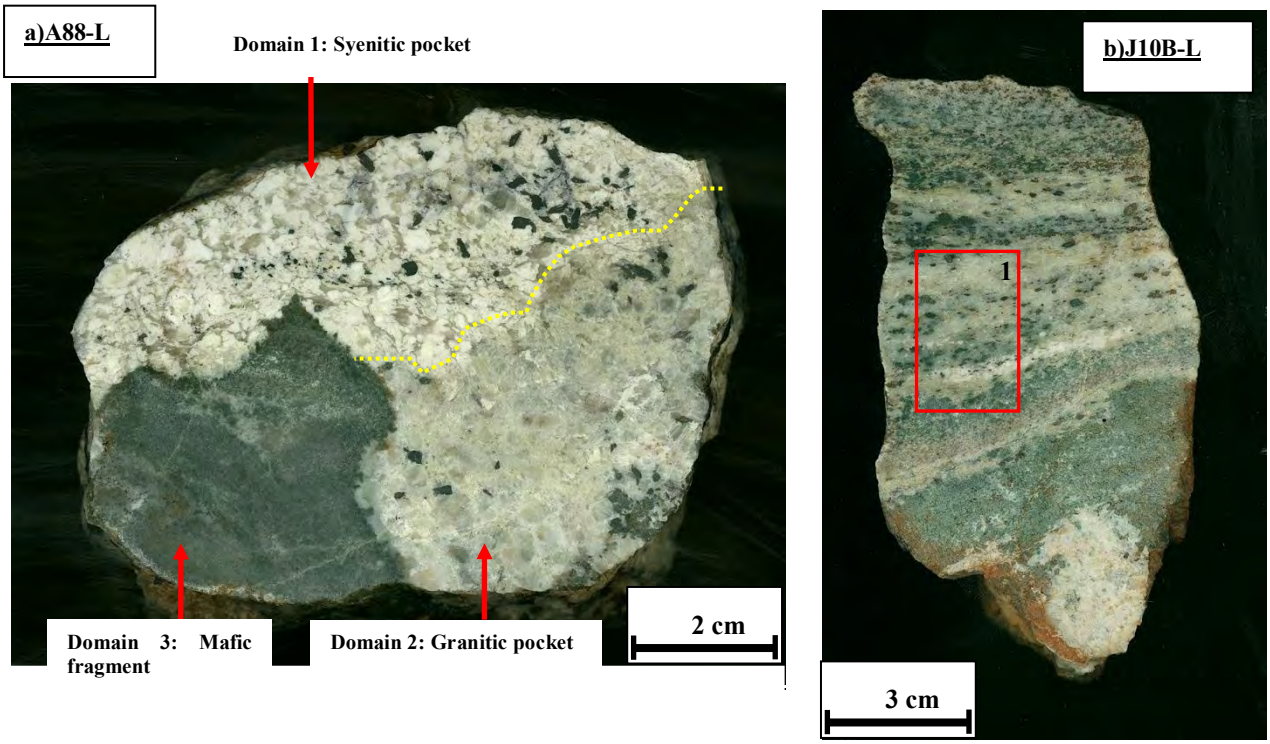

Figure 2.6. (a) Leucocratic sample A88-L. The specimen exhibits two discrete separate leucocratic pockets. Domain 1 is a syenitic pocket characterised by distinct vitreous white K-feldspar grains, quartz and minor plagioclase, and the other (domain 2) is granitic, characterised by little K-feldspar, with noticeable plagioclase and quartz. Both leucocratic pockets are separated by sharp contacts (highlighted by dashed yellow lines). (b) Stromatitic leucosome pocket J10B-L. The pocket is defined by successive leucocratic and melanocratic layers of variable thickness ranging from millimetre to centimetre scale. The numbered red rectangle indicates the sites for thin section observations (sample J10B-L; section 3.4).

2.1.3.3 Leucocratic networks

The leucocratic networks (location 982-Figure 2.7) are formed by anastomosing veins of various thickness and often irregular shape. They may occur from hand specimen scale (Figure 2.4 and 2.8) to outcrop-scale (Figure 2.10a, 2.10c domains 1, 2 and 3). The networks consist of medium- to coarse-grained (~0.5-2cm) quartz and alkali feldspar grains in addition to clinopyroxene fragments. Furthermore mafic fragments are also hosted within the networks (Figure 2.8 domains 1 and 4). A typical leucocratic network is developed at location 982 (Figure 2.1, location map), whereby the networks appear to stem from a fine-grained nebulitic mesosome with little *in-situ* leucosome (Figure 2.7 domain 1) into magmatic breccias zones (domain 2).

Figure 2.7. Location 982:Transition from metatexite nebulitic mesosomes (domain 1) to a magmatic breccia (domain 2). The leucocratic domains of the magmatic breccia zones penetrate the restitic mafic granulites.

Sample 982E (Figure 2.4) shows several thin (0.2-2 mm) leucocratic veinlets associated to stromatitic mesosomes grading into nebulitic mesosomes. Laterally the small network grades into distinct light-coloured larger-scale (0.5-1.5 cm-thick) leucocratic networks, and dark restitic domains. Location 982 (Figure 2.7) displays a leucocratic network formed by intrusive magma, penetrating restitic mafic granulite, forming elongate fragments within a vein network. Where this happens at a larger scale it forms magmatic breccias (domain 2). The hand specimen of sample 985A (Figure 2.8) shows an advanced stage of network evolution where spacing of mafic fragments are several centimetres apart. The separation of mafic fragments is about an order of magnitude larger than seen in sample 982E (Figure 2.4). In addition to mafic fragments, sample 985A shows a diffuse gradational contact with a grossularite-quartz-rich calc-silicate fragment (Figure 2.8, domain 3). Along the interface of leucocratic networks and calc-silicate fragments, fine grained (<0.5mm) light-greys scapolite is common (Figure 2.8-domain 2).

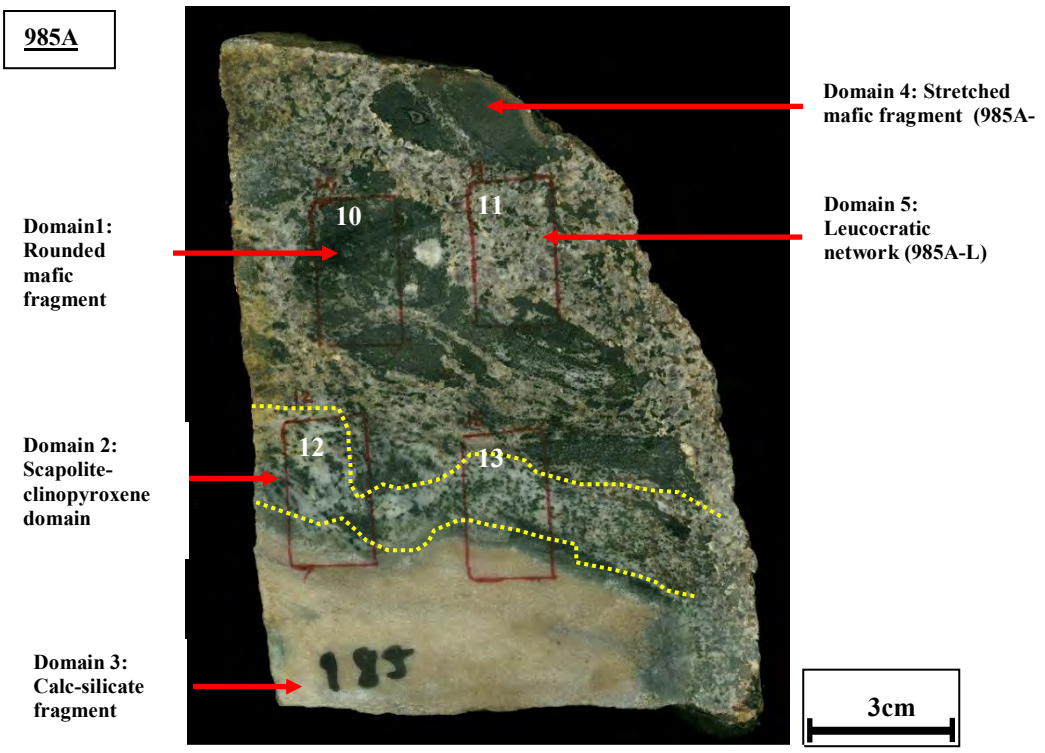

Figure 2.8. Scanned offcut from leucocratic network 985A. The sample contains dark green mafic (domains 1 and 4) and light brown calc-silicate fragments (domain 3). These in turn are surrounded by coarse-grained leucocratic syeno-granitic networks (domain 5). The interface between calc-silicate fragments and leucocratic networks are sharply separated by light grey medium-grained (~1mm) scapolite domains (domain 2). The highlighted rectangles indicate the sites for thin section observations (thin sections 985A 10-13; sections 3.1.3, 3.1.4, 3.1.7 and 3.1.8).

2.1.3.4 Mafic fragments:

Mafic fragments occur in a groundmass of leucocratic granite or granite vein networks and pools. They vary in shape and size, ranging from a few centimetres to as large a metre (Figure 2.10c). The gradual change from coherent mafic rocks of the Bysteek Formation to magmatic breccias is seen in zones that show increasing disruption of the Bysteek Formation by crosscutting granitic veins. The shape of fragments ranges from angular with sharp fragment boundaries to fragments with irregular boundaries or with reaction rims (Figures 2.6a, 2.8a and 2.9).

Many of the fragments are elongate in shape. Frequently leucocratic granite veins penetrate the fragments and intrude along foliation planes into the mafic fragments. This causes various degrees of disintegration and increases the nebulitic appearance of some fragments. With increasing interaction with the external magma the fragment boundaries become increasingly diffuse. However, in contrast to nebulitic domains in the central part of the Bysteek Formation, the nebulitic texture magmatic breccias may be related to intrusive granite rather than to *in-situ*

formed magma. Mafic fragments also occur in a dark green and pale brown variety. Dark green and fine-grained fragments are comprised almost entirely of clinopyroxene. Brown fragments are comprised almost entirely of calc-silicate material (Figure 2.8-domain 3). The outcrop appearance of the fragments is distinct due to their dark green-black colour hosted in a light grey leucocratic groundmass.

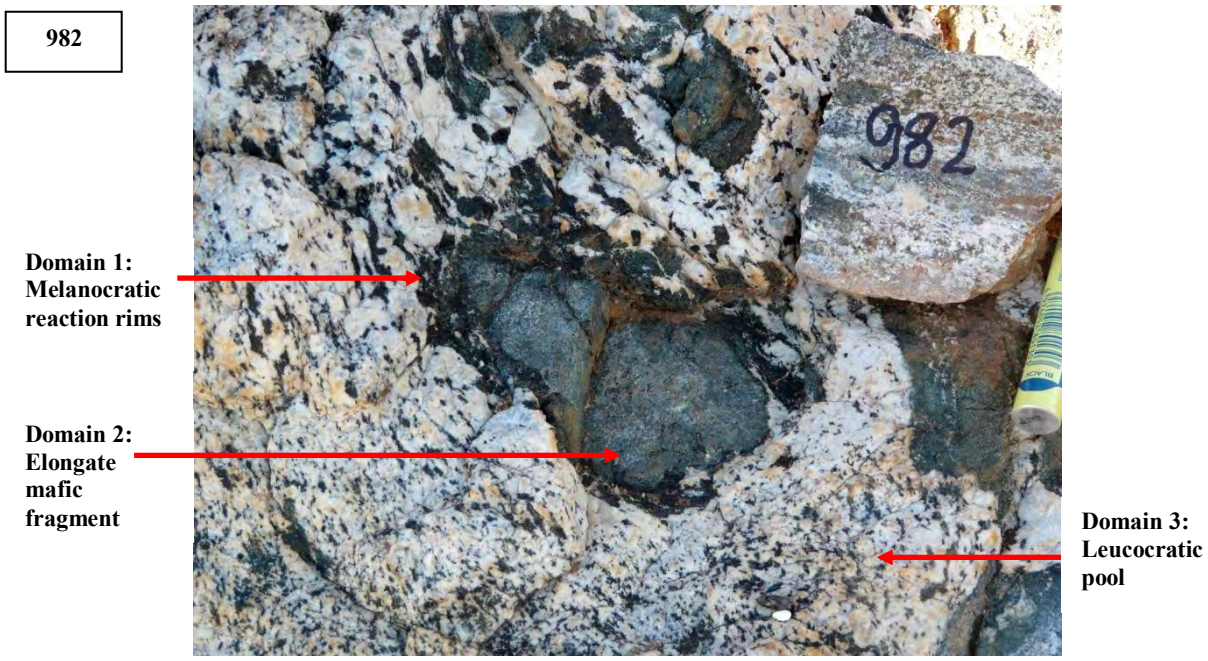

Figure 2.9. Location 982. The leucocratic part (domain 3) is comprised entirely of microcline phenocrysts. The elongate mafic fragment (domain 2) are ovoid in shape and display melanocratic reaction rims (domain 1) consisting of clinopyroxene along the interface with the hosting alkali feldspar-rich groundmass.

2.1.3.5 Leucocratic pools

Leucocratic granitoid pools occur where magma extracted from mesosomes gathers in spaces larger than 10 cm in diameter and no direct spatial relationship to the restitic source area exists. The pools are the largest sink of partial melt/magma formed in the Bysteek Formation mafic rocks that can be verified by connecting diffuse leucocratic veinlets, fracture networks and smaller magma pockets (Figure 2.10c, domains 2 and 3). Like the smaller pockets, the pools are essentially composed of alkali feldspar. The pool may contain mafic fragments from the Bysteek Formation mafic rocks (Figures 2.9 and 2.10b). These mafic fragments vary in scale from 10 to 150 cm (Figure 2.10c, domain 4). The pools vary in composition ranging from homogenous well defined re-crystallized microcline aggregates to mixed proportions of orthoclase, quartz and plagioclase (Figure 3.7).

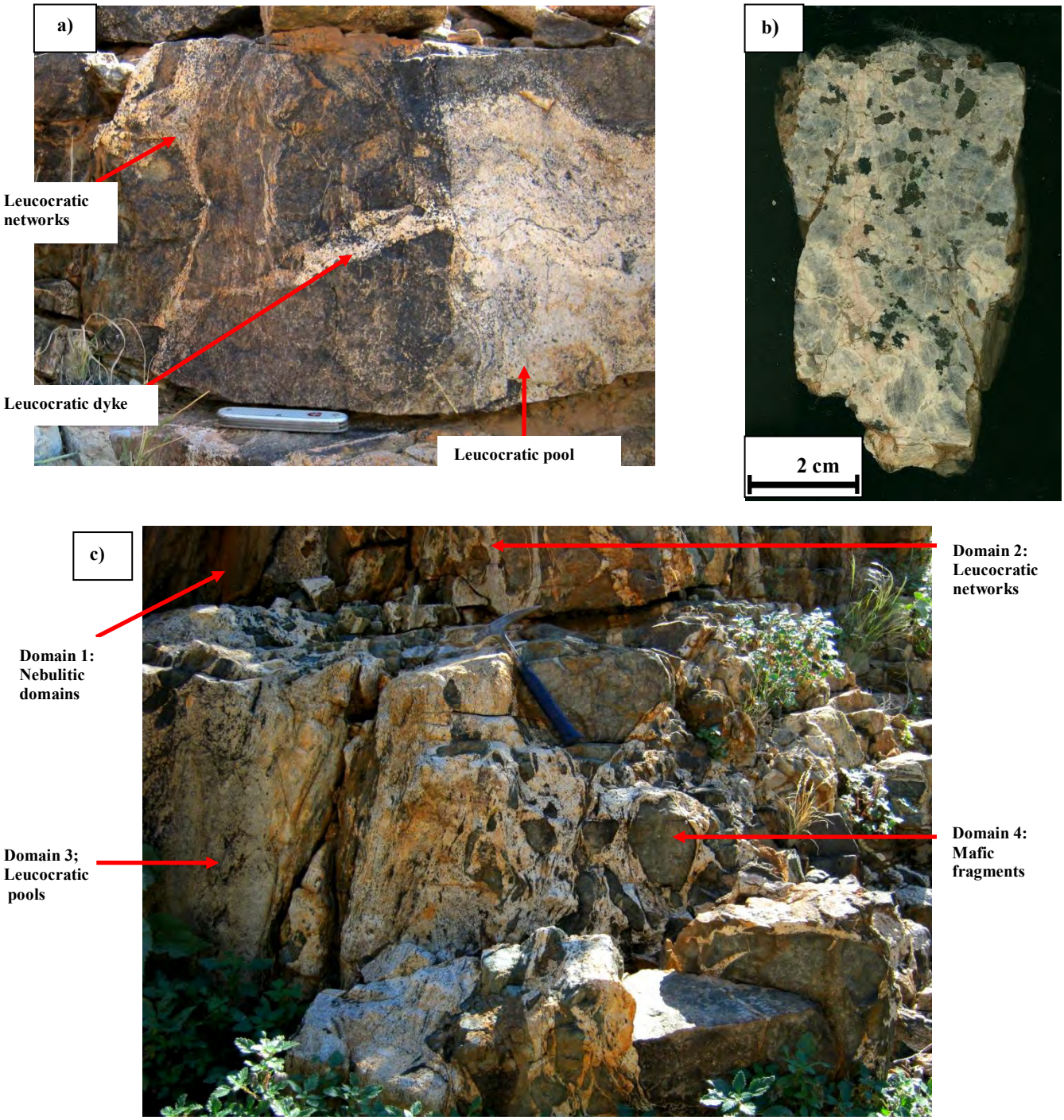

Figure 2.10. Leucocratic domains and magmatic breccia at Location 982. (a) The leucocratic dyke is joined at the left end by small-scale stromatitic veins and networks and is attached to a large leucocratic pool at the right end (b) Hand specimen of leucocratic pool sample J26A. The milky white domains are comprised microcline whereas the dark grey euhedral phenocrysts are orthoclase. The green grains are detached clinopyroxene xenocrysts most likely from neighbouring melanocratic domains (c) Large scale leucocratic networks and pools in a magmatic breccia. The networks appear to grade from nebulitic domains (domain 1) into larger scale networks (domain 2) and pools (domain 3). The mafic granulite fragments (domain 4) are, elongate and show roughly parallel orientation of their long axes. The mafic fragments are massive with various shapes and size. Hammer for scale.

2.2 Calc-silicates and related marble domains

Apart from the mafic granulites and anatexites, the Bysteek Formation contains a series of marbles and calc-silicate rocks with partly gradational transitions to each other. Coarse-grained (0.5 mm-2 cm sized) granoblastic marbles commonly show thick (1-3 cm) brown layers consisting of medium-grained (~0.5-1 mm) scapolite and garnet. The garnet-scapolite-rich layers may contain dark grey talc (location J1, Figure 2.11a). Other calc-silicate rocks host randomly oriented mafic fragments within marble units whereby the groundmass contains randomly oriented clinopyroxene grains (location T-64, Figure 2.11 b).

Furthermore, the leucocratic networks from the mafic granulite sequence have also incorporated calc-silicate fragments within its groundmass (sample 985A; Figure 2.8). Interlayerings of rheologically different rocks in the carbonate-calc-silicate-rich part of the Bysteek Formation often show convoluted folding with tight to isoclinal folds and often non-cylindrical or sheath fold geometry (location L25-Figure 2.12).

Intrusive vein networks of medium to coarse-grained syenitic composition containing mafic fragments also affect the calc-silicate rocks. Where magma came in contact with calc-silicate rocks of, for instance, grossularite-quartz-rich composition (sample 985A-Figure 2.8), the calc-silicate rock disintegrates along diffuse and irregular boundaries along of which felsic and calcic components appear to intermingle (sample J47-Figure 2.13).

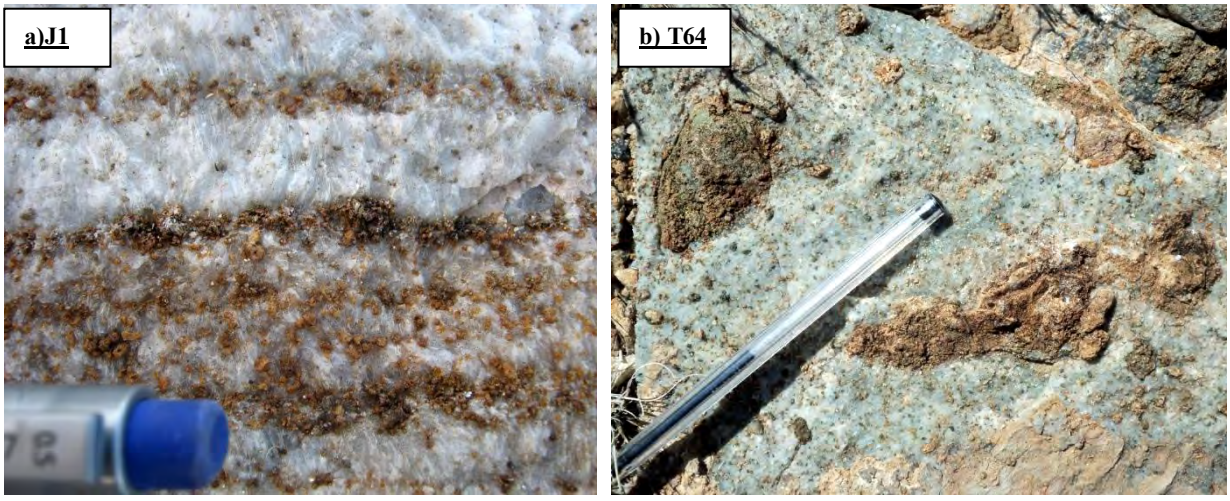

Figure 2.11. (a) Location J1 showing coarse-grained (0.5-2cm) granoblastic marble showing dark brown layers of garnet and scapolite along with dark grey talc layers. (b) Location T64 showing randomly oriented calc-silicate fragments within marble. Pen for scale.

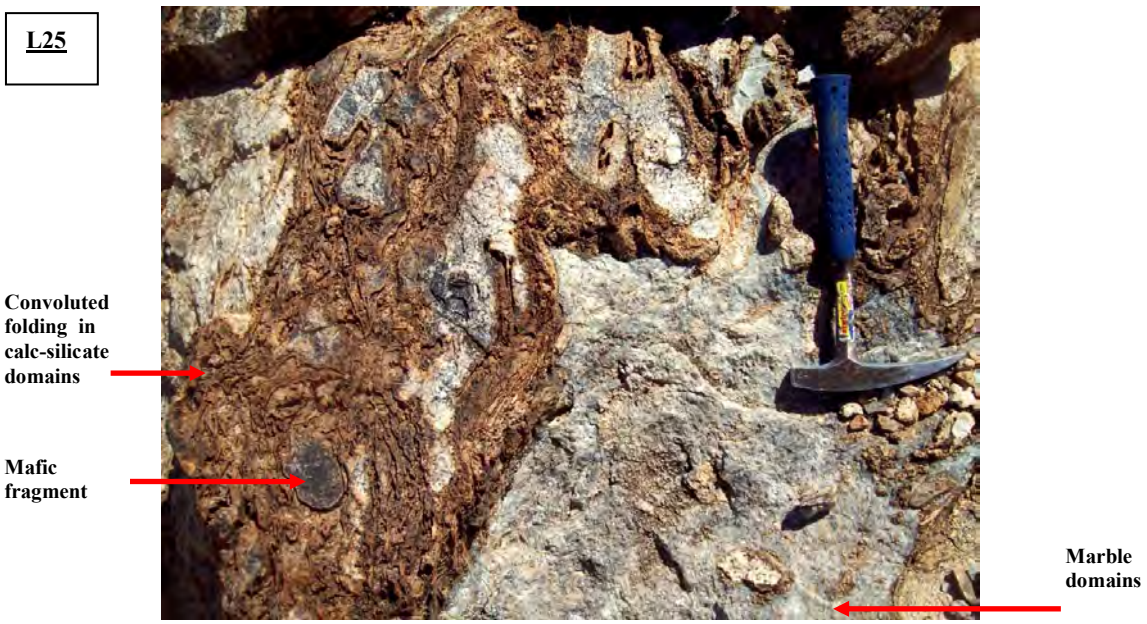

Figure 2.12. Location L25: Convoluted folding in calc-silicates with tight to isoclinal fold geometries. Additionally, the mafic fragments are located within the calc-silicate rock. Homogenous marble domains neighbour the calc-silicate domains. Hammer for scale.

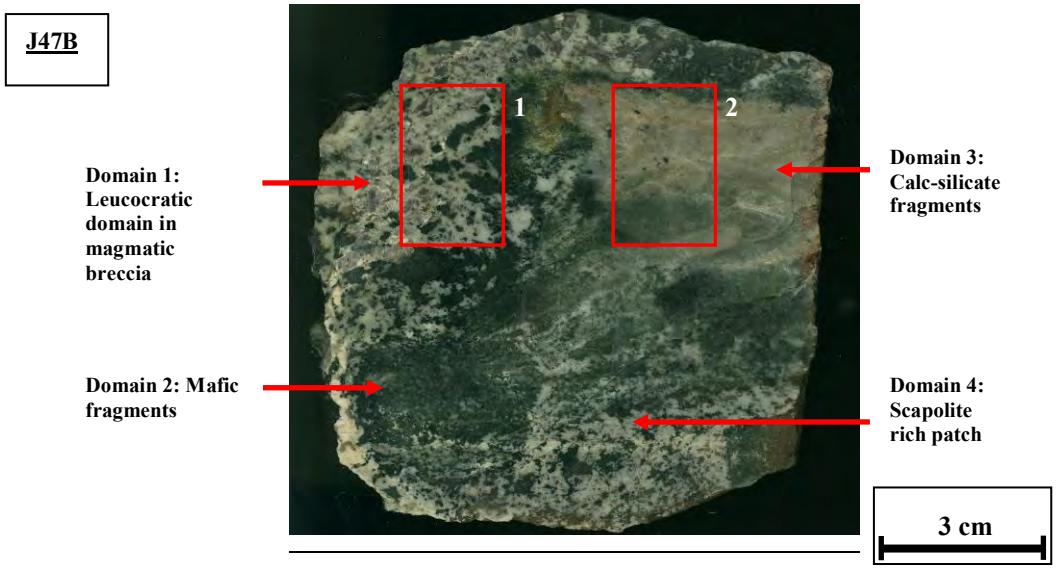

Figure 2.13. Hand specimen of calc-silicate J47B shows clear interaction between the leucocratic domain (domain1), mafic fragments (domain 2) and calc-silicate domains (domain 3). The leucosome in magmatic breccia contains near-spherical metabasite fragments of variable size and one larger calc-silicate rock fragment. The pale brown calc-silicates exhibit diffuse boundaries on its peripheries, grading from a pale brown colour to a light grey colour, where dark-green mafic fragments and leucocratic networks intersect. These light grey domains are comprised of scapolite similar to what is present in hand-specimen 985A (Figure 2.8; domain 3). All fragments show advanced stages of disintegration. The highlighted rectangles indicate the sites for thin section observations (thin sections J47-L1 and J47-2; sections 3.1.4 and 3.2).

2.3 Diatexites (kinzigites)

According to Brown's (1973) definition, diatexites are migmatites in which partial melting has destroyed any pre-anatectic features and which are characterised by homogenous grain coarsening textures. Diatexites are the dominant rock type of the Koenap Formation. Previously the rocks have been described as kinzigites (Moen and Toogood, 2007) which are rocks consisting of quartz-K-feldspar-plagioclase-rich groundmass with less abundant garnet (almandine/pyrope), cordierite, biotite, sillimanite (Mehnert, 1968). However, this assemblage is not always present and in this study the classification as diatexites is preferred since this covers the textural characteristics of large parts of the Koenap Formation.

The diatexites of the Koenap Formation typically are massive, poorly layered or isotropic rocks occurring in boulder outcrops essentially southwest of the Bysteek Formation (Fig.1.1 b-d). The mineral assemblage consists of quartz, alkali feldspar, biotite, almandine garnet, sillimanite, magnetite and occasionally cordierite. The diatexites vary in mineral modes (see Section 3.3, Tables 3.6-3.9) and mesoscopic textural characteristics. Although there are gradual transitions between different types they have been subdivided in (i) leucocratic diatexites, (ii) banded diatexites, (iii) nebulitic diatexites, and (iv) melanocratic domains.

2.3.1 Leucocratic diatexites

The pink to light grey leucocratic diatexites are medium- to coarse-grained (~0.5-0.8mm) and essentially consist of K-feldspar and quartz, and minor plagioclase, biotite and occasionally garnet. Leucocratic diatexites range from massive varieties to more or less diffusely banded types (Figure 2.14). Field observation does not show any systematic distribution of the different types within the study area.

Massive leucocratic domains (Sample 983D-Figure 2.14c) exhibit no recognisable layering or discrete domains where one mineral species would be enriched. The uniform fine to medium grain size (0.5-1cm) and light grey colour emphasises the homogenous field appearance of massive diatexites. The layered variations of leucocratic diatexites show segregations of material similar to the massive type, alternating with garnet-rich darker layers. The darker layers can vary substantially in thickness (Figure 2.14 a and b) and normally have little lateral extent, which distinguishes them from the banded diatexites (see next section). Occasionally, diffuse and finer-grained domains of nebulitic mesosome (Fig. 2.17) occur together with coarse-grained, pegmatoid domains rich in K-feldspar, medium-grained garnet and biotite forming a patchy variety of diatexite (Fig. 2.15b).

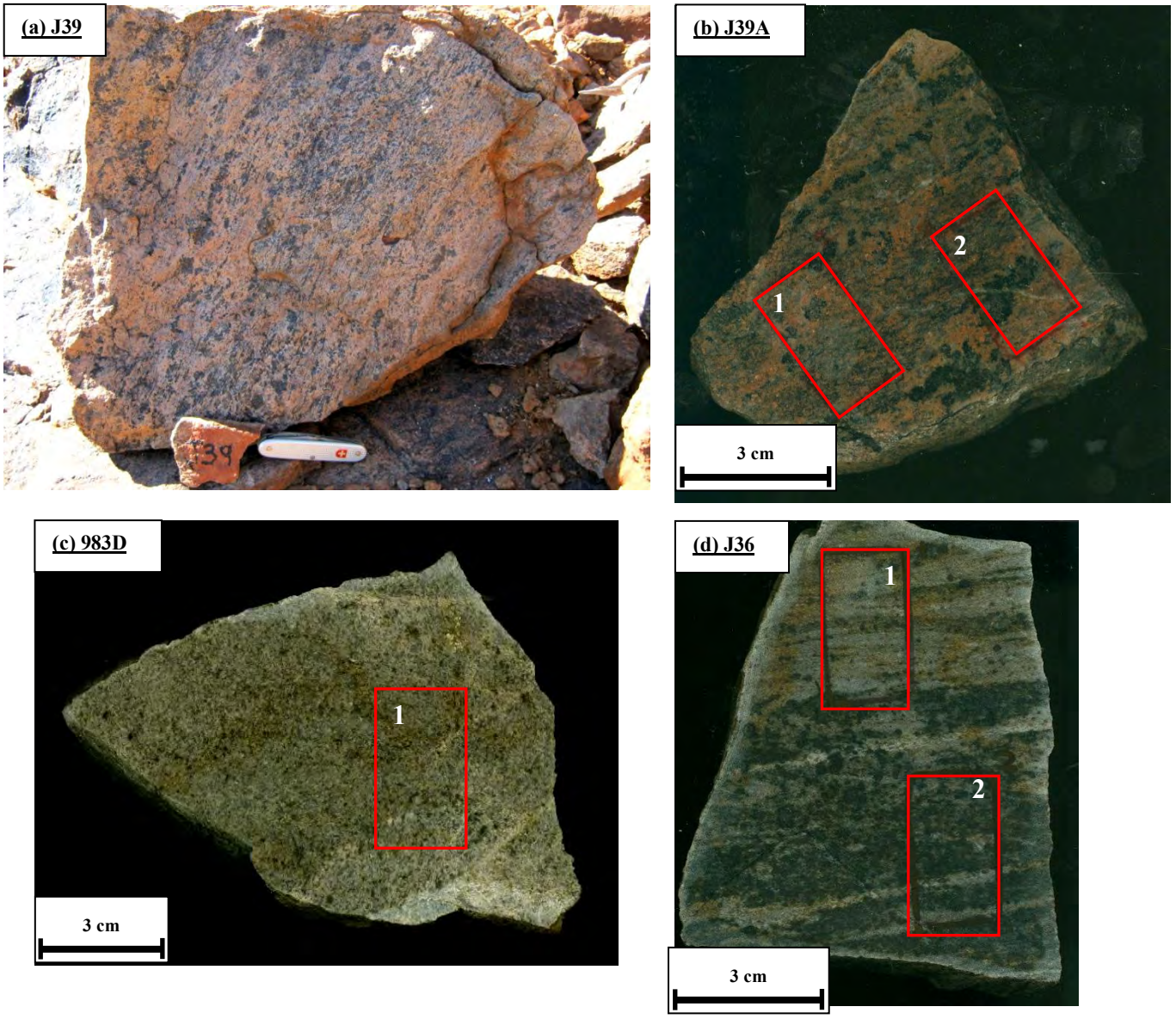

Figure 2.14. Field images and hand specimens of leucocratic diatexites. (a and b) Location/sample of J39 displaying a leucocratic diatexite containing diffusely banded and massive domains. It exhibits a diffuse layering formed by coarse-grained melanocratic garnet domains. (c) Specimen 983D is massive leucocratic diatexite. It is medium-grained (~0.5mm), homogenous with a small amount of melanocratic phases and without banding. (d) Specimen J36 displays a gradation from banded leucocratic domains with few melanosome areas to a nebulitic diatexite domain with further gradation into more melanocratic domains. Highlighted rectangles indicate sites for thin section analyses (thin sections J39A-1, 983D1, J36L-1; section 3.3.1).

2.3.2 Banded diatexites

The banded diatexites show a distinct interlayering of leucocratic, nebulitic or melanocratic domains. Typically the banding has considerable lateral extent and is penetratively developed. The spacing between layers varies between a less than 5 mm and ~2-3 cm (Figures 2.15 and 2.16). Banded diatexites show an anastomosing structure between dark grey-black biotite-

garnet domains and pink-light grey leucocratic domains, whereby the margins between both domains are generally diffuse (samples J20 and J40, Figure 2.15a- b, 2.16c-d). Coarse-grained maroon-red garnet (~0.5-1 cm) occurs in aggregates of up to 1 cm in diameter and show rims of fine-grained biotite. (Figure 3.3.4).

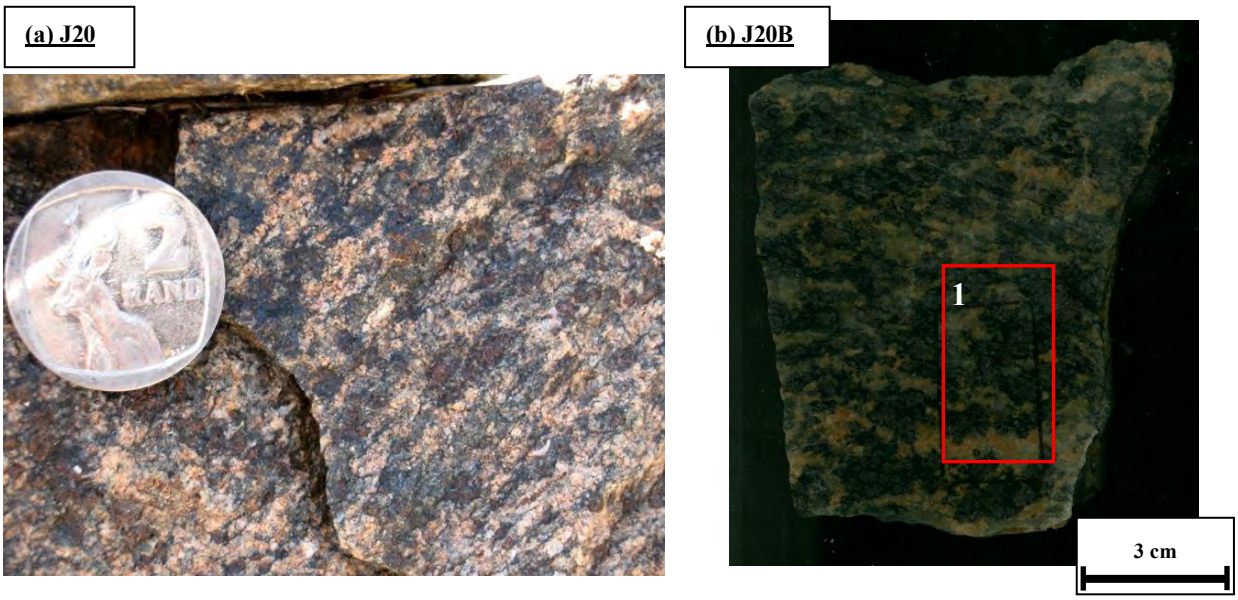

Figure 2.15. Location (a) and hand specimen (b) of banded diatexite J20. The anastomosing relationship occurs between layers rich in coarse-grained garnet (1-1.5 cm), biotite aggregates (>1mm) and a pink alkali feldspar-quartz groundmass. Highlighted areas indicates sites for thin section analyses (thin section J20B; section 3.3.4).

In typical banded diatexites (e.g. sample J33, Figure 2.16a) the margins between leucocratic and melanocratic domains are sharp and discrete. This provides the diatexite with a pronounced banding whereby the melanocratic and leucocratic domains are well distinguishable. Garnet-biotite-rich melanocratic layers are 1-2cm thick. Sample 983 (Figure 2.16b) is a poorly layered diatexite with some vague layering of maroon-red coarse-grained (0.5-5mm) garnet and more voluminous homogenous light grey-pink massive leucocratic layers. This is a transitional type to the more homogenous leucocratic diatexites which occur in the same exposure. This type differs from the well layered counterparts also by the absence of prominent biotite clusters surrounding garnet.

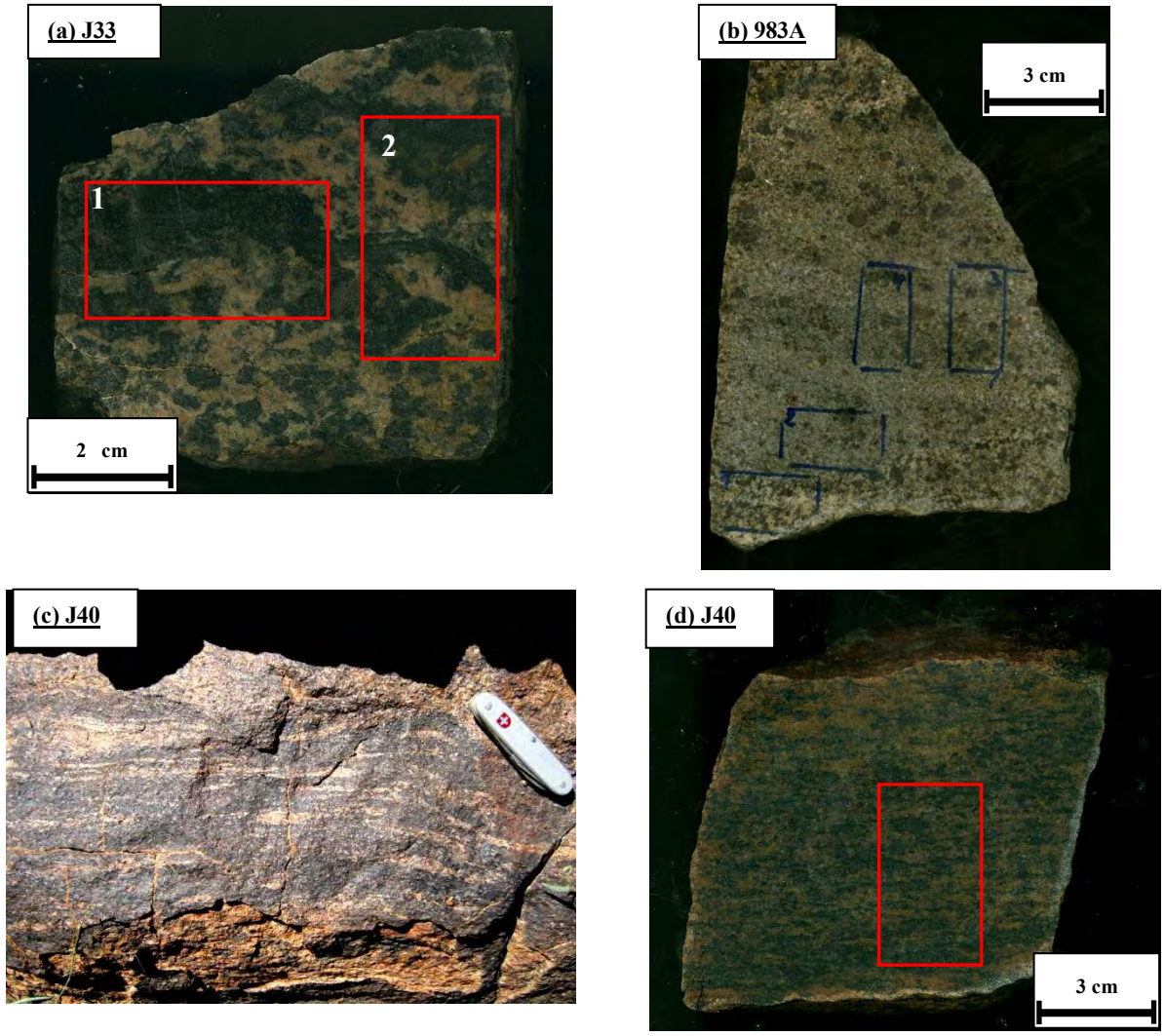

Figure 2.16. Field and hand appearance of banded diatexites J33, 983A and J40. **(**a) Irregularly shaped and partly disrupted garnet-biotite-rich layers intercalated with pink K-feldspar-quartz-rich leucocratic layers. The leucocratic layers also show abundant garnet aggregates. (b) Transitional diatexite between layered and the massive leucocratic type. A weakly layered specimen (983A) with clusters of garnet arranged in layers of light grey medium-grained groundmass. (c and d) Locality/sample J40 displays a stromatitic diffuse anastamosing interlayering between pink leucocratic and dark melanocratic domains. Leucocratic and melanocratic domains occur in an almost equal proportion whereby the domain thicknesses are uniform ranging between 1-3 mm. Highlighted rectangles indicate sites for thin section analyses (thin sections J33-1, J33-2; 983A1-4; J40; section 3.3.4).

2.3.3 Nebulitic diatexites

Nebulitic diatexites (samples J12, J37, J38, L38B; Figure 2.17) typically consist of leucocratic K-feldspar-quartz-plagioclase groundmass with variable proportions of garnet but always small amounts of biotite. Nebulitic diatexites are largely massive and lack layering but show distinctive domains with nebulitic texture associated with coarser-grained magmatic veins or patches (Figure 2.17). Particularly there are no melanocratic layers consisting of garnet or other mafic minerals. The grain size is variably medium-to coarse-grained (0.5-1mm).

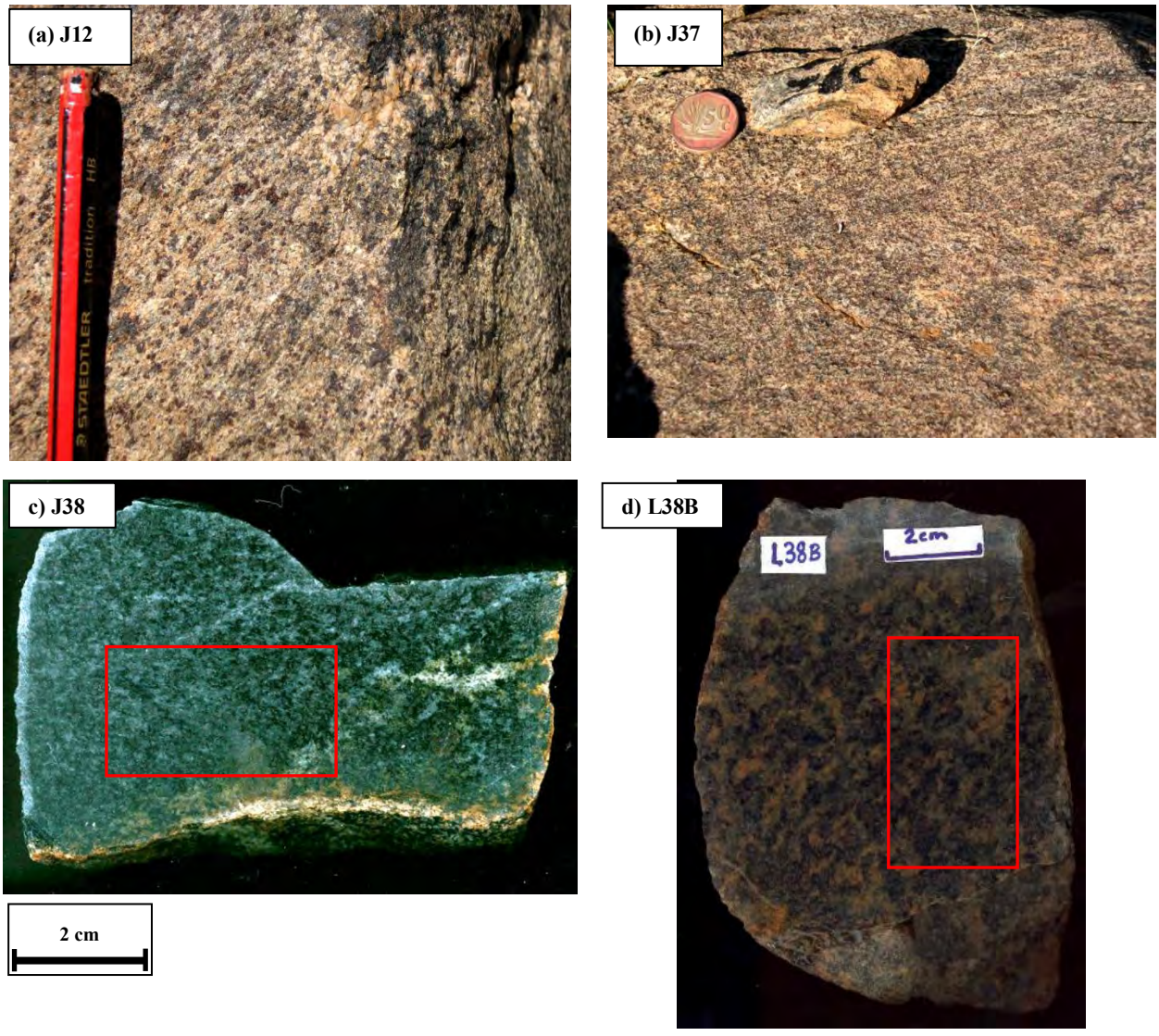

Figure 2.17. Field appearance of nebulitic diatexites (a) J12, (b) J37, (c) J38 and (d) L38B. All specimens show a weak layering, are medium-to coarse-grained containing pink garnet grains located within a pink-grey leucocratic groundmass. Highlighted rectangles indicate sites for thin section analyses (section 3.3.5).

2.3.4 Mafic lenses in the diatexites

The diatexite domains occasionally contain mafic lenses within the nebulitic domains. These lenses vary size (3-6cm), but are frequently elongate (sample 983E-Figure 2.18a) to lens shaped (Location A106A-Figure 2.18b). Additionally they are dark in colour and finer grained (<0.5cm) when in comparison to the neighbouring nebulitic diatexites (>0.5cm). A distinct sharp contact boundary is present between the peripheries of the nebulitic diatexite domains and the adjacent mafic enclave (Sample A106A-Figure 2.18c).

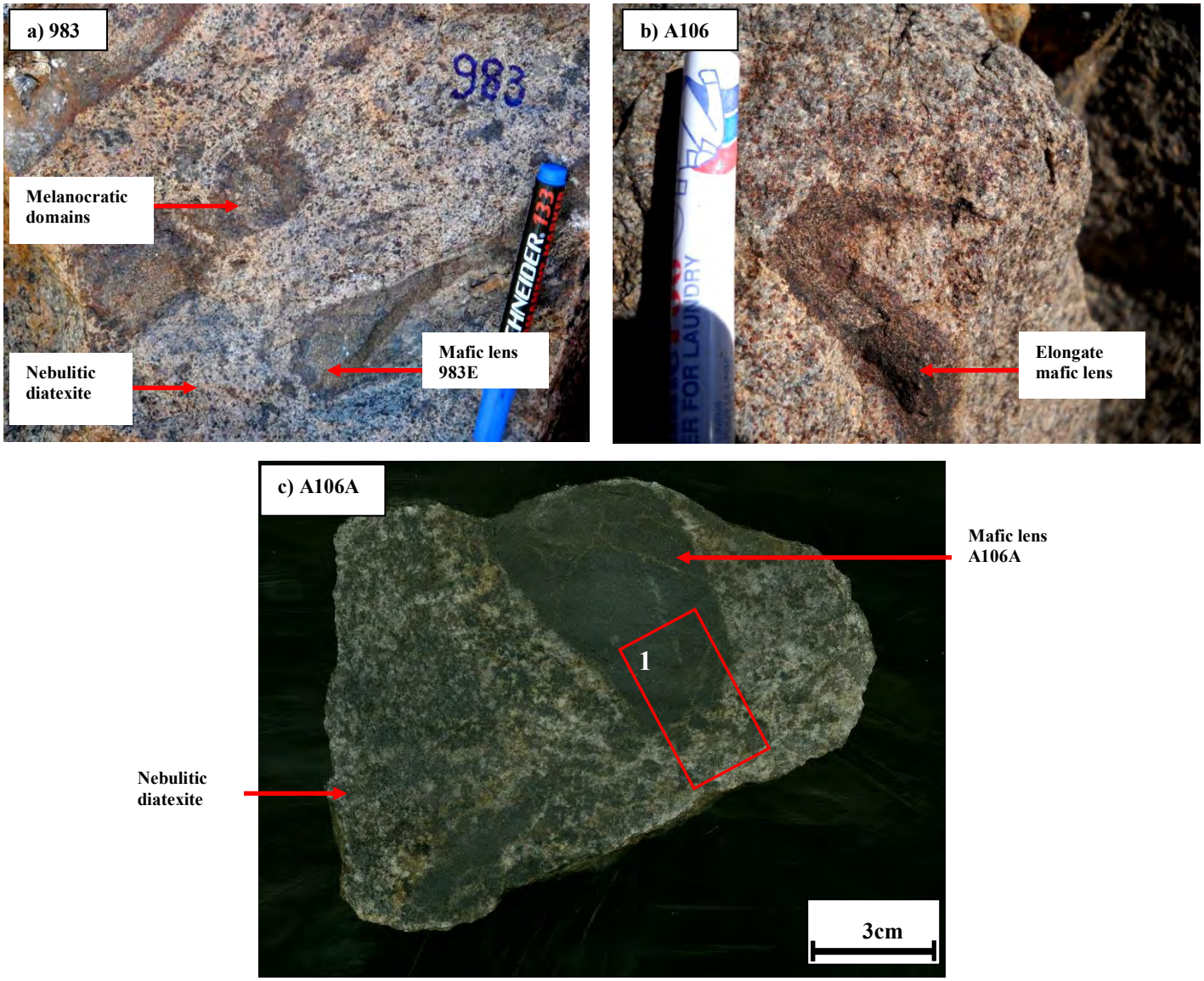

Figure 2.18. Mafic lens in diatexite domains. (a) Location 983: Nebulitic diatexite with distinct dark medium-grained (0.5-1mm) domains. Adjacent to these are finer-grained (<0.5mm) oval-shaped lenses. (b) Location A106 shows mafic lenses that are fine-grained and partly folded, suggesting that they have a pre-anatectic deformation history. (c) Hand specimen A106A shows fine-grained (<0.5mm) mafic lens with sharp boundaries to the neighbouring nebulitic diatexite. The rectangle indicates the position of the thin section (section 3.3.3).

3. Thin Section Petrography

This chapter is devoted to the petrographic evaluation of the Bysteek Formation mafic granulites and calc-silicate rocks, and the Koenap Formation diatexites. The marked positions on hand specimens shown on figures in the previous chapter indicate some of the sites used for microscopic analysis. Modal quantities of phases were quantified and assessed using three different processes: (i) Manual point counting on thin sections using a point counting device mounted on a petrographic microscope; (ii) Point counting on enlarged SEM back-scatter electron images (BSE) in addition to enlarged photomicrographs taken from thin section. This technique was used to support fine-grained domains such as nebulitic mesosomes; (iii) Image analysis of the BSE utilizing the phase analysis tool of the Oxford Instruments INCA EDS software package.

3.1 Mafic granulites and associated leucocratic domains

Petrographic observations were performed on mafic granulite mesosome (section 2.1.1), melanosome (section 2.1.2) and mafic fragment domains (section 2.1.3.4). Leucocratic domains were also evaluated: (i) *in-situ* leucosome domains (sample 976B-L) and veins (samples J9A-L and 982E-L; section 2.1.3.1); (ii) leucocratic pockets (samples J10B-L and 976A-L; section 2.1.3.2); (iii) leucocratic networks (samples 985A and J47-L; sections 2.1.3.3) and pools (sample J26-L and 982C section 2.1.3.5).

3.1.1 Mesosomes

The mesosomes from three specimens were analysed, sample 976A (Figure 2.2a), sample 976B (Figure 2.2b) and 982-mes (Figure 2.4) Mesosomes at location 976 are modally comprised of clinopyroxene (48-53 vol%), plagioclase (38-41 vol%), quartz (5-9 vol%), titanite (0.9-1.2 vol%), magnetite (0-3 vol%) and apatite (0.65 vol%) (Table 3.1).

The mesosome shows polygonal granular textures formed by clinopyroxene, plagioclase and ±quartz. The mesosomes are fine-to-medium-grained (<100-200µm) whereby both clinopyroxene and plagioclase exhibit polygonal shapes with straight to curved grain boundaries. Quartz is generally xenoblastic and displays irregularly shaped grain boundaries (Figure 3.1b). The magnetite in sample 976A-mes (Figure 3.1a) is often interstitial, but also occurs as exsolution lamellae within the clinopyroxene. Plagioclase shows lamellar twinning.

The stromatitic mesosome (982E-mes, Figure 3.1c) has mineral modes similar to the magnetite bearing mesosome 976A-mes (Table 3.1), but shows thin leucosome veins within the melanosome which are absent in sample 976A. Clinopyroxene at the periphery between melanosome and leucosome reacts forming aggregates of xenoblastic secondary amphibole and

minor biotite (Figure 3.1 c and d). The leucocratic veins are comprised of fine- to medium-grained (100-200µm) subhedral alkali feldspars and interstitial quartz.

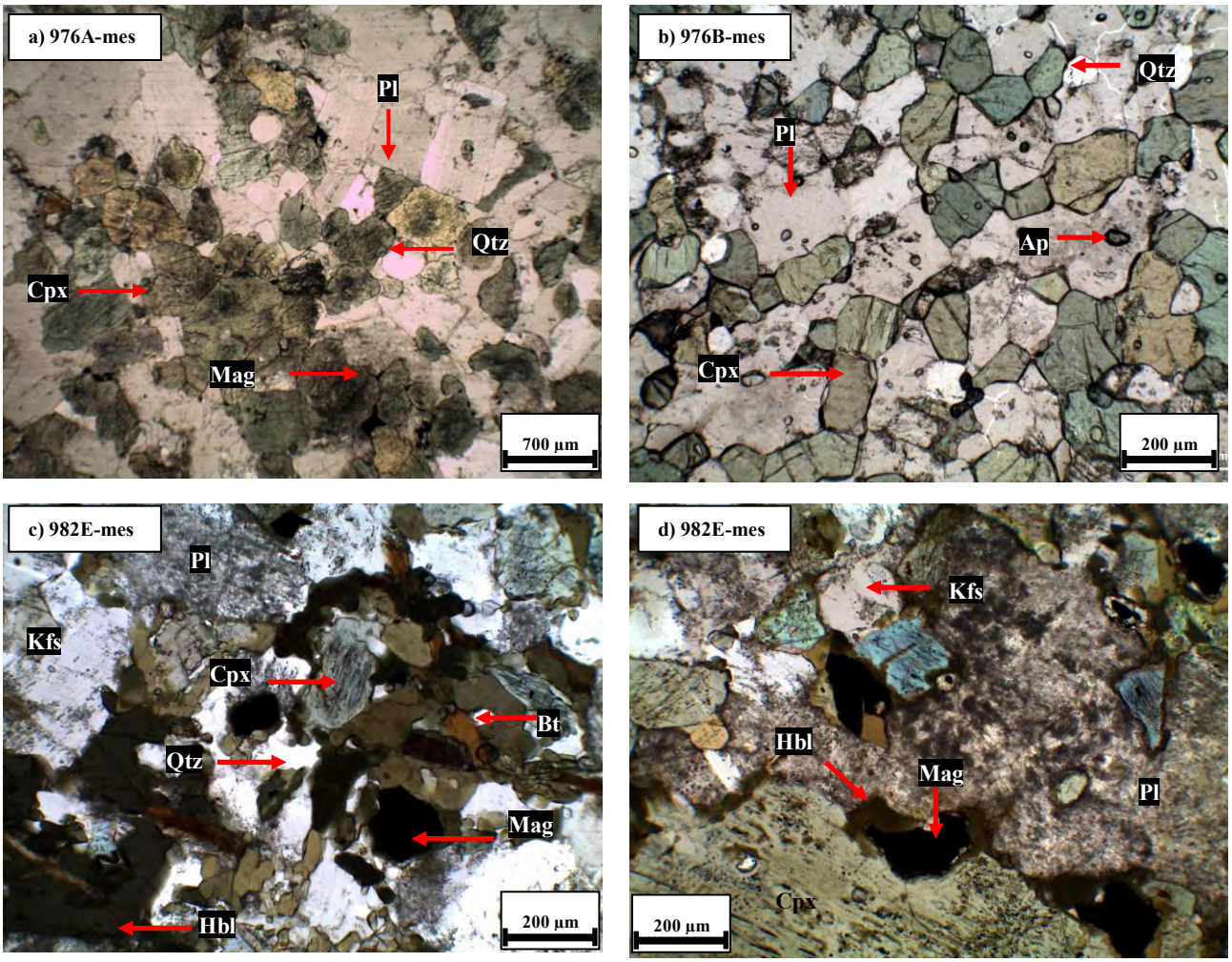

Figure 3.1. Photomicrographs from nebulitic and stromatitic mesosome domains. (a) Nebulitic mesosome 976A-mes (Figure 2.2a; rectangle 2). Plagioclase grains are medium-grained (300-600µm), tabular and subhedral with straight grain boundaries. Clinopyroxene is also medium-grained (300-600µm) and show polygonal shapes. Magnetite occurs as interstitial grains and as exsolution lamellae in clinopyroxene grains. (b) Nebulitic mesosome 976B (rectangle 2;Figure 2.2b). The clinopyroxene and plagioclase to a lesser degree show recrystallised foam textures indicated by their respective polygonal shapes. The mesosome of 976B is finer grained (100-200µm) in comparison to 976A (300-600µm). (c) Nebulitic mesosome domains from 982E (Figure 2.4; rectangle 1). (d) Stromatitic mesosome 982E (Figure 2.4; rectangle 3). Straight grain boundary faces occur between adjacent plagioclase and clinopyroxene. The grain boundaries of the clinopyroxene show breakdown to hornblende. Plagioclase is sausseritized in manner similar to the plagioclase grains in neighbouring nebulitic domains.

Table 3.1. Mineral modes of nebulitic mesosomes (976A-mes; 976B-mes) and stromatitic mesosome (982E-mes).

Domain	Nebulitic mesosome					Stromatic mesosome	
Sample	976A-mes			976B-mes		982E-mes	
Thin Section	976A1	976A2	976A3	976B2	976B4	982 E3	982 E4
Clinopyroxene	46.6	50.5	48.2	50.7	53.8	44.1	44.9
Quartz	9.2	7.5	5.5	8.5	6.5	7.7	7.0
K-feldspar	-	-	-	-	-	4.4	4.8
Plagioclase	38.8	38.4	41.6	39.4	38.4	37.4	37.2
Garnet	-	-	-	-	-	-	-
Biotite	-	-	-	-	-	0.3	0.1
Opaques	3.7	2.1	3.3	-	-	2.4	2.0
Apatite	0.6	0.4	0.4	0.5	0.7	0.5	0.5
Titanite	1.2	1.0	1.1	0.9	0.7	1.1	1.1
Hornblende	-	-	-	-	-	2.0	2.6
Total	100	100	100	100	100	100	100
Method	Point counter	Point counter	Point counter	Point counter	Point counter	Point counter	Point counter
Points counted	6479	7154	6351	7614	4681	3161	2794

3.1.2 Melanosomes

Four melanosome samples were analysed: 976A-mel (Figure 2.2a, domain 1), 976B-mel (Figure 2.2b, domain 4) 976B-2-g (Figure 2.2, domain 3) and J44-mel (Figure 2.3b). Melanosome 976B-mel is a homogenous garnet-free melanosome solely comprised of clinopyroxene (58-60 vol%) plagioclase (33-35 vol%) and quartz (4-5%) (Table 3.2). The melanosomes are located along the periphery of *in–situ* leucosome (976B-L) that locally forms folded veins. They are free of phases containing ferric iron such as magnetite or andradite, which are present in melanosomes 976B-2-g, 976A-mel, J44-mel, and mesosome 976A-mes.

The phases are similar in texture to mesosome 976B-mes, whereby clinopyroxene and plagioclase are fine- to medium-grained (<100-200µm) exhibiting straight grain boundaries with polygonal idiomorphic textures and interstitial quartz (Figure 3.2b).

Melanosome 976A-mel (Figure 3.2a) is texturally similar to 976B-mel but contains interstitial magnetite and interstitial quartz. Clinopyroxene is coarser-grained ranging between 300-800µm in comparison to 976B-mel which has finer-grained clinopyroxene in range of 100-200µm. Titanite is much coarser-grained (100-300 µm) compared to those of 976B-mel (10-50µm). Melanosome 976B is magnetite free, whereas 976A is magnetite bearing (3.1 vol%; Table 3.2). In its mineral modes, both melanosomes 976A and 976B are similar.

976B-2-g is a garnetiferous melanosome comprised of garnet (33-35 vol%), plagioclase (32-34 vol%), clinopyroxene (23-27 vol%), quartz (3-8 vol%) with minor titanite (~1 vol%) and apatite (~0.5 vol%) (Table 3.2). The melanosome exhibits a gradational contact relationship between the neighbouring garnet-free mesosome 976B-mes. Garnet is modally the most abundant and under plane polarised light (PPL) light brown in colour. It is fine- to medium-grained (100-500 µm), xenoblastic and often displays an amoeboid shape, growing along the interface of clinopyroxene and plagioclase (Figure 3.2c and 4.3 (Section 4.1.3)).Such garnet often shows round, probably resorbed, inclusions of clinopyroxene and plagioclase, and occasionally titanite or apatite (Figure 3.2b).

Sample J44 is located on the boundary of the Bysteek Formation mafic granulites and Koenap Formation diatexites (see sample map, Figure 2.1). The melanosome in this specimen is variable in grain size, exhibiting a gradational relationship between a medium-grained (200-400µm) and a fine-grained (<100-200µm) domain. Both domains show a similar assemblage orthopyroxene (31 vol%) clinopyroxene (5.9 vol%) , plagioclase (26 vol%), magnetite (2.1 vol%), hornblende (29 vol%), biotite (3.7 vol%) and quartz (0.8 vol%) but the fine-grained domain contains less clinopyroxene, magnetite and quartz, but shows some biotite that is absent in the coarse-grained domain (Table 3.2).

Both fine-and-medium-grained domains from melanosome J44 show polygonal granular textures formed by orthopyroxene, clinopyroxene, hornblende and plagioclase with straight grain boundaries. Magnetite is generally xenoblastic, occurring as interstitial grains or as exsolution lamellae in orthopyroxene, clinopyroxene and hornblende (Figure 3.2 d-e). Quartz is also interstitial and displays irregularly shaped grain boundaries.

The presence of hornblende and biotite together with orthopyroxene and clinopyroxene (Figures 3.2d and e) may be attributed to retrograde metasomatism at the expense of orthopyroxene and plagioclase. The formation of biotite may be indicative of a metasomatic influx of hydrous potassium/sodic bearing fluids possibly released from the cooling leucocratic material of the Bysteek Formation or from granitoid magmas from the neighbouring Koenap Formation diatexites.

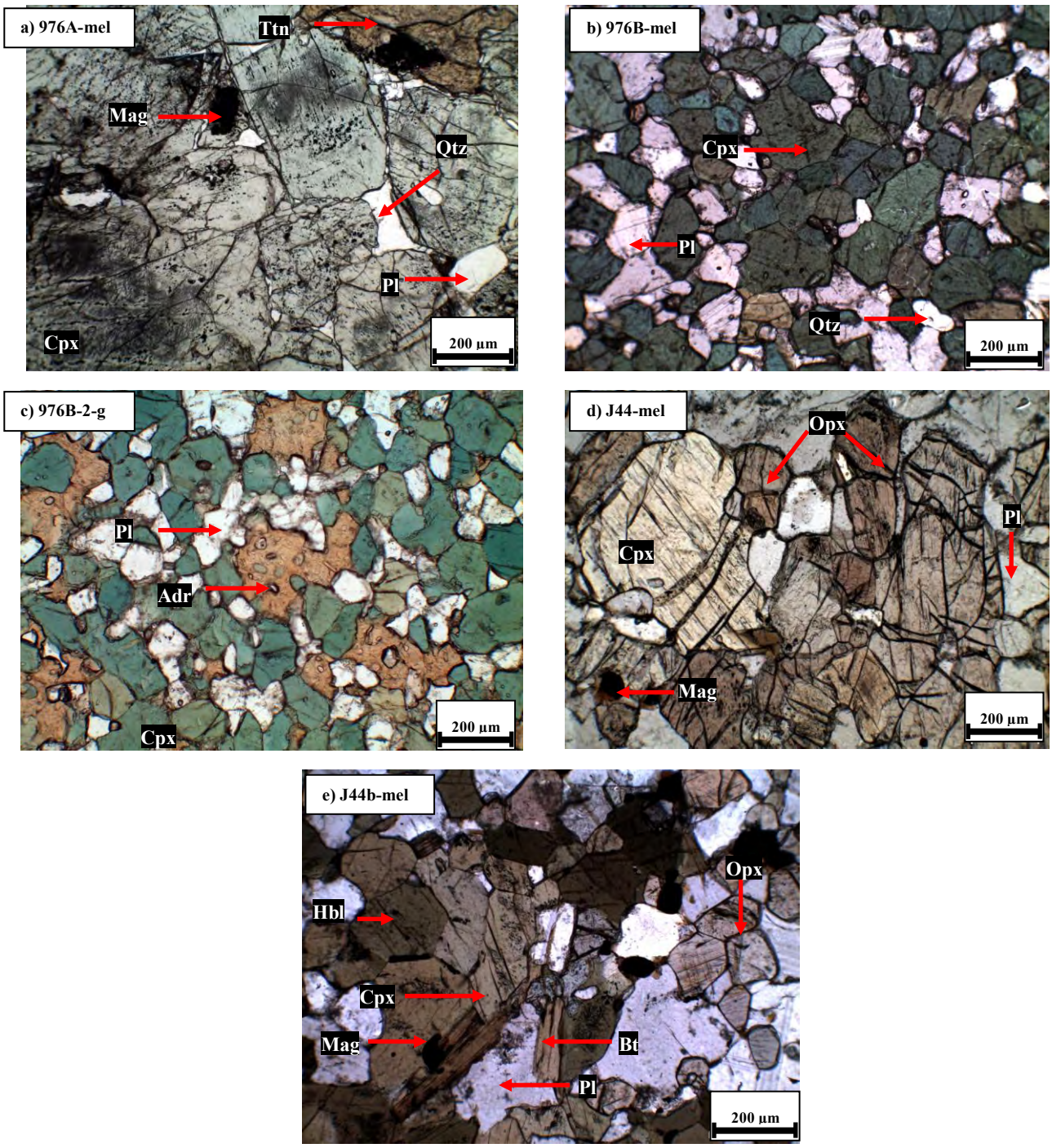

Figure 3.2. Photomicrograph from mafic granulite melanosome domains. All photos under PPL. (a) melanosome 976A-mel indicating idiomorphic clinopyroxene and plagioclase grains with interstitial quartz (Figure 2.2a; rectangle 1;domain 3). (b) Polygonal granular textures present within melanosome 976B-mel (Figure 2.2b; rectangle 3; domain 4). (c) Garnetiferous melanosome 976B-2-g displaying the amoeboid habit of andradite occupying interstitial spaces between clinopyroxene and plagioclase (Figure 2.2b;rectangle 2;domain 3). (d) Medium-grained (200-400µm) domain in melanosome J44-mel. The clinopyroxene grains are coarser in grain size (300-400µm) when in comparison to the neighbouring orthopyroxene grains (100-200µm). Amphibole and biotite are scarce in this domain. (e) Fine-to-medium-grained (80-150µm) domain of melanosome J44-b-mel. Hornblende shows polygonal habits with straight grain boundaries. Biotite often occurs along the grain boundaries of hornblende.

Table 3.2. Mineral modes in garnet free melanosome domains 976A-mel, 976B-mel, J44 and garnetiferous melanosome 976B-2-g.

Domain	**Melanosomes**							**Garnetiferous Melanosome**			
Sample	**976A-mel**		**976B-mel**				**J44**	**976B-2-g**			
Thin section	**976A1**	**976A4**	**976B2**			**976B3**	**J44**	**976B2**	**976B2**	**976B2**	**976B3**
Clinopyroxene	62.8	62.4	60.9	59.8	59.3	59.6	5.9	27.1	23.7	23.3	25.8
Quartz	6.2	4.2	5.3	4.6	5.8	4.3	0.8	3.8	7.9	5.4	3.7
K-Feldspar	-	-	-	-	-	-	-	-	-	-	-
Plagioclase	27.8	30.2	33.4	35.1	33.7	35.0	26.5	32.6	33.4	34.5	32.5
Garnet	-	-	-	-	-	-	-	35.4	33.4	34.5	35.6
Biotite	-	-	-	-	-	-	3.7	-	-	-	-
Opaques	3.1	2.9	-	-	-	-	2.1	-	-	-	-
Apatite	0.1	0.2	0.4	0.5	0.5	0.4	0.3	0.5	0.5	0.6	0.6
Titanite	0.1	0.2	-	-	0.7	0.7	0.8	0.7	1.1	1.8	1.8
Hornblende	-	-	-	-	-	-	28.8	-	-	-	-
Orthopyroxene	-	-	-	-	-	-	31.2	-	-	-	-
Total	100	100	100	100	100	100	100	100	100	100	100
Method	**Point counter**	**Point counter**	**Thin section grid**	**INCA area scan**	**Point counter**	**Point counter**	**Point counter**	**Thin section grid**	**INCA area scan**	**Point counter**	**Point counter**
Points counted	2047	4768	845	651	5981	6352	6749	782	681	5024	3257

3.1.3 Mafic fragments

The mafic fragments within the leucocratic networks (982E, 985A and 982C) are medium to coarse-grained (200-800µm) and largely homogenous in composition, largely comprised of clinopyroxene (85-92 vol%), magnetite (0.5-3 vol%) and titanite (0.5-1.6 vol%) (Table 3.3). Minor hornblende (1.5-2.6 vol%) occurs at the interface of clinopyroxene grains. Clinopyroxene is fine- to medium grained (200-400µm), statically recrystallised in foam structures showing straight grain boundaries, meeting at approximately 120° interface angles (Figure 3.3a). Coarse-grained (400-800µm) titanite is present within the groundmass of the mafic fragments. Plagioclase and occasionally quartz are present in interstitial spaces between clinopyroxene. The contacts of the mafic fragments and the neighbouring leucocratic pools or networks are typically sharp, with clear separation of the K-feldspar-quartz rich leucosome and the mafic domain of the fragments (Figure 3.3c).

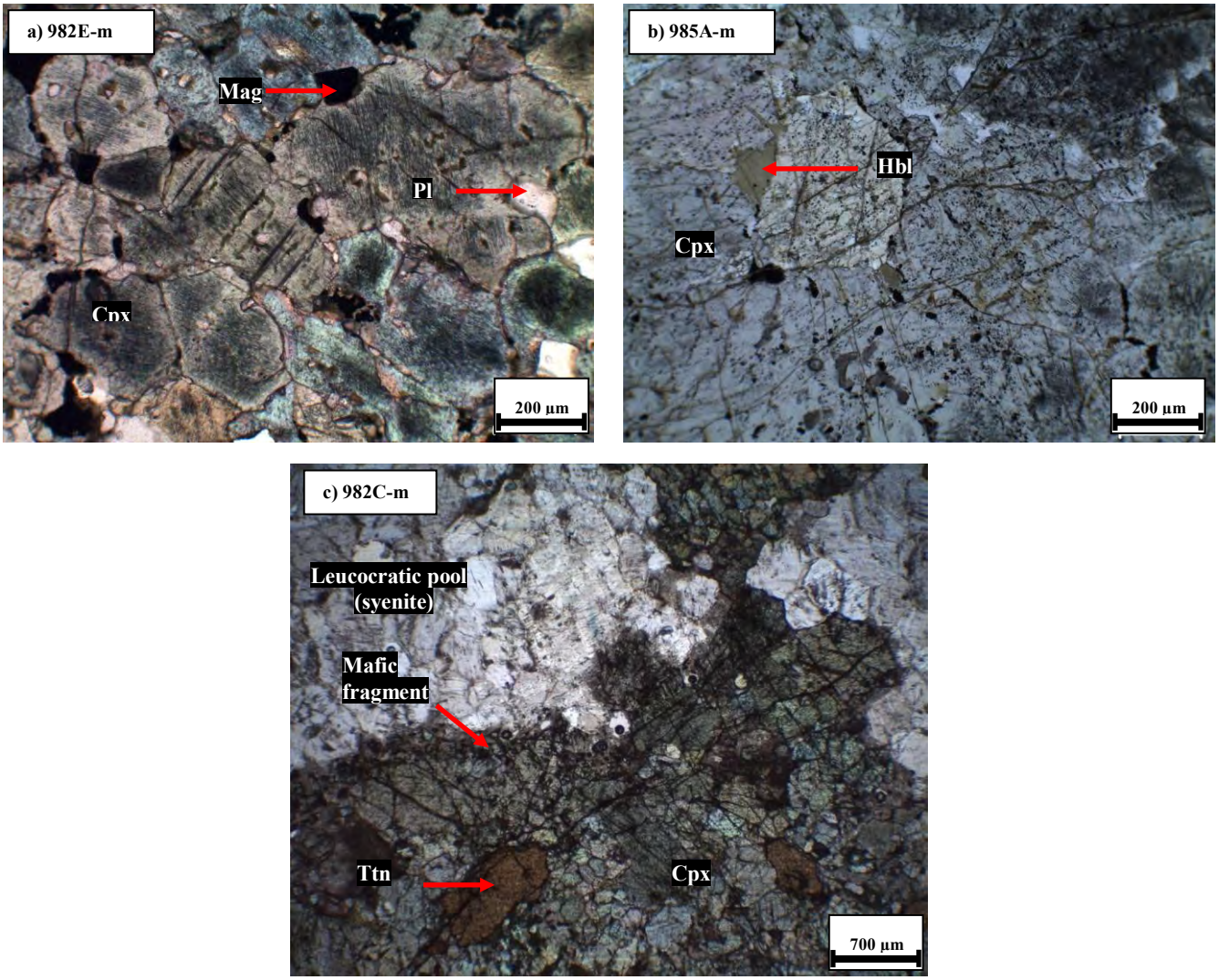

Figure 3.3. PPL photomicrographs of mafic fragments from mafic granulite leucocratic networks and pools. (a) Sample 982E (Figure 2.4; rectangle 6) covers a stretched mafic fragment from a diffuse leucocratic vein network. Clinopyroxene is statically recrystallised with straight grain boundaries

whereby magnetite occurs in interstitial spaces and as exsolution lamellae. (b) The mafic fragments from sample 985A (Figure 2.8; rectangle 10; domain 1) shows clinopyroxene grains exhibiting minor breakdown to hornblende. (c) The periphery between leucocratic pool and mafic fragment is typically sharp (sample 982C; Figure 2.9).

Table 3.3. Mineral modes of mafic fragments (982C-M, 985A-M and 982E-M) from leucocratic pools, networks and stromatitic vein domains.

Fragment location	**Pool**	**Leucocratic network**					**Stromatitic veins**	
Sample	**982C**	**985A**					**982E**	
Thin section	**982C1**	**985A2**	**985A5**	**985A7**	**985A8**	**985A10**	**982 E6**	**982 E5**
CPX	89.6	87.9	89.1	88.7	92.0	89.3	88.3	85.6
Quartz	0.8	-	1.4	0.9	1.6	-	5.1	3.2
K-Feldspar	-	-	-	-	-	-	-	-
Plagioclase	4.5	7.2	7.9	6.8	5.5	7.0	4.0	6.7
Garnet	-	-	-	-	-	-	-	-
Biotite	-	-	-	-	-	-	-	-
Opaques	2.3	1.1	1.7	1.4	0.9	2.0	2.6	3.1
Apatite	-	-	-	-	-	-	-	-
Titanite	-	1.5	-	0.5	-	1.6	-	-
Hornblende	2.8	2.3	-	1.6	-	-	-	1.5
Total	100	100	100	100	100	100	100	100
Method	**Point counter**	**Point counter**	**Point counter**	**Point counter**	**Point counter**	**Point counter**	**Point counter**	**Point counter**
Points counted	4606	4341	6074	6209	4117	3691	3154	1843

3.1.4 Leucocratic domains

The leucocratic domains present within the mafic granulite sequence have been classified as *in-situ* leucosomes, leucocratic veins, pockets, networks and pools (Section 2.1.3). On basis of normalised mineral modes the compositions of leucosomes from nine different samples and seven sample localities have been plotted in a Streckeisen diagram (Figure 3.4). The majority of leucosomes is K-feldspar-rich with variable amounts of quartz, plotting on the left-hand side of the diagram in the fields of alkali-feldspar and syeno-granite or in the syenite fields. Two samples show plagioclase-rich anorthositic leucosomes that plot in the gabbro field. However, the mafic components required for the classification as a gabbro are absent. A better classification might be ‘anorthosite’ for these rocks.

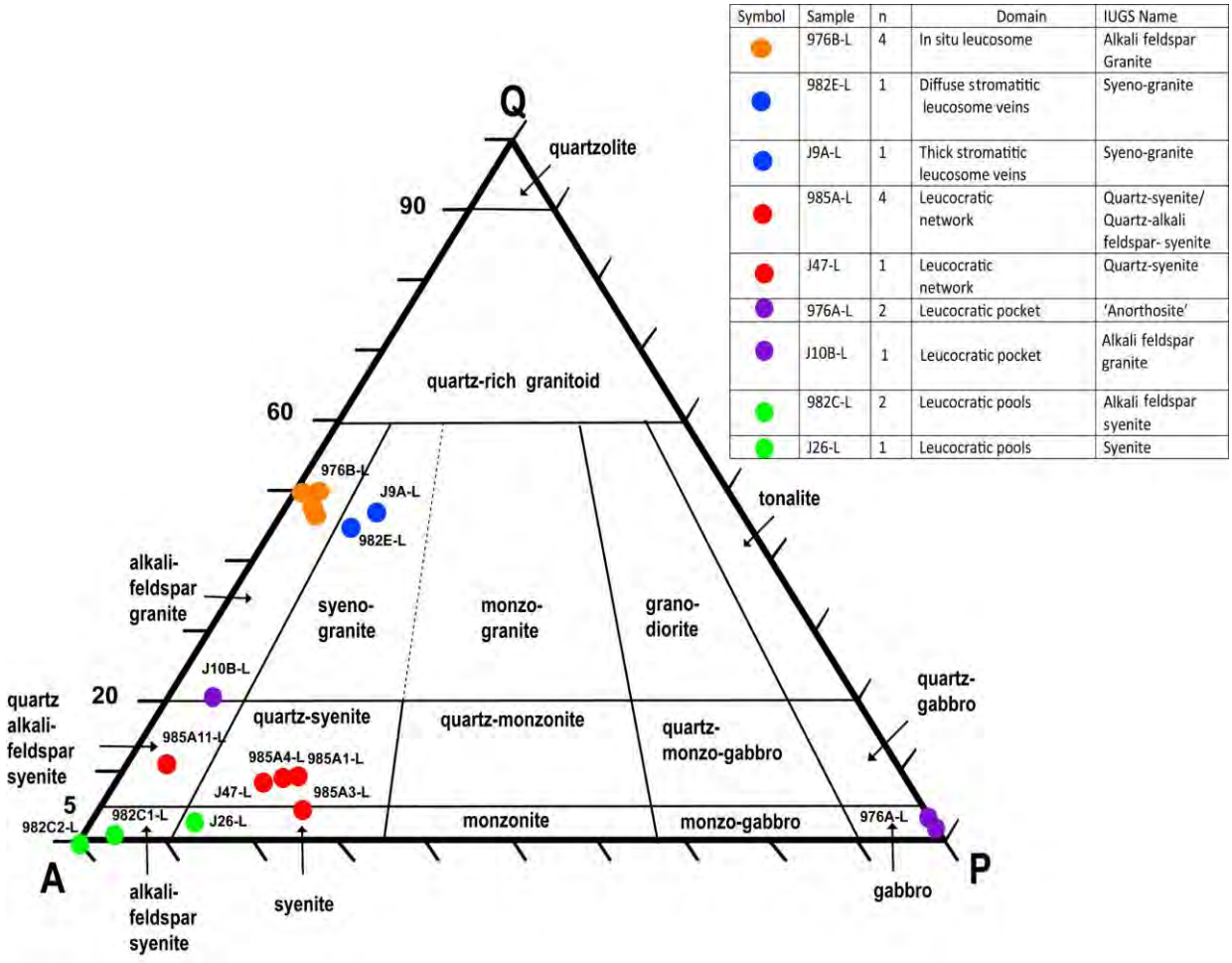

Symbol	Sample	n	Domain	IUGS Name
	976B-L	4	In situ leucosome	Alkali feldspar Granite
	982E-L	1	Diffuse stromatitic leucosome veins	Syeno-granite
	J9A-L	1	Thick stromatitic leucosome veins	Syeno-granite
	985A-L	4	Leucocratic network	Quartz-syenite/ Quartz-alkali feldspar- syenite
	J47-L	1	Leucocratic network	Quartz-syenite
	976A-L	2	Leucocratic pocket	'Anorthosite'
	J10B-L	1	Leucocratic pocket	Alkali feldspar granite
	982C-L	2	Leucocratic pools	Alkali feldspar syenite
	J26-L	1	Leucocratic pools	Syenite

Figure 3.4. QAP diagram (Streckeisen, 1976) for modal quantities from each analysed leucocratic domain. The green dots indicate leucocratic pools (alkali feldspar syenites, 982C-L and J26A-L), red dots are leucocratic networks (quartz alkali feldspar syenite;samples 985A-L and J47-L), blue dots are leucocratic veins (syeno-granites;samples 982E-L and J9A-L) and orange dots are *in-situ* leucosomes (alkali feldspar-granites; samples 976B-L). The purple dots are leucocratic pockets. Sample J10B-L plots on the periphery of alkali-feldspar granite and quartz alkali-feldspar syenite. Sample 976A-L plots in the gabbro field, yet the mafic phases required to classify it as a gabbro are absent. A more suitable classification for this leucosome pocket may be 'anorthosite'.

3.1.4.1 In-situ leucosomes and leucocratic veins

The mineral modes of *in-situ* leucosomes (sample 976B-L) show 39-43 vol% quartz, 40-42 vol% K-feldspar, 10-15 vol% scapolite and 2.2-3.0 vol% plagioclase, placing them in the quartz-rich part of alkali feldspar granite (Streckeisen; 1976; Figure 3.4). K-feldspar is medium-grained (100-300µm), tabular, with straight grain boundaries, suggesting that these are phenocrysts formed in the presence of melt (Vernon, 1986). The alkali feldspar grains are devoid of any perthitic textures (Figure 3.5b-c).Quartz is always anhedral and irregular in shape. Macroscopically the *in-situ* leucosomes often form rootless ptygmatic folds (Figure 2.2b, domain 1).

Scapolite is restricted to *in-situ* leucosome, and constitutes 10-15 vol% of the leucosome. Scapolite is colourless to pale-blue and medium-grained (200-250µm). It is randomly oriented in the leucosome groundmass as tabular to flaky sub-idiomorphic phenocrysts with straight grain boundaries (Figure 3.5b-c).

EDS analysis indicates that the scapolite is the meionite scapolite endmember (section 4.1.6, Table 4.7).

In-situ leucosomes are rimmed by thin marginal seams of homogenous Cpx-Pl-Qtz melanosomes (976B-mel, Figure 3.2b). The two domains show a diffuse and gradational transition. Detached clinopyroxene and plagioclase xenocrysts from the neighbouring melanosome may be present within the *in-situ* leucosome (Figure 3.5b).

Two specimens containing leucocratic veins (J9A-L and 982E-L) are part of the stromatitic mesosome mafic granulite domains (Figures 2.3c and 2.4). The veins are syeno-granitic in composition (Figure 3.4) comprised of 43-44 vol% quartz, 39-44 vol% K-feldspar and 8-9 vol% plagioclase (Table 3.4). The contact between the melanosome layers and leucocratic veins is relatively sharp. Quartz shows undulose extinction in old grains and foam textures, suggesting incomplete static recrystallisation (Figure 3.5d). Plagioclase and K-feldspar are fine- to medium-grained ranging from 200-300µm in size. They typically form subhedral phenocrysts occasionally with roundish quartz inclusions. Optical zonations are absent. K-feldspar does not show sodic exsolution lamellae. Plagioclase is medium-grained (200-300µm) and often neighbour clinopyroxene which has been altered along grain boundaries into secondary hornblende. The plagioclase adjacent the altered clinopyroxene is typically sausserized (Figure 3.5c).

Table 3.4. Mineral modes of *in-situ* leucosomes (976B-L), stromatitic veins (982E-L; J9A-L) and leucocratic networks (985A-L; J47-L).

Domain	**Rootless ptygmatic *in-situ* leucosomes**				**Leucocratic veins**		**Leucocratic networks**				
Sample	**976B-L**				**982E-L**	**J9A-L**	**J47-L**	**985A-L**			
Thin Section	**976B2-L**		**976B3-L**	**976B4-L**	**982 E7-L**	**J9A-L**	**J47-L1**	**985A1**	**985A4**	**985A3**	**985A11**
IUGS Name	**Alkali feldspar granite**				**Syeno-granite**		**Quartz syenite**			**Syenite**	**Quartz alkali feldspar syenite**
Quartz	42.9	42.8	39.7	40.7	43.8	44.8	8.6	9.3	9.1	4.7	11.2
Orthoclase	41.6	40.6	41.9	41.9	44.8	39.8	73.2	68.7	70.1	71.1	83.1
Microcline	-	-	-	-	-	-	-	-	-	-	-
Scapolite	10.0	14.4	15.4	14.8	-	-	-	-	-	-	-
Clinopyroxene	2.7	-	-	-	3.1	5.5	1.5	1.8	2.1	1.0	1.3
Plagioclase	2.3	2.2	3.1	2.6	8.3	10.0	16.6	20.2	18.7	23.3	4.3
Titanite	0.5	-	-	-	-	-	-	-	-	-	-
Hornblende	-	-	-	-	-	-	-	-	-	-	-
Magnetite	-	-	-	-	-	-	-	-	-	-	-
Total	100	100	100	100	100	100	100	100	100	100	100
Method	**Thin section grid**	**Thin section grid**	**Point counter**	**Thin section grid**	**Point counter**	**Point counter**	**Point counter**	**Thin section grid**	**Point counter**	**Point counter**	**Point counter**
Points counted	874	634	407	783	651	3471	512.00	379	926	866	752
Q	54.67	53.66	50.76	51.55	45.82	48.49	8.82	9.63	9.45	4.73	11.50
A	44.98	43.57	45.31	45.16	45.45	40.74	74.09	69.59	71.14	71.56	84.06
P	0.35	2.77	3.93	3.29	8.73	10.78	17.09	20.78	19.41	23.71	4.44

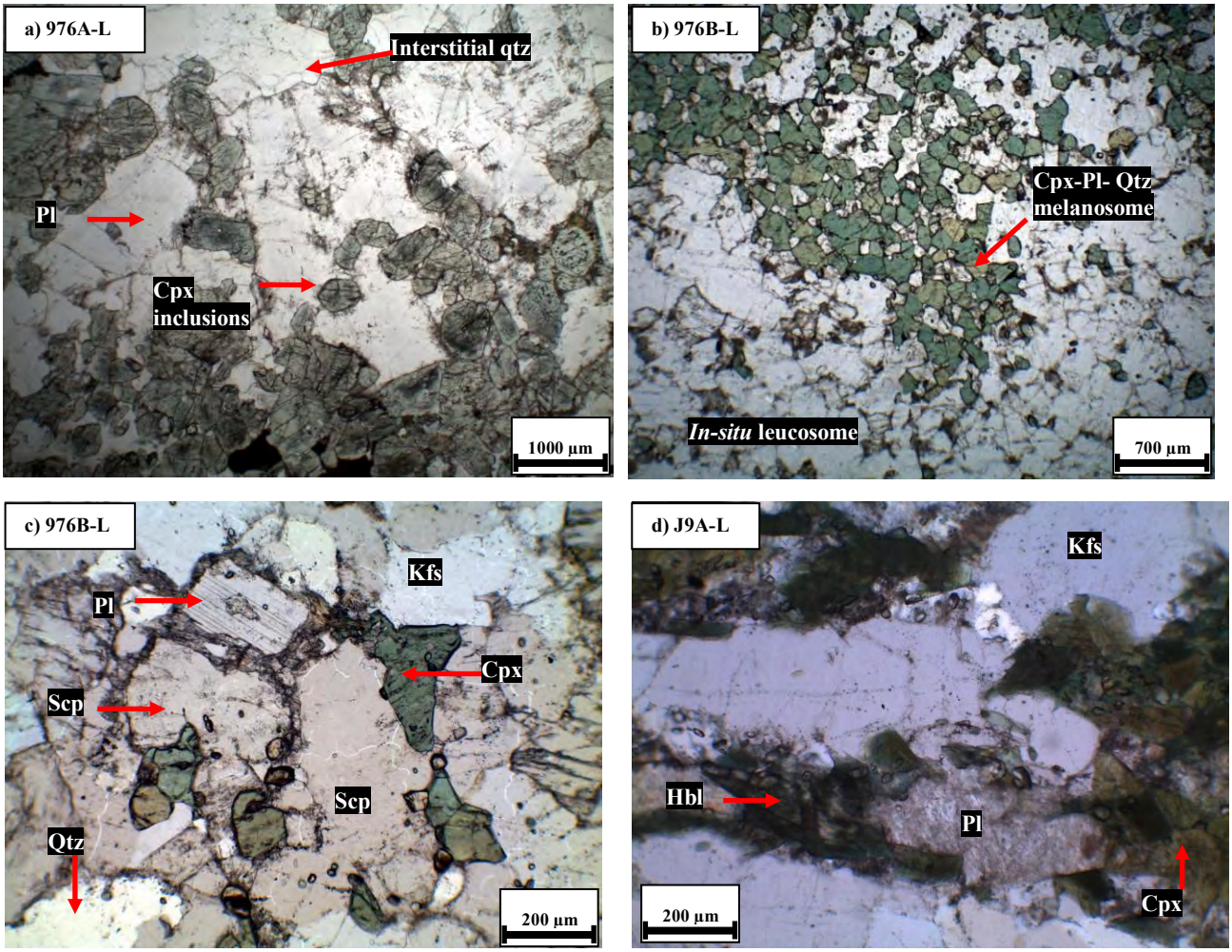

Figure 3.5. Photomicrographs of *in-situ* leucosomes and stromatitic veins. (a) The *in-situ* leucosomes of 976A (Figure 2.2a; rectangle 3) grade into leucocratic pockets. The leucosomes contain inclusions of clinopyroxene which show no preferred orientation. Plagioclase phenocrysts are medium- to- coarse-grained (500-1000µm) with straight grain boundaries. Quartz occurs as interstitial grains. (b-c: *In-situ* leucosomes of 976B-L; Figure 2.2b; rectangle 2). The neighbouring melanosome and leucosome show diffuse boundaries, whereby detached clinopyroxene xenocrysts occur in the leucosome groundmass. The groundmass displays recrystallised polygonal aggregates of quartz and to a lesser extent K-feldspar. Scapolite has no preferred orientation in the groundmass of the leucosome.(d)The stromatitic leucosome vein J9A-L (Figure 2.3b) display successive alternating veins of melanosome and leucosome that are frequently anastomosing. The quartz and K-feldspar grains display straight grain boundaries, whereas plagioclase grains are highly altered. Additionally, the clinopyroxene show strong breakdown into secondary hornblende aggregates.

3.1.4.2 Leucocratic pockets

Two leucocratic pockets were analysed. Sample 976A-L plots in the gabbro field of the Streckeisen diagram (Figure 3.4) but is not of gabbroic composition. It consists essentially of plagioclase (94-95 vol%) and with minor interstitial recrystallised quartz (2-3 vol%) (Table 3.5). A more suitable classification for this leucosome would be ‘anorthosite’. Plagioclase

forms coarse-grained euhedral phenocrysts (1000-2000µm sized), with fine polysynthetic twinning (Figure 3.6c). Grain boundaries are usually straight. Plagioclase shows minor saussuritisation. Occasionally near-spherical grains of quartz, alkali feldspar and clinopyroxene form inclusions in plagioclase (Figure 3.5a).

Sample J10B-L, sampled at a location nearby 976B and 976A (Figure 2.1), has alkali feldspar granite to quartz alkali feldspar syenite composition, plotting near the boundary of these two fields in the Streckeisen diagram (Figure 3.4). It modally consists of microcline 60 vol%, quartz (17 vol%), plagioclase (4 vol%) with mafic phases of clinopyroxene (9 vol%), and titanite (9 vol%) (Table 3.5). Based on textural similarity the mafic phases most likely are xenocrysts from the neighbouring mafic domains that have been incorporated into the leucocratic domains. K-feldspar is coarse-grained (~1000µm), have sutured grain boundaries and show interlocking to replacement perthitic exsolution (Figure 3.6a-b).

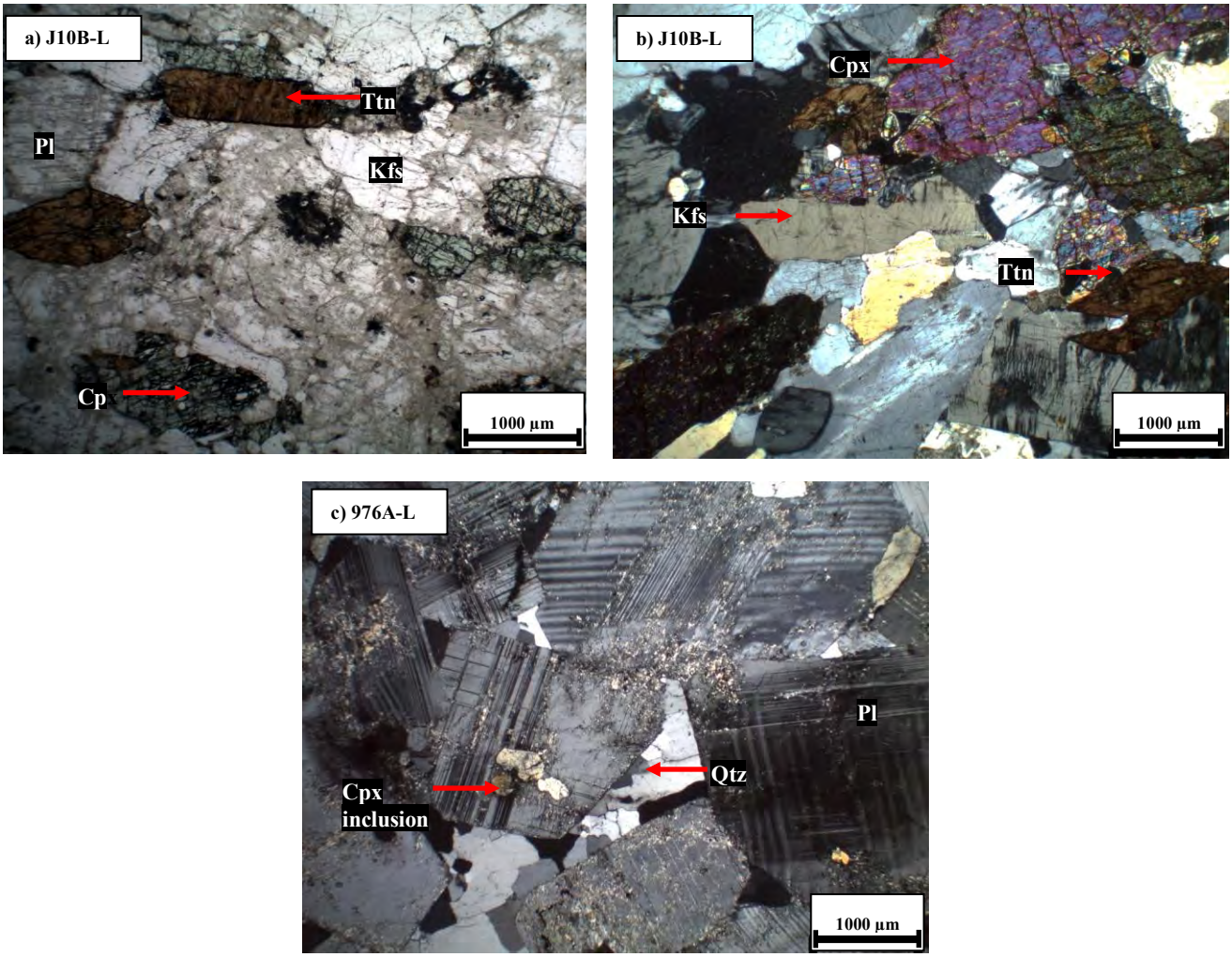

Figure 3.6. Photomicrographs from leucocratic pockets. (a-b: Sample J10B-L,Figure 2.6b) The isolated leucocratic pocket of J10B-L is stromatitic whereby all phases (mafic and leucocratic) are aligned partly parallel to one another (PPL and XPL). K-feldspar is coarse-grained (>1000µm) with sharp grain boundaries and meso-perthitic textures. (c) The leucocratic pocket of 976A-L (Figure 2.2b; rectangle 4).

indicate magmatic textures whereby plagioclase phenocrysts are coarse-grained (20 μm), show straight grain boundaries and display fine polysynthetic twinning. Additionally the interstitial spaces contain fine grained masses of recrystallised quartz. Clinopyroxene inclusions are present within the plagioclase phenocrysts.

Table 3.5. Mineral modes of leucocratic pockets (976A-L; J10B-L) and pools (982C; J26).

Domain	**Leucosome pockets**			**Leucocratic pools**		
IUGS Name	**'Anorthosite'**		**Alkali feldspar granite**	**Alkali feldspar syenite**		**Syenite**
Sample	**976A-L**		**J10B-L**	**982C-L**		**J26-L**
Thin section	**976A3-L**	**976A4-L**	**J10B2**	**982C1**	**982C2**	**J26-L1**
Quartz	3.1	2.0	17.3	1.2	0.8	3.0
Orthoclase	0.6	0.5	-	-	-	4.5
Microcline	-	-	60.3	78.1	81.9	84.5
Scapolite	-	-	-	-	-	-
Clinopyroxene	0.7	0.9	9.1	13.6	11.9	3.3
Plagioclase	95.6	96.6	4.0	2.5	3.1	4.7
Titanite	-	-	9.4	1.7	0.5	-
Hornblende	-	-	-	2.9	1.8	-
Magnetite	-	-	-	-	-	-
Total	100	100	100	100	100	100
Method	**Thin section grid**	**Point counter**	**Point counter**	**Point counter**	**Point counter**	**Point counter**
Points counted	918	545	2013	5846	6683	6265
Q	3.12	2.01	21.22	1.40	0.88	3.05
A	0.00	0.00	73.91	95.50	95.50	84.73
P	96.88	97.99	4.87	3.10	3.62	12.21

3.1.4.3 Leucocratic networks and pools

The leucocratic networks (samples 985A and J47; Figures 2.8 and 2.13) have quartz syenitic composition consisting of coarse-grained (500-2000μm) perthitic alkali feldspar grains (69-83 vol%), variable plagioclase (4-23 vol%) and quartz (4-11 vol%). Alkali feldspar phenocrysts exhibit magmatic textures, generally subhedral with straight to serrated grain boundaries. They also display string-perthitic textures (Figures 3.7a-b; samples J47-L and 985A-L). Quartz is present in the interstices between plagioclase and K-feldspar, is medium-grained (~500μm) and irregular in shape. Plagioclase is also coarse-grained (700-1000μm), tabular and shows distinct lamellar polysynthetic twinning (Figure 3.7b; sample 985A-L).

Two leucocratic pools (982C-L and J26A-L; Table 3.5) are homogenously comprised of K-feldspar (78-82 vol%) and accordingly plot in the syenite field (Figure 3.4) of the Streckeisen diagram (Figure 3.4). The majority of K-feldspar occurs as microcline with minor orthoclase

(4.4 vol%) displaying mesoperthitic textures. The grains are generally subhedral in shape, tabular in habit and medium grained (400-700µm). Detached medium-grained (400µm) clinopyroxene grains are present in the groundmass of the syenitic pools. Minor interstitial quartz is also present (1-2 vol%) (Table 3.5; Figure 3.7c; sample 982C-L).

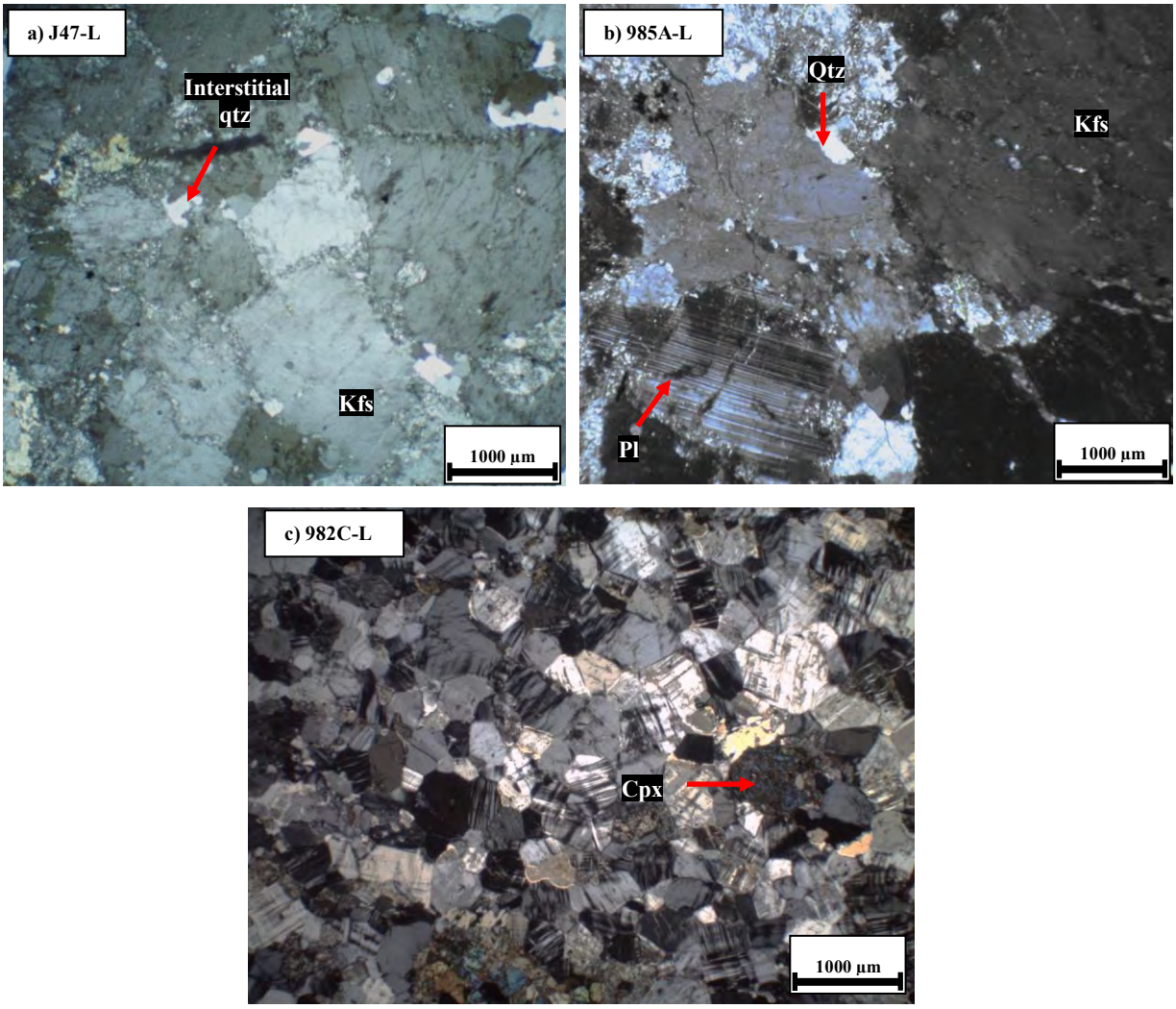

Figure 3.7. Photomicrographs of leucocratic networks (a) J47B-L (Figure 2.9; domain 1; rectangle 1) and (b) 985A-L (Figure 2.7a; rectangle 11). Both domains exhibit coarse-grained (>1000µm) meso-perthitic orthoclase phenocrysts with minor quartz and plagioclase. Plagioclase is also coarse-grained (>1000µm) and shows polysynthetic twinning. (c) Leucocratic pool 982C-L (Figure 2.6c) is essentially comprised of medium-grained (400-600µm) microcline with some clinopyroxene xenocrysts.

3.2 Calc-silicates and related marble domains

Calc-silicate rocks and marbles have not been used for thermodynamic modelling and are here only briefly described. Three lithological varieties have been analysed: (i) homogenous marble with minor calc-silicate phases (sample J1A, Figure 2.11a); (ii) grossularite-rich domains with cross-cutting leucocratic networks and mafic domains (sample J47B, Figure 2.13 domain 3); (iii) scapolite-rich domains located at the periphery of leucocratic networks and grossularite and mafic fragments (Figure 2.8; domain 3).

The homogenous marble mainly consists of coarse-grained (>2000µm sized) calcite but contains some grossularite, scapolite, talc and zoisite (Figure 3.8a). Grossularite is sub-idiomorphic and occurs in isolated grains in the calcite groundmass, is fine-grained (<100-150µm) and rarely containing calcite inclusions. Zoisite occurs as sub-idiomorphic medium-grained pink-greenish pleochroic grains of about 200-300µm in size. Talc is coarse-grained and randomly oriented. Occasionally minor bending of the crystals causes undulose extinction (Figure 3.7b).

The grossularite-rich domains within leucocratic networks crosscutting the calc-silicate bands (sample J47, Figure 3.8c) contain medium-grained (200µm) xenoblastic amoeboid grossularite aggregates associated with some quartz and calcite. These domains do not contain zoisite or talc.

The boundary between grossularite domains and the leucocratic networks are not always sharp. Along the contacts transitional zones consisting of aggregates of medium-grained scapolite are often present (Figure 3.8d). Mesoscopically these zones are white, fine-grained, and may show minor clinopyroxene (Figure 2.8a). In thin section, the scapolite is colourless, shows straight grain boundaries, and is randomly oriented. Close to the interface, and restricted to such positions, plagioclase in the leucocratic networks is highly saussuritised, suggesting stronger fluid-assisted alteration than elsewhere in the leucosome.

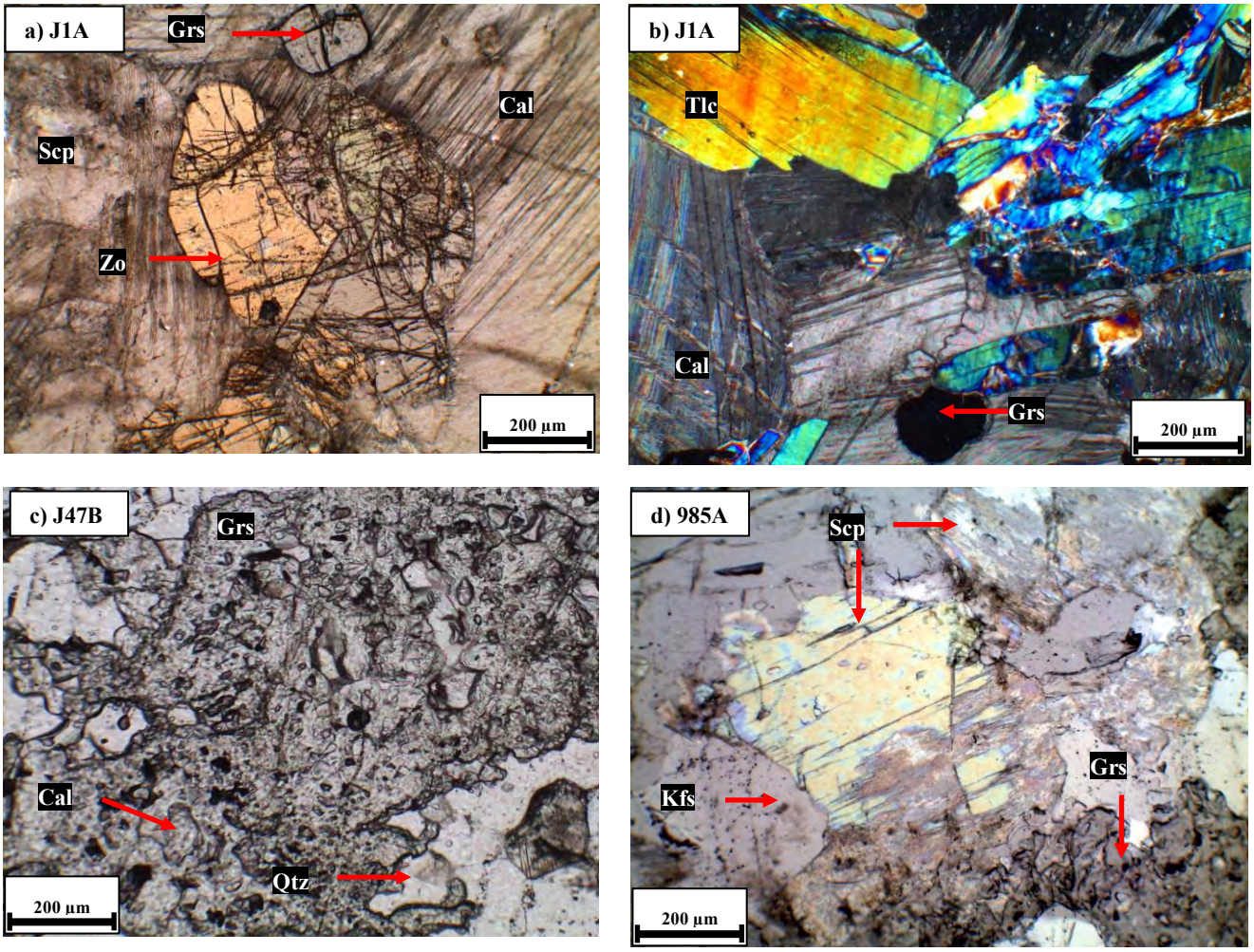

Figure 3.8. Photomicrographs from calc-silicate domains. (a-b: PPL images from calc-silicate marble J1A; Figure 2.11a). Grossularite, scapolite, and zoisite occur within coarse-grained granoblastic calcite groundmass. Talc occurs as fine- to medium-grained (200µm) subhedral clusters with no preferred orientation (c:PPL image of grossularite fragment from sample J47B-2; Figure 2.13; rectangle 2). The grossularite is fine-grained (<100µm), xenoblastic with irregular shaped grain boundaries. Fine-grained (<50µm) xenoblastic calcite and quartz inclusions occur within the grossularite fragment. (d) PPL image of the transitional contact between scapolite domains and grossularite fragments (Figure 2.8a; rectangle 13). Scapolite is medium-grained (200µm), with little alteration. It displays sharp grain boundaries to the adjacent grossularite fragment and alkali feldspar grains. The alkali feldspar grains are part of the neighbouring leucocratic network (985A-L).

3.3 Koenap Formation diatexite domains and mafic lenses

Petrographic observations were analyzed on leucocratic (section 2.3.1), banded (2.3.2), nebulitic (section 2.3.3) and melanocratic diatexite domains in addition to its associated mafic lenses (section 2.3.4).

3.3.1 Leucocratic diatexites

The leucocratic domains within the Koenap Formation diatexites are characterised by a homogenous distribution of quartz, alkali feldspar, plagioclase with minor biotite, garnet and cordierite. In samples 983D, J36L, and J39A (Figure 2.14a-d). The mineral modes of massive, and banded leucocratic diatexite are variable: quartz 42-49 vol%; alkali feldspar (35-38 vol%); plagioclase (6-13 vol%); and biotite (1.5-4 vol%) (Table 3.6). Garnet, sillimanite and pinite are minor phases that each occur less than 1-2 vol% of leucocratic diatexites.

Alkali feldspar is meso-perthitic, coarse-grained in the range of 300-1000µm, and subhedral in shape. Quartz occurs as medium-grained (100-300µm) interstitial grains in between meso-perthitic alkali feldspar and plagioclase with sharp to sometimes curved grain boundaries (Figure 3.9a-b). The plagioclase phenocrysts are fine-to-medium-grained (100-300µm), subhedral in shape, tabular in habit and display well-defined pericline and albite twins (Figure 3.9b) and intermittently occur as inclusions within alkali feldspar grains (Figure 3.9a). The massive leucocratic diatexites are almost garnet free (<1 vol% garnet) and contain fine-grained aggregates of inclusion free pinitised cordierite (Figure 3.9a).

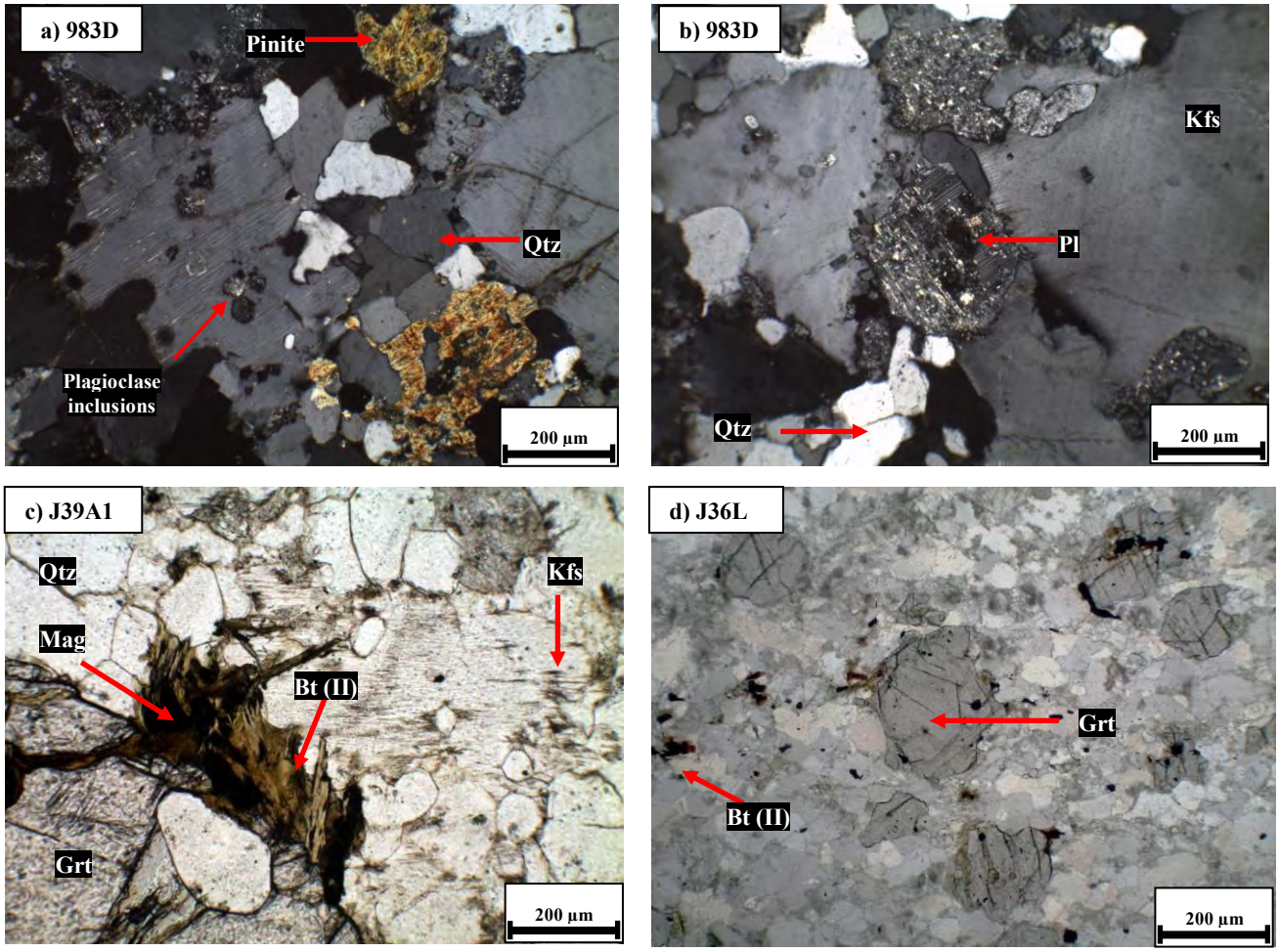

Figure 3.9. Photomicrographs from leucocratic diatexite domains. (a-b: Massive leucocratic diatexite 983D; section 2.3.1). The alkali feldspars show rod perthitic textures. Plagioclase inclusions occur within the alkali feldspar grains. Interstitial quartz grains are present between plagioclase and alkali feldspar showing sharp to sometimes curved grain boundaries. Pinitised cordierite is also present. Plagioclase grains exhibit pericline and albite twins. (c: Leucocratic domains from diffusely banded diatexite J39A (Figure 2.14a-b). The alkali feldspars shows rod perthitic textures that are similarly seen in sample 983D. The grain boundaries of the garnet grain shows breakdown into secondary biotite (Bt II; see section 3.3.2). (d: Diffusely banded leucocratic diatexite domain J36L;Figure 2.14). Entrained garnets constitute less than 1 vol% of the leucocratic diatexite domains. They are fine-grained (<100-200µm) and show little alteration along grain boundaries. Few secondary biotite grains are present in the Qtz-Kfs-Pl groundmass.

Table 3.6. Mineral modes in leucocratic domains 983D (massive), J36L (banded) and J39A (diffuse).

Diatexite domain	Massive leucocratic domain		Banded leucocratic domain		Diffuse leucocratic domain	
Sample	**983D**		**J36**		**J39**	
Thin section	**983D1**		**J36L-1**		**J39-A1**	**J39-A2**
Quartz	47.7	48.1	45.1	43.9	42.7	43.5
K-feldspar	36.8	38.9	37.5	35.3	38.9	36.6
Plagioclase	9.4	8.3	6.8	6.8	12.8	13.6
Garnet	0.8	0.2	-	-	-	0.8
Cordierite	-	-	-	-	0.9	1.1
Pinite	1.7	-	1.5	2.4	1.5	1.6
Biotite	1.5	1.5	4.0	3.6	1.3	1.8
Magnetite	1.1	1.5	1.2	1.5	1.4	0.7
Sillimanite	0.8	0.9	2.7	4.8	1.1	-
Rutile	0.1	0.6	0.4	0.7	-	-
Apatite	-	-	-	-	-	-
Titanite	-	-	-	-	-	-
Orthopyroxene	-	-	-	-	-	-
Zircon	-	-	0.1	0.2	0.2	0.3
Chlorite	-	-	0.7	0.9	-	-
Total	100	100	100	100	100	100
Method	**Point counter**	**Thin section grid**	**Point counter**	**Thin section grid**	**Point counter**	**Point counter**
Points counted	7594	950	3842	950	2076	2213

3.3.2 Melanocratic domains

The melanocratic diatexite domains in field appearance and hand-specimen show dark black restitic domains. Petrographic analysis on melanocratic diatexite domains include poorly banded coarse-grained anastomosing diatexite (sample J20B-Figure 2.15), moderately banded restitic domains (sample J33-Figure 2.16a; rectangle 2), well-foliated stromatitic melanocratic layers (sample J36M; Figure 2.14d), and melanocratic patches (sample J39-Figure 2.14b). These melanocratic domains in general, are formed by the mineral assemblage garnet-cordierite-biotite-sillimanite-magnetite-quartz.

The restitic domains in the melanocratic diatexites exhibit coarse-grained decussate aggregates of biotite, often overgrowing garnet. The grains are subhedral, coarse (200-500µm), pleochroic (light to dark brown), and often surround magnetite grains (Figure 3.10a). Isolated leucocratic domains are scarce in the melanocratic diatexites. Modal proportions (Table 3.7) indicate phase values of garnet (11-16 vol%), cordierite (4-4.8 vol%), quartz (15-18 vol%), biotite (21-23 vol%), alkali feldspar (7.5-8.6 vol%), and magnetite (4.8-6.9 vol%).

Thin section J33A covers a disrupted restitic layer in a banded diatexite neosome (sample J33-Figure 2.16a; rectangle 2).The domain displays pinitised cordierite that formed along garnet rims and is overgrown by biotite which might be a secondary breakdown product after cordierite. The secondary biotite (Bt II) forms fine-grained (<100µm), dark brown aggregates that are limited to the boundary of garnet and altered cordierite. This differs from the decussate aggregates of biotite (Bt I, Figure 3.10a) that occur as medium- to coarse-grained flaky aggregates (>200µm) within the groundmass.

Pinite along garnet rims contains inclusions of magnetite and secondary sillimanite which may also be a breakdown product of cordierite. This is attributed to the presence of oriented fibrolite occurring solely within pinitised domains and its distinct absence it the leucocratic diatexite domains (Figure 3.10b).

Garnet forms massive xenomorphic amoeboid clusters (300-1500µm) with resorbed grain boundaries that are replaced by pinite and biotite II. Fibrolitic sillimanite and spherical quartz inclusions are common in garnet cores.

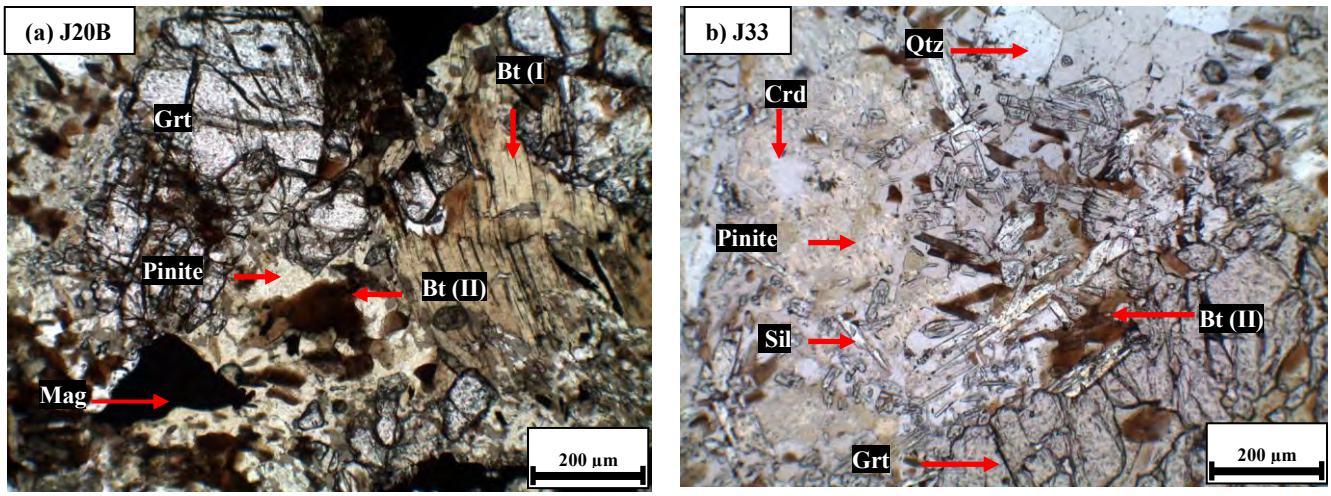

Figure 3.10. Photomicrographs from melanocratic diatexite domains from samples J20B (a) and J33A (b). The decussate biotite (Bt I; X_{Mg}=0.47; section 4.2.4; Table 4.10) occurs as medium-grained (>200µm) clusters. Along the grain boundaries of garnet and cordierite. A secondary biotite (Bt II; X_{Mg}=0.61; section 4.2.4; Table 4.10) forms fine-grained (<100µm) dark brown aggregates. The biotite forms in two preferred orientations that can be interpreted as parallel to cleavage planes in the former cordierite. The cordierite is generally xenoblastic, highly pinitised with little fresh relicts preserved in its core. The sillimanite and magnetite may be primary inclusions in the cordierite/pinite.

Table 3.7. Mineral modes of mafic lenses (983E; A106A) and melanocratic diatexite domains (J33, J36M and J39M).

Diatexite domain	**Mafic fragments**		**Melanocratic domains**			
Sample	**983E**	**A106**	**J33**		**J36**	**J39**
Thin section	**983E-M**	**A106A**	**J33**		**J36M**	**J39M**
Quartz	0.6	0.7	15.2	15.7	16.2	18.2
K-feldspar	-	-	7.6	8.4	8.6	8.2
Plagioclase	38.5	35.1	3.0	4.2	4.3	4.5
Garnet	-	-	16.6	15.5	11.7	13.9
Cordierite	-	-	4.0	4.7	4.9	4.5
Pinite	-	-	14.2	13.6	14.0	15.0
Biotite	2.3	1.5	22.3	20.6	23.6	21.5
Magnetite	3.7	4.8	6.1	6.9	5.1	4.8
Sillimanite	-	-	10.3	9.5	10.7	8.3
Rutile	-	-	0.4	1.1	0.9	0.9
Apatite	0.2	0.2	0.1	-	-	-
Titanite	-	-	0.2	-	-	-
Orthopyroxene	54.7	58.5	-	-	-	-
Zircon	-	-	0.1	-	-	0.2
Total	100	100	100	100	100	100
Method	**Point counter**	**Point counter**	**Point counter**	**Thin section grid**	**Point counter**	**Point counter**
Points counted	2093	2374	2153	950	3492	1921

3.3.3 Mafic lenses in diatexite domains

The mafic lenses present in the diatexites are homogenously comprised of orthopyroxene (54-58 vol%) and plagioclase (35-38 vol%) with minor magnetite (3.5 vol%) and biotite (2.2 vol%) (Table 3.9).Plagioclase and orthopyroxene show straight grain boundaries with faces in direct contact with each other. Orthopyroxene shows minor alteration whereby breakdown into secondary biotite occurs along its rims (Figure 3.11a).

The boundary between mafic lens and neighbouring diatexite is sharp, with little signs of reaction between entrained diatexite garnets and orthopyroxene grains. The garnet along the contact display xenoblastic habits and irregular shapes, whereby the garnets are in direct contact with orthopyroxene grains (Figures 2.18c; 3.11b). Conversely, the entrained garnet of the nebulitic diatexites are subhedral and are located in a K-feldspar-quartz-biotite groundmass that is free of orthopyroxene and plagioclase xenocrysts (Figure 3.11c).

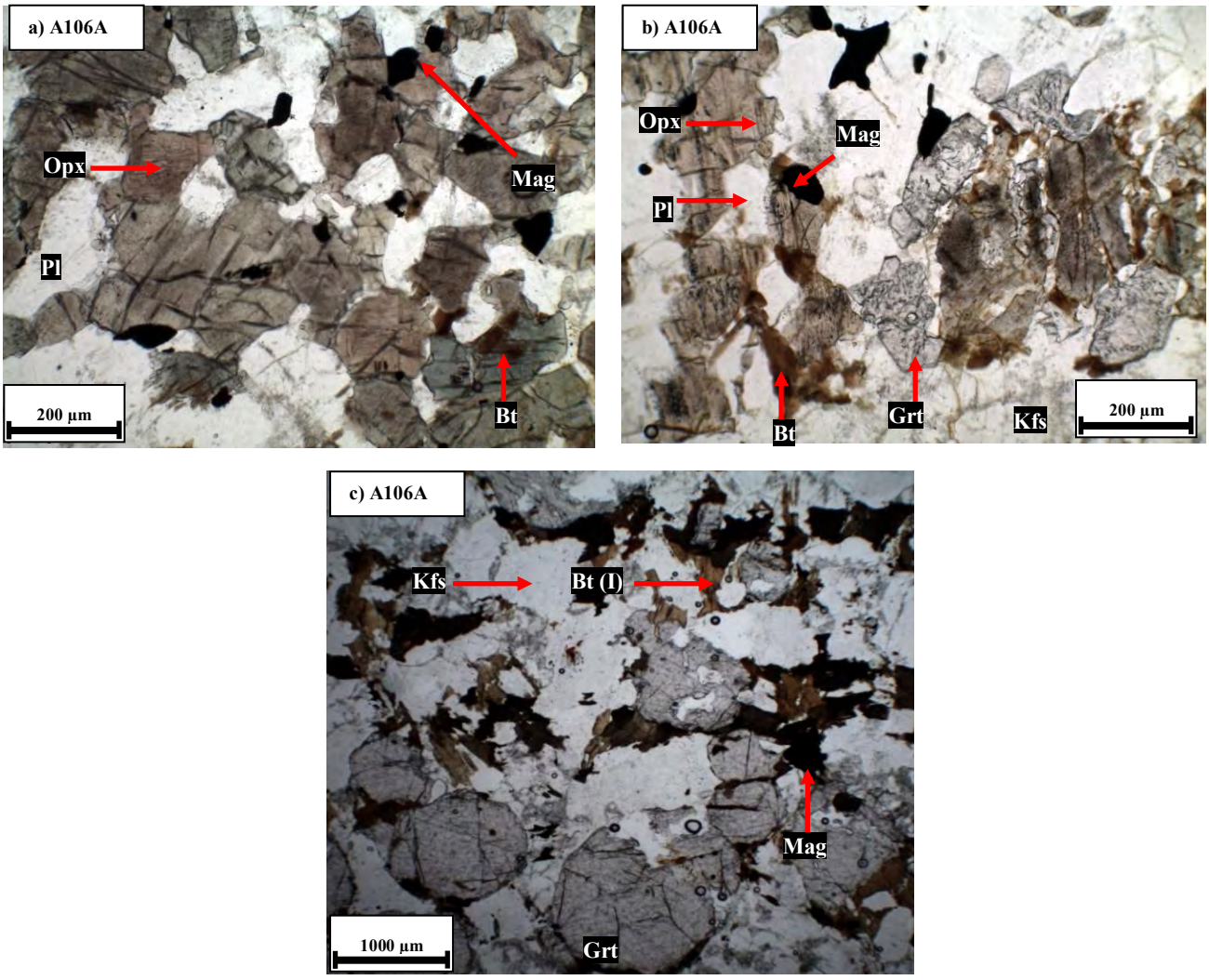

Figure 3.11. Photomicrographs of the mafic lenses in nebulitic diatexite A106A (Figure 2.18c-rectangle 1). All images taken under PPL (a) Micrograph taken from the groundmass of the mafic lens away from the contact of the nebulitic diatexite. Orthopyroxene and plagioclase is fine-to-medium grained (100-

200μm) and subhedral in shape with straight grain boundaries. The grain boundaries of the orthopyroxene show fine-grained (<100μm) aggregates of dark-brown biotite. This suggests it is a secondary breakdown product of the orthopyroxene. No xenocrysts of garnet, quartz, alkali feldspar or biotite from neighbouring diatexite domains are present. (b) Micrograph taken at the contact between mafic lens and diatexite shows all phases being relatively anhedral. The contact is sharp with little reaction between diatexite phases (garnet and alkali feldspar) and mafic lens phases (orthopyroxene and plagioclase). (c) Micrograph taken of the nebulitic diatexite away from the contact of the mafic lens. No orthopyroxene or plagioclase xenocrysts are present in the diatexite domain.

3.3.4 Banded diatexite

The banded diatexite is mesoscopically characterised by its weakly developed, diffuse anastomosing layering (section 2.3.1; Figures 2.15a-b; 2.16). Garnet is more abundant and coarser-grained (13-26 vol%) in the banded diatexites compared to the leucocratic diatexites (<1 vol%). It occurs in two forms, either in individual isolated inclusion-free subhedral crystals or amoeboid clusters. Individual garnet ranges in grain size from 400 mm to 1200 μm (Figure 3.12a-b). The amoeboid garnets are poikiloblastic hosting quartz, K-feldspar and fibrolite inclusions. Other garnet shows rounded or irregular boundaries, with breakdown products of pinitised cordierite and secondary biotite (Bt II) (Figure 3.12a; sample 983A).The amoeboid growth led to abundant inclusions of polygonal quartz aggregates or individual round quartz, some magnetite, and abundant sillimanite in the garnet cores (Figure 3.12c).

Cordierite occurs as aggregates within the groundmass or as xenoblastic grains along garnet margins. The cordierite in sample 983A is pinitised with no fresh relics (Figure 3.10a). Magnetite and sillimanite may be primary inclusions in cordierite/pinite but biotite forms in two preferred orientations that can be interpreted as parallel to cleavage planes in the former cordierite. This suggests that this biotite is a retrograde breakdown product (Figure 3.13c).

For similar reasons noted above and in the melanocratic domains (Section 3.3.2), the dark brown biotite forming along fractures of garnet and along garnet grain boundaries is interpreted as secondary retrograde breakdown reaction product. Such biotite ranges in size from 100-200μm (Figure 3.13a-b). Minor small biotite occurs as individual grains with random orientation in the Kfs-Qtz-rich leucosome groundmass (Figure 3.9d).

The leucosome groundmass is defined by quartz and alkali feldspar. Quartz occurs as medium- to coarse subhedral grains (100-500μm) that in monomineralic patches shows straight grain boundaries resembling foam textures. However, the lack of large and deformed old grains that

would grade into subgrains and foam textures, or any other evidence of recrystallisation, leaves open the possibility that these are in fact annealed primary grains of the leucosome. Alkali feldspar is perthitic and sporadically distributed within the quartz groundmass (Sample J39A2; Figure 2.14a-b). The grain size ranges from 100-400µm (Figures 3.9c and 3.12b).

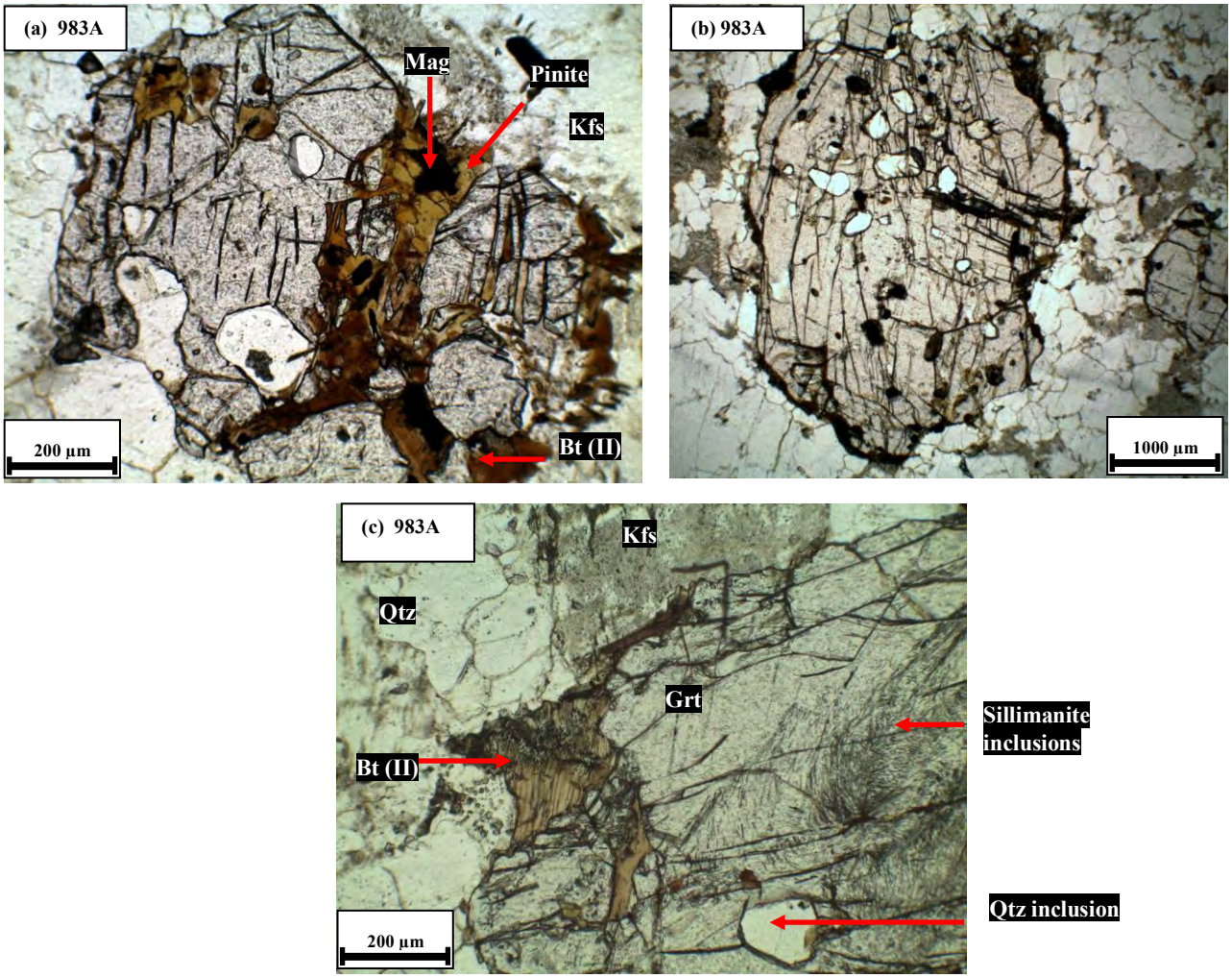

Figure 3.12. (a-b-c) Photomicrographs from poorly banded diatexite domain 983A (Figure 2.14c; section 3.3.4). The garnet clusters commonly show pinitised cordierite (yellow) in between neighbouring garnet grains. The yellow pinitised domains also contain magnetite. Fibrolitic sillimanite along with rounded quartz and alkali feldspar inclusions are also present within garnet. Such inclusions can be interpreted as part of the pre-anatectic or early anatectic mineral assemblage. Dark brown fine-grained (<100µm) biotite aggregates (Bt II) are common along the garnet grain boundaries and fractures. These textures are similarly seen in the melanocratic diatexite domains but not as extensive. These biotite grains may be interpreted as a secondary retrograde breakdown reaction product from garnet and cordierite.

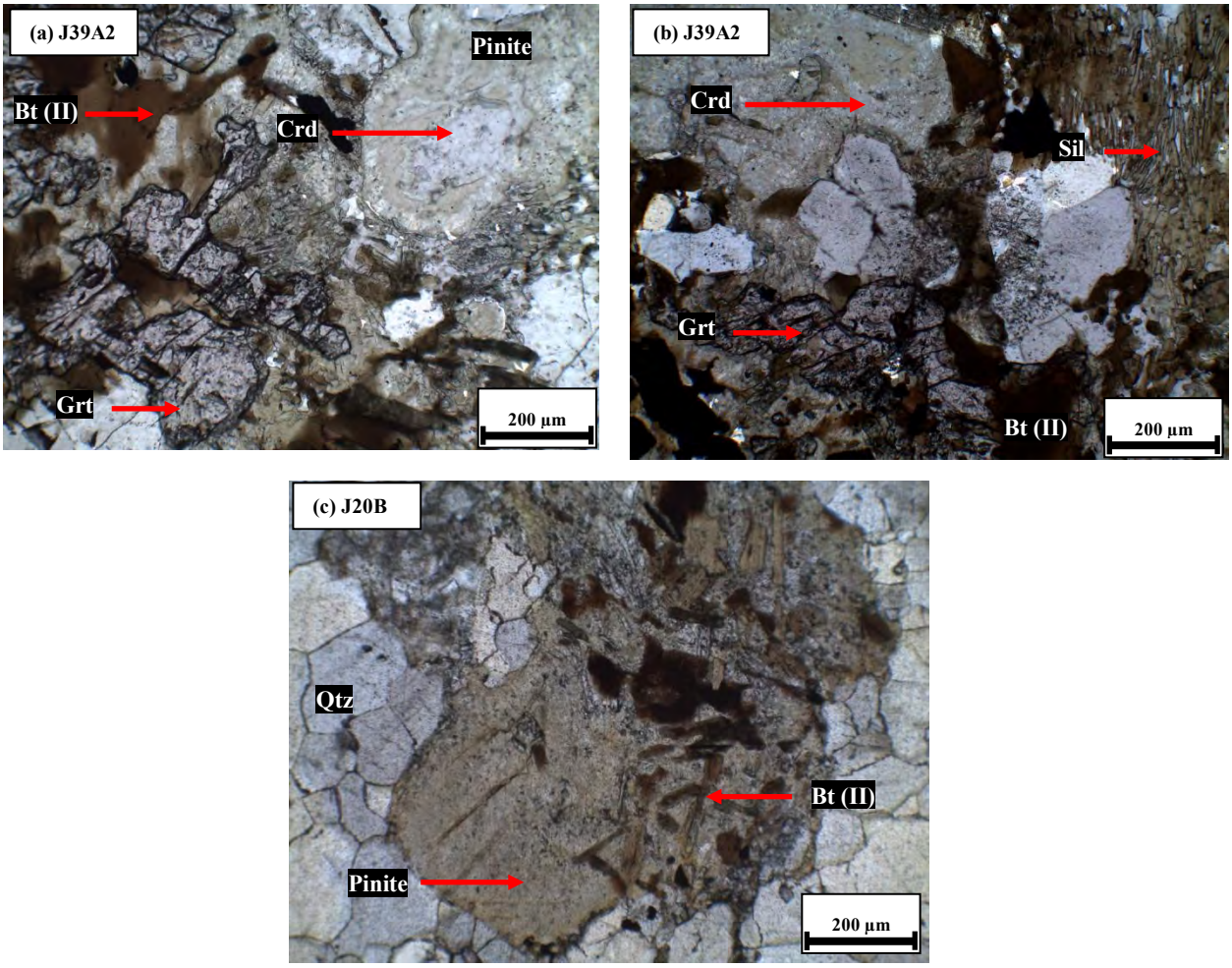

Figure 3.13. Photomicrographs from diffusely banded diatexite domains (sections 2.3.1; 2.3.2). (a-b) Sample J39A2 (Figure 2.14; section 2.3.1). Neighbouring the garnet grains are xenoblastic and partly pinitised cordierite with little fresh relicts preserved in its core. This may be seen as garnet breaking down to cordierite and in a second stage, garnet and cordierite forming secondary biotite (Bt II) as a retrograde product. The fibrolitic sillimanite clusters shows no preffered orirentation. The pinite forms after cordierite with secondary biotite (Bt II) growing parallel to the cordierite cleavage.

Table 3.8. Mineral modes in poorly banded (983A) and diffusely layered (J20B, J39A2 and J40) diatexite domains.

Diatexite domain	**Poorly-banded**						**Diffusely-layered**							
Sample	**983A**						**J20B**			**J39**			**J40**	
Thin section	**983A1**	**983A2**	**983A3**	**983A4**	**983C**	**983E**	**J20B**			**J39A2**			**J40**	
Quartz	34.5	32.0	33.0	31.8	36.8	33.6	19.8	21.4	23.2	34.0	36.5	38.1	13.7	17.2
K-Feldspar	35.2	36.8	33.1	34.6	32.0	17.7	20.0	19.3	24.2	45.9	42.9	42.6	27.9	32.4
Plagioclase	6.3	5.0	8.5	5.6	4.7	14.7	2.5	3.4	4.0	1.7	7.9	8.4	4.9	5.1
Garnet	13.9	15.4	14.0	17.5	15.1	20.9	16.3	15.4	14.1	2.2	2.0	2.7	26.4	26.4
Cordierite	-	-	-	-	-	-	2.9	2.2	-	2.3	-	-	3.0	-
Pinite	2.1	3.1	3.3	3.5	2.3	1.4	23.0	22.3	22.2	4.0	1.9	2.2	2.2	5.6
Biotite	4.8	5.1	4.8	4.3	4.8	5.7	7.8	7.6	8.1	7.0	3.5	3.4	15.5	12.4
Magnetite	2.4	1.8	1.9	2.0	3.0	3.1	3.0	2.7	3.0	0.9	1.1	0.8	1.0	0.9
Sillimanite	0.1	0.1	0.7	0.3	0.6	0.6	4.4	5.4	1.1	1.5	3.7	1.7	3.5	-
Rutile	0.4	0.6	0.3	0.5	0.8	0.3	0.3	0.5	-	-	-	-	1.0	-
Apatite	0.2	0.1	-	-	-	0.1	-	-	-	0.1	0.3	-	0.1	-
Titanite	0.1	-	0.3	-	-	0.2	-	-	-	0.2	0.1	-	0.3	-
Zircon	-	-	0.1	-	-	-	0.1	-	-	0.2	0.1	0.2	0.5	-
Chlorite	-	-	-	-	-	1.7	-	-	-	-	-	-	-	-
Total	100	100	100	100	100	100	100	100	100	100	100	100	100	100
Method	**Point counter**	**Point counter**	**Point counter**	**Point counter**	**Point counter**	**Point counter**	**Point counter**	**Thin section grid**	**Off-cut grid**	**Point counter**	**Point counter**	**Thin section grid**	**Point counter**	**Off-cut grid**
Points counted	6178	5832	5932	6412	5173	2084	7376	950	713	1893	1754	950	6896	674

3.3.5 Nebulitic diatexite

The nebulitic diatexite (samples J12, J37 and J38; Figure 2.17; section 2.3.3) forms anastomosing layers and vein patterns between garnet-cordierite-biotite-magnetite domains and the quartz-mesoperthitic groundmass. The diffuse macroscopic appearance of the diatexite is attributed to the garnets incorporating entire domains of quartz, perthitic alkali feldspar and melanocratic phases such as cordierite, biotite and magnetite into its structure (Figure 3.14). Garnet is coarse-grained ranging from 400-2500µm in size. Both the quartz and garnet exhibit irregular grain boundaries when the crystal faces are in contact with each other. Magnetite often occurs together with biotite aggregates and pinitised cordierite.

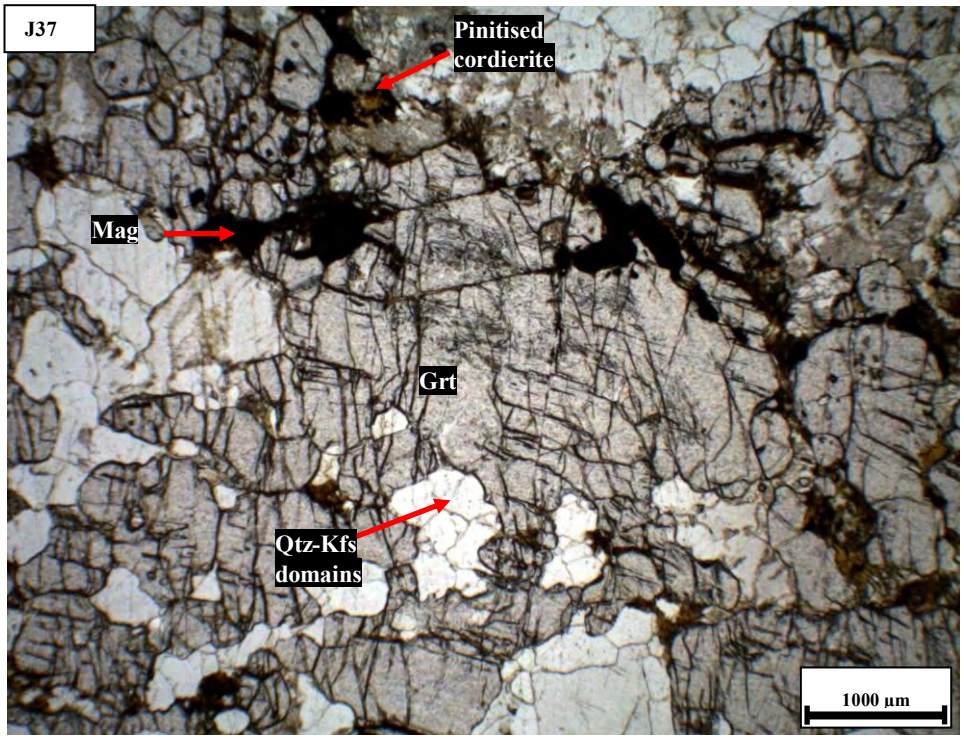

Figure 3.14. Photo-micrograph from nebulitic diatexite domains of sample J37A. The garnet clusters show amoeboid habits and curved grain boundaries. Quartz and alkali feldspar domains are enclosed within the garnet clusters. This provides the vein patterns observed in the nebulitic diatexite hand specimens (section 2.3.3). Adjacent to the garnet grains are xenoblastic cordierite that show similar alteration textures observed in the banded and melanocratic diatexite domains (section 3.3.2 and 3.3.3). The magnetite in the nebulitic diatexite domains are coarser-grained (500-1200µm) in comparison to the banded, leucocratic and melanocratic diatexite domains (100-500µm).

Table 3.9. Mineral modes of nebulitic diatexites J12, J37 and J38.

Sample	J12A	J37	J38
Quartz	32.4	27.9	31.9
K-feldspar	25.3	16.0	38.2
Plagioclase	7.3	2.4	3.9
Garnet	18.9	16.9	9.6
Cordierite	-	1.5	2.2
Pinite	3.8	8.4	3.2
Biotite	5.0	11.8	7.3
Magnetite	2.7	4.9	2.1
Sillimanite	4.6	9.2	1.5
Rutile	0.1	0.6	-
Apatite	-	-	-
Titanite	-	-	-
Zircon	-	0.6	-
Chlorite	-	-	-
Total	100	100	100
Method	**Point counter**	**Point counter**	**Point counter**
Points Counted	7063	7522	5902

4. Mineral Chemistry

The chemical compositions of minerals were determined using both Electron Probe Micro Analysis (EPMA) and Energy Dispersive Spectrometry (EDS) techniques. EPMA data acquisition was completed at the Department of Geology, Rhodes University, using a JEOL JXA-8230 Superprobe with four WD spectrometers. Natural mineral standards from SPI Supplies (www.2spi.com) were used for instrument calibrations. An acceleration voltage of 15 kV and a probe current of 20 nA were used for all analyses. Counting time on element peaks was 10 seconds and 5 seconds on the upper and lower backgrounds. The beam width for spot analysis is 1 micrometer. The JEOL software uses the ZAF matrix correction.

EPMA became available only towards the end of the project and has served as a tool to verify the bulk of the data set that was obtained from EDS analysis. EDS is less accurate in element quantification and has higher detection limits particularly for light elements. However, EDS and EPMA analysis from the same samples are always in good agreement within the requirement of this study.

The EDS data were produced using the SEM-based EDS at Rhodes University's Electronic Microscopy Unit. The Unit is equipped with a TESCAN Vega TS 5136LM SEM and an Oxford Instruments INCA PentaFET-x3 Si(Li) EDS Detector. The SEM was set to 15 kV acceleration voltage with a probe current setting of about 5. The probe current was fine-tuned as required to optimise the oxide totals. Cobalt was used as internal standard. Quant optimisation was performed after each 10-15 point analyses. Data processing and data reduction was done using the INCA Energy 350 EDS software from Oxford Instruments.

Due to careful setup of the instrument in terms of probe current and calibration most EDS analyses yielded oxide totals within 3% from the ideal mineral composition (100 wt% for anhydrous minerals; 93-98% for hydrous ones). However, for easier comparison EDS analyses have been normalised to 100 wt% for garnet, feldspars, and pyroxenes, 98 wt% for cordierite and amphibole, 96 wt% for biotite, and 93 wt% for scapolite.

4.1 Mafic granulites

Mineral analyses were obtained from six melanocratic domains from the Bysteek Formation mafic granulites and their associated leucocratic rocks: (i) nebulitic mesosomes (samples 976A, 976B-Figure 2,2); (ii) melanosomes (samples 976A ,976B-2-g, J44-mel-Figures 2.2 and 2.5); (iii) mafic fragments (985A-Figure 2.8) located within leucocratic networks; (iv*) in-situ*

leucosomes (976A and B); (v) leucocratic networks (985A); and (vi) leucocratic pools (J10B-Figure 2.6b). Mineral phases that have been analysed are clinopyroxene, orthopyroxene, plagioclase, garnet, amphibole, alkali feldspar, biotite and scapolite.

4.1.1 Clinopyroxene

The mafic granulites of the Bysteek Formation are dominated by clinopyroxene and plagioclase which are present at high modes in all mafic domains (Tables 3.1, 3.2 and 3.3).

4.1.1.1 Clinopyroxene in nebulitic mesosome domains

Clinopyroxene from the mafic granulites is largely uniform in Ca content but varies considerably in X_{Mg}. In the fine-grained nebulitic mesosomes of sample 976B-mes (Section 2.1.1.1, Figure 2.2a domain 2) are free of any phases hosting ferric iron where the average X_{Mg} is about 0.38 with only minor core-rim variation (Table 4.1; analysis 'g'). Clinopyroxene from the mesosome in sample 976A shows a significantly higher X_{Mg} of about 0.64 (Table 4.1; analysis 'f'). This sharp increase in X_{Mg} is possibly attributed to the presence of magnetite in sample 976A.

4.1.1.2 Clinopyroxene in melanosome domains

Four types of restitic melanosomes were analysed. They differ in mineral assemblages and modes (section 3.1.2; Table 3.2). Sample 976A shows clinopyroxene (57 vol%), plagioclase (35 vol%), quartz (7 vol%), and some magnetite (2 vol%). Clinopyroxene in the melanosome is slightly more diopside rich in comparison to that in the mesosomes (X_{Mg}= 0.66 *vs*. 0.64; analysis 'a' Table 4.1). Garnet free melanosomes from 976B often are crosscut by ptygmatically folded leucosome veins (Figure 2.2b) and are more diopside rich in comparison to the nebulitic mesosomes (X_{Mg}= 0.45. *vs*. 0.38; analysis 'b' Table 4.1). The clinopyroxene in garnetiferous melanosome 976B-2-g is similar in composition to that in the neighbouring garnet-free melanosome (X_{Mg}= 0.42-45. *vs*. 0.45; analysis 'c' Table 4.1).

Clinopyroxene grains from medium-and fine-grained domains from melanosome J44 (Figure 3.2 d-e) is the most diopside rich, featuring X_{Mg} values in range of 0.75-0.77 (analysis 'd-e'; Table 4.1; Figure 4.1).

4.1.1.3 Clinopyroxene in leucocratic domains

In sample 985A clinopyroxene occurs in lens-shaped mafic fragments as well as individual detached grains that are hosted in leucocratic networks. The clinopyroxene show X_{Mg} values between 0.66-0.68 (analyses 'd' and 'e'; Table 4.2).

The clinopyroxene xenocrysts located within the *in-situ* alkali feldspar granitic leucosomes of

sample 976B is approximately the same like that in the adjacent garnet-free melanosome, perhaps slightly more diopside rich (X_{Mg} =0.47; compared to 0.45; Table 4.2-analysis 'c', Figure 4.1).The dark grey anorthositic pockets and isolated leucosome domains in mafic granulite 976A contain clinopyroxene either as inclusions within large coarse-grained phenocrysts of plagioclase or as grains located within the leucocratic groundmass (Figure 3.5a). Both types show X_{Mg} values between 0.66-0.69 (Analyses 'a' and 'b' in Table 4.2). Groundmass clinopyroxene in the quartz-alkali feldspar syenite pockets of sample J10B is in the same range with X_{Mg} values of 0.70.

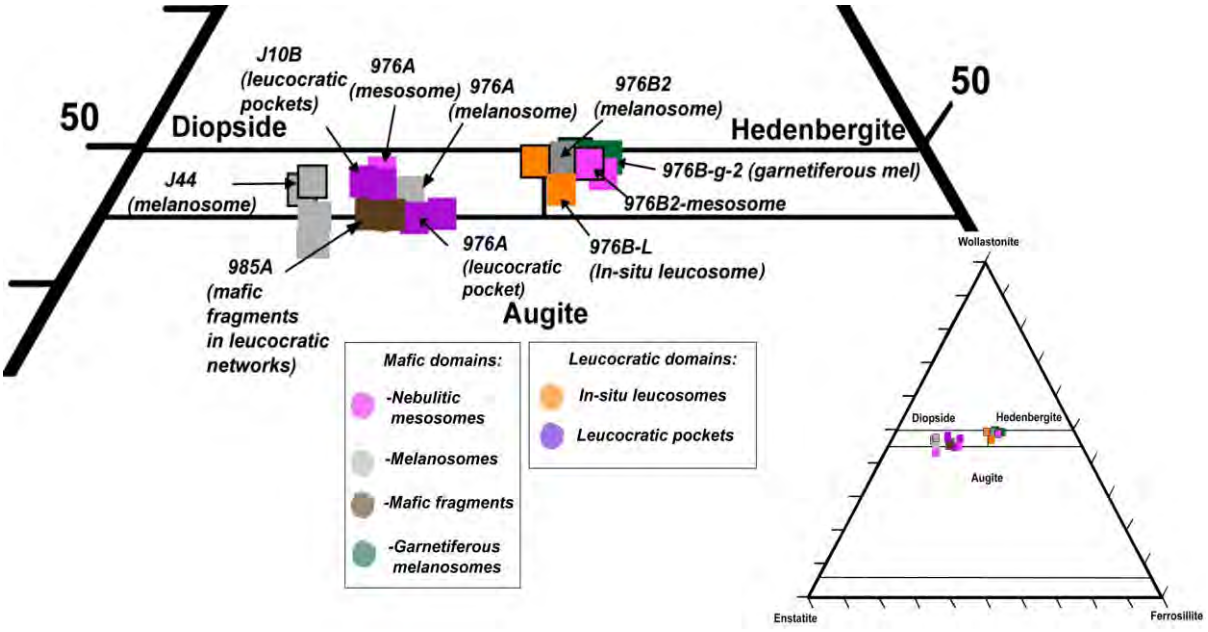

Figure 4.1. Pyroxene diagram (Morimoto, 1988) from EPMA and EDS analyses taken from nebulitic mesosomes, melanosome domains and leucocratic domains. Two populations of clinopyroxene exist in the mafic granulite sequence. Analyses taken from sample 976B (nebulitic mesosome, melanosome and *in-situ* leucosome) are hedenbergite rich (X_{Mg}: 0.45). Pyroxene analyses from mafic fragments, neighbouring melanocratic and leucocratic domains are more diopside rich (X_{Mg}: 0.65-0.70) .Squares with black frames are EPMA analyses, whereas squares without black frames are EDS analyses.

In summary the clinopyroxene compositions are uniform in calcium content with wollastonite contents of 45-49 mol% (Tables 4.1 and 4.2). The Mg-Fe ratio clinopyroxene shows two clusters, one around X_{Mg}: 0.40 and another ranging from 0.64-0.75. There is no systematic correlation between composition and provenance. For instance, clinopyroxene from different melanosomes may show either high or low X_{Mg} values. The same applies for xenocrysts in leucosomes. However, xenocrysts from leucocratic networks (X_{Mg}: 0.66-0.68) or pockets (X_{Mg}: 0.70) are similar in composition compared to the clinopyroxene in melanosomes or mesosomes nearby.

A possible explanation to why two clinopyroxene populations exist is probably because X_{Mg} variation correlates with the presence or absence of magnetite, which suggests oxygen fugacity variations. The presence of additional iron-rich phases such as magnetite, that may become stable with increasing oxygen fugacity, depletes the clinopyroxene in ferrous iron which then increases X_{Mg}.

Table 4.1. Average compositions of clinopyroxene from melanosome and mesosome domains. EDS oxide totals analyses are normalised to 100%. The un-normalised totals are given in an additional row. 'n.d': 'not-determined'- EPMA compositions do need to be re-normalised to 100%. See appendix 1 for the complete data set.

Sample	**976A-mel**	**976B-mel**	**976B-2-g**		**J44-mel**		**J44-mel**		**976A-mes**	**976B-mes**	
Domain Description	**Garnet free melanosome**	**Garnet free melanosome**	**Garnetiferous melanosome**		**Medium-grained orthopyroxene bearing melanosome**		**Fine-grained amphibole bearing melanosome**		**Garnet free mesosome**	**Garnet free mesosome**	
Mineral assemblage	**Cpx-Pl-Qtz-Mag**	**Cpx-Pl-Qtz**	**Grt-Cpx-Pl-Qtz**		**Cpx-Opx-Pl-Qtz-Hbl-Mag domain**		**Cpx-Opx-Pl-Hbl-Bt-Mag domain**		**Cpx-Pl-Qtz-Mag**	**Cpx-Pl-Qtz**	
Analyses	**a**	**b**	**c**		**d**		**e**		**f**	**g**	
Method	**EDS**	**EPMA**	**EPMA**	**EDS**	**EPMA**	**EDS**	**EPMA**	**EDS**	**EDS**	**EPMA**	**EDS**
Average number of analyses	**Average n=5**	**Average n=5**	**Average n=8**	**Average n=12**	**Average n=4**	**Average n=4**	**Average n=4**	**Average n=6**	**Average (n=2)**	**Average (n=4)**	**Average (n=5)**
SiO_2	53.01	48.50	48.88	50.94	49.97	53.01	50.27	52.98	52.12	48.14	52.33
TiO_2	0.21	0.14	0.11	0.13	0.31	0.28	0.33	0.24	0.34	0.11	0.26
Al_2O_3	1.82	2.03	1.81	2.03	2.78	2.61	2.96	2.98	2.41	2.09	1.81
Fe_2O_3	-	-	-	-	-	-	-	-	-	-	-
MgO	12.13	7.85	7.50	6.81	14.15	13.88	13.71	14.15	11.62	6.84	11.75
CaO	21.21	23.02	23.26	22.38	22.59	21.11	22.62	20.20	20.96	22.91	21.42
MnO	0.33	0.38	0.39	0.28	0.40	0.39	0.40	0.48	0.35	0.41	0.36
FeO	10.75	16.26	16.68	17.06	7.32	8.09	7.47	8.57	11.69	17.79	11.58
Na_2O	0.54	0.36	0.29	0.36	0.49	0.63	0.51	0.42	0.53	0.35	0.49
K_2O	-	-	-	0.01	-	-	-	-	-	-	-
Total:	100	98.58	98.95	100	98.00	100	98.28	100	100	98.67	100
Un-normalized EDS total	101.6	n.d	n.d	100.74	n.d	101.21	n.d	100.41	101.58	n.d	102.23

Table 4.1. (continued).

Sample	976A-mel	976B-mel	976B-2-g		J44-mel		J44-mel		976A-mes	976B-mes	
Domain Description	Garnet free melanosome	Garnet free melanosome	Garnetiferous melanosome		Medium-grained orthopyroxene bearing melanosome		Fine-grained amphibole bearing melanosome		Garnet free mesosome	Garnet free mesosome	
Mineral assemblage	Cpx-Pl-Qtz-Mag	Cpx-Pl-Qtz	Grt-Cpx-Pl-Qtz		Cpx-Opx-Pl-Qtz-Mag domain		Cpx-Opx-Pl-Hbl-Bt-Mag domain		Cpx-Pl-Qtz-mag	Cpx-Pl-Qtz	
Analyses	a	b	c		d		e		f	g	
Method	EDS	EPMA	EPMA	EDS	EPMA	EDS	EPMA	EDS	EDS	EPMA	EDS
Average number of analyses	Average n=5	Average n=5	Average n=8	Average n=12	Average n=4	Average n=4	Average n=4	Average n=6	Average (n=2)	Average (n=2)	Average (n=5)
Cations O=6											
Si	1.97	1.92	1.93	1.98	1.90	1.96	1.91	1.96	1.96	1.91	1.94
Ti	0.01	-	-	-	0.01	0.01	0.01	-	0.01	-	-
Al	0.07	0.09	0.08	0.09	0.12	0.11	0.13	0.13	0.11	0.09	0.10
Fe^{3+}	-	-	-	-	-	-	-	-	-	-	-
Mg	0.66	0.46	0.44	0.39	0.80	0.77	0.78	0.78	0.65	0.40	0.39
Ca	0.86	0.97	0.98	0.93	0.92	0.84	0.92	0.80	0.85	0.97	0.92
Mn	0.01	0.01	0.01	0.01	0.01	0.01	0.01	0.02	0.01	0.01	0.01
Fe^{2+}	0.37	0.53	0.55	0.55	0.23	0.25	0.24	0.27	0.37	0.59	0.63
Na	0.04	0.02	0.02	0.03	0.04	0.05	0.04	0.03	0.04	0.02	0.02
K	-	-	-	-	-	-	-	-	-	-	-
Total	4.00	4.04	4.03	3.99	4.04	4.00	4.03	3.99	3.99	4.04	4.01
Enstatite	34.95	23.42	22.35	20.97	41.02	41.32	40.14	42.26	34.94	20.56	20.07
Wollastonite	45.53	49.36	49.78	49.55	47.07	45.16	47.59	43.38	45.33	49.45	47.58
Ferrosillite	19.51	27.21	27.86	29.48	11.92	13.52	12.27	14.36	19.73	29.97	32.35
X_{Mg}	0.66	0.45	0.45	0.42	0.77	0.75	0.77	0.75	0.64	0.40	0.38
A	2.82	3.38	3.07	3.45	4.90	4.37	5.25	5.56	4.04	3.50	2.86
C	46.39	46.81	47.12	46.44	48.32	46.42	48.48	43.96	45.08	46.10	46.13
F	50.78	49.81	49.81	50.11	46.78	49.21	46.27	50.48	50.88	50.40	51.02

Table 4.2. Average compositions of clinopyroxene grains from leucosome domains. EDS oxide totals analyses are normalised to 100%. The un-normalised totals are given in an additional row. See appendix 2 for the complete data set.

Sample	**976A-L**	**976A-L**	**976B-L**		**985A-L**	**985A-L**	**J10B-L**
Domain description	**Inclusions in plagioclase phenocrysts**	**Leucocratic pocket**	***In-situ* leucosome**		**Mafic lens within network**	**Mafic fragments in networks**	**Mafic fragments in pockets**
Analyses	**a**	**b**	**c**		**d**	**e**	**f**
Method	**EDS**	**EDS**	**EPMA**	**EDS**	**EDS**	**EDS**	**EDS**
Average number of analyses	**Average (n=4)**	**Average (n=3)**	**Average (n=4)**	**Average (n=1)**	**Average (n=7)**	**Average (n=3)**	**Average (n=8)**
SiO_2	49.49	50.74	48.74	53.40	52.86	53.71	53.63
TiO_2	0.17	0.17	0.12	0.20	0.22	0.08	0.12
Al_2O_3	2.04	2.12	1.82	1.06	1.51	0.96	1.08
Fe_2O_3	-	-	-	-	-	-	-
MgO	6.62	7.19	8.21	12.27	12.04	12.64	12.52
CaO	21.85	22.36	23.05	21.18	21.24	21.35	22.42
MnO	0.40	0.27	0.40	0.32	0.41	0.41	0.25
FeO	19.12	16.76	15.71	11.18	11.27	10.48	9.61
Na_2O	0.31	0.38	0.37	0.39	0.46	0.37	0.38
K_2O	-	0.01	-	-	-	-	-
Total:	100	100	98.45	100	100	100	100
Un-normalised totals	101.25	101.62	n.d	100.99	102.09	102.41	102.79

Table 4.2. (continued).

Sample	976A-L	976A-L	976B-L		985A-L	985A-L	J10B-L
Domain description	Inclusions in plagioclase phenocrysts	Leucocratic pocket	*In-situ* leucosome		Mafic lens within network	Mafic fragments in networks	Mafic fragments in pockets
Analyses	a	b	c		d	e	f
Method	EDS	EDS	EPMA	EDS	EDS	EDS	EDS
Average number of analyses	Average (n=4)	Average (n=3)	Average (n=4)	Average (n=1)	Average (n=7)	Average (n=3)	Average (n=8)
Cations: O=6							
Si	2.00	1.98	1.93	1.96	1.99	2.01	2.00
Ti	-	0.01	-	0.01	0.01	-	-
Al	0.08	0.08	0.09	0.09	0.06	0.05	0.05
Cr	-	-	-	-	-	-	-
Fe3	-	-	-	-	-	-	-
Mg	0.69	0.66	0.48	0.47	0.68	0.70	0.70
Ca	0.85	0.87	0.98	0.91	0.86	0.87	0.90
Mn	0.01	0.01	0.01	0.01	0.01	0.01	0.01
Fe2	0.31	0.35	0.52	0.54	0.35	0.32	0.30
Na	0.04	0.04	0.03	0.03	0.03	0.03	0.03
K	-	-	-	-	-	-	-
Total	3.98	3.99	4.04	4.01	3.99	3.98	3.98
Enstatite	37.47	35.33	24.45	24.54	36.22	36.88	36.83
Wollastonite	45.61	46.27	49.31	47.34	45.34	46.09	47.32
Ferrosillite	16.92	18.40	26.23	28.12	18.44	17.04	15.85
X_{Mg}	0.69	0.66	0.48	0.47	0.66	0.68	0.70
A	3.46	3.58	2.97	1.46	2.28	1.30	1.55
C	43.96	46.30	47.21	46.43	46.19	46.96	49.27
F	52.58	50.12	49.83	52.11	51.53	51.75	49.18

4.1.2 Orthopyroxene, amphibole and biotite

Orthopyroxene, amphibole and biotite are scarce within the mafic granulites of the Bysteek Formation but occur in the melanosome of sample J44 (Figure 3.2 d-e). Modal compositions and petrography are presented in section 3.12. Orthopyroxene is enstatite rich with X_{Mg} values in range of 0.68-0.70 (Table 4.3, Figure 4.2a-b). Amphibole is a magnesium-hornblende with X_{Mg} values of 0.75-0.78. Biotite is also magnesium rich (X_{Mg} of 0.72-0.74) and has high TiO_2 values between 4.03-4.18 mol%. In general, orthopyroxene, hornblende and biotite compositions from both fine-and-medium grained domains are similar in X_{Mg} (0.70-0.77) differing by ~2 mol% (Table 4.2) and far higher compared to those in mafic granulites 976B (X_{Mg} : 0.40) and 976A (X_{Mg}:0.65).

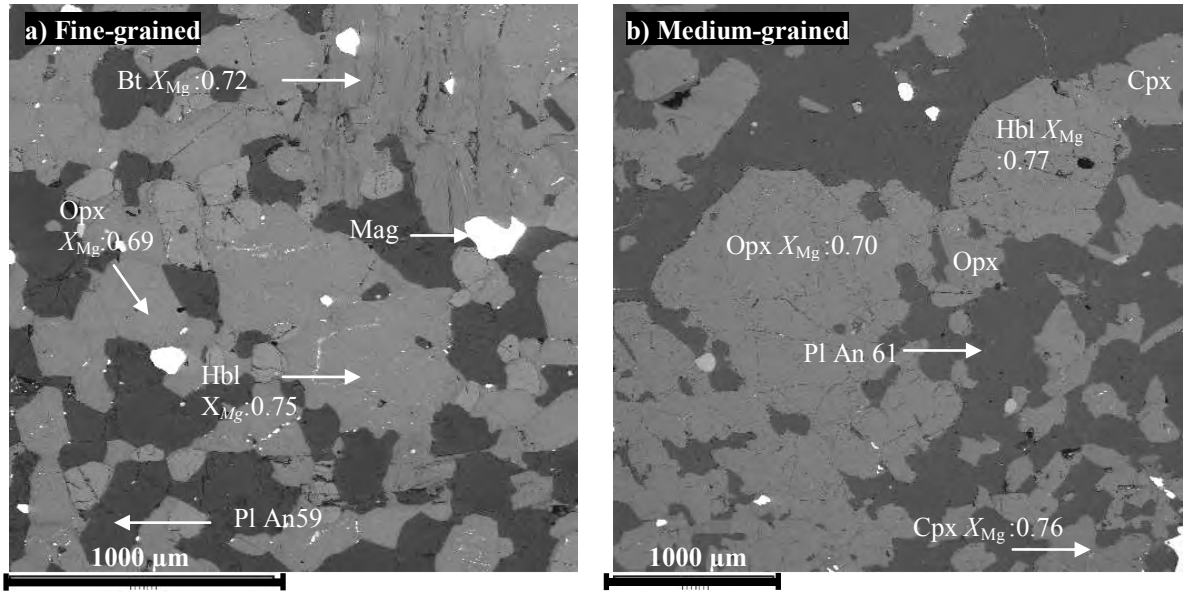

Figure 4.2. SEM backscatter images from (a) fine-grained and (b) coarse-grained domains from amphibole-biotite-orthopyroxene bearing melanosome J44-mel. The presence of hydrous phases amphibole and biotite are interpreted as a metasomatic product occurring during the retrograde metamorphic stage. Plagioclase is less anorthitic (An60) than in sample 976B (An91), yet compositionally higher to the plagioclase grains in magnetite bearing melanosome 976A (An47).

Table 4.3. Representative average EMPA and EDS analyses of orthopyroxene, amphibole and biotite from melanosome J44-mel. EDS oxide totals for orthopyroxene analyses are normalised to 100%. The un-normalised totals are given in an additional row. Ferric iron for amphiboles are calculated for best structural fit (see appendix 3 for complete data set).

Phase	**Orthopyroxene**				**Hornblende**					**Biotite**		
Domain	**Medium-grained**		**Fine-grained**		**Domain**	**Medium-grained**		**Fine-grained**		**Domain**	**Medium-grained**	**Fine-grained**
Method	**EPMA**	**EDS**	**EPMA**	**EDS**	**Method**	**EPMA**	**EDS**	**EPMA**	**EDS**	**Method**	**EPMA**	**EPMA**
Average Counts	**Average (n=6)**	**Average (n=7)**	**Average (n=4)**	**Average (n=7)**	**Average Counts**	**Average (n=4)**	**Average (n=4)**	**Average (n=4)**	**Average (n=5)**	**Average counts**	**Average (n=4)**	**Average (n=6)**
SiO_2	52.46	53.97	52.49	53.44	**SiO_2**	43.02	43.80	42.43	44.06	**SiO_2**	39.38	39.41
TiO_2	0.27	0.13	0.06	0.11	**TiO_2**	1.82	1.77	1.95	1.67	**TiO_2**	4.18	4.03
Al_2O_3	1.16	1.18	1.42	1.47	**Al_2O_3**	10.69	10.89	11.03	11.08	**Al_2O_3**	13.41	13.17
Cr_2O_3	-	-	-	-	**Cr_2O_3**	-	0.05	-	0.08	**Cr_2O_3**	0.13	0.09
MgO	24.85	24.42	24.50	23.72	**Fe_2O_3**	4.94	6.89	4.48	5.78	**MgO**	17.59	17.30
CaO	0.50	0.44	0.77	0.57	**FeO**	8.15	6.87	8.50	7.65	**CaO**	0.21	0.16
MnO	0.96	0.88	1.05	1.03	**MnO**	0.25	0.31	0.21	0.16	**MnO**	0.18	0.11
FeO	19.32	18.89	19.36	19.64	**MgO**	13.87	13.31	13.66	13.39	**FeO**	10.97	11.97
Na_2O	0.01	0.09	0.01	0.02	**CaO**	11.90	11.07	11.93	11.23	**BaO**	0.31	0.25
K_2O	-	-	-	-	**Na_2O**	1.71	1.55	1.68	1.56	**Na_2O**	0.20	0.16
Total	99.54	100	99.66	100	**K_2O**	1.65	1.46	1.79	1.55	**K_2O**	9.45	9.33
Un-normalised total	n.d	99.79	n.d	99.88	**BaO**	-	-	0.07	-	**Total (dry)**	96.00	96.00
					H_2O*	2.04	2.05	2.03	2.06	**Total (with water)**	100.05	100.09
					Total (with water)	100.03	100.08	99.70	100.46			
					Total (dry)	97.99	98.03	97.67	98.40			

Table 4.3. (continued)

Phase	Orthopyroxene				Phase	Hornblende				Phase	Biotite	
Domain	Medium-grained		Fine-grained		Domain	Medium-grained		Fine- grained		Domain	Medium - grained	Fine-grained
Method	EPMA	EDS	EPMA	EDS	Method	EPMA	EDS	EPMA	EDS	Method	EPMA	EPMA
Average Counts	Average (n=6)	Average (n=7)	Average (n=4)	Average (n=8)	Average Counts	Average (n=4)	Average (n=4)	Average (n=4)	Average (n=6)	Average Counts	Average (n=4)	Average (n=6)
Cations: O=6					Cations: O=23					Cations: O=24		
Si	1.94	1.97	1.94	1.97	Si	6.33	6.4	6.27	6.42	Si	5.74	5.76
Ti	0.01	-	-	-	Al tot	1.85	1.87	1.92	1.9	Ti	0.46	0.44
Al	0.05	0.05	0.06	0.06	Al iv	1.67	1.6	1.73	1.58	Al	2.3	2.27
Cr	-	-	-	-	Al vi	0.18	0.27	0.2	0.32	Cr	0.01	0.01
Fe^{3+}	-	-	-	-	Ti	0.2	0.19	0.22	0.18	Mg	3.82	3.77
Mg	1.37	1.34	1.35	1.3	Cr	-	0.01	-	0.01	Ca	0.03	0.03
Ca	0.02	0.02	0.03	0.02	Fe^{3+}	0.55	0.76	0.5	0.63	Mn	0.02	0.01
Mn	0.03	0.03	0.03	0.03	$Fe2^{+}$	1	0.84	1.05	0.93	Fe	1.34	1.46
Fe^{2+}	0.6	0.58	0.6	0.6	Mn	0.03	0.04	0.03	0.02	Ba	0.02	0.01
Na	-	0.01	-	-	Mg	3.04	2.9	3.01	2.91	Na	0.06	0.05
K	-	-	-	-	Ca	1.88	1.73	1.89	1.75	K	1.76	1.74
Total	4.02	4	4.02	4	Na	0.49	0.44	0.48	0.44	Total	15.55	15.55
Enstatite	68.92	69.11	68.22	67.48	K	0.31	0.27	0.34	0.29	X_{Mg}	0.74	0.72
Wollastonite	1	0.88	1.53	1.17	Ba	-	-	-	0.01	A	4.47	11.05
Ferrosillite	30.07	30	30.25	31.35	OH*	2.00	2.00	2.00	2.00	C	0.62	0.48
X_{Mg}	0.7	0.7	0.69	0.68	Total	17.67	17.45	17.71	17.49	F	94.92	88.46
A	2.47	2.38	2.81	3.12	X_{Mg}	0.75	0.78	0.74	0.76			
C	1.07	0.95	1.46	1.23	A	26.42	31.89	25.99	29.78			
F	96.46	96.66	95.73	95.65	C	25.63	23.9	25.74	24.33			
					F	47.95	44.21	48.27	45.89			

4.1.3 Garnet

Garnet in the mafic granulite sequence are present in the melanosome of sample 976B (see Figure 3.3c).

Backscattered images and EDS element mapping of garnet show zonation patterns with increasing iron content towards the rim and highest aluminium content within the core. The endmember calculation shows increasing andradite and decreasing grossularite concentrations from core to rim (Table 4.4). Almandine contents are around 5 mol% (EPMA); manganese and magnesium contents are low, irrespective of textural position. The highest andradite (71 mol%) and lowest grossularite contents shows garnet growing as thin rims along Cpx-Pl grain boundaries (Figure 4.3b).

The growth of andraditic garnet in a matrix that is free of ferric iron, and increasing incorporation of ferric iron in garnet towards the rims, suggest increasing oxygen fugacity at the time of garnet growth. The reverse trend of aluminium enrichment and low X_{Adr} within garnet cores may also suggest an exchange reaction between Al^{3+} and ferric iron ions (Figure 4.3 a-b).

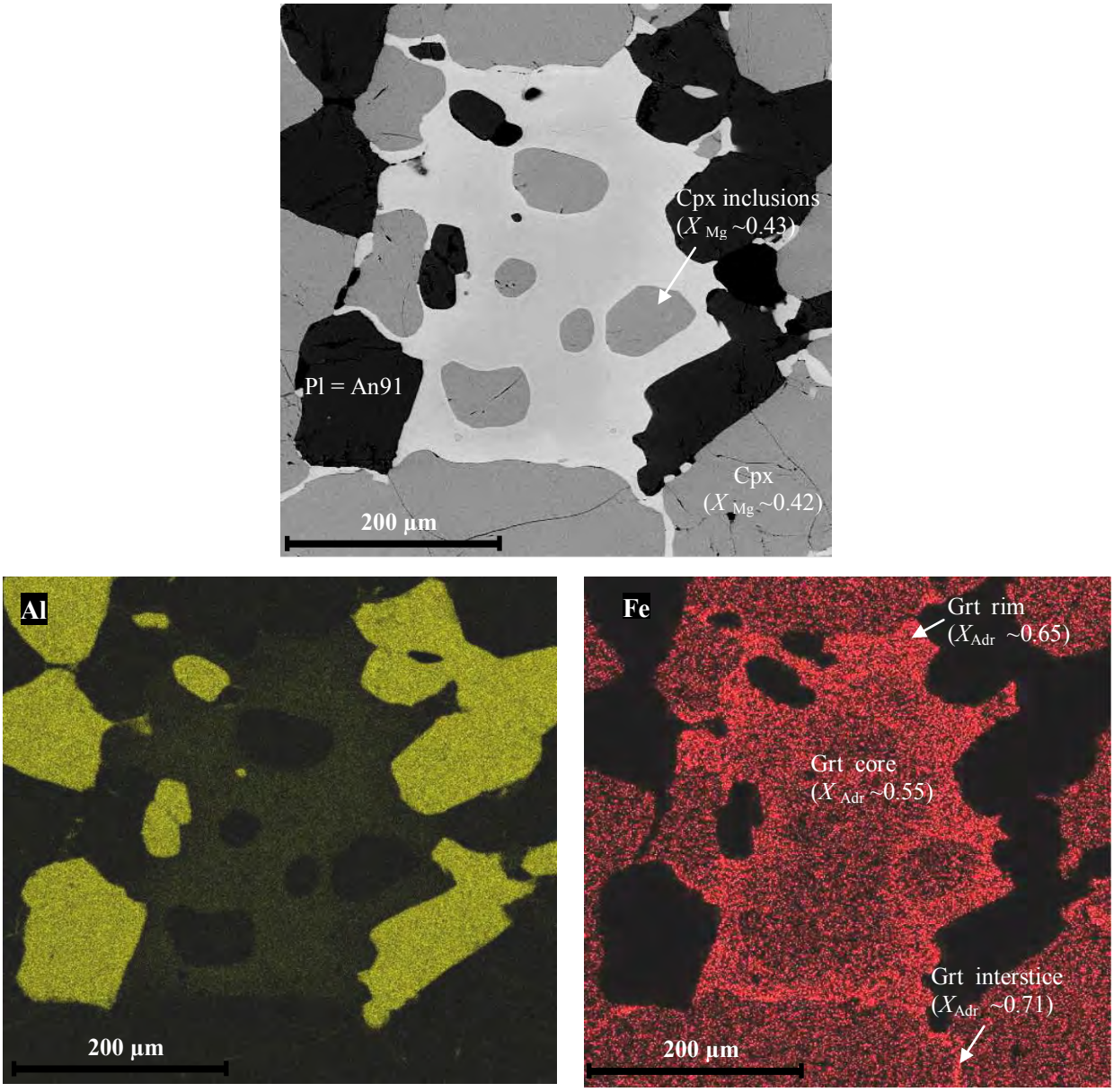

Figure 4.3. Al (left) and Fe (right) element mappings for amoeboid garnet, clinopyroxene and plagioclase in 976B-2-g. The interstitial domains (X_{Adr}: 0.71) and rims (X_{Adr}: 0.65) are more ferric in comparison to the core (X_{Adr}: 0.55). Conversely, cores are more aluminous in comparison to the rims. The backscatter SEM image centred above shows clinopyroxene and plagioclase inclusions located within the garnet.

Table 4.4. Representative EDS and EPMA garnet analyses from sample 976B-2-g. EDS oxide totals analyses are normalised to 100%. The un-normalised totals are given in an additional row. Ferric iron is calculated for best structural fit (see appendix 4 for complete data set).

Method	**EDS**			**EPMA**		
Location	**core**	**rim**	**interstices**	**core**	**rim**	**interstices**
Average number of analyses	**Average n=2**	**Average n=5**	**Average n=3**	**Average n=3**	**Average n=4**	**Average n=2**
SiO_2	38.16	37.39	36.99	36.62	36.17	36.45
TiO_2	0.85	0.72	0.59	0.77	0.76	0.32
Al_2O_3	9.24	6.86	5.11	9.40	7.77	6.96
Cr_2O_3	0.03	0.07	0.06	0.00	0.00	0.00
Fe_2O_3	15.96	19.54	22.27	17.28	19.15	21.09
MgO	0.14	0.10	0.14	0.20	0.17	0.11
CaO	31.13	29.90	29.84	32.60	31.46	31.51
MnO	0.30	0.55	0.48	0.42	0.49	0.74
FeO	4.19	4.87	4.52	1.51	2.28	2.32
Total	100	100	100	98.80	98.25	99.50
Un-Normalized	102.78	101.10	100.74	n.d	n.d	n.d
Cations: O=24						
Si	6.13	6.11	6.10	5.96	5.98	5.99
Ti	0.10	0.09	0.07	0.09	0.09	0.04
Al	1.75	1.32	0.99	1.80	1.51	1.35
Cr	-	-	-	-	-	-
Fe^{3+}	1.93	2.41	2.77	2.12	2.38	2.61
Mg	0.03	0.02	0.04	0.05	0.04	0.03
Ca	5.36	5.23	5.27	5.69	5.57	5.55
Mn	0.04	0.08	0.07	0.06	0.07	0.10
Fe^{2+}	0.56	0.67	0.62	0.21	0.31	0.32
Total	15.92	15.93	15.94	15.98	15.97	15.99
X_{Mg}	0.06	0.10	0.09	0.19	0.16	0.23
Uvarovite	0.11	0.23	0.20	-	-	-
Andradite	50.76	62.23	70.82	55.28	61.95	66.22
Grossular	38.50	24.82	16.90	39.54	30.95	26.29
Almandine	9.38	11.07	10.37	3.42	5.25	5.32
Spessartine	0.68	1.26	1.12	0.97	1.14	1.73
Pyrope	0.57	0.39	0.59	0.79	0.71	0.44
A	23.86	23.69	23.85	24.67	24.52	24.80
C	68.60	66.59	66.94	71.33	70.12	69.57
F	7.54	9.72	9.22	3.99	5.36	5.63

4.1.4 Plagioclase and alkali feldspar

Plagioclase compositions were determined for melanosome, mesosome and leucosome domains. Alkali feldspar is present only in the leucosome. Amongst domains of different types, plagioclase shows compositions ranging from anorthite to labradorite and andesine (Figure 4.4). Individual crystals are homogenous and free of compositional zonation. Alkali feldspar is either orthoclase or microcline (Figures 3.5-3.7).

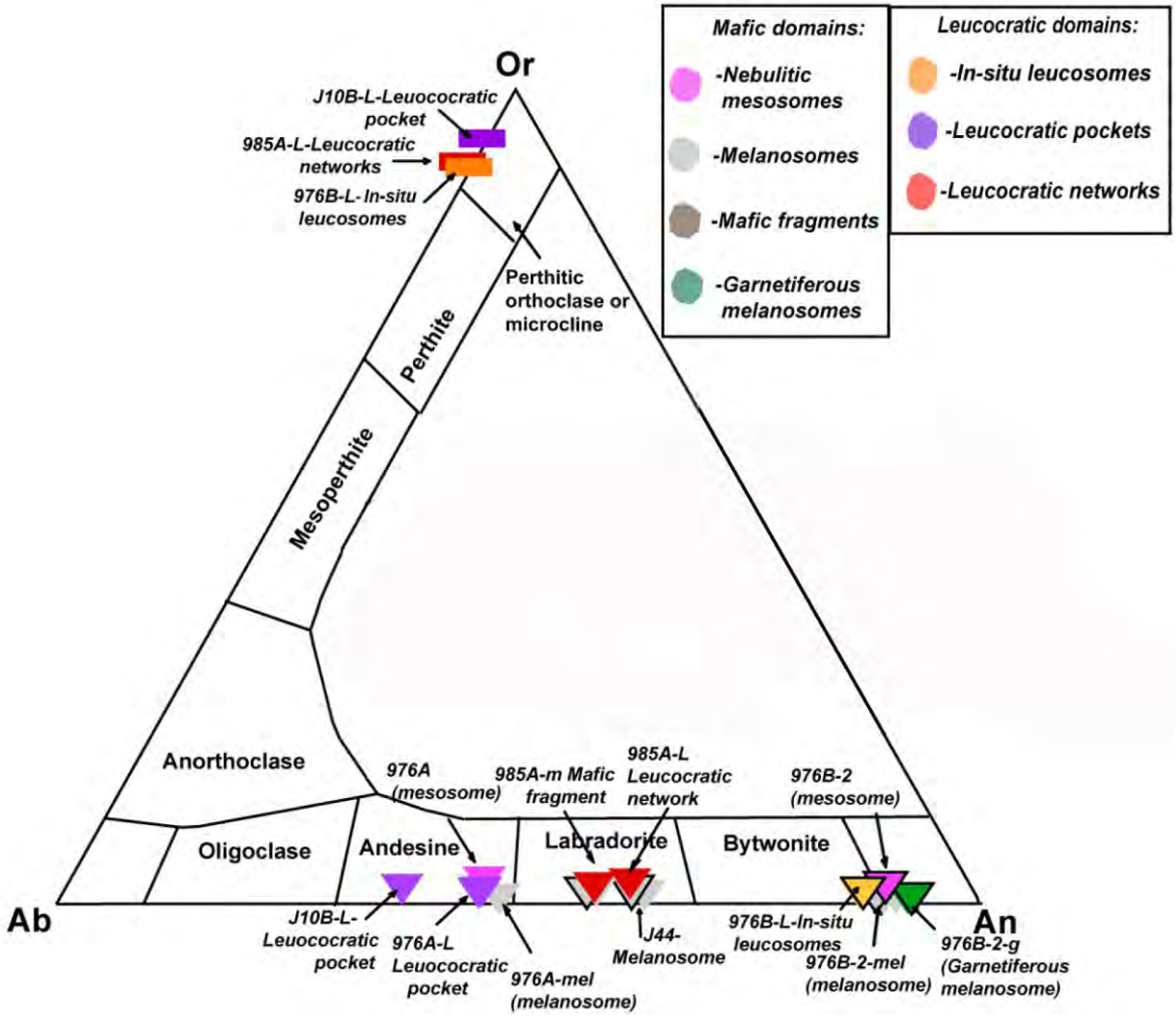

Figure 4.4. Feldspar diagram (O'Connor, 1965) of EPMA and EDS analyses taken from nebulitic mesosomes, melanosome domains, leucocratic networks, pockets and *in-situ* leucosome domains. Plagioclase analyses from sample 976B are all anorthitic (An90), whereas nebulitic mesosomes and melanosomes from mafic granulite 976A are andesine rich (An47). Leucocratic pockets J10B-L are also andesine rich (An44), whereas plagioclase grains from networks 985A are and melanosome J44 are labradorite rich (An60). All alkali feldspars (rectangles) from analysed domains are orthoclase or microcline. Triangles with black frames are EPMA analyses, whereas rectangles without black frames are EDS analyses.

4.1.4.1 Plagioclase in melanosomes

Plagioclase of the garnet, magnetite-free Cpx-Pl-Qtz melanosome (sample 976B, Figure 3.3b) are anorthite (An88-89). In the garnetiferous melanosome (sample 976B-2-g; Figure 3.2c) of the same sample the anorthite content is almost identical (An91). Plagioclase in the magnetite bearing melanosome of sample 976A are with an anorthite content of An47. significantly more albitic. In the coarse-grained domains of melanosome J44 (Figure 3.2d), anorthite contents are intermediate, with values around An61-62, with slightly lower values in finer-grained parts (An58-59) (Table 4.5).

4.1.4.2 Plagioclase in mesosomes

Plagioclase in the magnetite bearing mesosomes of 976A are almost identical to those in the neighbouring melanosomes (An45), yet more orthoclase rich (Or4) in comparison to the plagioclase in the adjacent melanosome (Or2; Table 4.6). Plagioclase in the garnet, magnetite-free mesosomes of 976B are similar to those in the adjacent melanosome, yielding An90-91. The variations in plagioclase compositions in the mesosome may reflect the textural appearance of poorly separated leucosome and melanosome.

4.1.4.3 Plagioclase in leucosome domains

Macroscopically dark grey plagioclase phenocrysts in the 'anorthosite' pockets of sample 976A-L (Figure 2.2a; domain 4) are andesine (An48; Table 4.6) which is similar to those located in the neighbouring nebulitic mesosome. Plagioclase in alkali-feldspar-granite *in-situ* leucosome domains of 976B-L are anorthite-rich (An88-89), similar to those in adjacent nebulitic mesosome of 976B-mes. The mafic fragments (sample 985A; Figure 3.7b; domain 1) hosted in the quartz syenitic leucocratic networks, show anorthite contents of An57 in plagioclase; similar to plagioclase in the quartz syenitic leucocratic networks (sample 985A-L; An60; Figure 2.8). The alkali feldspar granitic pockets in sample J10B show plagioclase with anorthite contents of An44.

4.1.5 Alkali feldspar

EDS analyses were conducted on alkali feldspars from *in-situ* leucosome domains (sample 976B-L; Figure 2.2b), leucocratic networks (sample 985A-L; Figure 2.8) and pockets (sample J10B-L; Figure 2.6b). Petrographic observations and backscatter images from *in-situ* leucosome (Figure 3.5b-c; 4.5) show no evidence for unmixing. The alkali feldspars exhibit orthoclase content of Or89 (Table 4.6). The alkali feldspars from network 985A-L shows compositionally similar orthoclase content (Or89) to those from *in-situ* leucosome 976B-L, yet show string-perthitic textures (Figure 3.7b).

Alkali feldspars from leucocratic pocket J10B-L shows the highest orthoclase content (Or 94; Figure 4.4; Table 4.6). Unmixing is also common as they show interlocking to replacement perthitic textures (Figure 3.6a-b)

Table 4.5. Average compositions of plagioclase in mafic granulite melanosome domains (see appendix 5 for complete data set). EDS oxide totals analyses are normalised to 100%. The un-normalised totals are given in an additional row.

Sample	**976A-mel**	**976B-mel**		**976B-2-g**		**J44-mel**			
Domain description	**Magnetite bearing**	**Garnet, magnetite-free melanosome**		**Garnetiferous melanosome**		**Medium-grained**		**Fine-grained**	
Location	**Average (n=6)**	**Average (n=1)**	**Average (n=1)**	**Average (n=5)**	**Average (n=8)**	**Average (n=5)**	**Average (n=5)**	**Average (n=10)**	**Average (n=5)**
Method	**EDS**	**EDS**	**EPMA**	**EDS**	**EPMA**	**EPMA**	**EDS**	**EPMA**	**EDS**
SiO_2	57.19	47.07	43.88	46.65	43.40	51.12	53.64	51.16	54.73
Al_2O_3	27.02	33.55	36.06	33.90	36.71	31.58	29.70	31.31	28.81
MgO	-	-	-	-	-	-	-	-	-
CaO	9.66	17.79	17.81	18.01	18.51	12.43	12.46	12.13	11.79
MnO	0.03	-	-	0.02	-	-	-	-	-
FeO	0.14	0.40	-	0.40	-	-	-	-	-
BaO	0.02	-	-	0.06	-	-	-	-	-
Na_2O	5.64	1.20	1.25	0.94	0.94	4.11	4.07	4.33	4.52
K_2O	0.29	-	0.10	0.02	0.06	0.19	0.14	0.23	0.15
Total	100	100	99.09	100	99.61	99.43	100	99.16	100
Un-normalised EDS totals	100.77	101.44	n.d	101.76	n.d	n.d	99.82	n.d	99.45

Table 4.5. (continued).

Sample	976A-mel	976B-mel		976B-2-g		J44-mel			
Domain description	Magnetite bearing	Garnet, magnetite-free melanosome		Garnetiferous melanosome		Medium-grained		Fine-grained	
Location	Average (n=6)	Average (n=1)	Average (n=1)	Average (n=5)	Average (n=8)	Average (n=5)	Average (n=5)	Average (n=10)	Average (n=5)
Method	EDS	EDS	EPMA	EDS	EPMA	EPMA	EDS	EPMA	EDS
Cations :O=8									
Si	2.57	2.16	2.04	2.15	2.01	2.33	2.42	2.34	2.47
Al	1.43	1.82	1.98	1.84	2.01	1.70	1.58	1.69	1.53
Mg	-	-	-	-	-	-	-	-	-
Ca	0.46	0.88	0.89	0.89	0.92	0.61	0.60	0.59	0.57
Mn	-	-	-	-	-	-	-	-	-
Fe	0.01	0.02	-	0.02	-	-	-	-	-
Ba	-	-	-	-	-	-	-	-	-
Na	0.49	0.11	0.11	0.08	0.08	0.36	0.36	0.38	0.39
K	0.02	0.00	0.01	-	-	0.01	0.01	0.01	0.01
Total	4.97	4.98	5.03	4.98	5.03	5.01	4.97	5.02	4.97
Or	1.70	-	0.60	0.07	0.33	1.11	0.84	1.37	0.90
An	47.81	89.15	88.22	91.26	91.32	61.87	62.33	59.89	58.48
Ab	50.49	10.85	11.18	8.65	8.35	37.02	36.84	38.73	40.62
A	49.45	48.98	51.15	49.23	51.05	52.13	50.22	52.04	49.77
C	49.86	50.15	48.85	49.86	48.95	47.87	49.78	47.96	50.23
F	0.69	0.88	-	0.91	-	-	-	-	-

Table 4.6. Average compositions of plagioclase and alkali feldspar in mesosome and leucosome domains. EDS oxide totals analyses are normalised to 100%. The un-normalised totals are given in an additional row. (see appendix 6 for complete data set).

Phase	**Plagioclase**									**Alkali-feldspar**		
Sample	**976A-mes**	**976B-mes**		**976A-L**	**976B-L**		**985A-L**		**J10B-L**	**976B-L**	**985A-L**	**J10B-L**
Domain Description	**Nebulitic mesosome**	**Nebulitic mesosome**		**Pocket**	***In-situ* leucosome**		**Mafic fragments**	**Leucocratic networks**	**Pocket**	***In-situ* leucosome**	**Leucocratic network**	**Pocket**
Average number of analyses	**Average (n=2)**	**Average (n=4)**	**Average (n=4)**	**Average (n=6)**	**Average (n=3)**	**Average (n=2)**	**Average (n=4)**	**Average (n=4)**	**Average (n=4)**	**Average (n=5)**	**Average (n=5)**	**Average (n=6)**
Method	**EDS**	**EDS**	**EPMA**	**EDS**	**EDS**	**EPMA**	**EDS**	**EDS**	**EDS**	**EDS**	**EDS**	**EDS**
SiO_2	57.88	46.68	43.68	57.03	47.33	43.96	58.94	59.51	55.23	64.90	65.60	65.88
Al_2O_3	26.46	33.83	36.16	27.15	33.46	35.89	25.93	25.42	28.45	17.88	17.82	17.70
MgO	0.03	0.01	-	-	-	-	-	-	-	0.02	-	-
CaO	9.04	17.92	18.10	9.72	17.50	17.80	8.38	7.83	11.20	0.42	0.11	0.05
MnO	-	0.02	-	-	0.04	-	-	0.04	0.02	0.02	0.03	0.01
FeO	0.18	0.45	-	0.14	0.32	-	-	0.11	0.12	0.10	0.05	0.06
BaO	0.09	-	-	0.05	0.07	-	-	0.05	-	1.47	0.89	0.38
Na_2O	5.53	1.07	1.09	5.62	1.26	1.36	6.54	6.90	4.86	0.88	1.05	0.68
K_2O	0.77	0.03	0.10	0.28	0.02	0.04	0.20	0.14	0.12	14.30	14.46	15.24
Total	100	100	99.13	100	100	99.05	100	100	100	100	100	100
Un-normalised EDS totals	100.78	100.50	n.d	100.76	103.60	n.d	98.99	99.99	102.10	100.41	100.04	100.92

Table 4.6. (continued).

Phase	Plagioclase									Alkali feldspar		
Sample	976A-mes	976B-mes		976A-L	976B-L		985A-L		J10B-L	976B-L	985A-L	J10B-L
Domain Description	Nebulitic mesosome	Nebulitic mesosome		Pocket	*In-situ* leucosome		Mafic fragments	Leucocratic networks	Pocket	In-situ leucosome	Leucocratic network	Pocket
Average number of analyses	Average (n=2)	Average (n=4)	Average (n=4)	Average (n=6)	Average (n=3)	Average (n=2)	Average (n=4)	Average (n=4)	Average (n=4)	Average (n=5)	Average (n=5)	Average (n=6)
Method	EDS	EDS	EPMA	EDS	EDS	EPMA	EDS	EDS	EDS	EDS	EDS	EDS
Cations O=8												
Si	2.60	2.15	2.03	2.56	2.17	2.05	2.63	2.66	2.49	3.01	3.03	3.03
Al	1.4	1.83	1.98	1.44	1.81	1.97	1.36	1.34	1.51	0.98	0.97	0.96
Mg	-	-	-	-	-	-	-	-	-	-	-	-
Ca	0.43	0.88	0.9	0.47	0.86	0.89	0.4	0.37	0.54	0.02	0.01	-
Mn	-	-	-	-	-	-	-	-	-	-	-	-
Fe	0.01	0.02	-	0.01	0.01	-	-	-	-	-	-	-
Ba	-	-	-	-	-	-	-	-	-	0.03	0.02	0.01
Na	0.48	0.1	0.1	0.49	0.11	0.12	0.57	0.6	0.42	0.08	0.09	0.06
K	0.04	-	0.01	0.02	-	-	0.01	0.01	0.01	0.85	0.85	0.9
Total	4.97	4.98	5.03	4.97	4.98	5.03	4.97	4.98	4.97	4.96	4.96	3.03
Or	4.65	0.18	0.61	1.63	0.12	0.24	-	0.79	0.69	89.41	89.62	94.43
An	45.25	90.07	89.6	48.07	88.25	87.61	57.84	60.91	43.69	2.19	0.55	0.35
Ab	50.1	9.75	9.79	50.3	11.5	12.15	42.16	38.21	55.62	8.4	9.84	5.22
A	49.62	49.07	51	49.61	49.24	50.94	49.52	49.08	49.7	-	-	-
C	49.33	49.9	49	49.82	49.95	49.06	50.48	50.15	49.81	-	-	-
F	1.05	1.04	-	0.57	0.81	-	-	0.77	0.49	-	-	-

4.1.6 Scapolite

The scapolite grains of *in-situ* leucosomes of 976B-L (Figure 3.5b) are meionitic in composition (0.75-0.78; Table 4.7). They are also high in CaO (~17 wt%), Al_2O3 (~27 wt%) with minor sodium (2.40 wt%).

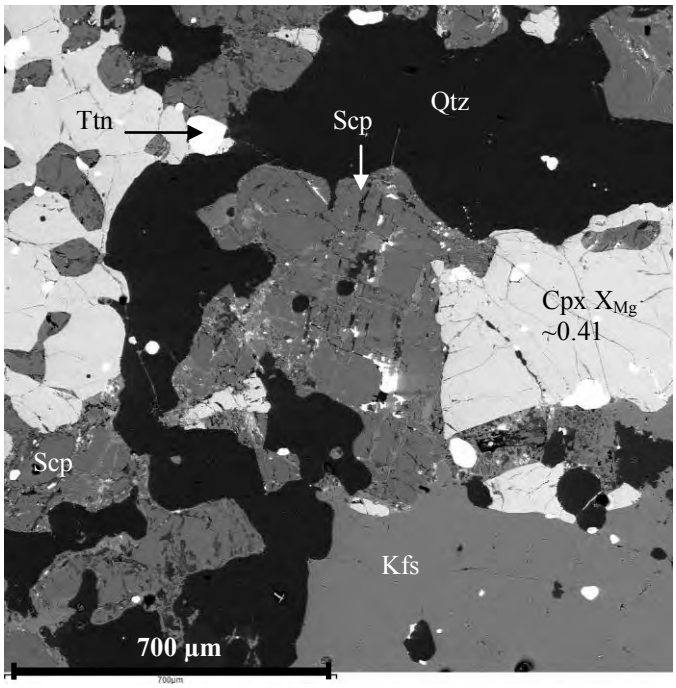

Figure 4.5. Backscatter image of scapolite grains located within *in-situ* leucosome 976B-L. The scapolite grains are randomly oriented neighbouring detached clinopyroxene xenocrysts, quartz and alkali feldspar. The clinopyroxene show similar X_{Mg} values to those in neighbouring mesosomes and melanosomes (X_{Mg}: 0.40).The alkali feldspar grains show no unmixing textures.

Table 4.7. Compositions of scapolite grains located from *in-situ* leucosome domain 976B-L. The O_2, H_2O and CO_2 amounts required for the channel volatiles have been added to the 18 oxygen atoms that charge-balance the cationic scapolite components. Me[a]: meionite content = Ca+Mg+Fe+Mn+Ti / Ca+Mg+Fe+Mn+Ti+Na+K *100).

Method	EDS	EDS	EDS	EDS	EDS
Analyses	1	2	3	4	Average (n=4)
SiO_2	45.14	45.08	45.09	45.06	45.09
TiO_2	0.06	0.07	-	0.05	0.05
Al_2O_3	25.68	25.35	25.23	25.26	25.38
MgO	-	-	0.03	-	0.01
CaO	16.67	15.99	15.96	16.40	16.26
MnO	0.10	-	0.07	-	0.05
FeO	0.30	0.37	0.33	0.13	0.28
Fe_2O_3	-	-	-	-	-
Na_2O	2.45	2.47	1.90	2.13	2.24
K_2O	0.56	0.63	0.36	0.23	0.45
BaO	0.02	0.12	0.18	0.01	0.08
Cr_2O_3	0.05	0.07	0.09	0.01	0.06
P_2O_5	0.09	0.09	0.19	0.02	0.10
H_2O	2.42	2.38	2.36	2.37	2.37
CO_2	3.20	3.29	3.24	3.29	3.26
O_2	0.45	0.47	0.47	0.48	0.47
Total	99.08	99.14	99.23	100.03	99.37
Total (dry)	92.58	92.57	92.73	93.51	92.84
Cations: O =18					
Si	5.16	5.18	5.22	5.21	5.20
Al	3.45	3.43	3.37	3.43	3.42
Fe^{3+}	-	-	-	-	-
Cr	-	-	-	-	-
Ti	-	-	-	-	-
Fe^{2+}	0.03	0.04	0.03	0.01	0.03
Mg	-	-	-	-	-
Mn	0.01	-	0.01	-	-
Ca	2.11	2.08	2.05	2.06	2.08
Na	0.53	0.55	0.62	0.66	0.59
K	0.08	0.09	0.05	0.03	0.06
Ba	-	-	0.01	-	0.00
OH	0.35	0.36	0.35	0.35	0.35
Molecules CO_2	0.35	0.37	0.36	0.33	0.36
Molecules O_2	0.11	0.10	0.10	0.12	0.10
PO_4	0.01	0.01	0.02	-	0.01
Total	12.20	12.22	12.21	12.21	12.21
Me [a]	78.18	76.78	75.71	74.99	76.41

4.2 Diatexites

Mineral analyses were conducted on four diatexite samples from different domains of the Koenap Formation. The analysed domains include: (i) nebulitic diatexites (samples J20B, J37, L38B and A106A); (ii) diffusely banded diatexite (sample J39A); (iii) poorly banded diatexite (sample 983A) and (iv) melanocratic domains (sample J33A). Mineral phases that have been analysed are garnets, cordierite, plagioclase, alkali feldspar and biotite.

4.2.1 Garnet

Garnet in diatexites are homogenous and in particular do not show any systematic zonation patterns.

Garnet in the fine-grained diffusely banded diatexite domains of sample J39A2 are almandine-rich with X_{Mg} values varying between ~0.18-0.19 (EPMA, EDS). Calcium and manganese contents are low (<1 wt% and <3 wt% of the oxides, respectively; Table 4.8). Re-calculations of the EPMA analyses for best stoichiometric fit show that calcium is contained in the andradite and not in the grossularite endmember.

The coarse-grained nebulitic diatexite (J20B), characterised by its anastomosing texture between pink leucocratic and dark grey melanocratic domains, exhibits garnet of similar composition, yielding X_{Mg} values of 0.19. This garnet is almandine-rich (77 mol%). The pyrope content is still significant (18 mol%), with minor spessartine and andradite (2.5 mol%) (Table 4.8; Figure 4.6).

Sample J33 is well banded diatexite with distinguishable leucocratic and melanocratic domains (Figures 2.16a and 3.10b). Garnet in sample J33 is compositionally similar to garnet in the samples described above (J20B and J39A; Table 4.8). The garnet occurs in a groundmass of thick biotite aggregates, pinitised cordierite and some magnetite.

Garnet from poorly banded and nebulitic diatexite varieties (samples L38B, 983A3, A106A, (Figure 2.1-sampling map) contain somewhat more magnesium and less iron causing higher X_{Mg} values of about 0.25. Otherwise these garnets are similar in composition compared to garnet from other diatexites types (Table 4.8).

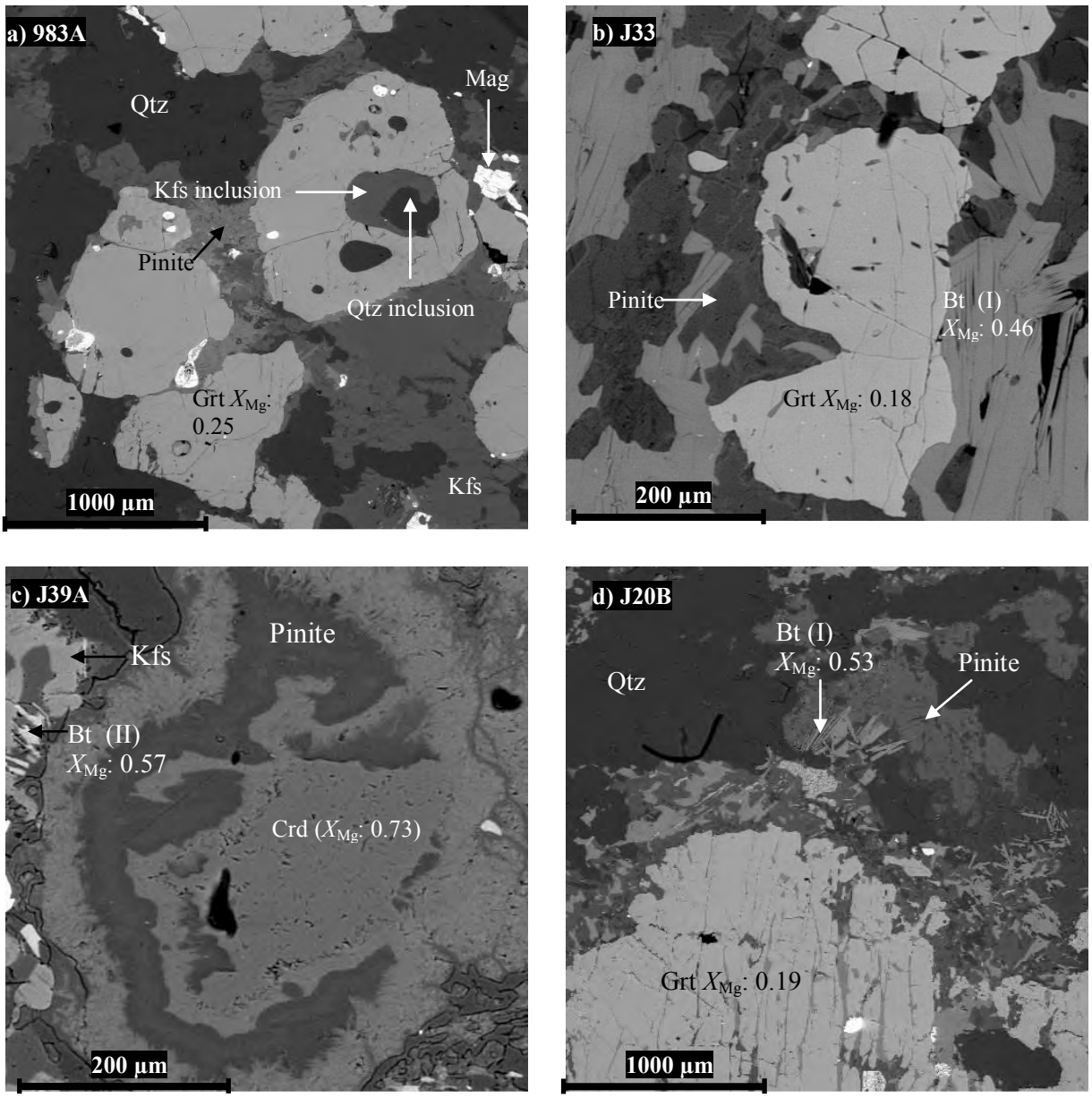

Figure 4.6. SEM backscatter images from analysed diatexite domains. (a) 983A is a poorly layered diatexite whereby garnets are almandine rich with X_{Mg} values of 0.25. Pinitised domains occur in between adjacent garnet grains. The garnets also contain quartz and alkali feldspar inclusions with rounded grain boundaries. The alkali feldspar grains show rod perthitic textures. (b) Melanocratic domains from sample J33A show garnet grains (X_{Mg}: 0.18) surrounded by biotite flakes (Bt I: X_{Mg}: 0.46) and strongly pinitised domains. (c) Diffusely banded domains from J39A exhibit partly pinitised cordierite where the cores remain unaltered. The cordierite cores have X_{Mg} values of 0.73. Surrounding the cordierite are few Bt II grains with X_{Mg} of 0.57. (d) Nebulitic diatexite J20B shows biotite variety Bt I as fine-grained (<100µm) clusters around almandine garnet (X_{Mg}: 0.19). These biotite grains are less iron rich (X_{Mg}: 0.53) compared to those in melanocratic domain J33 (X_{Mg}: 0.46).

Table 4.8. Average EDS and EPMA garnet compositions in diatexites. See appendix 8 for all mineral analyses.

Domain	Diffusely banded diatexite		Nebulitic	Banded (melanocratic domains)	Nebulitic	Poorly banded	Nebulitic
Sample	J39A-2		J20B	J33	L38B	983A3	A106A
Method	EPMA	EDS	EDS	EDS	EDS	EDS	EDS
Average number of analyses	Average (n=7)	Average (n=6)	Average (n=9)	Average (n=8)	Average (n=6)	Average (n=9)	Average (n=2)
SiO_2	37.25	37.75	37.78	37.56	38.28	38.17	37.05
TiO_2	0.01	0.01	0.02	0.06	0.04	0.03	0.06
Al_2O_3	20.08	20.16	20.08	20.02	20.24	20.26	20.57
Cr_2O_3	-	0.01	0.02	0.02	0.02	0.06	0.17
Fe_2O_3	0.51	0.51	0.73	0.56	0.96	0.86	1.04
MgO	4.59	4.31	4.70	4.56	6.10	6.18	6.38
CaO	0.54	0.55	0.86	0.76	1.18	0.99	1.50
MnO	1.29	1.16	0.92	1.08	0.63	0.54	0.95
FeO	35.26	35.37	34.71	35.04	32.43	32.82	32.12
Total	99.53	99.83	99.80	99.65	99.88	99.87	99.84
Cations :O=24							
Si	6.02	6.07	6.06	6.05	6.06	6.05	5.90
Ti	-	-	-	0.01	0.01	-	0.01
Al	3.82	3.82	3.79	3.83	3.78	3.78	3.86
Cr	-	-	-	-	-	0.01	0.02
Fe^{3+}	0.06	0.06	0.09	0.07	0.11	0.10	0.12
Mg	1.11	1.03	1.12	1.06	1.44	1.46	1.52
Ca	0.09	0.09	0.15	0.13	0.20	0.17	0.26
Mn	0.18	0.16	0.13	0.14	0.08	0.07	0.13
Fe^{2+}	4.76	4.75	4.65	4.75	4.30	4.35	4.28
X_{Mg}	0.19	0.18	0.19	0.18	0.25	0.25	0.26
Uvarovite	-	0.03	0.06	0.07	0.06	0.18	0.51
Andradite	1.53	1.55	2.25	1.82	2.99	2.60	3.17
Grossular	-	-	0.18	0.31	0.34	0.16	0.97
Almandine	77.58	78.70	76.89	78.06	71.30	71.78	68.90
Spessartine	2.89	2.62	2.07	2.36	1.40	1.20	2.07
Pyrope	18.00	17.10	18.54	17.39	23.91	24.07	24.39
A':	24.01	24.30	24.28	24.12	24.42	24.27	24.37
K:	-	-	-	-	-	-	-
F:	75.99	75.70	75.72	75.88	75.58	75.73	75.63
A:	0.24	0.24	0.24	25.64	0.24	0.24	0.24
F:	0.81	0.82	0.81	63.72	0.75	0.75	0.74
M:	0.19	0.18	0.19	10.63	0.25	0.25	0.26

4.2.2 Cordierite

Fresh cordierite is rare but occurs in sample J39A2, a diffusely banded diatexite domain (Figure 4.5c) and in a nebulitic variety, sample L38B (Figure 2.17d). Cordierite is anhedral and typically occurs together with garnet, forming along its rims. Secondary biotite (see section 3.3.2, Figure 3.10b) is frequently associated with garnet and cordierite. Cordierite often shows orange pinitisation along grain boundaries and cleavage planes. Cordierite in both samples is homogenous with X_{Mg} values around 0.72-0.74 (EPMA, EDS; Table 4.9).

4.2.3 Plagioclase and alkali feldspar

Plagioclase and alkali feldspar chemistry were analysed from three diatexite varieties: leucocratic domains from diffusely banded diatexite J39A2 (section 3.3.1), banded (samples 983A and J20B ; sections 2.3.2 and 3.3.4) and nebulitic (L38B; Figure 2.17d; section 2.3.3).

Plagioclase compositions from poorly banded diatexite are oligoclase exhibiting anorthite content of An27 (Table 4.9; Figure 4.7). The plagioclase from sample J39A are also oligoclase with EPMA and EDS analyses showing anorthite content between An17-22. Plagioclase from nebulitic diatexite L38B is andesine with anorthite content of An35 (Table 4.9).

Alkali feldspar grains from leucocratic domains of diffusely banded diatexite J39A2 show rod perthitic textures (Figure 3.9c). They exhibit orthoclase content of Or84 (Table 4.9). The alkali feldspars from poorly banded diatexite 983A are compositionally similar with orthoclase content of Or85 (Figure 4.7). Backscatter images similarly show rod perthitic unmixing textures (Figure 4.6a). Alkali feldspar grains from nebulitic diatexite J20B shows a higher orthoclase content (Or92) in comparison to samples J39A2 and 983A (Table 4.9; Figure 4.7).

Table 4.9. Average EDS and EPMA mineral analyses of K-feldspar, plagioclase and cordierite from diatexites. Feldspar EDS oxide totals are normalised to 100%. The un-normalised totals are given in an additional row. Ferric iron content in cordierite is calculated for best structural fit (18 O + oxygen for CO_2 and H_2O) (see appendix 9 for complete data set).

Phase	**Alkali-Feldspar**			**Plagioclase**				**Cordierite**			
Sample	**J39-A2**	**J20B**	**983A3**	**J39A-2**	**J39A-2**	**L38**	**983A**	**Sample**	**J39A**	**J39A**	**L38**
Method	**EDS**	**EDS**	**EDS**	**EPMA**	**EDS**	**EDS**	**EDS**	**Method**	**EPMA**	**EDS**	**EDS**
Average	**Average (n=3)**	**Average (n=4)**	**Average (n=3)**	**Average (n=4)**	**average (n=3)**	**average (n=1)**	**average (n=3)**	**Average**	**average (n=4)**	**Average (n=13)**	**Average (n=9)**
SiO_2	66.62	66.46	66.31	63.14	64.92	60.71	62.72	**SiO_2**	46.86	49.51	49.75
Al_2O_3	18.15	17.99	18.08	24.87	22.14	24.86	23.53	**TiO_2**	0.00	0.02	0.03
MgO	-	-	-	-	-	-	-	**Al_2O_3**	34.38	31.57	31.57
CaO	0.02	0.06	0.06	3.92	3.46	7.02	5.44	**MgO**	8.83	9.46	9.62
MnO	-	-	-	-	-	0.07	-	**CaO**	-	0.02	0.03
FeO	-	-	-	-	-	0.04	-	**MnO**	0.04	0.07	0.06
BaO	-	-	-	-	-	-	-	**FeO**	6.24	6.29	6.13
Na_2O	1.73	0.84	1.54	7.54	9.41	7.15	8.15	**Fe_2O_3**	-	0.50	0.22
K_2O	13.49	14.64	14.01	0.20	0.07	0.15	0.16	**Na_2O**	0.07	0.16	0.16
Total	100	100	100	99.66	100	100	100	**K_2O**	0.03	0.01	0.01
Un-normalised total	98.74	98.54	99.28	n.d	99.71	99.89	99.69	**H_2O**	2.16	2.19	2.19
								CO_2	0.34	0.31	0.31
								Total	98.95	100.10	100.07
								Total (dry)	96.45	97.60	97.57

Table 4. 9. (continued).

Phase	Alkali feldspar			Plagioclase				Phase	Cordierite		
Sample	J39-A2	J20B	983A3	J39A-2	J39A-2	L38	983A	Sample	J39A	J39A	L38
Method	EDS	EDS	EDS	EPMA	EDS	EDS	EDS	Method	EPMA	EDS	EDS
Average	Average (n=3)	Average (n=4)	Average (n=3)	Average (n=4)	average (n=3)	average (n=1)	average (n=3)	Average	average (n=4)	Average (n=13)	Average (n=9)
Cations: O=8								Cations: O=18			
Si	3.03	3.04	3.03	2.78	2.86	2.7	2.77	Si	4.87	5.09	5.11
Al	0.97	0.97	0.97	1.29	1.15	1.3	1.23	Ti	0	0	0
Mg	-	-	-	-	-	-	-	Al	4.22	3.83	3.82
Ca	-	-	-	0.18	0.16	0.33	0.26	Mg	1.37	1.45	1.47
Fe	-	-	-	-	-	-	-	Ca	-	-	-
Ba	-	-	-	-	-	-	-	Mn	-	0.01	0.01
Na	0.15	0.07	0.14	0.64	0.8	0.62	0.7	Fe^{2+}	0.54	0.54	0.53
K	0.78	0.85	0.82	0.01	0	0.01	0.01	Fe^{3+}	0	0.04	0.02
Total	4.95	4.94	4.96	4.91	4.97	4.96	4.97	Na	0.01	0.03	0.03
An	0.11	0.32	0.31	22.04	16.82	34.83	26.69	K	-	-	-
Ab	16.34	8.01	14.31	76.65	82.77	64.25	72.39	Total	11.02	10.99	10.99
Or	83.55	91.67	85.38	1.32	0.42	0.92	0.92	X_{Mg}	0.72	0.73	0.74
A'	4.38	3.93	1.71	98.54	99.21	97.58	98.43	A'	52.25	48.93	48.66
K	95.62	96.07	98.29	1.46	0.79	1.44	1.57	K	47.71	51.05	51.32
F	-	-	-	-	-	0.99	-	F	0.04	0.02	0.02
A	100	100	100	100	100	99.57	100	A	50.42	49	48.88
F	-	-	-	-	-	0.16	-	F	13.5	13.85	13.46
M	-	-	-	-	-	0.27	-	M	36.07	37.16	37.66

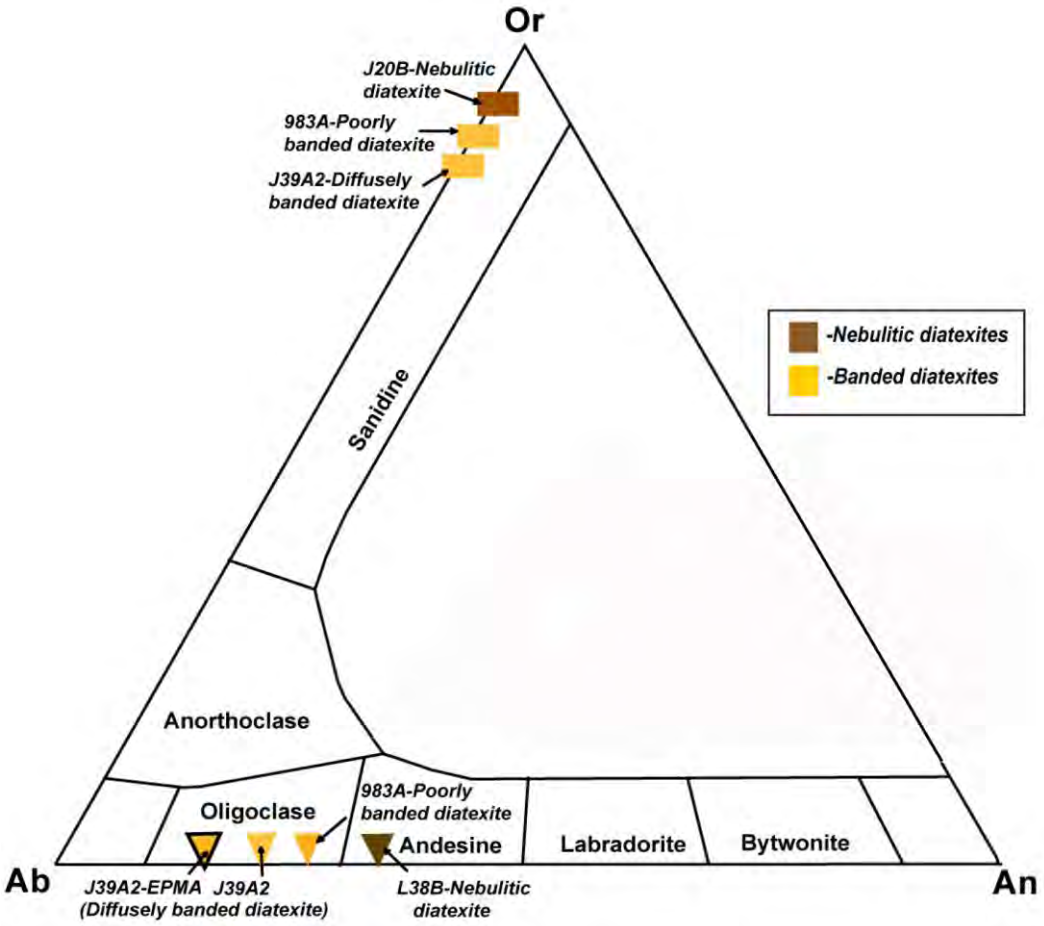

Figure 4.7. Feldspar diagram showing compositions from diatexite domains (O'Connor, 1965). Plagioclase from banded diatexite domains (orange triangles, sample J39A2 and 983A) fall in the oligoclase field, whereas plagioclase from nebulitic domains (brown triangle, sample L38B) reside in the andesine field. Triangles with black frames are EPMA analyses, whereas squares without black frames are EDS analyses. All alkali feldspars (rectangles) from analysed domains are perthitic orthoclase.

4.2.4 Biotite

Biotite analyses from melanocratic, leucocratic, banded and nebulitic diatexite domains show X_{Mg} values in range between 0.46 and 0.62. Petrographic observations from diatexite domains show two varieties of biotite (section 3.3.2). The first variety (Bt I) occur as fine- to medium-grained (200-400µm) that occur as decussate clusters in the diatexite groundmass, often neighbouring garnet and xenoblastic cordierite grains (Figure 3.10). They show TiO_2 content between 3.7 and 4.4 wt% and X_{Mg} values of 0.46-0.53 (Table 4.10). The second variety (Bt II) occurs as fine grained (<200µm) secondary retrograde breakdown product after garnet and cordierite (Figures 3.10, 3.13; 4.6). They show X_{Mg} values of 0.57-0.62 and TiO_2 content between 2.2 and 4.4 wt% (Table 4.10).

Table 4.10. Representative EDS biotite compositions from analyzed banded, melanocratic and nebulitic diatexite domains (See appendix 10 for all biotite analyses).

Sample	J39-A2		J20B		L38B		983A3		J33
Diatexite Type	Diffusely banded diatexite		Nebulitic diatexite		Nebulitic diatexite		Banded diatexite		Banded diatexite
Domain where biotite occurs	Nebulitic domains	Diffuse leucocratic	Melanocratic domains	Nebulitic domain	Adjacent cordierite and garnet	Melanocratic domains	Adjacent cordierite and garnet	Massive leucocratic domains	Melanocratic domains
Biotite variety	Bt II	Bt II	Bt I	Bt I	Bt II	Bt I	Bt II	Bt II	Bt I
Average counts	Average (n=3)	Average (n=3)	Average (n=5)	Average (n=2)	Average (n=2)	Average (n=2)	Average (n=5)	Average (n=5)	Average (n=4)
SiO_2	37.46	37.88	36.52	36.31	37.57	36.73	36.82	36.38	35.46
TiO_2	2.22	2.29	3.70	4.15	4.43	4.40	4.05	4.16	4.04
Al_2O_3	17.21	17.29	16.34	16.27	15.81	16.70	16.19	16.34	16.68
Cr_2O_3	0.03	0.05	0.14	0.16	0.16	0.01	0.26	0.22	0.20
MgO	12.66	12.75	9.89	11.55	13.32	9.36	14.35	13.56	9.72
CaO	0.01	0.01	0.14	0.04	0.02	0.03	0.10	0.07	0.03
MnO	0.08	0.03	0.01	0.00	0.03	0.00	0.03	0.05	0.19
FeO	16.76	16.18	19.67	17.97	15.33	19.16	15.95	17.66	20.34
BaO	0.19	0.11	0.31	0.20	0.00	0.00	0.01	0.11	0.08
Na_2O	0.14	0.09	0.11	0.12	0.20	0.19	0.17	0.19	0.24
K_2O	9.25	9.34	9.18	9.23	9.13	9.42	8.07	7.26	9.03
Total (dry)	96.00	96.00	96.00	96.00	96.00	96.00	96.00	96.00	96.00
Total (with water)	99.94	99.95	99.73	99.64	99.92	99.99	99.96	100.16	99.76

Table 4.10. (continued).

Sample	J39-A2		J20B		L38B		983A3		J33
Diatexite Type	Diffusely banded diatexite		Nebulitic diatexite		Nebulitic diatexite		Banded diatexite		Banded diatexite
Domain where biotite occurs	Nebulitic domains	Diffuse leucocratic	Melanocratic domains	Nebulitic domain	Adjacent cordierite and garnet	Melanocratic domains	Adjacent cordierite and garnet	Massive leucocratic domains	Melanocratic domains
Biotite variety	Bt II	Bt II	Bt I	Bt I	Bt II	Bt I	Bt II	Bt II	Bt I
Average counts	Average (n=3)	Average (n=3)	Average (n=5)	Average (n=2)	Average (n=2)	Average (n=2)	Average (n=5)	Average (n=5)	Average (n=4)
Cations : O=24									
Si	5.58	5.61	5.54	5.46	5.56	5.54	5.44	5.4	5.4
Ti	0.25	0.26	0.42	0.47	0.49	0.5	0.45	0.46	0.46
Al	3.02	3.02	2.92	2.89	2.76	2.97	2.82	2.86	2.99
Cr	-	0.01	0.02	0.02	0.02	-	0.03	0.03	0.02
Mg	2.81	2.82	2.24	2.59	2.94	2.11	3.16	3	2.21
Ca	-	-	0.02	0.01	-	-	0.02	0.01	0.01
Mn	0.01	-	-	-	-	-	-	0.01	0.02
Fe	2.09	2.01	2.5	2.26	1.9	2.42	1.97	2.19	2.59
Ba	0.01	0.01	0.02	0.01	-	-	-	0.01	-
Na	0.04	0.02	0.03	0.04	0.06	0.06	0.05	0.05	0.07
K	1.76	1.77	1.78	1.77	1.72	1.81	1.52	1.37	1.75
Total	15.56	15.51	15.48	15.52	15.45	15.41	15.47	15.4	15.54
X_{Mg}	0.57	0.58	0.47	0.53	0.61	0.47	0.62	0.58	0.46
A	37.44	37.93	36.18	36.06	36.04	37.57	35.3	34.89	36.28
F	35.02	34.1	41.92	38.36	33.59	41.37	33.41	36.15	42.58
M	27.54	27.97	21.91	25.59	30.37	21.06	31.29	28.96	21.14

4.2.5 Mafic lens

Mineral compositions of one of the rare mafic lenses in the diatexites (sample A106A; Figures 2.18; 3.11) have been analysed and are presented here in the context of the hosting diatexites. Modal compositions and petrography are presented in section 3.3.3.

Orthopyroxene is a hypersthene with uniform composition. The X_{Mg} values are 0.50 and the calcium contents are low (0.20 wt% CaO; Table 4.11). Plagioclase core compositions are slightly lower in anorthite content (77.5 mol%) compared to rim compositions (81.3 mol%). Biotite is secondary and formed along the boundaries of the orthopyroxene. It is chemically homogenous with X_{Mg} values of 0.52 and with TiO_2 contents of 4.04 mol%.

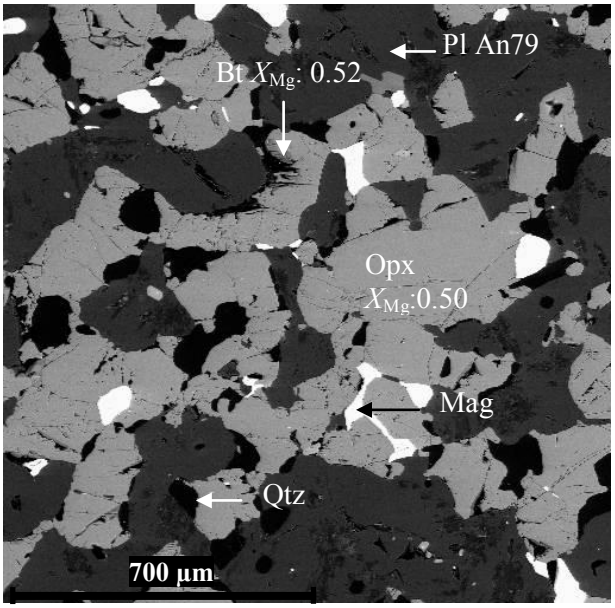

Figure 4.8. Backscatter images of mafic lens A106A. Biotite is scarce (1.4-2.3 vol%) occurring at the grain boundaries of orthopyroxene. Interstitial magnetite and quartz are also present in between orthopyroxene and plagioclase grains.

Table 4.11. Representative EDS analyses of orthopyroxene, plagioclase and biotite compositions from mafic lens within nebulitic diatexite A106A (see appendix 11 for all biotite analyses). EDS oxide totals for plagioclase analyses are normalised to 100%. The un-normalised totals are given in an additional row.

Phase	**Orthopyroxene**	**Plagioclase**		**Biotite**	
Sample	**A106A**	**Sample**	**A106A**	**Sample**	**A106A**
Method	**EDS**	**Method**	**EDS**	**Method**	**EDS**
Average	**Average (n=9)**	**Average**	**Average (n=4)**	**Average**	**Average (n=2)**
SiO_2	49.92	**SiO_2**	49.72	**SiO_2**	38.54
TiO_2	0.03	**Al_2O_3**	32.18	**TiO_2**	4.04
Al_2O_3	2.40	**MgO**	0.01	**Al_2O_3**	14.83
Cr_2O_3	-	**CaO**	15.51	**Cr_2O_3**	0.07
Fe_2O_3	-	**MnO**	0.03	**MgO**	13.01
MgO	17.03	**FeO**	0.30	**CaO**	0.09
CaO	0.20	**BaO**	-	**MnO**	0.08
MnO	0.37	**Na_2O**	2.20	**FeO**	21.28
FeO	29.86	**K_2O**	0.04	**BaO**	0.09
Na_2O	0.11	**Total**	100	**Na_2O**	0.11
K_2O	0.01	**Un-normalised EDS Total**	99.74	**K_2O**	7.73
Total	99.92	**Cations: O=8**		**Dry**	96.00
Cations: O=6		**Si**	2.27	**Total**	99.88
Si	1.93	**Al**	1.73	**Cations : O=24**	
Ti	-	**Mg**	-	**Si**	5.58
Al	0.11	**Ca**	0.76	**Ti**	0.44
Cr	-	**Mn**	-	**Al**	2.53
Fe^{3+}	-	**Fe**	0.01	**Cr**	0.01
Mg	0.98	**Ba**	-	**Mg**	2.81
Ca	0.01	**Na**	0.19	**Ca**	0.01
Mn	0.01	**K**	-	**Mn**	0.01
Fe^{2+}	0.97	**Total**	4.97	**Fe**	2.58
Na	0.01	**Or**	0.24	**Ba**	0.01
K	-	**An**	79.37	**Na**	0.03
Total	4.02	**Ab**	20.40	**K**	1.43
Enstatite	50.19			**Total**	15.44
Wollastonite	0.42			**X_{Mg}**	0.52
Ferrosillite	49.39				
X_{Mg}	0.50				

5. *Whole rock chemistry*

Representative major oxide whole rock chemical compositions from selected hand specimen domains were obtained using three methods, (i) X-ray fluorescence (XRF); (ii) Electron Dispersive Spectrometry (EDS) area scans, and (iii) compositions calculated from mineral compositions and modes using the 'Rock-Maker' software (Büttner, 2012).

Coarse to medium-grained rocks, such as leucocratic domains present in the Bysteek Formation mafic granulite sequence, or nebulitic diatexite domains from the Koenap Formation, were analysed using XRF techniques. Where geometrically possible, individual domains, such as melanosomes, were marked, mechanically separated, crushed and prepared for XRF analysis utilizing the fusion disc technique after Norrish and Hutton (1969). This method requires approximately 0.28g of the crushed material to be fused with 1.5g of flux and 0.028g of $NaNO_3$ and is then chemically analysed using the X-ray analyzer (see section 1.3.4). EDS area scans were used for the bulk analysis of fine-grained domains as well. The area scan tool of the EDS software interface allows the definition of polygonal areas of interest to be analysed.

The iron concentration in XRF and EDS area scans are reported as $FeO_{(tot)}$. Where ferric iron concentrations are known, such as in rocks where Fe_2O_3 is present in andraditic garnet and magnetite, the ferric iron in the whole rock has been calculated using Rock Maker (Büttner, 2012).

5.1 Mafic granulites and associated leucocratic domains

5.1.1 Nebulitic and stromatitic mesosomes

Three nebulitic mesosome samples (976B1-mes, 976B2-mes and 976A-mes) as well as a stromatitic mesosome (982E-n) were analysed using XRF and Rock Maker (Table 5.1). Nebulitic mesosomes show their variation in leucocratic and melanocratic portions at small scale that mechanically cannot be separated. Melanosomes and *in-situ* leucosomes are often so small in volume that again no material for XRF could be separated (see hand specimen section 2.1.1, Figures 2.2 and 2.3). Hence, these rocks were crushed as a whole and with their respective host, and analysed in order to identify the integrated composition of the whole rock before segregation of the anatectic components.

Nebulitic mesosomes are moderately rich in silica with 55-58 wt% SiO_2 containing 5.4-9.2 vol% of quartz. CaO contents are relatively high ranging between 12.5 and 15.0 wt %. Nebulitic mesosome 976A-mes has higher MgO wt% values (6.78-8.35 wt%) compared to those of 976B-mes (3.61-3.7 wt%). This is attributed to the higher X_{Mg} (0.65) in the

hedenbergite-rich clinopyroxene, compared to those of 976B-mes, where diopside-rich clinopyroxene has an average X_{Mg} of 0.40 (Table 4.1-analysis g, section 4.4.1).

The stromatitic mesosome in sample 982E-n is a specimen hosting *in-situ* leucocratic veinlets separated by alternating melanocratic bands and nebulitic domains. The SiO_2, Al_2O_3, MgO, $FeO_{(tot)}$ and CaO concentrations are similar to those of samples 976B-mes and 976A-mes. However, the stromatitic mesosome is more sodic (2.54-2.83 wt % Na_2O) in composition compared to those values observed in the analysed nebulitic mesosomes (Na_2O: 0.7-2.31 wt%). Conversely, 976B-mes is more potassic (2.34-3.94 wt% K_2O) than 976A-mes (0.13-0.12 wt% K_2O) and 982E-n (0.64-1.9 wt% K_2O). This is attributed to the quartz-alkali feldspar granite composition of the *in-situ* leucosomes present in 976B-mes, the anorthositic pockets and *in-situ* leucosome domains of 976A-mes and the syeno-granitic composition of the leucosome veins of 982E (see Section 3.1.4; Figure 3.5; Section 4.1.4; Table 4.6).

Table 5.1. Normalised mafic granulite nebulitic and stromatitic mesosome whole rock chemistry.[1]

Sample	**976B1-mes**	**976B2-mes**	**976A-mes**		**982E-mes**	
Domain	**Nebulitic mesosome**		**Nebulitic mesosome**		**Stromatitic mesosome**	
Method	**XRF**	**XRF**	**XRF**	**Rock Maker**	**XRF**	**Rock Maker**
SiO_2	57.87	57.31	55.73	54.92	55.91	53.32
TiO_2	1.12	0.75	0.62	0.64	0.95	0.85
Al_2O_3	13.03	12.16	10.04	9.82	11.41	10.53
Fe_2O_3	6.58	7.62	8.15	0.28	9.23	0.08
FeO	-	-	-	9.01	-	8.49
MnO	0.26	0.68	0.33	0.14	0.22	0.2
MgO	3.61	3.7	6.78	8.35	5.06	7.76
CaO	12.52	14.39	15.04	14.14	13.28	13.94
Na_2O	0.77	0.7	1.79	2.31	2.83	2.54
K_2O	3.94	2.34	1.2	0.13	0.64	1.91
P_2O_5	0.3	0.35	0.32	0.26	0.46	0.38
Total	100	100	100	100	100.00	100
Un-normalized Total	102.54	103.89	102.84	n.d	101.37	n.d
LOI	0.33	1.06	0.78	n.d	0.26	n.d
FeO (tot)	5.92	6.85	7.33	9.26	8.30	8.56
A	27.47	26.55	20.1	19.93	23.34	17.64
C	38.03	38.51	38.51	34.54	34.34	35.84
F	34.5	34.94	41.38	45.54	42.32	46.52
FeO (tot) + MgO	9.53	10.55	14.11	17.61	13.36	16.32
$Na_2O + K_2O$	4.71	3.04	2.99	2.44	3.47	4.45

[1] n.d: 'not –determined'- Rock Maker WR compositions do not need to be re-normalised as modal quantities total to 100%

5.1.2 Melanosomes

Three separate melanosome domains were analysed using EDS area scans, XRF and Rock Maker techniques (Table 5.2). 976B-mel is a magnetite free melanosome located along the periphery of the *in-situ* leucosomes (Figure 3.3b).The melanosome has the assemblage clinopyroxene (59-60 vol%), plagioclase (33-35 vol%) and quartz (4-5 vol%). The melanosome is basic with low silica values (50-53 wt% SiO_2) and high CaO values (18.54-18.92 wt%). The MgO values vary between 7.46-7.96 wt% whereas iron values range between 8.79-10.90 wt% $FeO_{(tot)}$. The Na_2O (0.69-0.73 wt%) and K_2O (0 wt%) values are lower than those occurring in the mesosomes, yet higher than those values from the mafic fragments due to the higher modal abundance of anorthitic plagioclase (33-35 vol%) (see Tables 3.2 and 3.3).

The melanosome (976B-2-g) shows a gradational transition from mesosome 976B-mes which does not contain phases with ferric iron into a domain containing andraditic garnet (Figure 3.3c). Andraditic garnet, present at modal values of 33-35 vol% (Table 3.2) causes high Fe_2O_3 concentrations in garnetiferous melanosomes (5.9-12.13 wt%). Ferrous iron contents are lower (4.39 wt% FeO) than those for the other garnet free melanosomes (8.11-9.77 wt%), mesosomes (6.58-9.19 wt%) and mafic fragments (6.7-9.3 wt%) (see Tables 5.1; 5.2 and 5.3). Due to the lower modal abundance of clinopyroxene (23-27 vol%), MgO wt% values are also significantly lower (3.56-4.34 wt %) compared to 7.37-7.96 wt% in garnet-free melanosomes.

J44-mel is a fine-grained melanosome with the assemblage orthopyroxene-amphibole-plagioclase-biotite ±clinopyroxene ±magnetite ±quartz (Figures 3.3d-e). In comparison to the melanosomes from 976B-mel and 976B-2-g, they are more aluminous (17.8-18.3 wt% Al_2O_3), sodic (2.34-2.71 wt% Na_2O) and potassic (1.11-1.82 wt% K_2O) due to the high abundance of hornblende amphibole (28 vol%) and less anorthitic plagioclase (26 vol%) (Table 3.2). As a result they are significantly less calcic exhibiting 9.16-9.87 wt % CaO (Table 5.2). However $FeO_{(tot)}$ values are similar (9.95-10.16 wt%) to those in 976B (8.79-10.90 wt%).

Table 5.2. Normalised mafic granulite melanosome whole rock chemistry.

Sample	**976B-mel**		**976B-2-g**			**J44A**	
Method	**EDS Area Scan**	**Rock Maker**	**EDS Area Scan**	**XRF**	**Rock Maker**	**EDS Area Scan**	**Rock Maker**
SiO_2	50.68	53.28	49.75	50.29	49.77	48.61	47.76
TiO_2	0.45	0.42	0.59	1.06	0.70	0.96	0.83
Al_2O_3	11.06	11.20	14.00	11.23	12.75	18.27	17.84
Fe_2O_3	9.77	-	11.5	12.13	5.90	9.95	0.21
FeO	-	8.11	-	-	4.39	-	9.95
MnO	0.24	0.13	0.19	0.37	0.17	0.22	0.12

Table 5.2. (continued).

Sample	976B-mel		976B-2-g			J44A	
Method	**EDS Area Scan**	**Rock Maker**	**EDS Area Scan**	**XRF**	**Rock Maker**	**EDS Area Scan**	**Rock Maker**
MgO	7.96	7.37	3.56	4.31	4.34	9.17	8.72
CaO	18.92	18.54	19.09	19.18	21.15	9.16	9.87
Na_2O	0.73	0.69	0.71	0.55	0.59	2.34	2.71
K_2O	0.00	0.00	0.21	0.56	0.00	1.11	1.82
P_2O_5	0.17	0.26	0.37	0.32	0.25	0.22	0.17
Total	100	100	100	100	100	100	100
Un-normalised total	103.22	n.d	102.04	104.72	103.03	102.57	n.d
LOI	n.d	n.d	n.d	0.457	n.d	n.d	n.d
FeO (tot)	8.79	8.11	10.34	10.90	10.29	9.95	10.16
A	12.62	13.72	25.19	21.15	21.97	35.28	32.49
C	43.42	44.95	50.48	50.81	53.37	19.79	22.35
F	43.96	41.34	24.33	28.04	24.66	44.93	45.15
FeO (tot) + MgO	16.75	15.48	13.90	15.21	14.63	18.12	18.88
$Na_2O + K_2O$	0.73	0.69	0.92	1.11	0.59	3.45	4.53

5.1.3 Mafic fragments

Three mafic fragments located within syenitic pools and quartz-syenitic leucocratic networks were analysed (Table 5.3). As expected the mafic fragments are basic in composition, exhibiting low silica (48-52 wt% SiO_2) high $FeO_{(tot)}$ (6.17-9.35 wt%), high MgO (11.45-16.31 wt%) and CaO (19.06-20.82 wt%). This is due to the high modal abundance of hedenbergite-rich clinopyroxene (85-92 vol%) and andesine (4.0-7.8 vol%) (see Tables 3.3 and 4.2).

Table 5. 3. Metabasite mafic fragment whole rock chemistry located in the leucocratic domains.

Sample	985A-m		982E-m		982C-m	
Domain	**Leucocratic network**		**Stromatitic mesosome**		**Leucocratic pool**	
Method	**XRF**	**Rock Maker**	**XRF**	**Rock Maker**	**XRF**	**Rock Maker**
SiO_2	48.69	50.12	50.92	52.82	50.49	51.42
TiO_2	0.48	0.31	0.22	0.30	0.63	0.37
Al_2O_3	7.23	7.97	3.27	2.88	6.63	7.02
Fe_2O_3	8.89	0.15	6.86	0.36	7.11	0.27
FeO	-	9.25	-	7.18	-	7.48
MnO	0.74	0.42	0.7	0.42	0.30	0.48
MgO	12.04	11.45	16.31	15.57	13.62	12.11
CaO	20.82	19.9	20.79	20	19.06	20.35
Na_2O	0.53	0.43	0.27	0.46	0.91	0.5
K_2O	0.4	-	0.41	0.01	1.06	-

Table 5.3 (continued).

Sample	985A-m		982E-m		982C-m	
Domain	**Leucocratic network**		**Stromatitic mesosome**		**Leucocratic pool**	
Method	**XRF**	**Rock Maker**	**XRF**	**Rock Maker**	**XRF**	**Rock Maker**
P_2O_5	0.18	-	0.25	-	0.19	-
Total	100	100	100	100	100	100
Un-normalised total	103.63	n.d	102.12	n.d	101.84	n.d
LOI	0.46	n.d	0.63	n.d	0.54	n.d
FeO (tot)	8.00	9.38	6.17	7.50	6.40	7.72
A	13.34	4.21	6.00	5.92	10.93	3.87
C	41.94	44.45	42.98	42.72	41.75	44.04
F	44.72	51.35	51.01	51.36	47.32	52.09
FeO (tot) + MgO	20.04	20.83	22.48	23.07	20.02	19.83
Na_2O + K_2O	0.93	0.43	0.68	0.47	1.97	0.5

5.1.4 Leucocratic domains

Leucocratic domains have been subdivided based on their field appearance and petrographic analysis (Figure 3.4, Section 3.1.4), which shows a strong segregation of quartz and K-feldspar into leucosomes whereas clinopyroxene, anorthitic plagioclase and titanite are retained in the solid residual. This section presents the chemical composition of the leucosome veins, networks, pockets and pools and presents their position in the TAS diagram (Figure 5.1; Middlemost, 1985).

Sample 976B-L (Figures 2.2b and 3.5b) is an *in-situ* leucosome of alkali feldspar composition (Figure 3.4-Streckeisen diagram) hosted within a nebulitic mesosome (976B-mes). Rock Maker calculations based on modal and mineral compositions yield results similar to EDS area scans (Tables 4.6) falling in range of the 'granite' field on the TAS diagram (Figure 5.1).

Leucocratic veins analysed from stromatitic mesosomes J9A-L and 982E-L are also granitic in composition. XRF and Rock Maker values indicate compositions of 75-77 wt% SiO_2, 12-13.3 wt% Al_2O_3. The leucosome veins are slightly more calcic (4.56-5.48 wt% CaO) and sodic (2.67-3.33 wt% Na_2O) than those of the *in-situ* leucosomes of 976B-L, but are much less potassic (1.74-2.82 wt% K_2O; Table 5.4).

Leucocratic pockets from two separate domains were analysed: sample 976A-L (Figure 2.2a; domain 4; Figure 3.5a) and J10B-L (Figure 2.6b). Sample 976A-L is anorthositic in composition (Figure 3.4) and is modally comprised of 94-95 vol% plagioclase, 2-3 vol % quartz, 2 vol% clinopyroxene with minor quantities of alkali feldspar (0.5 vol %). The XRF and

Rock Maker compositional results show a leucosome that is calcic (8.05-8.47 wt% CaO) and sodic rich (4.36-5.69 wt% Na_2O) with minor K_2O (1.95-2.22 wt%). The modal composition according to the Streckeisen classification (Streckeisen, 1976) is that of an 'anorthosite' (Figure 3.4; Table 3.5) and that of a monzonite according to the TAS classification (Middlemost, 1985). Leucocratic pocket J10B-L differs from 976A-L as it is quartz-monzonitic in composition (Figure 5.1). It is about 10% more silicic (68-70 wt% SiO_2), highly potassic (9.05-9.55 wt % K_2O), less sodic (1.31-1.51 Na_2O wt%) and calcic (2.73-3.12 wt% CaO). The Streckeisen classification indicates that it falls on the periphery of the alkali feldspar granite and quartz alkali feldspar syenite field (Figure 3.4). The modal and chemical differences (Tables 3.5 and 5.4) of pocket 976A-L (Figures 3.4 and 5.1) may imply a different mechanism to its origin in comparison to the other leucosome domains.

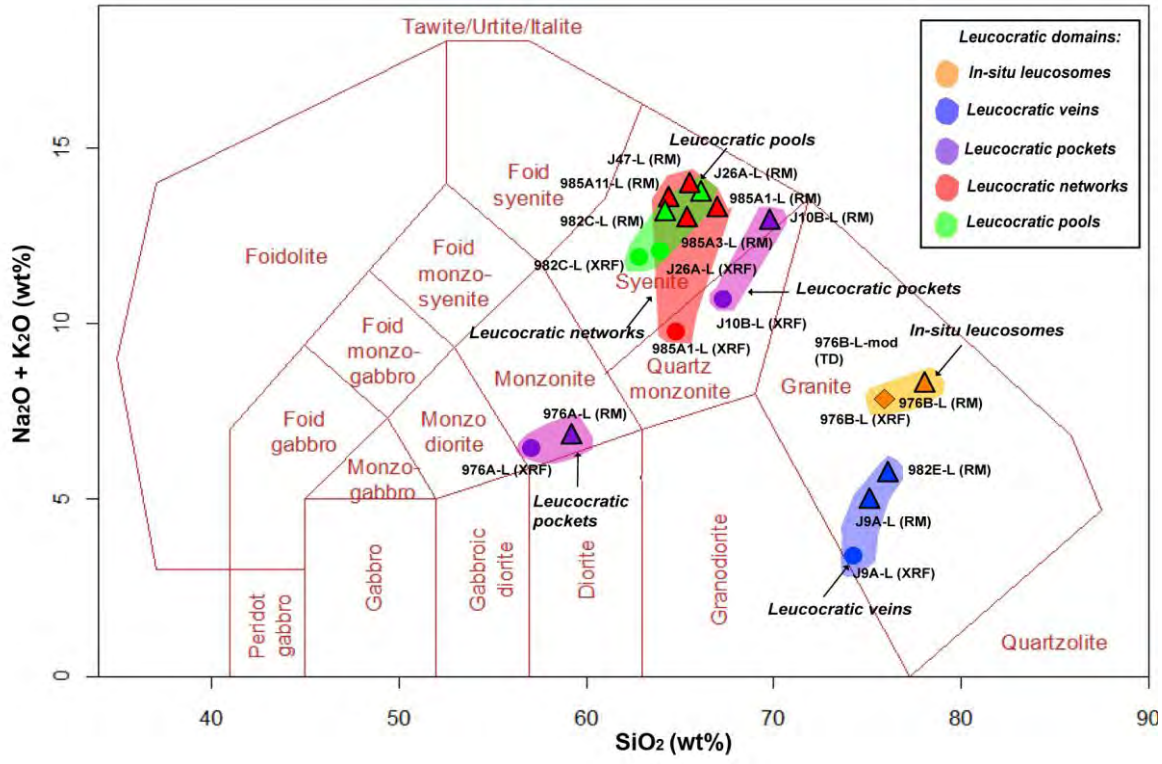

Figure 5.1. TAS diagram for leucocratic domains in mafic granulites of the Bysteek Formation (Middlemost, 1985). The *in-situ* leucosomes (orange field) and leucocratic veins (blue field) plot within the granite field. Leucocratic pockets (purple fields) plot within both monzonite and quartz-syenite/syenite fields. The leucocratic networks (red fields) and pools (green fields) both occur within the syenite fields as well. Triangles: whole-rock chemistries determined using the Rock Maker; circles: XRF data; diamonds: EDS area scans. The TAS classification was used on only the leucocratic domains and not the mafic domains of the mafic granulite sequence in order to compare and support the modal classification based on the Streckeisen diagram (Figure 3.4).

Table 5.4. Whole rock chemistry from mafic granulite *in-situ* leucosomes, leucocratic veins and pockets.

Domain	***In situ* leucosome**		**Leucocratic Veins**			**Leucocratic Pockets**			
Sample	**976B-L**		**J9A-L**		**982E-L**	**976A –L**		**J10B-L**	
IUGS Name (Streckeisen, 1976)	**Alkali feldspar Granite**		**Syenitic granite**		**Syenitic granite**	**Anorthosite**		**Alkali feldspar granite**	
TAS (Middlemost, 1985)	**Granite**		**Granite**		**Granite**	**Monzonite**		**Quartz monzonite**	**Syenite**
Method	**EDS-Area Scan**	**Rock Maker**	**XRF**	**Rock Maker**	**Rock Maker**	**XRF**	**Rock Maker**	**XRF**	**Rock Maker**
SiO_2	75.70	77.18	75.21	77.06	77.33	58.14	58.68	68.76	70.98
TiO_2	0.07	-	0.3	-	-	0.49	-	0.96	-
Al_2O_3	12.47	11.69	13.28	12.09	12.05	24.19	25.63	15.06	15.35
Fe_2O_3	0.15	-	0.88	-	-	0.94	-	0.81	-
MnO	-	-	0.59	-	-	0.17	-	0.18	-
MgO	0.16	-	0.53	-	-	0.91	-	0.43	-
CaO	3.36	2.97	4.63	5.48	4.56	8.47	8.05	2.73	3.12
Na_2O	1.31	1.09	2.67	3.33	3.24	4.36	5.69	1.35	1.51
K_2O	6.59	7.07	1.74	2.04	2.82	2.22	1.95	9.55	9.04
P_2O_5	0.19	-	0.17	-	-	0.11	-	0.17	-
Total	100	100	100	100	100	100	100	100	100
Un-normalized total	99.83	n.d.	101.37	n.d.	n.d.	101.49	n.d.	103.64	n.d.
LOI	n.d	n.d	0.431	n.d	n.d	0.30	n.d	0.831	n.d
FeO (tot)	0.13	-	0.79	-	-	0.85	-	0.73	-
FeO (tot) + MgO	0.29	-	1.32	-	-	1.76	-	1.16	-
$Na_2O + K_2O$	7.85	8.16	4.41	5.37	6.05	6.47	6.74	10.67	12.72
$Na_2O + CaO$	4.67	4.06	7.3	8.81	7.8	12.83	13.74	4.08	4.63

Table 5.5. Whole rock chemistry from mafic granulite leucocratic networks and pools.

Domain	Leucocratic Networks					Leucocratic Pool			
Sample	985A1 –L		985A3	985A11	J47	982C-L		J26L	
IUGS Name (Streckeisen, 1976)	Quartz syenite	Syenite	Quartz syenite	Quartz-alkali feldspar syenite	Quartz syenite	Alkali feldspar syenite		Syenite	
TAS (Middlemost, 1985)	Syenite-quartz monzonite	Syenite	Syenite	Syenite	Syenite	Syenite		Syenite	
Method	XRF	Rock Maker	Rock Maker	Rock Maker	Rock Maker	XRF	Rock Maker	XRF	Rock Maker
SiO_2	65.40	66.87	64.20	64.22	64.86	62.24	64.02	63.76	66.57
TiO_2	0.35	-	-	-	-	0.55	-	0.50	-
Al_2O_3	17.41	18.62	19.96	17.65	18.11	17.61	19.03	17.62	17.69
Fe_2O_3	1.77	-	-	-	-	1.94	-	1.80	-
MnO	0.65	-	-	-	-	0.19	-	0.18	-
MgO	0.23	-	-	-	-	1.03	-	1.32	-
CaO	3.74	2.86	2.68	2.67	1.72	4.06	3.65	2.58	2.35
Na_2O	1.94	2.20	1.49	2.16	2.92	2.15	2.7	2.16	2.79
K_2O	8.20	9.45	11.68	13.29	12.39	9.82	10.6	9.87	10.61
P_2O_5	0.31	-	-	-	-	0.41	-	0.21	-
Total	100	100	100	100	100	100	100	100	100
Un-normalized total	102.06	n.d.	n.d	n.d	n.d	102.61	101.06	103.57	n.d
LOI	0.108	n.d	n.d	n.d	n.d	0.451	0.238	0.917	n.d
FeO (tot)	1.59	-	-	-	-	1.75	-	1.62	-
FeO (tot) + MgO	1.82	-	-	-	-	2.78	-	2.94	-
$Na_2O + K_2O$	10.14	12.88	13.17	14.43	13.62	11.97	13.38	12.03	15.02
$Na_2O + CaO$	5.68	5.06	4.17	4.83	4.64	6.21	6.35	4.74	5.14

Leucocratic network samples from two separate locations (985A and J47; Figures 2.8 and 2.13) were analysed in order to compare their modal and bulk compositions. The modal compositions of the samples are presented in section 3.1.4 (Table 3.4)

Rock Maker and XRF results (Tables 5.4 and 5.5), plotted in the TAS diagram, (Figure 5.1) show the primarily syenitic to quartz-monzonitic composition of the leucocratic networks. Similar results are obtained from the Streckeisen diagram (Streckeisen, 1976), where normalised values plot in the fields of quartz-alkali feldspar syenite (samples 985A and J47, Figure 3.4)

XRF and Rock Maker analysis were performed on two separate leucocratic pools (sample 982C-L and J26L, Figures 2.10 and 3.6e), both showing similar syenitic compositions. The investigated pools are almost free of quartz (Table 3.5).

5.1.5 Mesosome, melanosome and leucosome segregation trends

Most of the leucosomes in the mafic granulites of the Bysteek Formation concentrate either alkali feldspar or sodic plagioclase, and often are quartz-rich. The melanosome retains clinopyroxene and anorthitic plagioclase. In order to describe this segregation of mafic and felsic domains the compositions of the different analysed domains have been plotted on FeO_{tot}+MgO *vs.* Na_2O+K_2O and FeO_{tot}+MgO *vs.* SiO_2 diagrams (Figure 5.2). These two diagrams are considered to describe best the separation of leucosomes from melanosomes, and hence the segregation of the protolith during anatexis.

The mafic fragments hosted in the leucocratic networks and pools are iron and magnesium rich (19-22 wt% FeO_{tot}+MgO) and show SiO_2 contents of 48-50 wt%. Alkali contents are variable (0.4-0.93 wt% Na_2O+K_2O). CaO contents vary between 19-20 wt% (Table 5.3). The variations in compositions are attributed to the variable modal abundance of secondary amphibole, most likely caused by metasomatic processes (See section 3.1.2, Figure 3.2d-e).

Compared to the fragments in networks and pools, the nebulitic mesosomes are similar yet richer in the alkalis (Na_2O+ K_2O 2.4-4.7 wt%) but slightly more silicic (53-58 wt% SiO_2). They are lower in FeO_{tot}+MgO content (10-17 wt% compared to 17-25 wt%). The stromatitic mesosome compositions (sample 982E-n) are similar to the nebulitic mesosome compositions (Table 5.1).

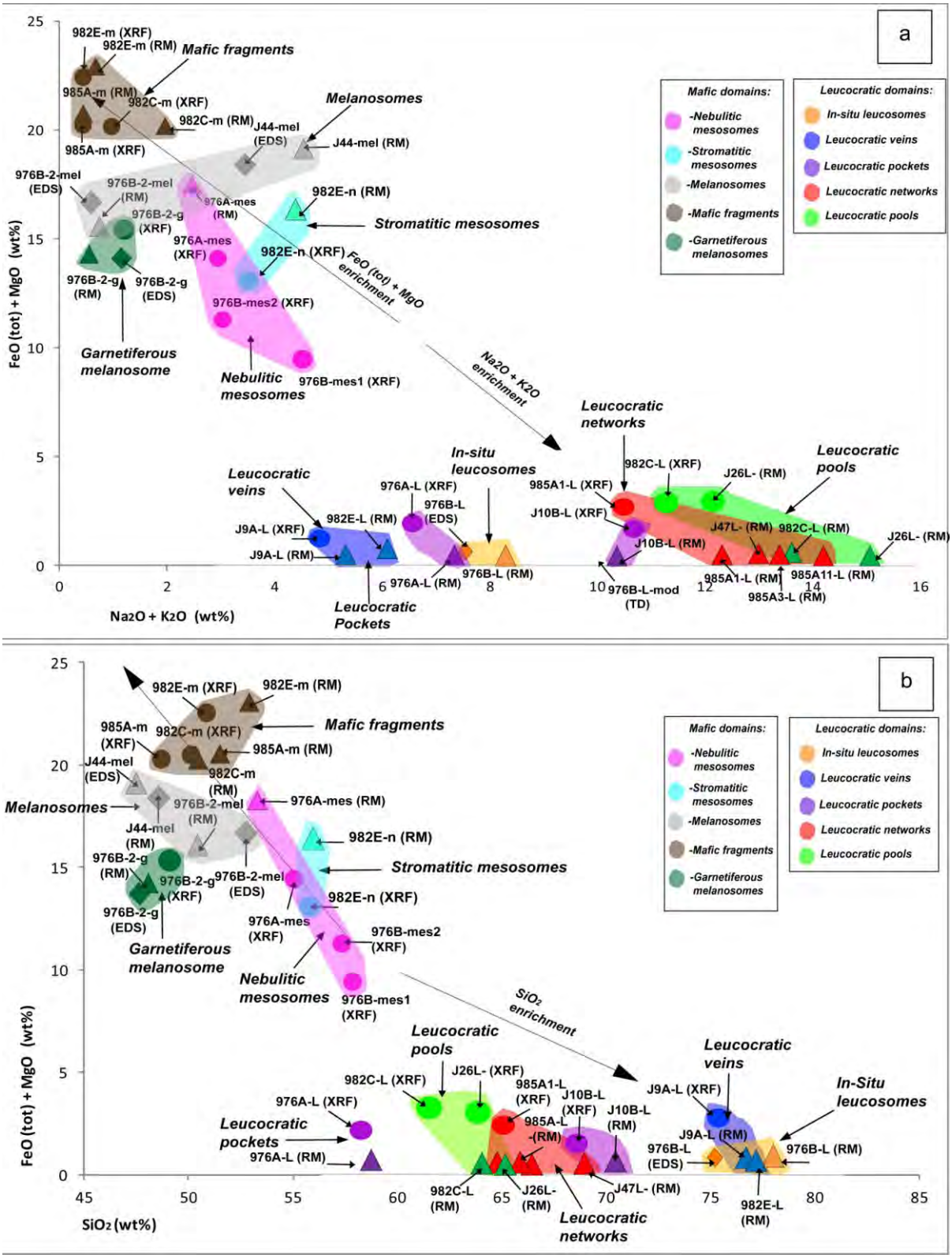

Figure 5.2. Compositional trends between the nebulitic (pink fields), stromatitic mesosomes (pale blue fields), garnet-free melanosomes (grey fields), garnetiferous melanosomes (dark green fields), mafic fragments (brown fields) and leucocratic domains of the Bysteek Formation mafic granulites. A negative linear correlation exists, whereby mafic domains are enriched in $FeO_{(tot)}$ + MgO, yet depleted in Na_2O, K_2O and SiO_2. Triangles: whole-rock chemistries determined using the Rock Maker; circles: XRF data; diamonds: EDS area scans.

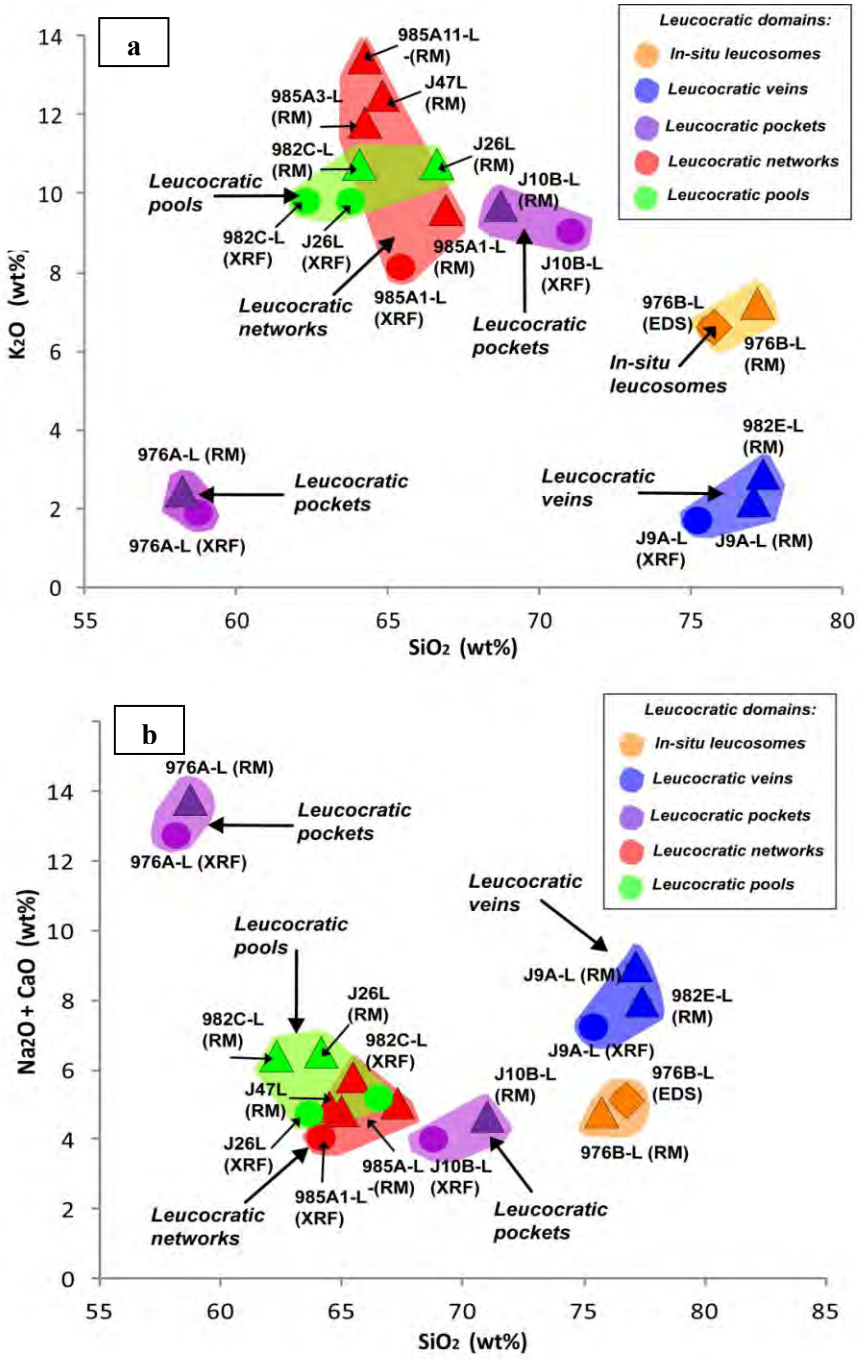

Figure 5.3. Variation diagram for leucosome domains from the mafic granulite sequence. A negative linear correlation is present in (a) whereby leucocratic veins (blue fields) and *in-situ* leucosomes (orange fields) are less potassic (1.74-9.55 wt%) than leucocratic pools (green fields), networks (red fields) and pocket J10B (8.2-13.3 wt%). Conversely, in (b) a positive linear correlation occurs whereby the *in-situ* leucosomes and veins are richer in silica and Na_2O + CaO in comparison to networks, pools and pockets. The exception being pocket 976A-L which is comprised of andesine plagioclase (94 vol%) and minor quartz (2-3 vol%). This accounts for its low K_2O and high Na_2O + CaO (wt%) (Tables 5.4-5.5). Triangles: whole-rock chemistries determined using the Rock Maker; circles: XRF data; diamonds: EDS area scans.

The garnetiferous melanosome 976B-2-g has both low SiO_2 and Na_2O+K_2O (Table 5.2) which is due to the high modal abundance (38 vol%) of andraditic garnet. The leucosome domains are generally FeO and MgO free, however the presence of high mafic oxides is due to the incorporation of detached mafic phases (frequently clinopyroxene) that have broken from its source and crystallised within the leucocratic domain (Figures 3.5-3.7)

Figure 5.2 shows a systematic trend to less mafic and more alkalic compositions from mafic fragments and melanosomes via stromatitic mesosomes to nebulitic mesosomes. All segregated leucosomes are largely free of iron and magnesium or contain less than 5 wt% of the oxides. Similar to the negative correlation between $FeO_{tot}+MgO$ and Na_2O+K_2O, melanosomes and mesosomes also show decreasing $FeO_{tot}+MgO$ with increasing SiO_2 (Figure 5.2).

Various types of leucosomes (pools, networks, pockets) show variable Na_2O+K_2O compositions ranging from 3-15 wt%. A similar variability is seen in the SiO_2 content of the leucosomes which range from 55-75 wt% (Figure 5.3). The Na_2O+K_2O *vs*. SiO_2 (TAS) diagram for the leucosomes (Figure 5.1) shows a negative linear correlation for different leucosome types other than leucocratic pockets (sample 976A-L). This trend reflects the variation in modal contents in quartz, plagioclase and alkali feldspar (Tables 3.4-3.5, section 3.1.4). Similarly the Na_2O+CaO *vs.* SiO_2 diagram (Figure 5.3b) shares the negative linear correlation showing leucocratic pocket J10B-L, networks and pools exhibiting Na_2O+CaO (wt%) values between 2.5-6.5 wt%, whereas in-situ leucosome domains and leucocratic veins having higher Na_2O + CaO values (4-8.5 wt%).

The trends shown in Figures 5.1-5.3 are interpreted to reflect various degrees of segregation of leucosome and melanosome during anatexis with stromatitic and nebulitic mesosomes representing a poorly segregated variety of anatexites in the mafic series whereas leucosomes and melanosome compositions are endmembers of the segregation trends, confirming their field relationships as physically separated rocks. The variability amongst the various types of leucosomes is caused by variable modes of quartz and feldspar. Given that some of the rocks are coarse-grained, nugget effects of large quartz or feldspar crystals might have contributed to the variation seen in the leucosome compositions.

5.2 Diatexite whole rock chemistry

Whole rock chemical analyses of diatexites from the Koenap Formation allow the comparison of leucocratic, nebulitic, banded and melanocratic diatexite types. Thirteen samples were analysed in total. The nebulitic diatexites and melanocratic domain whole rock chemistry falls in range of the pelitic field of the AKF ternary diagram (Winkler, 1967). The banded diatexites however fall in both pelitic and greywacke fields, whereas the leucocratic domains range between greywacke and alkali granite fields (Figure 5.4).

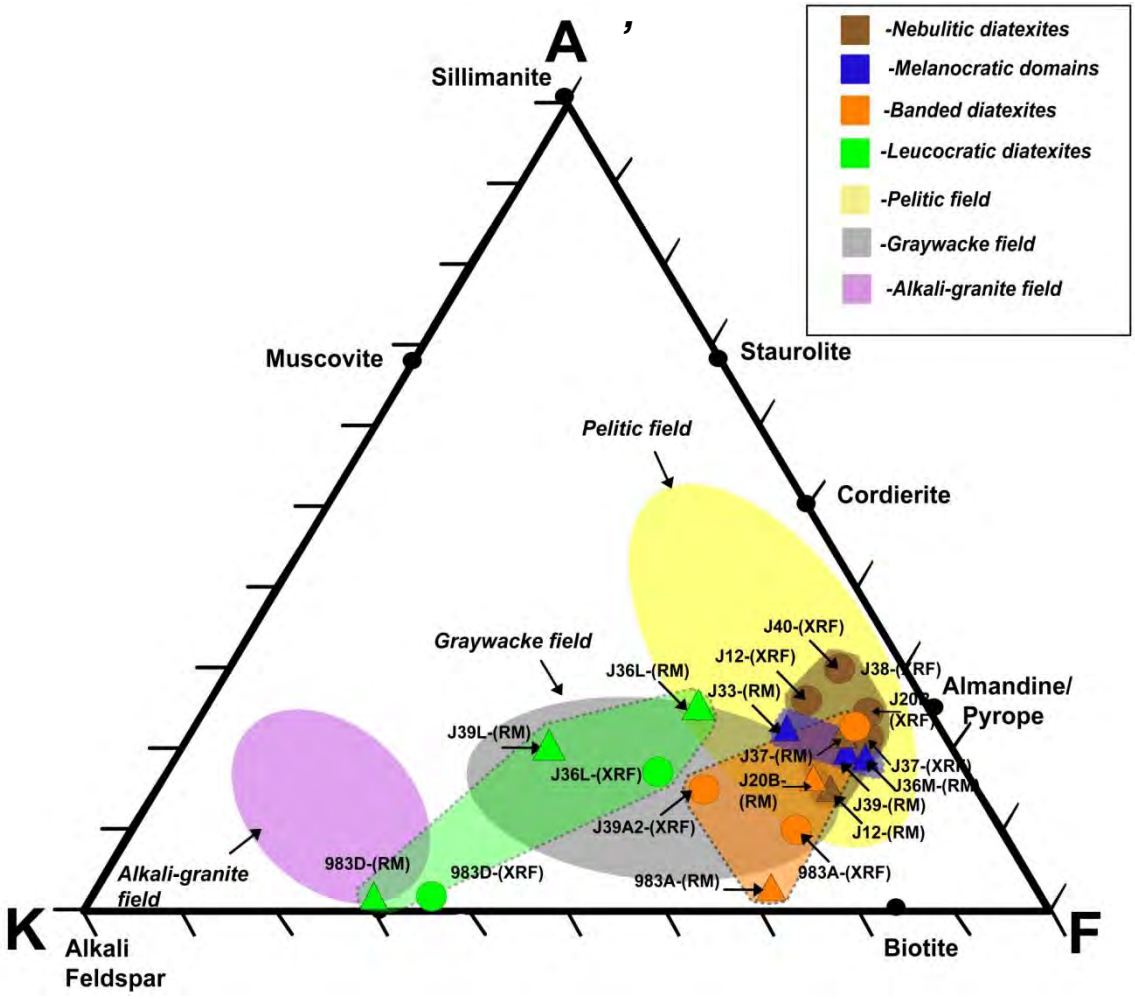

Figure 5.4 A'KF chemographic representation of analysed diatexite whole rock chemistries (Winkler, 1967). The nebulitic diatexite domains (highlighted in brown) and melanocratic domains (blue) reside within the pelitic field. Banded domains (orange) extend between the pelitic and greywacke field. However, the leucocratic diatexite domains (green) range between greywacke and alkali-granite fields. Triangles: Rock Maker calculations; circles: XRF data.

5.2.1 Leucocratic diatexites

Two varieties of leucocratic diatexites have been analysed (Table 5.6): the massive leucocratic sample 983D (Figure 2.14c) and banded leucocratic domains (samples J36L, J39L- Figures 2.14 a and d). They exhibit variably high modal abundances of quartz (42-48 vol%) alkali feldspar (35-38 vol%) and generally low presence of garnet or cordierite. This in turn results in high values of SiO_2 (73-78 wt%), and K_2O (3.25-6.73 wt.%). Due to the low modal contents of garnet, cordierite and biotite, MgO and $FeO_{(tot)}$ values are low (0.88-3.54 wt%). Calcium and sodium are present in significant amounts in the leucocratic domains with CaO values ranging between 0.68-1.57 wt% and Na_2O between 1.03-4.89 wt% respectively.

Table 5.6. Leucocratic diatexite domain whole rock chemistry

Domain	**Massive leucocratic domain**		**Banded leucocratic domain**			
Sample	**983D**		**J36L**		**J39A-L**	
Method	**XRF**	**Rock Maker**	**XRF**	**Rock Maker**	**EDS-Area Scan**	**Rock Maker**
SiO_2	76.55	78.92	74.83	77.47	73.23	74.85
TiO_2	0.5	-	0.68	-	0.19	-
Al_2O_3	11.43	10.64	12.53	11.71	14.41	14.64
Fe_2O_3	1.81	0.02	3.32	0.1	1.10	0.12
FeO	-	1.1	-	3.45	-	0.77
MnO	0.15	-	0.18	-	0.11	-
MgO	0.54	0.64	1.00	1.53	0.47	0.76
CaO	1.27	0.68	1.4	0.81	1.57	1.15
Na_2O	1.72	1.27	1.57	1.03	4.89	4.46
K_2O	5.94	6.73	4.38	3.9	3.84	3.25
P_2O_5	0.09	-	0.11	-	0.19	-
Total	100	100	100	100	100	100
Un-normalised Total	102.65	n.d.	103.42	n.d.	99.64	n.d.
LOI	0.712	n.d.	0.673	n.d.	n.d.	n.d.
FeO (tot)	1.63	1.12	2.99	3.54	0.99	0.88
A'	0.43	0.21	37.55	40.60	43.93	55.24
F	61.00	69.45	31.15	26.09	39.88	30.43
K	38.58	30.34	31.29	33.31	16.20	14.33
A	74.27	76.90	63.31	56.78	84.14	82.11
F	16.79	11.48	23.84	24.50	9.12	7.07
M	8.93	11.62	12.85	18.72	6.74	10.82

5.2.2 Nebulitic diatexites

Three nebulitic diatexite samples (J12, J37 and J38) were chemically analysed (Table 5.8). The abundant garnet (9-18 vol%), biotite (5-11% vol%) and pinitised cordierite (3-8 vol%) are reflected in moderately high silica content (60-67 wt% SiO_2) and $FeO_{(tot)}$ (7.16-12.88 wt%). The MgO (1.76-3.46 wt%) and K_2O (2.02-3.47 wt%) contents are higher than in the leucocratic diatexites, yet lower than in banded and melanocratic domains (Table 5.7).

Table 5.7. Nebulitic diatexite whole rock chemistry

Domain	**Nebulitic diatexite**				
Sample	**J37**		**J38**	**J12A**	
Method	**XRF**	**Rock Maker**	**XRF**	**XRF**	**Rock Maker**
SiO_2	60.54	60.39	63.80	67.32	65.67
TiO_2	1.68	-	1.67	1.63	-
Al_2O_3	15.03	16.66	15.47	15.01	15.95
Fe_2O_3	14.10	-	10.63	7.96	-
FeO	n.d	12.88	n.d	n.d	7.33
MnO	0.25	-	0.29	0.27	-
MgO	3.46	3.33	2.73	1.76	2.44
CaO	0.78	1.04	1.63	1.22	2.35
Na_2O	0.72	0.88	1.36	1.63	2.63
K_2O	3.34	4.16	2.31	3.08	3.47
P_2O_5	0.10	-	0.11	0.12	-
Total	100	100	100	100	100
Un-normalised total	101.73	n.d	103.29	100.62	n.d
LOI	0.574	n.d	0.749	0.691	n.d
FeO (tot)	12.69	12.88	9.56	7.16	7.33
A'	22.50	22.80	39.76	41.85	36.68
K	8.83	11.15	8.84	13.91	16.59
F	68.67	66.05	51.40	44.24	46.72
A	34.31	37.61	41.31	48.84	48.67
F	45.71	43.37	40.27	36.72	32.50
M	19.98	19.03	18.42	14.44	18.83

5.2.3 Banded diatexites

The banded diatexites are defined by their banded-layered appearance between leucocratic and melanocratic domains (Figures 2.15-16). The banded diatexite domains vary between poorly banded (sample 983A-Figure 2.16b) to diffusely banded (samples J20B and J39A2). Samples 983A and J20B exhibit similar whole rock chemistries with $FeO_{(tot)}$ ranging between 8-13 wt % and Na_2O varying between 0.69 and 1.79 wt % (Table 5.8). However diffusely banded domains

from sample J39A-2 exhibits higher Na_2O (3.41-3.54 wt%) and lower $FeO_{(tot)}$ (2.91-3.03 wt%). This is attributed to the lower modal abundance of garnet (2-2.7 vol%) when in comparison to the sample 983A and J20B (14-17 vol%). Additionally the lower modal quantities of biotite (3-7 vol%) and higher quantities of alkali feldspar (43-46 vol%) in J39A2 further contribute to high K_2O content (Table 3.8).

Table 5.8. Poorly banded and diffusely banded diatexite whole rock chemistry.

Domain	**Poorly Banded Diatexite**		**Diffusely Banded Diatexite**				
Sample	**983A**		**J20B**		**J39A2**		**J40**
Method	**XRF**	**Rock Maker**	**XRF**	**Rock Maker**	**XRF**	**Rock Maker**	**XRF**
SiO_2	66.46	67.31	62.87	60.97	71.3	72.73	65.68
TiO_2	1.29	-	1.5	-	0.69	-	1.77
Al_2O_3	13.29	12.06	14.97	15.49	14.77	13.12	15.41
Fe_2O_3	8.91	0.23	11.45	0.38	2.91	0.02	11.32
FeO	-	9.81	-	13.06	-	3.01	-
MnO	0.26	-	0.32	-	0.15	-	0.34
MgO	1.64	1.53	3.26	2.52	1.26	1.52	0.99
CaO	1.31	1.05	1.18	1.15	1.92	2.02	1.39
Na_2O	1.79	1.34	0.85	0.69	3.41	3.54	0.98
K_2O	4.93	6.67	3.5	5.74	3.45	4.04	2.02
P_2O_5	0.12	-	0.1	-	0.14	-	0.10
Total	100.00	100.00	100.00	100.00	100.00	100.00	100.00
Un-normalised total	102.28	n.d	101.76	n.d	103.02	n.d	101.14
LOI	0.711	n.d	0.433	n.d	0.606	n.d	0.529
FeO (tot)	8.02	10.02	10.30	13. 48	2.61	3.03	10.19
A'	10.99	3.30	34.89	28.00	43.68	29.23	43.32
K	21.42	27.95	12.51	19.39	25.07	33.36	7.86
F	67.59	68.75	52.59	52.62	31.25	37.41	48.81
A	44.20	39.95	37.98	37.86	66.86	61.75	45.36
F	42.04	47.25	41.16	46.56	18.71	20.22	47.24
M	13.76	12.80	20.86	15.58	14.43	18.02	7.39

5.2.4 Melanocratic diatexite domains and mafic lenses

Three melanocratic diatexite domain samples were analysed (J33M, J36M and J39M; section 3.3.2). These samples comprise largely of garnet (7-15 vol%), pinite (11-16 vol%), magnetite (5-7 vol%), biotite (5-31 vol%), and secondary sillimanite (9-10 vol%) and show only minor or no quartz and feldspar (Figure 3.3.5). This accounts to their high aluminium content (17.3- 20.5 wt% Al_2O_3), high K_2O (5.06-7.0 wt%), MgO and $FeO_{(tot)}$ contents (6.47-8.03 and 8.55-12 wt% respectively), and relatively low lower SiO_2 content (55-57 wt%) compared to the leucocratic,

nebulitic and banded diatexite domains (60-77 wt SiO_2%; Tables 5.6, 5.7, 5.8). The whole rock compositions of the melanocratic domain reflects its mafic mineralogy with FeO contents between 8 and 12 wt% and SiO_2 below 65 wt%. Magnesium (~7 wt% MgO) is high due to the abundance of cordierite (Table 5.9).

Samples from two mafic lenses (section 2.3.4 samples 983E-m and A106A) were analysed. They are comprised of orthopyroxene (54-58 vol%) plagioclase (35-38 vol%) and minor biotite (1.4-2.3 vol%) with little quartz (0.6-0.7 vol%). They accordingly show low SiO_2 (47-53 wt%) and high $FeO_{(tot)}$ (11-16 wt%) and MgO content (5.73-9.26 wt%) (Table 5.9).

Table 5.9. Mafic lens and melanocratic diatexite domain whole rock chemistry

Domain	**Mafic lenses**				**Melanocratic domains**		
Sample	**983E**	**983E-b**	**A106A**	**A106A**	**J33**	**J36M**	**J39M**
Method	**Rock Maker**	**Rock Maker**	**EDS Area Scan**	**Rock Maker**	**Rock Maker**	**Rock Maker**	**Rock Maker**
SiO_2	47.69	50.41	51.43	53.36	56.03	55.22	57.01
TiO_2	1.35	0.00	0.83	-	-	-	-
Al_2O_3	14.35	16.47	19.98	17.78	20.48	18.08	17.32
Fe_2O_3	0.12	0.17	-	0.22	0.68	0.51	0.33
FeO	16.67	14.23	12.17	16.52	7.94	11.54	11.88
MnO	0.74	-	0.06	-	-	-	-
MgO	7.72	9.26	5.73	7.32	6.47	8.03	7.13
CaO	9.55	7.20	7.87	5.23	0.75	1.2	0.71
Na_2O	0.16	0.31	1.27	1.34	0.65	0.4	0.02
K_2O	1.41	1.95	0.47	0.33	7.0	5.02	5.6
P_2O_5	0.24	-	0.19	-	-	-	-
Total	100	100	100	100	100	100	100
Un-Normalised Total	n.d	n.d	99.73	n.d	n.d	n.d	n.d
FeO (tot)	16.78	14.38	12.17	16.72	8.55	12.00	12.18
A'	-	-	-	-	23.55	19.31	31.51
K	-	-	-	-	16.43	10.40	15.59
F	-	-	-	-	60.02	70.29	52.91
A	24.86	27.29	38.63	24.86	41.73	32.57	32.86
F	41.31	33.89	33.35	41.31	24.94	30.82	32.92
M	33.83	38.83	28.02	33.83	33.33	36.61	34.22

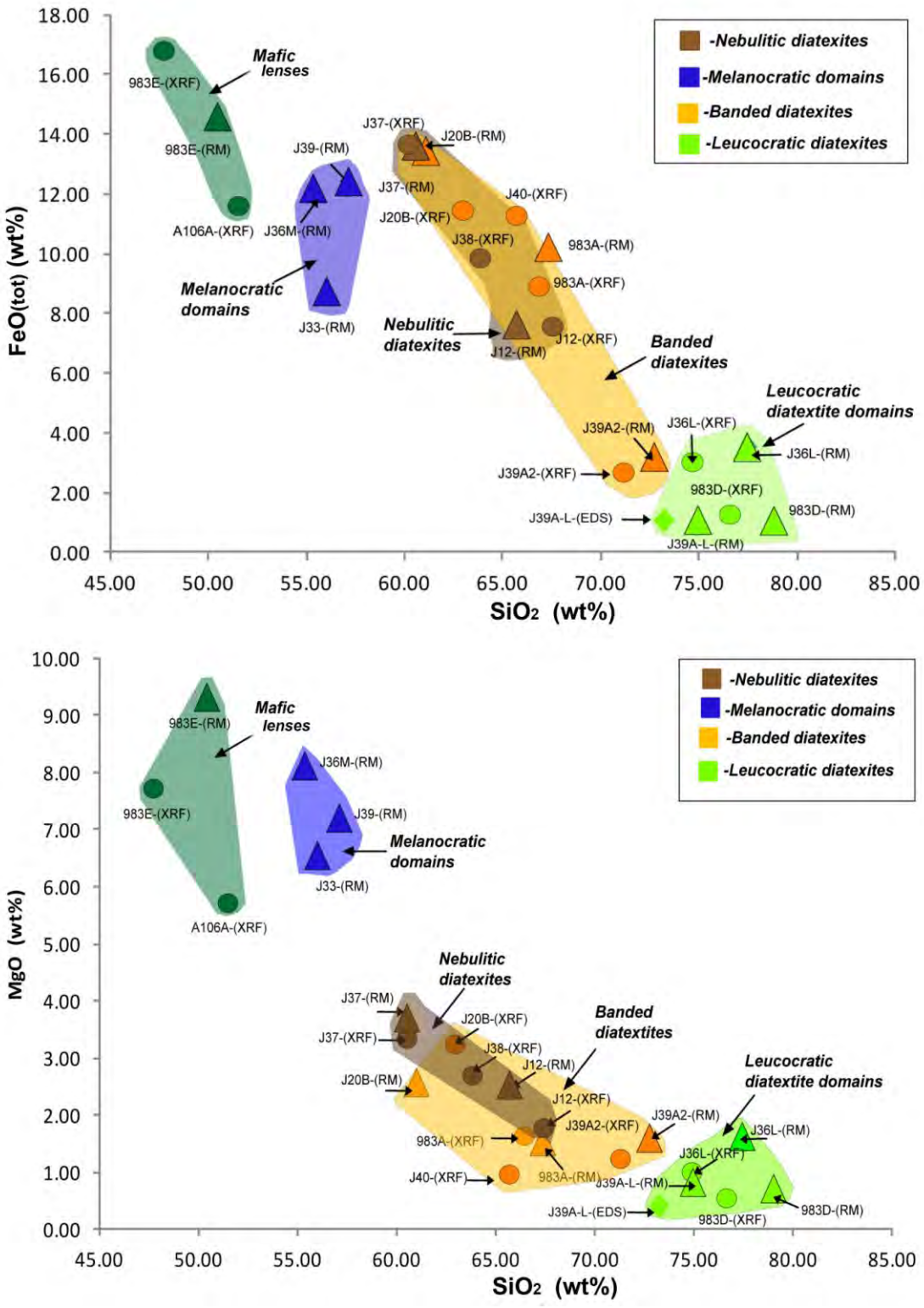

Figure 5.5. Harker variation diagram of $FeO_{(tot)}$ and MgO *vs.* SiO_2 for diatexite leucocratic, nebulitic, banded, melanocratic domains and mafic fragments. A systematic negative trend occurs for MgO and $FeO_{(tot)}$, whereby mafic lenses and melanocratic domains are typically richer in $FeO_{(tot)}$ and MgO due to a higher modal abundance of garnet and cordierite (in melanocratic domains) and orthopyroxene (in mafic lenses). Conversely leucocratic domains are richer in silica. The nebulitic diatexites and some banded domains exhibit intermediate compositions with as high $FeO_{(tot)}$, similar to melanocratic domains, and fair amounts of silica (60-67 wt%).

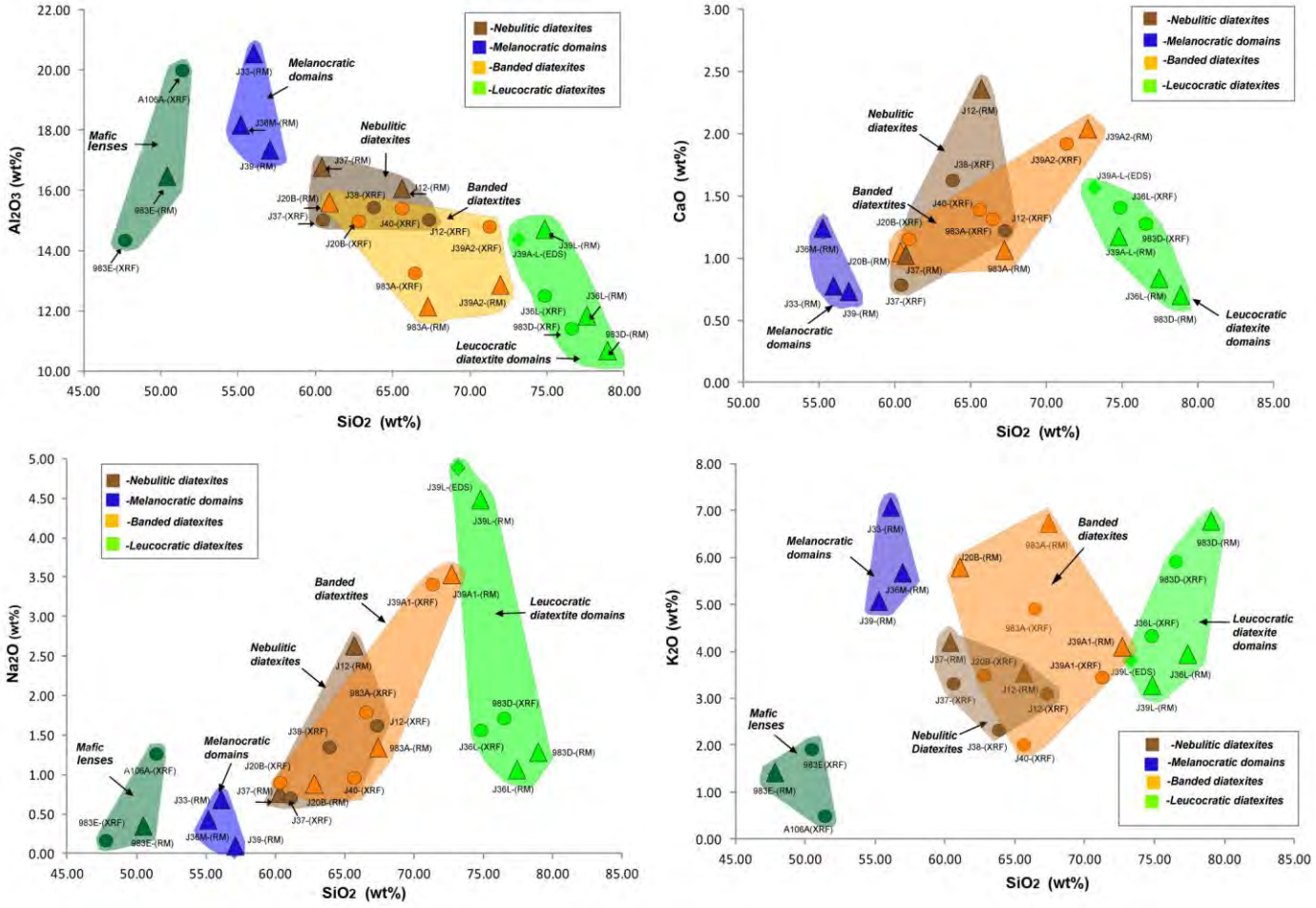

Figure 5.6. Harker variation diagram of Al_2O_3, CaO, Na_2O and K_2O for diatexite leucocratic, nebulitic, banded, melanocratic domains and mafic lenses. CaO and Na_2O concentrations are unsystematic in the diatexites depending on the modal quantities of plagioclase which are generally low and variable in diatexite domains (1-13 vol%). Only two domains (J39A1 and J39L) exhibit high modal sodic content (An16-22; ~13 vol%). Potassium content is similarly unsystematic and is high wherever biotite and alkali feldspar is present. K_2O is typically low in mafic fragments due to the absence of alkali-feldspar. Al_2O_3 concentrations exhibit a negative systematic trend, whereby melanocratic domains are high due to the presence of aluminium rich phases such as garnet, cordierite and biotite.

In summary of the major element variations, Harker diagrams (Figure 5.4-5.5) show less systematic trends compared to the trends seen in the mafic series of the Bysteek Formation (Figures 5.2-5.3). Only $FeO_{(tot)}$ and MgO *vs.* SiO_2 show systematic negative correlations which can be expected due to the low silica content of mafic minerals, which are more or less abundant in different samples. Similarly, the aluminium contents in the mafic domains are slightly higher than in more leucocratic domains, due to high garnet and cordierite contents. The contribution of the aluminium-rich plagioclase in some leucocratic domains (samples J36-L; J39-L and 983D; Figures 3.9; Table 3.6) is counteracted by high quartz contents, which reduces the Al_2O_3 content in the samples in favour of high SiO_2 concentrations. CaO and Na_2O vary unsystematically amongst the various diatexite domains depending upon their plagioclase content, which is low in the melanocratic domain and the mafic lens. Potassium is high where abundant alkali feldspar or biotite is present.

These unsystematic relationships argue against a systematic differentiation within the diatexites, for which also no convincing field evidence exists. However, the intense anatexis may have caused mobilisation of melt from which leucocratic domains crystallised. Peritectic garnet and cordierite, forming secondary biotite later, may have remained closer to the source, forming mafic layers and domains.

5.3 Chemographic mineral and whole rock relationships

ACF and AFM ternary phase diagrams were used illustrate the compositional relationship between whole rock and mineral chemistries of selected domains and associated mineral assemblages.

5.3.1 Mafic granulite compositions

The ACF diagram (Orville, 1969) in Figure 5.7 shows the relationship between mineral and whole rock composition in mafic rocks of the Bysteek Formation. On the left hand side, clinopyroxene, calcic-garnet and anorthitic plagioclase constitute the corners of a triangle. Accordingly, the garnet bearing melanosomes (sample 976B-2-g) plot within that triangle whereas those mafic granulites that are free of garnet plot on the tie line connecting clinopyroxene and plagioclase, the main phases in these rocks. The shifting of the garnet bearing rocks away from that tie line is caused by the oxidation of some of the ferrous iron. Ferric iron is added to the aluminium proportion and subtracted from the iron component, casing the rocks composition plotting further left and up from the other mafic granulites, inside the triangle.

On the right hand side of the ACF diagram orthopyroxene, clinopyroxene and plagioclase form a second triangle. Secondary amphibole plots on the orthopyroxene-plagioclase tie line. In a subsequent fluid-assisted breakdown, biotite forms after amphibole (section 3.1.2, Figure 3.2d-e). The anorthite content in the plagioclase of J44 is substantially lower than in other melanosomes (~An60 *vs.* ~An90), correlating with the higher sodium content (Table 4.5). It is therefore likely that the metasomatic fluid that led to the formation of amphibole and plagioclase also reacted with the plagioclase.

The WR composition of J44 plots close to the tie line connecting the secondary biotite with plagioclase but much higher in the ACF diagram than other mafic granulites. This shifting is interpreted as expression of the metasomatism in the sample.

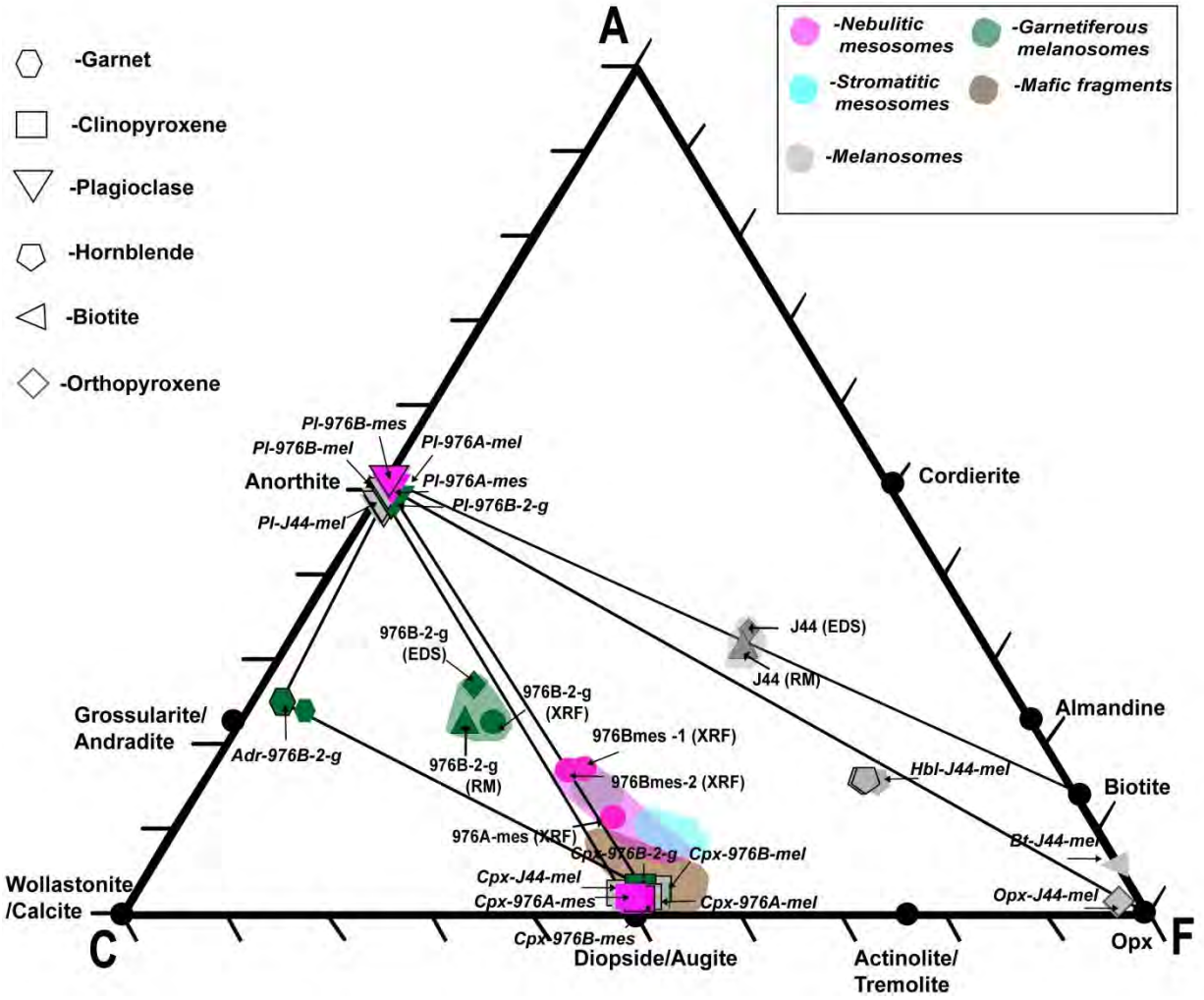

Figure 5.7. ACF diagram (Orville, 1969) showing mineral phase and WR compositions from Bysteek Formation mafic granulites. On the left-hand side of the ACF triangle plagioclase, clinopyroxene and andraditic-garnet constitute the corners of a triangle, whereby garnetiferous melanosome WR compositions (sample 976B-2-g; dark-green fields) occurs within that triangle. Garnet-free mafic granulite domains (nebulitic, stromatitic mesosomes, and mafic fragments) plot on or close to the plagioclase-clinopyroxene tie-line. Towards the right-hand side of the ACF triangle, plagioclase, orthopyroxene and clinopyroxene form a second-triangle with secondary amphibole from melanosome J44-mel occurring on the plagioclase-orthopyroxene tie-line. The WR composition of J44-mel plots higher on the ACF diagram compared to the other garnet-amphibole-biotite free mafic granulite domains as it plots on the plagioclase-biotite tie-line. The symbols representing phases correspond to its respective WR chemical domain (same as in Figure 5.2; pink: nebulitic mesosomes; pale blue: stromatitic mesosomes; brown: mafic fragments; dark green: garnetiferous melanosomes; grey: melanosomes). Triangles: Rock Maker calculations; circles: XRF data; diamonds: EDS area scans.

5.3.2 Diatexite compositions

The peak assemblage of diatexites shows garnet and cordierite with melt. Retrograde biotite and occasionally sillimanite (Figures 3.10; 3.13) form by partial garnet, cordierite, and alkali feldspar breakdown. This can be demonstrated by the tie line intersections in the AFM diagram (Figure 5.8). This retrograde reaction is qualitatively the same like the one that most likely produced garnet, cordierite and melt at the thermal peak (Bt_1+Sil_1+Qtz=Grt+Crd+Kfs+Liq). However, considering the position of most WR compositions in the left part of the AFM diagram, this prograde $biotite_1$ must have had a lower X_{Mg} (~0.25, or even less) compared to the retrograde biotite that are plotted in the diagram (Figure 5.8).

Melt or magma extraction or migration at the thermal peak might have changed the composition of the diatexites. For instance, the extraction of quartz and alkali feldspar, forming syenitic pools elsewhere, would increase the aluminium, and decrease the potassium content of the residual diatexite, which then would plot further up in the AFM diagram. The scattering of the WR compositions in Figure 5.5-5.6 may have been caused by the migration of melt or magma at or shortly after the thermal peak.

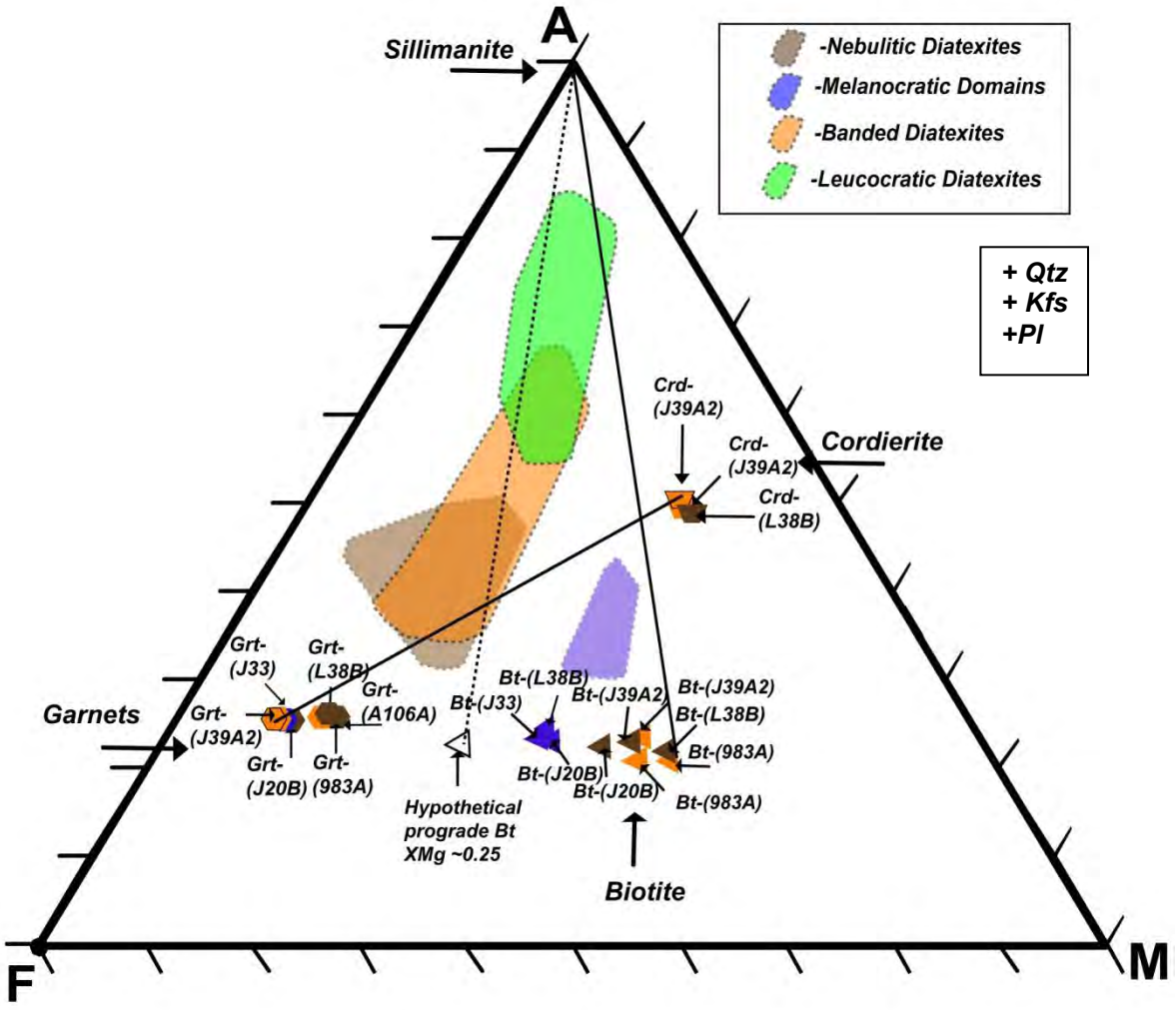

Figure 5.8. AFM diagram (projected through alkali feldspar and in excess of quartz, K-feldspar and plagioclase; Thompson, 1957) showing phases and WR compositions from nebulitic (brown fields), melanocratic (blue fields), banded (orange fields) and leucocratic (green fields) domains from the Koenap Formation diatexites. The peak metamorphic assemblage is shown by the tie-line joining garnet and cordierite in the presence of leucocratic melt. The retrograde assemblage is formed via the partial breakdown of garnet and cordierite into secondary biotite and sillimanite. However given the positions of garnet on the left-hand side of the AFM triangle, the primary prograde biotite most likely had a lower X_{Mg} in comparison to the secondary biotite (Bt II; X_{Mg}: 0.58). Therefore, a hypothetical prograde biotite (biotite$_1$) with an X_{Mg} of 0.25 is plotted and joined to the sillimanite point (dashed line), providing intersections with the garnet-cordierite tie-lines and the diatexite WR composition fields.

6. Petrogenesis, thermodynamic modelling and thermobarometry

This chapter investigates the *P-T* conditions experienced by the mafic granulites of the Bysteek Formation and the diatexites of the Koenap Formation. The stability range particularly of the peak mineral assemblages in mafic granulites and diatexites was determined using multi-phase equilibria, calculated using Theriak Domino (De Capitani and Petrakakis, 2010), and conventional geothermometers and barometers.

Holland and Powell's (1998) current database (tcdb55c2d) in Theriak-Domino (De Capitani and Petrakakis, 2010) has been used to calculate pseudosections for the Bysteek Formation mafic granulites and the Koenap Formation diatexites. Prerequisite for the calculation of meaningful results is the determination of a realistic bulk composition that existed and reacted at the point of interest on the *P-T* path of the investigated rock.

The Fe, Mg, Ca, Na, K, Si and Al oxide compositions of the rocks used for thermodynamic modelling were obtained from EDS area scans and XRF analysis (Section 5). Crucial for the determination of the solid mineral assemblage and the formation of melt during anatexis is the proportion of hydrous fluid at the thermal peak. This proportion cannot be measured directly, but the approximate amount of melt that may have been present during anatexis has been estimated petrographically by adding the modes of magmatic quartz, plagioclase and alkali feldspar in the investigated mesosomes. In both investigated mafic mesosomes this volume proportion is about 24%.

Since the volume of melt produced in the WR composition determined by XRF and EDS correlates with the fluid content, these 24 vol% of former melt have been used to model the fluid content. This has been done in an iterative process using numerous Theriak Domino runs, aiming to re-produce the observed mineral modes and compositions, and the observed melt volume as a stable assemblage in a narrow *P-T* field.

Equally unknown is the precise oxygen fugacity during the formation of the investigated assemblages. The presence or absence of phases containing ferric iron, such as andraditic garnet or magnetite, however, provides some constraints. In a similar approach like for the estimation of the fluid content, excess oxygen has been added where such phases were observed. The modes of magnetite or andradite served as guidance for the amount of oxygen added.

Where such whole rock composition at the *P-T* stage of interest not sufficiently well known and cannot be estimated with satisfactory accuracy, the calculated pseudosections will not provide reliable information (Vernon *et al.* 2008). Furthermore, the thermodynamic data sets used in

Theriak Domino are not well suited to calculate the stability of certain amphiboles. Therefore, the results from pseudosections were supplemented by conventional thermobarometry that uses the composition of individual mineral compositions of paragenetic mineral phases.

Since in granulite facies rocks and diatexites relics of the prograde *P-T* evolution usually are obliterated, and no such relics have been identified in the petrographic studies, the focus of the *P-T* investigations are the metamorphic peak conditions and the retrograde stages of the *P-T* paths.

6.1 Thermodynamic modelling

Estimated peak *P-T* conditions were investigated using two mafic granulite nebulitic mesosomes (976B-mes, Figure 2.2b; 976A-mes, Figure 2.2a), a garnetiferous melanosome (sample 976B-2-g; Figure 2.2b; domain 3) and diffusely banded diatexite J39A2 (Figure 2.14a-b).

6.1.1 Nebulitic mesosome 976B-mes (Cpx-Pl-Qtz)

Sample 976B-mes (Cpx-Pl-Qtz) is a fine-grained (<100µm) nebulitic mesosome containing domains of melanosomes and hosting *in-situ* leucosome domains (Figure 2.2b). Hence it appears that after partial melting a substantial amount of magma remained close to its source and that therefore bulk composition of the sampled rock might be similar to the composition that reacted at the thermal peak. Therefore the sample's composition (Table 5.1) has been used for thermodynamic modelling after adding an appropriate amount of hydrous fluid phase (Figure 6.1; see bulk composition at the top of the diagram). The mineral assemblage is not suitable for conventional thermobarometry but the pseudosection reveals the stability field of the observed mineral assemblage.

The pseudosection (Figure 6.1) shows fields of parageneses stable in specific *P-T* intervals. Since titanite and apatite show no exchange reactions with the observed mineral assemblage (Cpx-Pl-Qtz), to simplify peak P-T calculations, titanite and apatite have not been considered in the thermodynamic modelling. The remaining assemblage that was present at the metamorphic peak in sample 976B-mes is Cpx-Pl-Qt and leucocratic melt. Its stability field is highlight in purple. At mid- and lower crustal levels (5-10 kbar) it is stable between ~850-1100 °C. In order to identify the *P-T* conditions more accurately the diagram shows contours of modal proportions of plagioclase and clinopyroxene with its respective anorthite content and X_{Mg} values.

The observed compositions and modes of the solids, clinopyroxene (X_{Mg}: 0.40; 57-59 vol%), plagioclase (An89; 35 vol%) and quartz (7 vol%) is stable at 8.1-9.5 kbar and ~900-990 ˚C

(Figure 6.1; blue polygon). The liquid that exists at these conditions can be determined using Theriak Domino. It has a granitic composition equivalent to 48 vol% quartz; 46 vol% alkali feldspar and 5.7 vol% plagioclase, which is similar to the observed compositions from the *in-situ* leucosomes of 976B-L (Tables 6.1). The composition of the melt allows the crystallisation of an assemblage similar to the leucocratic phases seen in sample 976B-mes, and the melt volume of ~24 vol% corresponds to their modal proportion (Table 3.4). The hydrous fluid content of the melt (6.33 wt%) is not represented in the sample, which entirely consists of anhydrous phases, and may have been extracted during the metamorphic peak or soon thereafter.

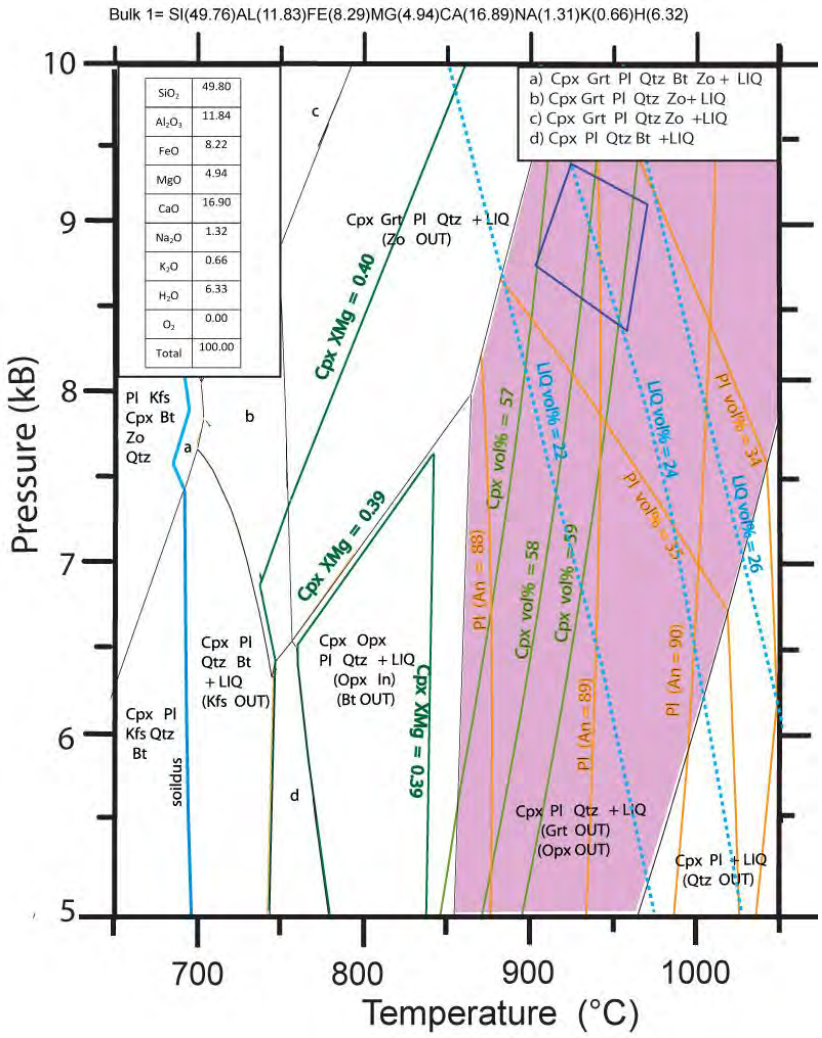

Figure 6.1. Pseudosection for sample 976B-mes. The light green contours show clinopyroxene modes whereas dark green contours indicate clinopyroxene X_{Mg}. The plagioclase modes (34-35 vol%) and anorthite content (An88-90) is shown in orange contours. The blue polygon outlines the best fit between observed and calculated mineral modes and compositions, which is interpreted as the likely peak metamorphic conditions of mafic mesosome. This occurs in a *P-T* range of ~890-990 °C and 8.2-9.4 kbar. The light blue dashed lines indicate the volume of extracted leucosome at thermal peak (24-25 vol%), which corresponds to 6.33 wt% water under oxygen free conditions.

Table 6.1. Comparison between analysed leucosome compositions (XRF, EDS area scans and Rock Maker) to those established at theoretical thermal peak using Theriak Domino.

Rock type	**Mafic granulite leucocratic domains**						**Diatexite leucocratic domains**				
IUGS Name (Streckeisen , 1976)	**Alkali feldspar granite**			**'Anorthosite'**			**Granite**			**Granite**	
TAS (Middlemost, 1985)	**Granite**			**Monzonite**		**Granite**	**Granite**			**Granite**	
Sample	**976B-L**			**976A-L**			**J39A-L**			**983D**	
Method	**EDS-Area Scan**	**Rock Maker**	**Theriak Domino**	**XRF**	**Rock Maker**	**Theriak Domino**	**EDS-Area Scan**	**Rock Maker**	**Theriak Domino**	**XRF**	**Rock Maker**
SiO_2	75.70	77.18	77.82	58.14	58.68	77.81	73.23	74.85	79.63	76.55	78.92
TiO_2	0.07	-	-	0.49	-	-	0.19	-	-	0.50	-
Al_2O_3	12.47	11.69	11.88	24.19	25.63	13.18	14.41	14.64	11.19	11.43	10.64
Fe_2O_3	0.15	-	-	0.94	-	-	1.10	0.12	-	0.01	0.02
FeO	-	-	-	-	-	-	-	0.77	-	1.80	1.10
MnO	-	-	-	0.17	-	-	0.11	0.00	-	0.15	-
MgO	0.16	-	-	0.91	-	-	0.47	0.76	-	0.54	0.64
CaO	3.36	2.97	2.41	8.47	8.05	2.43	1.57	1.15	0.72	1.27	0.68
Na_2O	1.31	1.09	1.93	4.36	5.69	1.68	4.89	4.46	2.23	1.72	1.27
K_2O	6.59	7.07	5.97	2.22	1.95	4.90	3.84	3.25	6.24	5.94	6.73
P_2O_5	0.19	-	-	0.11	-	-	0.19	-	-	0.09	-
Total	100	100	100	100	100	100	100	100	100	100	100

6.1.2 Nebulitic mesosome 976A-mes (Cpx-Pl-Qtz-Mag)

Fine-grained nebulitic mesosomes and melanosomes in sample 976A-mes host *in situ* leucosomes (Figure 2.2a). No suitable parageneses are present for conventional thermobarometry. The pseudosection in Figure 6.2 uses a bulk composition suitable to estimate the peak metamorphic conditions. Magnetite is present in the assemblage, with petrographic evidence suggesting that it is secondary (Section 3.1.2; Figure 3.2a). Therefore peak metamorphic conditions were calculated without the effect of oxygen, whereby the magnetite composition was re-integrated into the existing clinopyroxene (X_{Mg}: 0.65). The resulting re-integrated clinopyroxene exhibits an X_{Mg} of 0.43, similar to the clinopyroxene compositions in mesosome 976B (X_{Mg}: 0.40). The hydrogen content of 9.4 atoms in the bulk assemblage is sufficient to allow melt formation comparable to the leucosome volume observed in the field.

While the mineral assemblage of clinopyroxene, plagioclase and quartz is stable over a wide range between ~720 and 1000 °C (pink field in Figure 6.2), the observed modes and compositions of this assemblage, however, fit best in a *P-T* field similar to that determined for sample 976B (Figure 6.1), but at slightly lower pressures and temperatures of ~850-900 °C and ~8.0-9.2 kbar (blue polygon in Figure 6.2). At these conditions and with the water content used for the calculation (6.7 vol%) the system produces 22-25 vol% of granitic melt at the thermal peak. The composition of the melt is dominated by quartz (45 vol%), alkali feldspar (48 vol%) and plagioclase (6.6 vol%) (Table 6.1); which is in agreement with the compositions of the *in-situ* leucosomes seen in the mesosome 976B (granite), but differs to the leucocratic pockets present in 976A (monzonite). A possible explanation for this is that during cooling fluid escapes, most likely together with dissolved Si, K and Na components, of which leucocratic pockets crystallize post peak-metamorphism. The granitic leucosome WR compositions (section 5.1.4; Table 5.4) coincide with the theoretical granitic compositions (Table 6.1) and most likely represent peak-metamorphic leucosome.

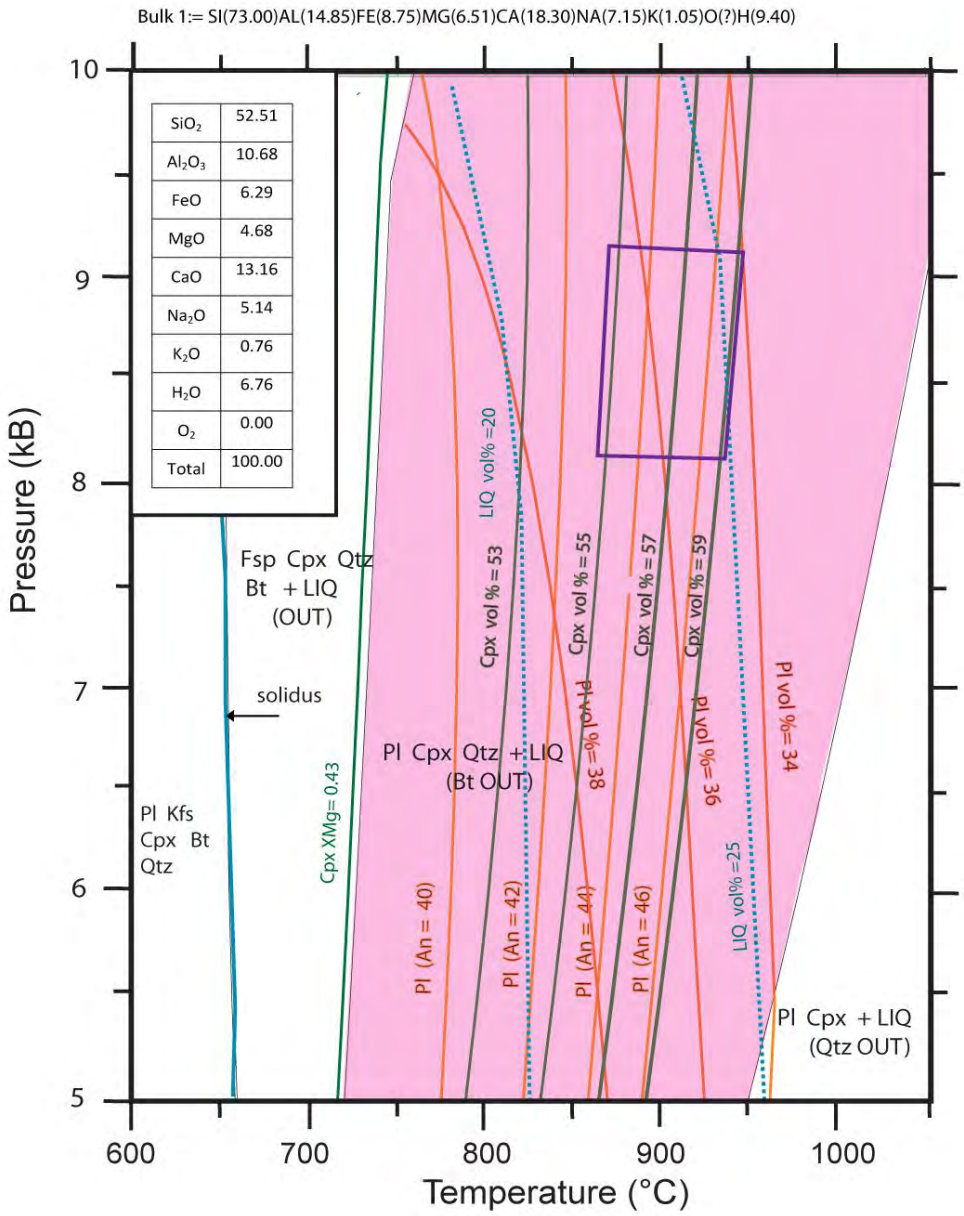

Figure 6.2. Pseudosection for the composition of sample 976A-mes. The likely peak metamorphic conditions of mafic mesosome is outlined by the purple polygon which indicates the best fit between observed and calculated mineral modes and compositions. This occurs in a *P-T* range of ~850-920 °C and 8.0-9.1 kbar. 6.7 wt% water (i.e. 9.4 hydrogen atoms) allow the formation of melt volumes that are in agreement with the observed volume of leucocratic magmatic phases (Tables 5.4 and 6.1). The plagioclase modes (34-38 vol%) and anorthite content (An40-46) is shown in orange contours. The light green contours show clinopyroxene modes whereas dark green contours indicate clinopyroxene X_{Mg}.

6.1.3 Garnetiferous melanosome 976B-2-g

Sample 976B-2-g is the garnetiferous melanosome with the assemblage andradite-clinopyroxene-plagioclase-quartz and minor titanite and apatite (Section 4.1.3). The melanosome shows a diffuse gradational contact to the adjacent mesosome 976B-mes (Figure 4.3).

Petrographic observations (Section 3.1.2; Figure 3.3c) suggest that garnet grows in the solid state within the melanosome, after the potassium-rich extraction of melt, and at the expense of clinopyroxene and anorthitic plagioclase. The presence of ferric iron in the andraditic endmember also suggests increasing oxygen fugacity. In order to estimate the *P-T* conditions of garnet growth the melanosome composition with additional oxygen but without hydrous fluid phase has been used for thermodynamic modelling.

The pseudosection (Figure 6.3) shows the stability of garnet, clinopyroxene and plagioclase over a large temperature range at pressures above ~ 4 kbar (Figure 6.3, pink field). The observed mineral compositions in sample 976B-2-g, are An_{91}, (32-34 vol%; Table 3.2), X_{Mg} in clinopyroxene of 0.45 (23-27 vol%) and andradite contents in garnet (33-35 vol%) of ~0.55 mol%. Calculated mineral modes and compositions fit the observed ones along a *P-T* corridor (yellow polygon; Figure 6.3) from 650-750 °C at 4.5 kbar to 850-1000 °C at 8 kbar. The different contours show a similar slope which renders it difficult to locate an area of meaningful intersections. Therefore the *P-T* conditions cannot be narrowed down further than the highlighted corridor. Since garnet in the melanosome shows a strong andradite component the bulk composition for thermodynamic modelling includes 2.6 atoms of additional oxygen.

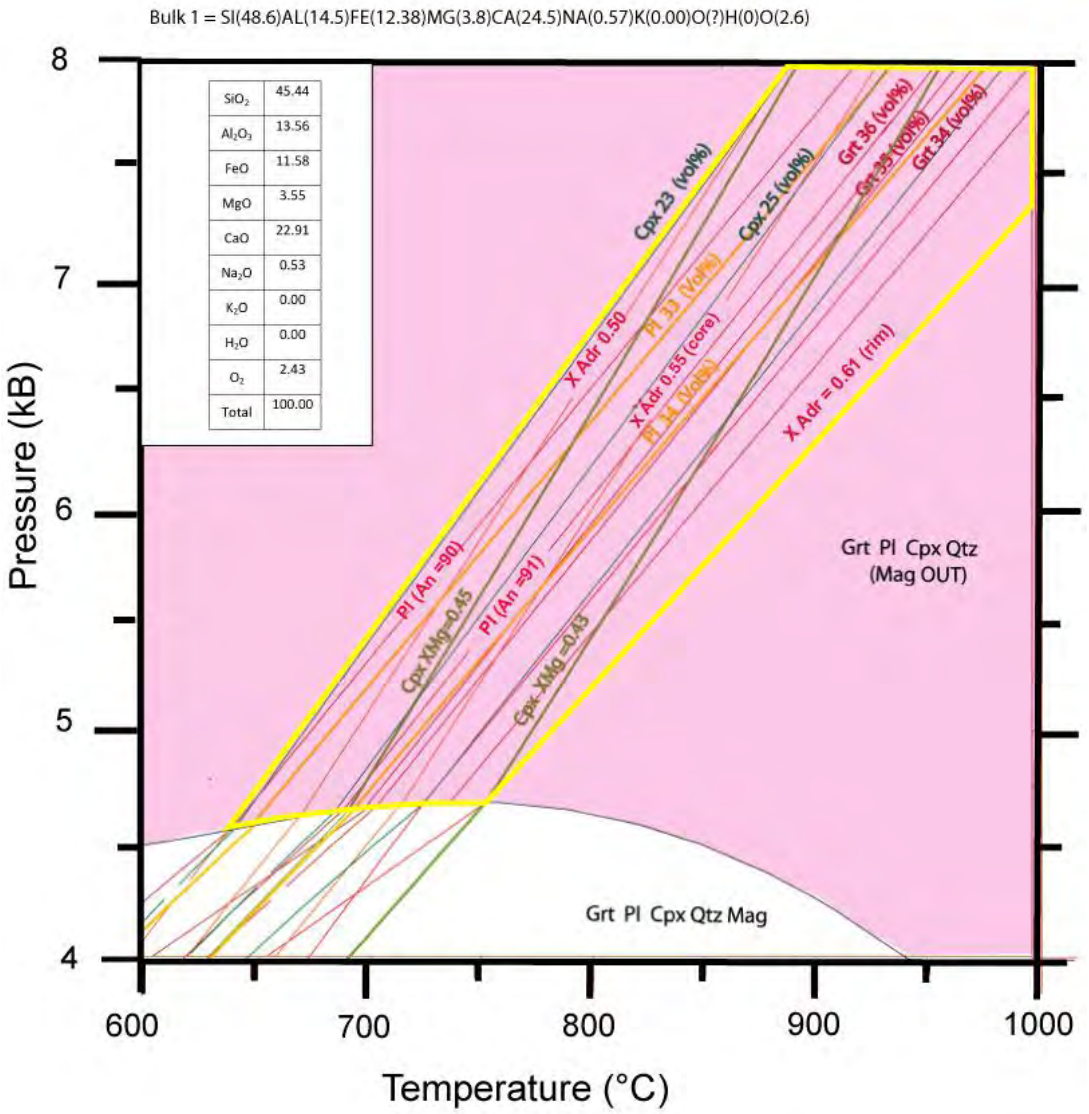

Figure 6.3. Pseudosection for the growth of garnet in melanosome 976B-2-g. The absence of magnetite in garnetiferous melanosomes restricts the likely growth of andraditic garnet to pressures exceeding 4.5 kbar. The stability of the observed assemblage with the approximate mineral modes and compositions covers a wide corridor (yellow polygon) between ~700 °C at 4.7 kbar and 950 °C at 8 kbar. The corridor continues to higher pressures.

6.1.4 Diffusely banded diatexite –sample J39A2

Sample J39A2 is a diffusely banded diatexite with the assemblage quartz-alkali feldspar garnet-cordierite-plagioclase-biotite ±magnetite. Petrographic analysis show well equilibrated textures between garnet and cordierite. Furthermore, garnet shows poikiloblastic textures, hosting rounded inclusions of alkali-feldspar, quartz and fibrolite. This might suggest that biotite-sillimanite breakdown played a role in garnet growth.

Mineral compositions and modes in sample J39A-2, are An16-22 (1.6-8.7 vol%; Table 3.7), X_{Mg}: 0.71 in cordierite (0-2.3 vol%) and X_{Mg} 0.18-0.19 in garnet (2-2.7 vol%).

As suggested by the coarse-grained nature, granitic patches and pockets, and abundant magmatic microfabrics (Sections 2.3.1 and 3.3.1 Figures 2.1.4; 3.9a-b), the proportion of melt in the diatexite must have been high. However, the precise volume of melt is difficult to determine petrographically and may have ranged between relatively small volumes to proportions that are comparable to granitoid magmas.

In the following section, a *P-T* pseudosection for the diatexite were calculated with 9.52 wt% H_2O in the starting compositions. The resulting stability fields of the solid assemblage show melt proportions varying between 40-50 vol% (blue dashed lines; Figure 6.4; Table 6.1) with mode and composition contours in a *P-T* range of 750-890 °C and 3.7-6 kbar (pink field; Figure 6.4) . The leucocratic melt is granitic with calculated modal assemblages (43 vol% quartz; 46 vol% alkali feldspar, 9.7 vol% plagioclase) being similar to the observed volumes in leucocratic diatexite domains (Table 3.6).

The composition used for modelling is the proportional mass of the oxides of Si, Al, Fe, Mg, Ca, Na, K in the WR composition of the sample J39A2. Since garnet in the diatexite shows a minor andradite component the bulk composition for thermodynamic modelling includes 0.45 atoms of additional oxygen.

These modes and compositions have been modelled using Theriak Domino but the result is not fully satisfactory. The results indicate that the calculated garnet composition in the *P-T* field (stability field ‘a’, Figure 6.4, pink polygon) has a higher magnesium content corresponding to an X_{Mg} of 0.24. The observed garnet composition (X_{Mg}: 0.18) is not stable together with the observed assemblage. Conversely the observed cordierite composition (X_{Mg}: 0.71) occurs with the calculated garnet composition in the assemblage ‘Kfs-Pl-Grt-Sil-Crd-Qtz-Mag+LIQ’ (stability field ‘b’; Figure 6.4). However the higher magnesium content in garnet may be supported by observed X_{Mg} values of 0.25 in garnet from diatexites L38B, A106A and 983A (section 4.2.1; Table 4.8).

The sillimanite present in the observed assemblage occurs as relic inclusions within garnet grains (Figure 3.12c), rather than being a stable phase in the Kfs-Qtz-Pl groundmass. Therefore, the assemblage to be modelled is one where primary sillimanite is not present (Kfs-Pl-Grt-Crd-Qtz-Mag +LIQ; stability field ‘a’; Figure 6.4).

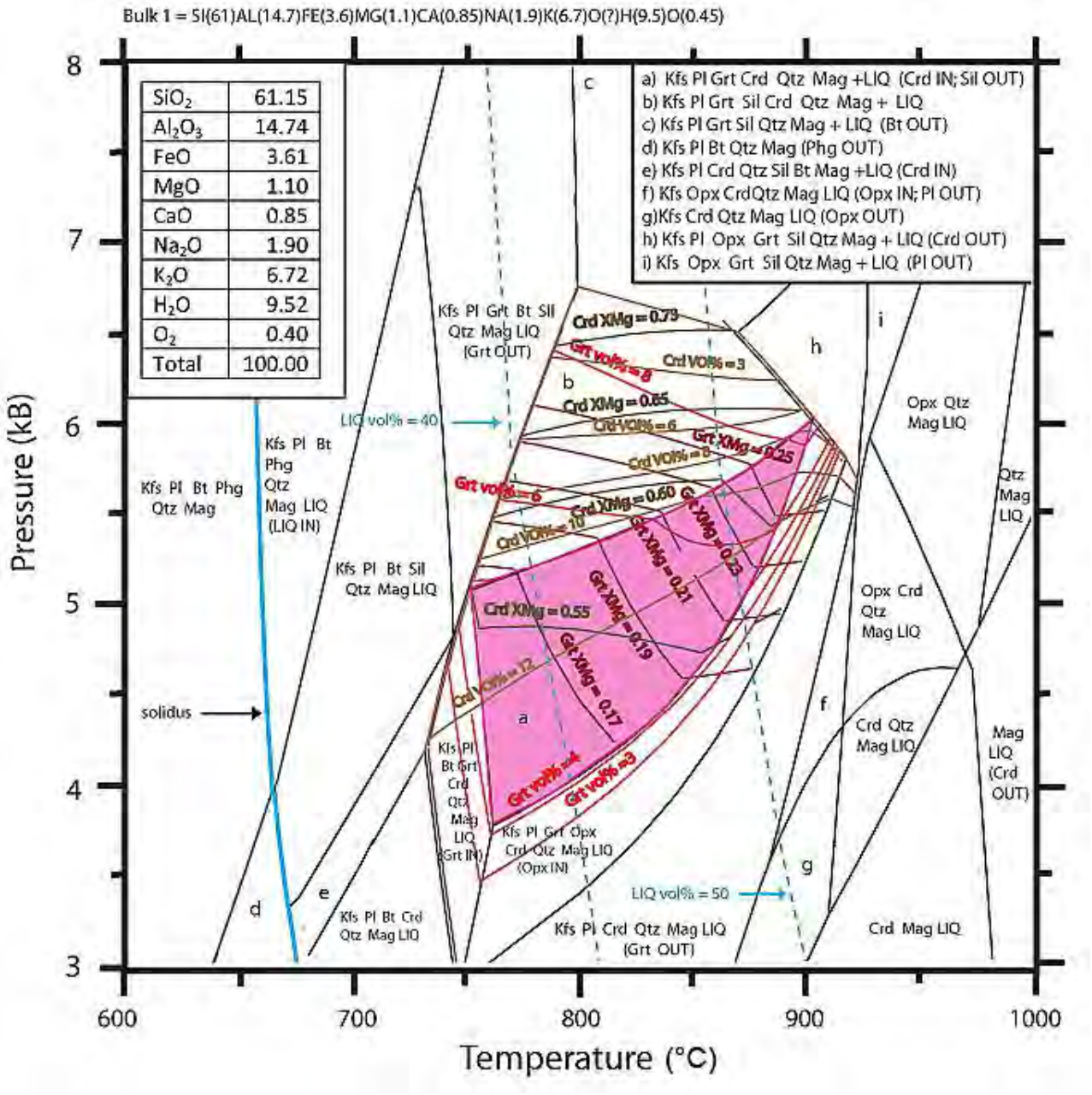

Figure 6.4. Pseudosection for diffusely banded diatexite J39A2. The pink stability field outlines the likely metamorphic conditions of the diatexite indicating by the best fit between observed and calculated mineral modes and compositions. This occurs at temperatures between ~750-900 °C and a wide pressure range of 3.7-6 kB. The maroon lines show X_{Mg} values for garnets (0.17-0.25), whereas brown lines are X_{Mg} values for cordierite (0.55-0.73). The blue dashed lines indicate the volume of granitic melt occuring between 40-50 vol % between a range of 800-900 °C (Table 6.1).

6.2 Conventional thermobarometry

Conventional thermobarometry was used wherever the mineral assemblage shows suitable phases in parageneses. This applies to amphibole or garnet bearing mafic granulites and to cordierite-garnet and garnet-plagioclase-aluminosilicate bearing diatexites.

Due to only minor core-rim variation, temperatures and pressures were calculated using either EMPA core, rim or average analyses from phases co-existing in contact with each other and showing equilibrium textures. Apart from the zoned andraditic garnet in mafic granulite 976B-2-g, core, rim and average compositions differ only slightly from each other (Section 4.1, Tables 4.1-4.2; 4.4-4.6; complete data set in the appendix). Unless stated otherwise the text in the next sections always refers to average compositions.

6.2.1 976B-2-g (Grt-Cpx-Pl-Qtz- melanosome)

Sample 976B-2-g is a fine-grained mafic granulite melanosome domain with the metamorphic assemblage of retrograde garnet growing at the expense of clinopyroxene and plagioclase (sections 3.1.2 and 4.1.3, Figures 3.2c and 4.3). This assemblage has been used for Grt-Cpx thermometry (Raheim and Green, 1974; Krogh, 1988) and Grt-Cpx-Pl-Qtz barometry (Eckert *et al.* 1991). Average garnet core compositions (X_{Adr}=0.55), core clinopyroxene (X_{Mg}=0.45) and core plagioclase compositions (An91), yield a pressure ranging between 7.5-8.3 kbar at a temperature between 790-900 °C (Figure 6.5).

Thermometry calibrated for crustal mafic granulites after Raheim and Green (1974) and Krogh (1988) uses the following Fe-Mg exchange between garnet and clinopyroxene:

$$1/3\ Mg_3Al_2Si_3O_{12} + CaFeSi_2O_6 = 1/3\ Fe_3Al_2Si_3O_{12} + CaMgSi_2O_6$$

$$\text{pyrope} + \text{hedenbergite} = \text{almandine} + \text{diopside} \qquad \text{(R1)}$$

Barometric calculations were obtained utilizing the calibration of Eckert *et al.* (1991) for gradual anorthite breakdown of anorthite and diopside in crustal mafic granulites:

$$CaAl_2Si_2O_8 + CaMgSi_2O_6 = 2/3\ Ca_3Al_2Si3O_{12} + 1/3\ Mg_3Al_2Si_3O_{12} + SiO_2$$

$$\text{anorthite} + \text{diopside} = \text{grossularite} + \text{pyrope} + \text{quartz} \quad \text{(R2)}$$

Using core compositions of garnet, clinopyroxene and plagioclase the barometer of Eckert *et al*. (1991) yields a pressure of approximately 6 kbar. The intersections of the two

thermometers are close together at 780 and 810 °C, respectively (Figure 6.5).

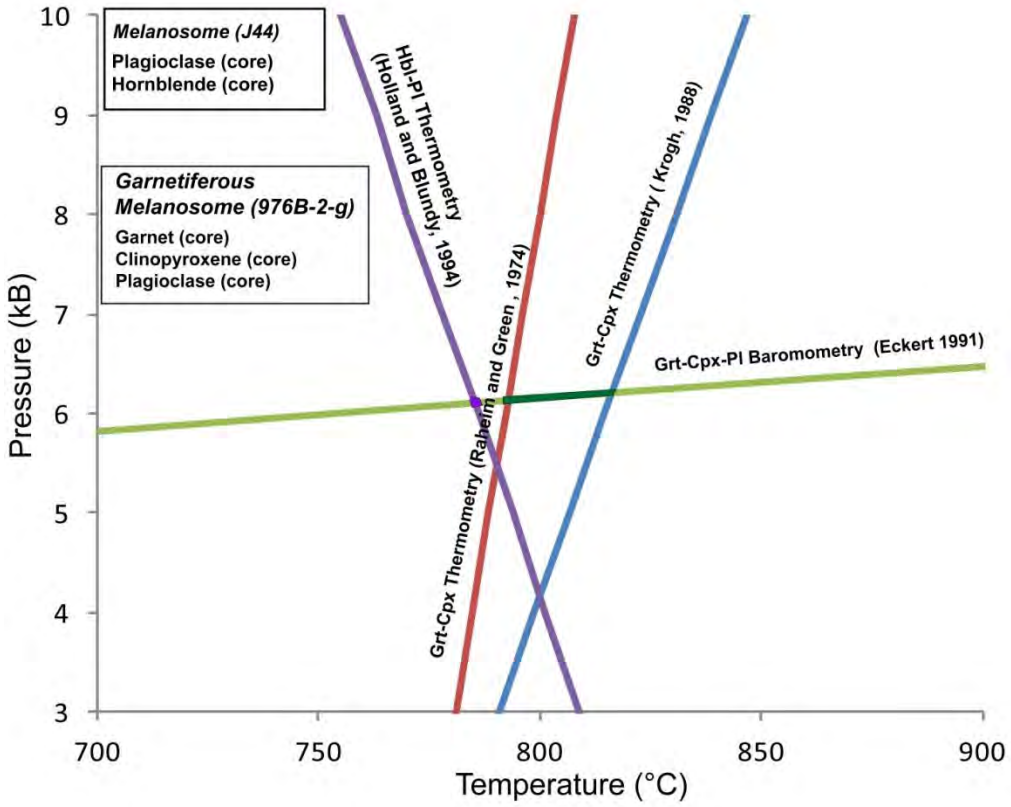

Figure 6.5. Thermobarometry for garnetiferous melanosome 976B-2-g using core compositions of garnet, clinopyroxene and plagioclase. Thermobarometry after Eckert et al. (1991), Raheim and Green (1974) and Krogh (1988) yields ~780-810 °C and ~6 kbar. Amphibole-plagioclase thermometry (Holland and Blundy, 1994) from sample J44 yields retrograde temperatures of ~770˚C at 7-8 kbar.

6.2.2 J44-mel (Opx-Cpx-Hbl-Pl-Bt-Mag-Qtz melanosome)

The melanosome sample J44 shows the assemblage orthopyroxene-clinopyroxene-plagioclase-hornblende±biotite-magnetite-quartz. The melanosome grades from a fine-to-medium grained domain (<300µm grain size) into a medium-grained domain (>300µm). The mineral modes in both domains change to some extent between the domains. Amphibole and biotite most likely are retrograde mineral phases (section 3.1.2.; Figures 3.2d-e).

The mineral assemblages of the medium-grained domain permit estimations for equilibration temperatures for two-pyroxene thermometry, which was conducted using the Fe-Mg exchange thermometer by Bertrand and Mercier (1985):

$$(Ca, Fe)_2 Si_2O_6 + MgSiO_3 = (Ca, Mg)_2 Si_2O_6 + FeSiO_3$$

hedenbergite + enstatite = diopside + ferrosillite (R3)

Amphibole and plagioclase from the neighbouring fine-grained domain has been used for amphibole-plagioclase thermometry after Holland and Blundy (1994):

$$NaCa_2Mg_5Si_4 (AlSi_3)O_{22}(OH)_2 + NaAlSi_3O_8 = Na (Ca, Na) Mg_5 Si_8O_{22} (OH)_2 + CaAl_2Si_2O_8$$

edenite + albite = richerite + anorthite (R4)

Pressures were calculated utilizing the empirical calibration of the reaction between the Ca-Tschermakite component within clinopyroxene, anorthite and quartz (McCarthy and Patiño-Douce, 1998):

$$CaAl_2SiO_6 + SiO_2 = CaAl_2Si_2O_8$$

Ca-Tschermakite (within clinopyroxene) + quartz = anorthite (R5)

Cpx-Pl barometry (McCarthy and Patiño-Douce, 1998) was compared with pressure estimations from GASP barometry from the diatexite J39A2. This sample comes from a location close to J44 (Figure 2.1-sample locations). Field observations suggest that the field relationships between the two sample locations have not qualitatively changed since the metamorphic peak.

EPMA mineral analyses were taken from core positions of orthopyroxene, clinopyroxene, plagioclase and amphibole. Cpx-Pl barometry (McCarthy and Patiño-Douce, 1998) and Cpx-Opx thermometry (Bertrand and Mercier, 1985) intersect at ~865 ˚C and 8.1 kbar (Figure 6.6), which is well compatible with the results of thermodynamic modelling for the Bysteek Formation mafic granulites (800-950 °C, 8-9 kbar; Section 6.1). In addition, the results of GASP barometry from the nearby diatexite (see section 6.2.3 below) intersects with both the Cpx-Pl barometer and the Cpx-Opx thermometer in the same *P-T* region, suggesting that the *P-T* determination is fairly robust and probably reflects conditions close to the peak metamorphism.

Holland and Blundy's (1994) plagioclase-amphibole thermometer yields temperatures that are ~80 ˚C below the Cpx-Opx temperatures. This is in agreement with the textural observation that amphibole is a retrograde phase .The two barometers, GASP and Cpx-Pl, are not likely to provide valid pressures for the amphibole-plagioclase thermometer because they intersect at the thermal peak.

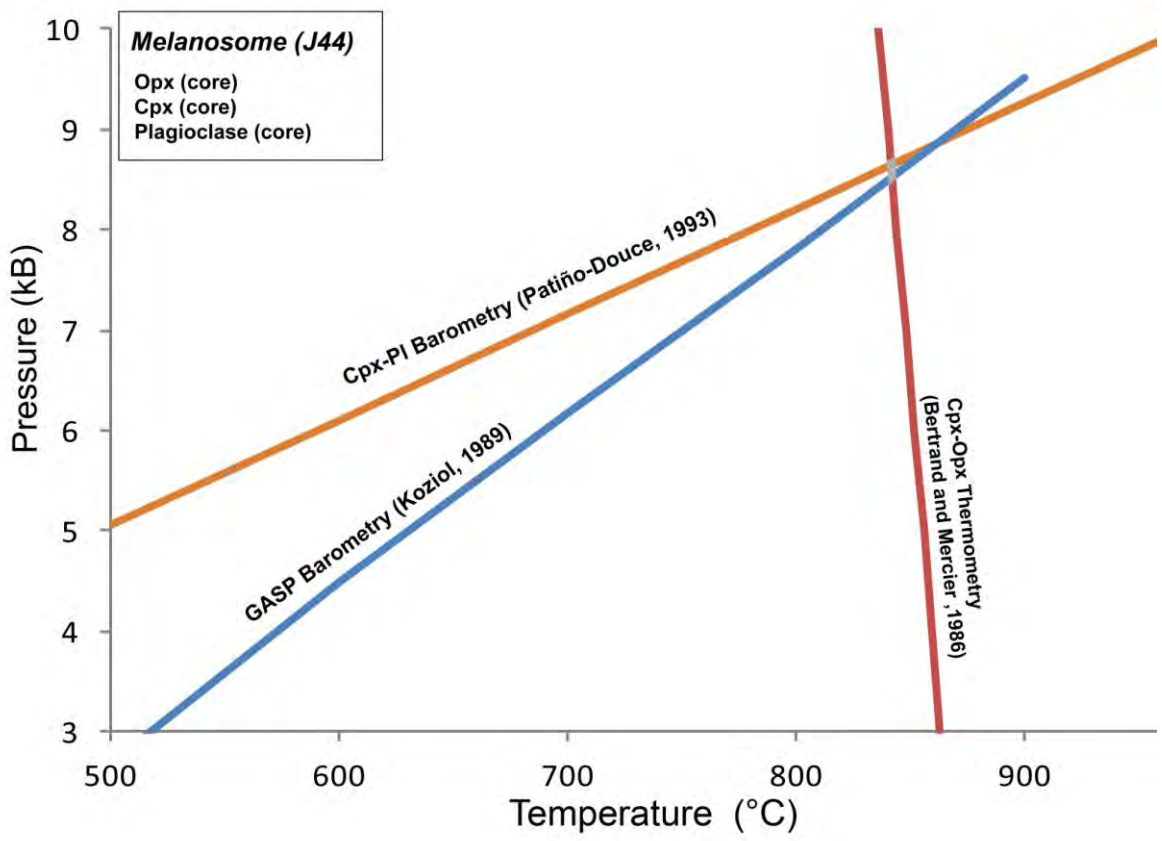

Figure 6.6. *P-T* thermobarometry for sample J44-mel, using core compositions from clinopyroxene, orthopyroxene and plagioclase. Cpx-Opx pairs from medium-grained domain were used for Fe-Mg exchange thermometry (Bertrand and Mercier, 1986). Cpx-Pl barometry (McCarthy and Patiño-Douce, 1998) is used in addition with the GASP barometer (Koziol, 1989) from the neighbouring diatexite domains. Both barometers intersect the Cpx-Opx thermometer at ~8.1 kbar and ~865 °C.

6.2.3 J39A1-Diffusely banded diatexite

The diffusely banded diatexite domain of sample J39A2 is well-suited for conventional thermobarometry, containing garnet, cordierite, sillimanite and plagioclase. The Grt-Crd geothermometer of Bhattacharyya *et al.* (1988) was used to calculate equilibrium temperatures:

$$2Fe_3Al_2Si_3O_{12} + 3Mg_2Al_4Si_5O_{18} = 2Mg_3Al_2Si_3O_{12} + 3FeAl_4Si_5O_{18}$$

almandine + Mg-cordierite = pyrope + Fe-cordierite (R7)

The Grt-Crd geothermometer was used in conjunction with a garnet-aluminosilicate-quartz-plagioclase (GASP) geobarometer after Koziol (1989):

$$Ca_3Al_2Si_3O_{12} + 2Al_2SiO_5 + SiO_2 = 3CaAl_2Si_2O_8$$

grossularite + sillimanite + quartz = anorthite (R8)

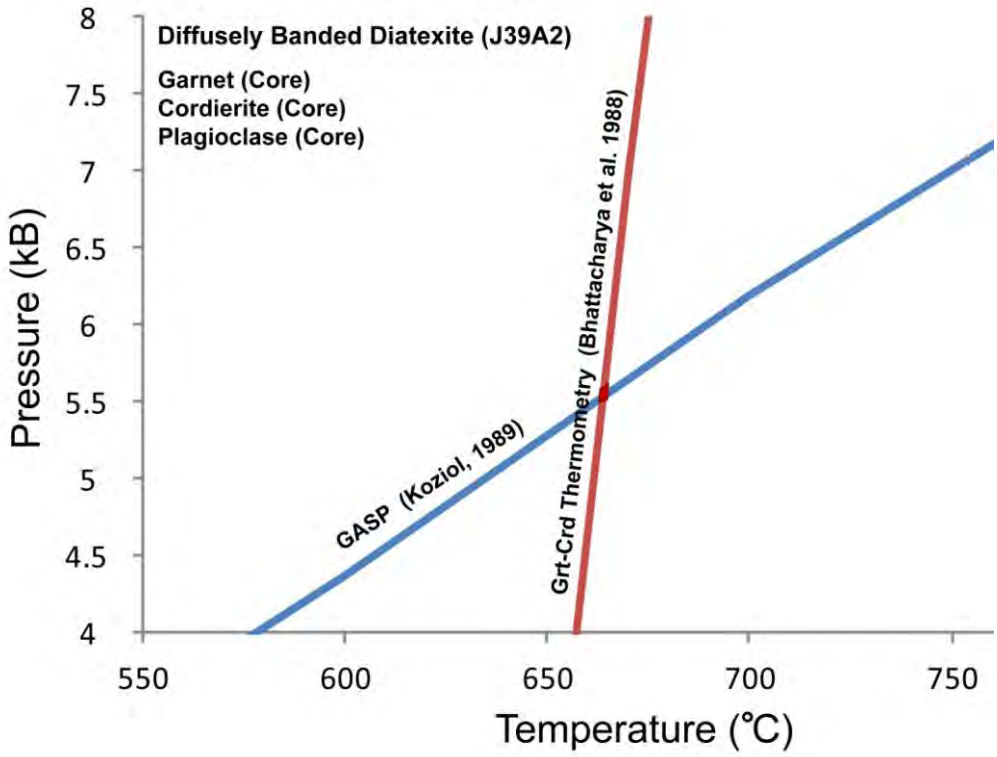

Figure 6.7. Thermobarometric calculations for diffusely banded diatexite (J39A2), using core compositions from garnet, cordierite and plagioclase. The Fe-Mg exchange thermometer between garnet and cordierite (R7) after Bhattacharya *et al.* (1988) along with GASP barometry (R8) after Koziol (1989) were used. *P-T* intersections occur at ~660 ˚C and 5.5 kbar.

GASP barometry and Grt-Crd thermometry results intersect at ~660 ˚C and 5.5 kbar (Figure 6.7). However, it is likely that the Fe-Mg exchange between garnet and cordierite outlasted the formation of the Ca-component in garnet and therefore the GASP barometer is valid for the thermal peak, when garnet formed, but the garnet-cordierite temperatures reflect a retrograde stage. This renders the intersection shown in Figure 6.7 invalid as a meaningful *P-T* datum for the diatexites.

7. Discussion

7.1 Field relationships, timing of events, and principal metamorphic processes

The Bysteek and Koenap Formations form a coherent sequence of high-grade metamorphic rocks that are associated with granitic to syenitic plutons of the Polisiehoek Gneiss and the Swartoup "Enderbite". This discussion covers essentially metamorphic processes in the mafic granulites of the Bysteek Formation and the diatexites of the Koenap Formation.

Rocks of these groups show roughly NW-SE striking layers which, at the scale of mapping, show non-planar contacts to each other and occasionally transitional boundaries. The latter exist essentially between anatectic mafic granulites and calc-silicate rocks within the Bysteek Formation, and, along the north-eastern boundary of the Bysteek Formation, between anatectic mafic granulites and magmatic breccias and the Swartoup "Enderbites".

The close spatial relationship of probably intrusive alkali feldspar granites or syenite of the Swartoup "Enderbite" and plagioclase-rich, clinopyroxene xenocryst bearing magmatic breccias of the Bysteek Formation may have caused incorrect sampling and classification as an enderbite by Moen and Toogood (2007). The intrusive Polisiehoek Gneiss, which in the study area shows some mylonitic zones of substantial thickness, but away from them is largely undeformed, is the youngest pluton, forming dikes that penetrate the older Swartoup "Enderbite". Only late pegmatites postdate the Polisiehoek "Gneiss", completing the magmatic history in the study area.

The Bysteek and Koenap Formations contain the metamorphic rocks which host the younger plutons. From their lithological nature and association it is likely that the protolith of the Bysteek Formation was a calcic sedimentary sequence, now consisting of marbles and calc silicate rocks that graded in the more mafic unit that now is the anatectic mafic granulites series. The protolith of the mafic granulites might either have been marls, reflecting a gradational intake of pelitic sediments into the carbonate sedimentation. This is supported by the structurally overlying Koenap Formation which shows a mineral assemblage compatible with a pelitic/greywacke protolith. This may suggest that a sedimentary series of limestones continuously developed into a pelitic series (or vice versa, since the stratigraphic way up is unknown). Or the mafic granulites of the Bysteek Formation might have been mafic or intermediate igneous rocks of volcanic or intrusive

origin. Field evidence in this regard has been obliterated during anatexis and deformation of the Namaquan orogeny.

The timing of the high-T events in the region is poorly constraint. U-Pb monazite data, published as age distribution but without background data in Moen and Toogood (2007), show the well-known two metamorphic events at ~1200 and ~1100 Ma for the metapelitic Narries Subsuite on the northern side of the Hartebeest River shear zone. These data are similar to U-Pb zircon data for the emplacement of the Twakputs granite-gneiss at ~1220 Ma, which was followed by prolonged ductile shearing at granulite and upper amphibolite facies conditions, that ended only at about 1100 Ma (Mzde *et al.,*2011). The end of ductile shearing correlates in time with the emplacement of the Naros granite at ~1103 Ma (Mdze *et al.*2011; U-Pb zircon). The Naros granite must be younger than the high-T metamorphism since it cuts the Koenap Formation, the Polisiehoek and Twakputs granitic gneisses discordantly about 5 km north of the study area.

Hence, the timing of the metamorphism in the study area requires more age dates, which are currently under production, but most likely such investigations will yield an age comparable to the intrusion of the Twakputs gneiss (i.e. ~1200 Ma) for the high-T event in the study area.

7.1.1 Metamorphism in mafic granulites of the Bysteek Formation

Internally, and along their boundaries to other lithologies, the rocks of the Bysteek Formation are characterised by the variable abundance of leucosome, which may occur, in increasing order of volume, as (i) rootless folded thin veins, (ii) interconnected vein networks, (iii) patches and pools, and (iv) magmatic breccias. The composition of the leucosome varies (Figures 5.1; 5.2 and 5.3) and ranges from plagioclase-rich (sample 976A-L) to quartz-alkali feldspar-rich (sample 985A-L) and granitic (sample 976B-L).

This variability in the leucosomes is unlikely to be the result of different breakdown processes in different protolith, because the residual melanosomes are fairly uniform in mineralogy and composition, containing essentially clinopyroxene, anorthitic plagioclase, quartz, and minor titanite and apatite (Figures 3.1, 3.2; Tables 3.1, 3.2). More likely is the variable extent of potassic/silicic melt extraction and retention of andesine plagioclase, which implies that this andesine forms as a cotectic or early magmatic phase in leucosome close to the source (Sample 976A -976B, Sections 2.1.1 and 6.1.1-6.1.2).

Where such K- and Si-rich melt is quantitatively extracted, the leucosome close to the source (i.e. present in the context of melanosome and mesosome) will contain much plagioclase (Samples 976A-mes; 976B-mes; Figure 2.2a domain 2; Figure 2.2b domain 2) and little or no alkali feldspar. Where the bulk of anatectic melt was retained and crystallised *in-situ*, in veins or in pools together with early magmatic or cotectic plagioclase, the leucosome will be more granitic (sample 976B-L, 985A-L).

Although leucosome veins often show ptygmatic folding (Figure 2.2b-domain 1), they lack evidence of deformation in the solid state, and also the hosting mafic rocks do not show evidence of deformation patterns post-dating the thermal peak. Hence, the folding must have occurred in presence of melt, at the thermal peak. This syn-magmatic deformation probably mobilised anatectic melt and promoted its segregation and extraction from the source.

The abundant segregation of leucosome (quartz, alkali feldspar, some andesine) suggests depletion of the melanosome in potassium, silica, sodium, and some aluminium and calcium. The mesosomes, which show no or incomplete segregation of leucosome from melanosome, reflect this trend and therefore were considered to be closest to the whole rock composition before anatexis (Figure 5.2).

The precise mineralogy and composition of the Bysteek Formation mafic granulites before segregation is unknown but, re-integrating the components seen in the leucosome, or using the composition of mesosomes, it is likely that the plagioclase present before anatexis was more sodic than the anorthite now seen in the melanosomes, and that a potassium-rich phase must have been present. This phase most likely was biotite which, when its temperature limit was reached, released water that triggered the formation of potassium-rich melt. The pseudosections (Figures 6.1 and 6.2) show biotite stable up to ~750 °C. The stability of biotite might have been even higher than that because the Theriak Domino does not consider the titanium as a component which might have stabilised biotite (Patiño-Douce, 1993).

Dehydration melting of Ti-rich biotite as the source of potassic melts in the mafic granulites is supported by fairly abundant titanite in the melanosomes and mesosomes, which may have captured the titanium released from biotite during breakdown.

At peak metamorphic conditions or soon thereafter no hydrous phase other than occasional scapolite was formed in the mesosome, neither in the melanosome nor in any of the

leucocratic veins or pools, suggesting that substantial amounts of hydrous fluid available from biotite breakdown must have escaped during cooling and solidification of the Bysteek Formation. Within this fluid phase most likely silica and alkali metal cations were dissolved. Such fluids, or fluid-rich melts, could have formed pegmatites which are common in the Namaqua basement.

7.1.2 Diatexites of the Koenap Formation

The diatexites are in contact with the Bysteek Formation mafic granulites along boundaries parallel and oblique to the regional NE-SE strike. The reasons for the stepping geometry of the contact are not evident from field observation but the rheological contrast between the felsic diatexites and the mafic granulites resulting in boudinage, or even primary processes might account it. The usually sharp contacts, nowhere show any tectonic overprint, suggesting that no relative displacement between the Bysteek and the Koenap Formations occurred after the thermal peak. Therefore, and because of the spatial proximity of the sample locations (Figure 2.1 sample locations), peak conditions of metamorphism and the retrograde *P-T* paths of diatexites and mafic granulites should be identical.

The diatexites do not show clear segregation patterns of leucosome and melanosome as they are typical for the mafic granulites. The high degree of anatexis and the resulting mobility of magma and melt have obliterated clear lithological boundaries, if any ever existed, which has led to a situation of gradational contacts between domains showing different textures. Coarse-grained diatexites with abundant feldspar phenocrysts often resemble *in-situ* granites. At the other extreme, fine- to medium-grained, and often garnet-rich granofelses without such phenocrysts show the character of felsic granulites. Layering, although occasionally present (Sections 2.3.1-2.3.4; Figures 2.14-2.18), is nowhere penetrative or laterally continuous. This also is interpreted as a result of anatexis and magma mobility.

The inconsistent anatectic patterns in the field and their gradational nature caused by melt and magma mobility make it difficult to estimate the whole rock composition at a given place at the temperature peak, when anatexis took place. This renders the correct determination of the correct composition of the reactive rock volume used for thermodynamic modelling problematic and introduces some uncertainty into the results.

The mineral assemblage of quartz, alkali feldspar, plagioclase, garnet, and cordierite is stable over a large *P-T* field and on its own is as inconclusive as the mineral assemblage in the mafic granulites. However, partial melting in mafic granulites and diatexites in felsic rocks point to granulite facies *P-T* conditions.

Sillimanite inclusions in garnet suggest that garnet formed by a breakdown involving sillimanite that, in the light of the common presence of garnet in a granitic leucocratic assemblage, also produced melt. The obvious primary Fe-Mg phase, again, would have been biotite, that in the diatexites entirely was consumed at the end of the prograde *P-T* path. The absence of hydrous phases at the peak other than cordierite in the diatexites and occasional scapolite in some leucosomes of the mafic granulites support the estimation of granulite facies *P-T* conditions. In addition, restitic diatexites sampled nearby and investigated by a group from Kiel University (Germany) show pseudomorphs after osumilite (pers. commun. Bial, 2012). In other Koenap Formation diatexites, spinel and quartz was stable, showing partial retrograde breakdown to garnet (pers. commun., Kanime, Büttner, 2011). These observations support high and ultra-high temperature metamorphism in the region.

A crucial factor for the interpretation of such extreme temperatures is the pressure at which they existed and the retrograde *P-T* path that followed the thermal peak. The results of thermobarometric calculations are discussed in section 7.2.

7.1.3 Retrograde mineral reactions and metasomatism

The cooling history of the terrain is poorly known but from the retrograde mineral assemblage, or, rather, its general absence, it is evident that the conditions of the retrograde *P-T*-d-t path were not suitable to produce a significant overprint on the peak assemblages and structures.

In the study area some features of retrograde metamorphism are seen in both the mafic granulites and the diatexites. In the mafic granulite sample J44 the formation of hornblende at the expense of orthopyroxene and plagioclase, and the formation of biotite, indicate the influx of hydrous potassium bearing fluids that either could have been released from the cooling leucosome within the Bysteek Formation, or, via a longer pathway, from the abundant granitoid magmas solidifying in the vicinity (Polisiehoek granite gneiss, Swartoup “Enderbite”, Koenap Formation diatexites). All of these fluids can be expected to contain potassium. According to the results of amphibole-plagioclase

thermometry (Figure 6.5) the amphibole grew still at lower granulite facies conditions of ~750-780 °C), which closely associates the retrograde overprint with the thermal peak.

A solid state feature that post-dated the thermal peak is the growth of andraditic garnet in the melanosome of sample J44. The textural characteristics (sections 3.1.2 and 4.1.3, Figure 3.2c and 4.3) clearly show that garnet consumes well-equilibrated plagioclase and clinopyroxene and grows along the interfaces of the pre-existing phases. The ferric iron content in garnet implies increasing oxygen fugacity after the equilibration of clinopyroxene and plagioclase in melanosomes. Zonation patterns in garnet with increasing andradite content towards the rim suggest that the increase in oxygen fugacity occurred in at least two steps.

In the diatexites the retrogression of the peak assemblage consisting of garnet-cordierite-K-feldspar/melt is restricted to the breakdown of garnet and cordierite to secondary biotite and sillimanite, partly reversing the prograde formation of these phases. The required fluid might well have been released from crystallising melt nearby. No thermobarometric data are available for this retrograde stage but the absence of white mica as a retrograde phase suggests that the secondary assemblage grew in the upper amphibolite facies.

Apart from pinitisation of cordierite, which may have occurred at lower amphibolite or greenschist facies temperatures, no observation indicates any significant mineral reaction or deformation event below upper amphibolite facies temperatures. This is in agreement with an investigation of retrograde ductile shear zones north of the Hartebees River shear zone, including the Oup shear zone, which also became inactive before the crust cooled down to mid-amphibolite facies temperatures (Mdze, 2010; Mdze et al. 2011).

7.2 Thermobarometry

The *P-T* conditions have been quantified via thermodynamic modelling and conventional thermobarometry. The results mutually support or complement each other.

In the mafic granulites of the Bysteek Formation the pseudosections show two different fields at high temperature and pressures equivalent to lower crustal levels between 7.5 and 9.5 kbar and 800 and 950 °C (Figure 7.1). Both investigated samples come from the same locality (976; Figures 2.1 and 2.2). The melanosome domains (sample 976B-mel, Figure 3.2b) which delivers the higher temperatures, is a well-equilibrated rock showing clinopyroxene in foam textures. Plagioclase is anorthitic and X_{Mg} in clinopyroxene is about 0.40.

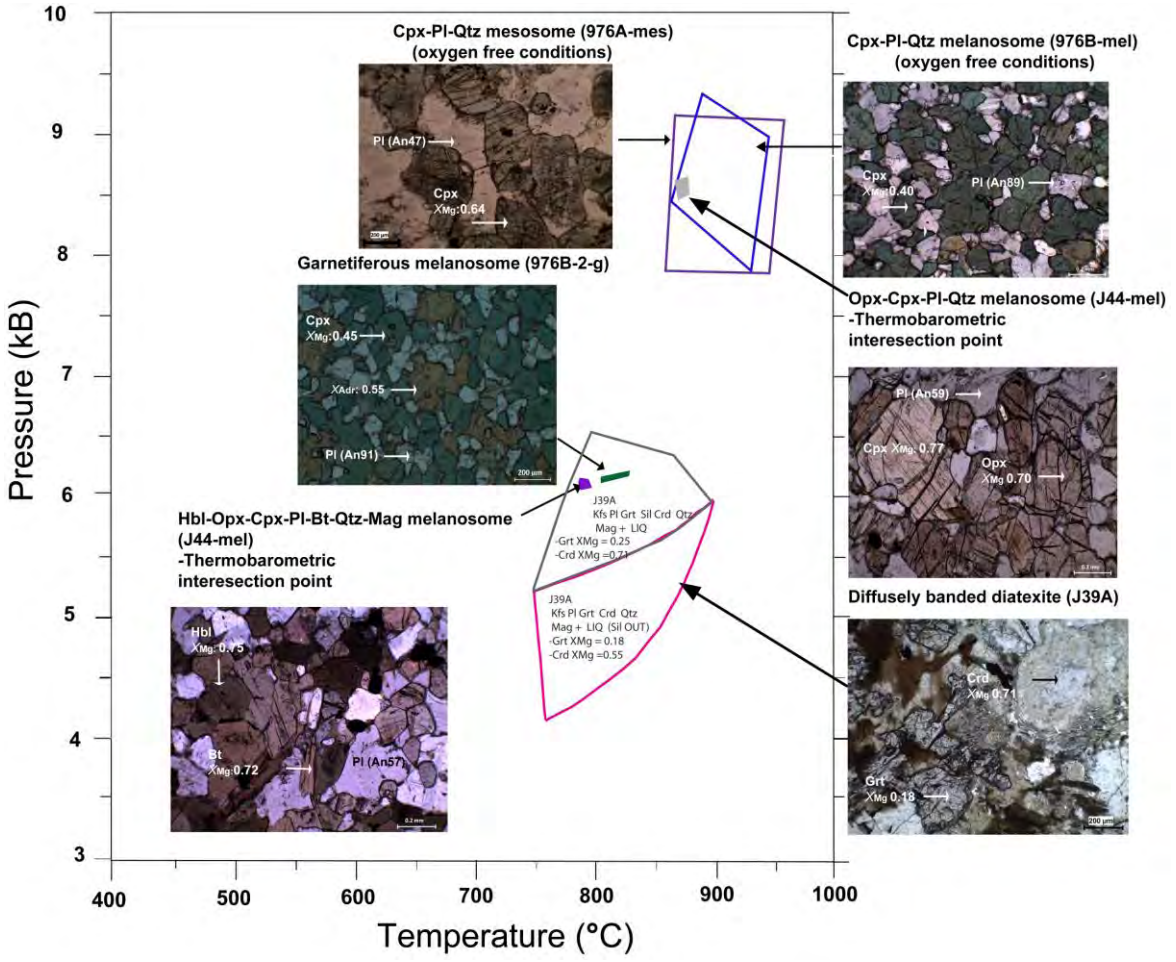

Figure 7.1. Summary of *P-T* thermobarometry and pseudosection results. The thermobarometric intersection point using orthopyroxene-clinopyroxene thermometry with Cpx-Pl barometry (McCarthy and Patiño-Douce, 1998) and a GASP barometer (Koziol, 1989) from melanosome J44 (Figure 6.6) coincide with peak *P-T* stability fields calculated from mesosomes 976A (purple polygon) and 976B (blue polygon). This suggests that peak metamorphism occurred in range between 800-950 °C and 7.8-9.2 kbar. Retrograde metamorphic conditions are indicated by the close proximity of *P-T* intersection points from garnetiferous melanosome 976B-2-g and the amphibole-biotite bearing melanosome domains from J44-mel (~780-810 °C and ~6 kbar; Figure 6.5). The calculated stability fields for the diatexite domains occur in a temperature range of 710-890 °C and 4-6.5 kbar.

In contrast the melanosome in sample 976A-mel shows more anatectic patterns with coarsened clinopyroxene and plagioclase and no foam structures. The clinopyroxene (X_{Mg}: 0.64) and plagioclase (An47) in 976A-mel are different in composition from those in sample 976B-mel. Particularly the higher sodium content in plagioclase suggests that here feldspar might have reacted with, or crystallised from melt, and that in sample 976A-mel the alkali content has not been removed as efficiently into the leucosome as from sample

976B-mel. The higher X_{Mg} in clinopyroxene in 976A-mes can be explained by the lamellar exsolution of magnetite, which extracts iron under oxidising conditions. This in turn suggests increasing oxygen fugacity which probably correlates in time with the andradite growth in sample 976B-2-g (Figure 3.2c) and is therefore a secondary process that took place during the retrograde stage.

Conventional thermobarometry of the melanosome in sample J44 (medium-grained domain; Cpx-Opx thermometry in combination with Cpx-Pl barometry; Figure 6.6) produces a *P-T* intersection at ~865 °C and 8.7 kbar, which is in the *P-T* region where the determined stability fields of the pseudosections for 976A-mes and 976B-mes overlap. Since no observation suggests a *P-T* path moving between the stability fields outlined in the pseudosections for the two mesosomes (Figures 6.1 and 6.2), this overlap and the *P-T* intersection for sample J44 are interpreted as the best estimation of the peak metamorphism in the mafic granulites of the Bysteek Formation.

Like the retrograde exsolution of magnetite in clinopyroxene, andraditic garnet growth in sample 976-2-g is also associated with increasing oxygen fugacity. The pseudosection (Figure 6.3) does not provide good constraints in terms of pressure and temperature for this process. Figure 6.3,which in the *P-T* field provides a 100 °C wide corridor between ~700°C/4.7 kbar and ~900 °C/8 kbar, possibly extending to higher pressures. Conventional thermobarometry provides a better solution with intersections of Grt-Cpx-Pl barometry and Grt-Cpx thermometry at ~6 kbar and ~800 °C (Figure 6.5).

Amphibole-plagioclase thermometry in sample J44-mel is well compatible with these *P-T* conditions. At 6 kbar the temperature of amphibole and plagioclase equilibration, ~785 °C, is almost identical to the result of the Grt-Cpx thermometry in sample 976-2-g (Figure 6.5). Although there is no direct barometric result for the amphibole growth it can be assumed that, due to their proximity in the field, the samples 976-2-g and J44 were at the same crustal depth when they were exposed to the same temperature. Hence the pressure estimation of 6 kbar for the andradite growth should also be valid for the growth of amphibole.

The diatexites do not show evidence of a metamorphic stage comparable in pressure to the peak event in the mafic granulites. The stable assemblage of garnet, cordierite and granitic melt typically forms at lower pressure than 8-9 kbar and the pseudosection of diffusely banded diatexite sample J39A2 supports this, suggesting *P-T* conditions of ~750-890 °C;

3.7-6 kbar, which suggests further isothermal decompression after the retrograde decompression stage documented in the mafic granulites that formed garnet and amphibole.

However, the close association of diatexites and mafic granulites in the field, with no evidence of a tectonic juxtaposition after the thermal peak, suggests that an assemblage stable in the diatexites at ~8-9 kbar, as seen in the mafic granulites, has been destroyed during the decompression to a retrograde stage, or has not been discovered during this study. The osumilite, reported as pseudomorphs by Bial *et al.* (2012) may have formed during that stage.

Conventional GASP and Garnet-Cordierite thermobarometry (Figure 6.7) produces an intersection at ~660 ˚C and 5.5 kbar. These conditions are unlikely to produce the observed assemblage and the high amounts of anatectic melts that are evident from the granitic textures in the field. They result most likely from continuous Fe-Mg exchange between cordierite and garnet during slow crustal cooling.

7.3 Regional geological implications

There is no well substantiated tectonic scenario yet published for the central Namaqua belt with which the evolution of the Bysteek and Koenap Formation could be compared. The propositions that either the Hartebeest River shear zone or the Onseepkans Thrust served as a terrane boundary (Moen and Toogood, 2007; Sithole, 2011; Kanime, 2011) have not been supported by hard data, such as *P-T*-d-t paths, in the respective literature. To some extend the data presented in this thesis may add some information that can contribute to a better understanding of the tectonic processes in this part of the Namaqua Metamorphic Province.

High to ultra-high temperature metamorphism has not been recorded previously for the central Namaqua belt but is well known in other parts of the Namaqua Metamorphic Province (Robb, 1999; Waters, 1986, 1988, 1989). Remarkable is the peak pressure of 8-9 kbar observed in the mafic granulites of the Bysteek Formation which is 1-2 kbar higher than previously recorded (Cornell *et al*., 1992).

However, the pressure is still well in the range of crust of normal thickness and therefore does not support tectonic scenarios involving subduction or duplication of lithosphere during continent collision, which would be expected to be present if the Hartebeest River shear zone had been a terrane boundary during an accretionary Namaquan event.

The decompression from the peak at ~8-9 kbar to ~5 kbar is not significant compared to the decompression reported in collisional orogens like the Alps (Pazzaglia et al., 2007; Selverstone 1984, 1985, 1988) or in regions that experience post-collisional crustal collapse, such as the Variscan belt (Franke, 2006). Problematic in this respect is that the time required for the decompression from 8-9 to 5 kbar is not known. For instance, if the recorded peaks of monazite and zircon formation of ~1200 and ~1100 Ma reflect time between the 8-9 kbar and the ~5 kbar stage of the recorded *P-T* path, the pressure difference would be seen as insignificant, and the more relevant question would be the environment that allowed the crust to stay hot over such a long time period. However, until precise age data for the Koenap and Bysteek Formations are available, these questions must remain open.

8. Conclusions

The mafic granulites of the Bysteek Formation and the felsic diatexites of the Koenap Formation underwent high- to ultra-high temperature metamorphism at pressures suggesting mid- to lower crustal levels, whereby the pressure peak of 8-9 kbar in the mafic granulites is not recorded in the mineral assemblage of the diatexites. From their field relationships, however, it is likely that the two formations share the conditions of the thermal peak at ~865 °C and ~8.6 kbar but that phases stable at these conditions (e.g. orthopyroxene) were replaced by cordierite during near-isothermal decompression to ~5-6 kbar/~800 °C. Associated with this lower pressure stage is the increase of oxygen fugacity in the mafic granulites that locally produced andraditic garnet and iron exsolution producing magnetite in clinopyroxene. Minor fluid influx led to the growth of amphibole at the expense of orthopyroxene and plagioclase.

The retrograde overprint following the high-T stage at 6 kbar is limited to replacement of garnet and cordierite by secondary biotite and sillimanite at higher amphibolite facies temperatures. The lack of white mica, even in the regional shear zones (including those nearby in the Polisiehoek Gneiss or in the larger Hartebeest River or Oup shear zones (Mdze, 2010; Mdze et al., 2011), suggests that as soon as the middle or lower amphibolite facies temperatures were reached, cooling rates were high and the regional deformation ceased.

Deformation within the study area occurred at the thermal peak and in the presence of melt. The main fabric is the ptygmatic folding of leucosome veins. Due to the high melt content in the diatexites at that time, no conspicuous deformation patterns are preserved from that stage but it can be expected that magma or melt were mobilised, causing granitic and granulitic domains to form. Layering in the diatexites might have been common at lower degrees of partial melting but, apart from relics, was largely destroyed when the maximum volume of melt was generated and mobilised.

During continent-continent collisional tectonics *P-T* conditions at ~8-9 kbar normally do not exceed temperatures of ~750-780 °C (Collins, 2002a; Collins 2002b). As suggested by Mdze *et al.* (2011), the *P-T*-d evolution in the Twakputs Gneiss, which are well compatible with those in the Bysteek and Koenap Formations, are more in better agreement with thin lithospheric mantle and thin or only moderately thickened crust in a continental back-arc setting (Collins, 2002a; Hyndman et al., 2005). The lack of

significant retrograde deformation at temperatures below upper amphibolite facies conditions supports such a setting, since it suggests low strain during crustal cooling, which also is untypical for the evolution of a collisional orogen, such as the Alps or the Variscan belt (Selverstone *et al*. 1984; Selverstone 1985, 1988; O'Brien and Rötzler, 2003; Carswell and O'Brien, 1993, O'Brien et al., 1992). All this makes it very unlikely that the Hartebeest River shear zone ever was a terrane boundary or collisional suture zone, as suggested or implied in the existing literature.

9. References

Bertrand, P. and Mercier, J.C.C. (1985). The mutual solubility of coexisting ortho- and clinopyroxene: toward an absolute geothermometer for the natural system? *Earth Planet Science Letters.*, **76**,109–122.

Bial, J., Schenk, V., Büttner, S. and Appel, P. (2012). Evidence for Mesoproterozoic UHT metamorphism and two metamorphic events in the central Namaqualand Metamorphic Complex (Kakamas Terrane), European Mineralogical Conference., Kiel, Germany.

Bhattacharya, A., Mazumdar, A.C. and Sen, S.K. (1988). Fe-Mg mixing in cordierite: Constraints from natural data and implications for cordierite-garnet thermometry in granulites. *American Mineralogist.,* **73**, 338–344.

Brown, M. (1973). The definition of metatexis, diatexis and migmatites. *Proceedings of the Geologist Association.*, **84**, 371-382.

Brown, M. (1994). The generation, segregation, ascent and emplacement of granitic magma: the migmatites-to-crustally-derived granite connection to thickened oregons. *Earth Science Reviews.,* **36**, 83-130.

Büttner, S.H. (2012). Rock Maker: an MS Excel^{TM} spreadsheet for the calculation of rock compositions from proportional whole rock analyses, mineral compositions, and modal abundance, *Mineralogy and Petrology*, **104**, 129-135.

Carswell, D. A. and O'Brien, P. J. (1993). Thermobarometry and geotectonic significances of high-pressure granulites: examples from the Moldanubian Zone of the Bohemian Massif in Lower Austria. *Journal of Petrology.*, **34**, 427–459.

Collins, W.J. (2002a). Nature of extensional accretionary orogens, *Tectonics*, **21**, 1024-1036.

Collins, W.J. (2002b). Hot orogens, tectonic switching, and creation of continental crust, *Geology*, **30**, 535–538.

Colliston .W.P. and Schoch ,A.E. (1998). Tectono-stratigraphic features along the Orange River in the western part of the Mesoproterozoic Namaqua mobile belt, *South African Journal of Geology.*, **101**, 91–100.

Colliston, W.P and Schoch, A.E. (2002). The structural development of the Aggeneys Hills, Namaqua Metamorphic Complex , *South African Journal of Geology.*, **105**, 301–324.

Colliston, W.P. and Schoch, A.E. (2003). A mid-Proterozoic volcano-sedimentary sequence in the Aggeneys Hills duplex, Namaqua Metamorphic Complex , *South African Journal of Geology.*, **106**, 343–360.

Colliston, W.P. and Schoch, A.E. (2006). The distribution and diagnostic features of deformed plutonic rocks in two terranes of the Namaqua mobile belt along the Orange (Gariep) River, South Africa. *South African Journal of Geology.*, **109 (3),** 369-392.

Cornell, D.H., Humphreys, H., Theart, H.F.J. and Scheepers, D.J. (1992). A collision-related pressure-temperature-time path for Prieska copper mine, Namaqua-Natal tectonic province, South Africa. *Precambrian Research.*, **59**, 43-71.

Cornell, D.H., Thomas, R.J., Moen, H.F.G., Reid, D.L., Moore, J.M. and Gibson, R.L. (2006). The Namaqua-Natal Province. In: Johnson, M.R., Anhauesser, C.R. and Thomas, R.J. (Eds.), The Geology of South Africa. The Geological Society of South Africa, Johannesburg, South Africa, 325-379.

De Capitani, C. and Petrakakis, K. (2010). The computation of equilibrium assemblage diagrams with Theriak/Domino software. *American Mineralogist.*, **95**, 1006–1016.

Didier, J. (1973). Granites and their enclaves: The bearing of enclaves on the origin of granites, Development in Petrology: **3**, Amsterdam, Elsevier.

Du Plessis, G. (1979). A metamorphic-magmatic study from the rocks of the Namaqua Metamorphic Complex along the Orange River, east of Onseepkans. M.Sc. thesis (unpubl.), University of O.F.S.

Eckert Jr, J.O., Newton, R.C. and Kleppa, O.J. (1991). ΔH of reaction and recalibration of garnet-pyroxene-plagioclase-quartz geobarometers in CMAS system by solution calorimetry of stoichiometric mineral mixes, *American Mineralogist.*, **76**, 148–160.

Eglington, B.M. (2006). Evolution of the Namaqua-Natal Belt, southern Africa – a geochronological and isotope geochemical review. *Journal of African Earth Sciences.*, **46**, 93-111.

Ehlers, E.G. and Blatt, H. (1982). Petrology, Igneous, Sedimentary, and Metamorphic. W.H Freeman, San Francisco.

Holland, T. and Powell R. (1998). An internally consistent thermodynamic dataset for phases of petrological interest. *Journal of Metamorphic Geology*., **16**, 309-343.

Franke, W. (2006). The Variscan orogen in Central Europe: construction and collapse. Geological Society of London, **32**, 333-344.

Holland, T. and Blundy, J.(1994). Non-ideal interactions in calcic amphiboles and their bearing on amphibole-plagioclase thermometry. *Contributions to Mineral Petrology.*, **116**, 433-47.

Joubert, P. (1986). Namaqualand – a model of Proterozoic accretion? *Transactions of the Geological Society of South Africa.*, **89(2)**, 79-96.

Hyndman, R.D., Currie, C.A., Mazzotti, S.P. (2005). Subduction zone backarcs, mobile belts, and orogenic heat, *GSA Today*, **15 (2)**, 4–10.

Kanime, T. (2011). Field relations and petrography of high-grade metamorphic and plutonic rocks in the Central Namaqua Belt, Northern Cape Province. Hons thesis (unpubl.) Rhodes University.

Kenah, C and Hollister, L.S. (1983). Anatexis in the Central Gneiss Complex, British Columbia. In: M.P, Atherton and C.D.Gribble, (Eds.), Migmatites, melting and metamorphism. Shiva, Nantwich, U.K.

Koziol, A.M. (1989). Recalibration of the garnet-plagioclase-Al_2SiO_5-quartz (GASP) geobarometer and application to natural parageneses. *EOS Transactions, American. Geophysical Union.*, **70**, 493.

Kretz, R. (1983). Symbols for rock-forming minerals. *American Mineralogist.*, **68**, 277-279.

Krogh, E.J. (1988). The garnet-clinopyroxene Fe-Mg geothermometer - a reinterpretation of existing experimental data. *Contributions to Mineralogy and Petrology.*, **99**,44–48.

McCarthy, T.C. and Patiño-Douce, A.E. (1998). Empirical calibration of the silica-Ca-tschermak-anorthite (SCAn) geobarometer. *Journal of Metamorphic Geology.*, **16**, 675–686.

Mdze, M., Büttner, S.H. and Frei, D. (2010). The P-T-d-t evolution of the Twakputs gneiss: Implications for the tectonic setting of the central Namaqua belt. Hons thesis (unpubl.) Rhodes University.

Mdze, M., Büttner, S.H. and Frei, D. (2011). The P-T-d-t evolution of the Twakputs gneiss: Implications for the tectonic setting of the central Namaqua belt. IMSG 2011, Stellenbosch.

Mehnert, K. R. (1968). Migmatites and the origin of granitic rocks. Development in Petrology: **3**, Amsterdam, Elsevier.

Middemost, E.A.K. (1985). Magmas and magmatic rocks. An introduction to igneous petrology. London, Longman.

Moen, H.F.G. and Toogood, D.J. (2007). The geology of the Onseepkans area. Explanation sheet 2818 Onseepkans, 1:250000. Council for Geoscience, South Africa.

Morimoto. N, (1988), Nomenclature of pyroxenes. *Mineralogy Magazine*., **52**, 535-50.

Norrish, K. and Hutton. J.T. (1969). An accurate X-ray spectrographic method for the analysis of a wide range of geological samples. *Geochemica et Cosmochimica Acta.,* **33**, 431-453.

O'Brien, P.J and Rotzler, J. (2003). High-pressure granulites: formation, recovery of peak conditions and implications for tectonics, *Journal of Metamorphic Geology.*, **21**, 3–20.

O'Brien, P.J., Rohr, C., Okrusch, M. and Patzak, M. (1992). Eclogite facies relics and a multistage breakdown in metabasites of the KTB pilot hole, NE Bavaria: implications for the Variscan tectonometamorphic evolution of the NW Bohemian Massif. *Contributions to Mineralogy and Petrology.*, **112**, 261–278.

O'Connor, J. T. (1965). A classification for quartz-rich igneous rocks based on feldspar ratio. *United States Geological Survey Professional Paper.,* **525B**, 79–84.

Orville, P.M (1969). A model for the metamorphic differentiation origin of thin-layered amphibolites. *American Journal of Science.*, **267**, 64-86.

Patiño-Douce, A. E. (1993). Titanium substitution in biotite: an empirical model with applications to thermometry, O_2 and H_2O barometries, and consequences for biotite stability. *Chemical Geology.,* **108**,133-162.

Raheim, A. and Green, D.H. (1974). Experimental determination of the temperature and pressure dependence of the Fe-Mg partition coefficient for coexisting garnet and clinopyroxene. *Contributions to Mineralogy and Petrology,* **48**,179–203.

Robb, L.J., Armstrong R.A., and Waters, D.J. (1999). The history of granulite-facies metamorphism and crustal growth from single zircon U–Pb geochronology: Namaqualand, South Africa, *Journal of Petrology*, **40**, 1747-1770.

Sawyer, E.W. (1998). Formation and evolution of granite magmas during crustal reworking: the significance of diatexites, *Journal of Petrology*, **39**, 1147-1167.

Sawyer, E.W. (2008). Atlas of Migmatites. The Canadian Mineralogist Special Publication 9. Mineralogical Association of Canada, Quebec; NRC Research Press, Ottawa.

Sithole, A.L. (2011). Petrography and structural analysis in high-grade metamorphic basement rocks of the Gordonia Subprovince. Hons thesis (unpubl.) Rhodes University.

Selverstone, J., Spear, F.S., Franz, G., and Morteani, G. (1984). High-pressure metamorphism in the SW Tauern Window, Austria: P-T paths from hornblende-kyanite-staurolite schists. *Journal of Petrology.*, **25**, 501-531.

Selverstone, J. (1985). Petrologic constraints on imbrication, metamorphism, and uplift in the SW Tauern Window, Eastern Alps. *Tectonics.*, **4**, 687-704.

Selverstone, J. (1988). Evidence for east-west crustal extension in the Eastern Alps: implications for the unroofing history of the Tauern Window. *Tectonics.*, **7**, 87-105.

Stowe, C.W. (1986). Synthesis and interpretation of structures along the north-eastern boundary of the Namaqua Tectonic Province, South Africa. *Transactions of the Geological Society of South Africa.*, **89**, 185–198.

Streckeisen, A. (1976). To each plutonic rock its proper name, *Earth-Science Reviews.*, **12**, 1-33.

Thomas, R.J., von Veh, M.W. and McCourt, S. (1993). The tectonic evolution of southern Africa. *Journal of African Earth Sciences.*, **16/1-2**, 4-24.

Thomas, R.J., Agenbacht, A.L.D., Cornell, D.H. and Moore, J.M. (1994). The Kibaran of Southern Africa: Tectonic evolution and metallogeny. *Ore Geology Reviews.*, **9**, 131-160.

Thompson, J.B. Jr. (1957). The graphical analysis of mineral assemblages in pelitic schists. *American Mineralogist.*, **42**, 842-858.

Vernon, R.H. (1986). K-feldspar megacrysts in granites-phenocrysts not porphryoblasts, *Earth-Science Reviews.*, **23**,1-63.

Vernon, R.H., White, R.W. and Clarke, G.L. (2008). False metamorphic events inferred from misinterpretation of microstructural evidence and P-T data. *Journal of Metamorphic Geology.*, **26**, 437-449.

Waters, D.J. (1986). Metamorphic zonation and thermal history of pelitic gneisses from western Namaqualand, S. Africa. *Transactions of the Geological Society of South Africa*., **89**, 97–102.

Waters, D.J. (1988). Partial melting and the formation of granulite facies assemblages in Namaqualand, *South African Journal of Geology.*, **99**, 169-184.

Waters, D.J. (1989). Metamorphic evidence for the heating and cooling path of Namaqualand granulites. In: Daly, J. S., Cliff, R. A. & Yardley, B. W. D. (eds) Evolution of Metamorphic Belts. *Geological Society*, London, Special Publication, **43,** 357–363.

Wimmenauer, W. and Bryhni, I. (2007). A systematic nomenclature for metamorphic rocks: Migmatites and related rocks. A proposal on behalf of the IUGS Subcommission on the Systematics of Metamorphic Rocks.

Winkler, H.G.F. (1967). Petrogenesis of metamorphic rocks. Springer-Verlag, New York

Winter, J.D. (2001). An introduction to igneous and metamorphic Petrology. Prentice-Hall Inc, Upper Saddle River, New Jersey.

Orthopyroxene-EDS analyses-sample A106A								
Domain	**Mafic lens in nebulitic diatexite**							
Location	**Core**	**Core**	**Core**	**Core**	**Core**	**Rim**	**Rim**	**Rim**
SiO_2	50.21	49.52	49.52	50.01	49.17	50.04	49.52	50.51
TiO_2	0.01	0.00	0.00	0.00	0.00	0.26	0.00	0.03
Al_2O_3	2.37	2.31	2.31	2.03	2.68	2.51	2.31	2.55
Cr_2O_3	0.00	0.00	0.00	0.00	0.00	0.00	0.00	0.00
Fe_2O_3	0.00	0.00	0.00	0.00	0.00	0.00	0.00	0.00
MgO	16.96	17.43	17.43	17.23	16.78	16.88	17.43	16.79
CaO	0.23	0.12	0.12	0.29	0.19	0.23	0.12	0.27
MnO	0.42	0.26	0.26	0.73	0.35	0.17	0.26	0.35
FeO	29.75	30.07	30.07	29.70	30.58	29.63	30.07	29.43
Na_2O	0.03	0.06	0.06	0.00	0.22	0.21	0.06	0.03
K_2O	0.01	0.00	0.00	0.00	0.03	0.04	0.00	0.01
Total	99.99	99.78	99.78	100.00	100.00	99.97	99.78	99.96
Cations based on 6 Oxygen atoms								
Si	1.94	1.92	1.92	1.94	1.91	1.93	1.92	1.94
Ti	0.00	0.00	0.00	0.00	0.00	0.01	0.00	0.00
Al	0.11	0.11	0.11	0.09	0.12	0.11	0.11	0.12
Cr	0.00	0.00	0.00	0.00	0.00	0.00	0.00	0.00
Fe^{3+}	0.00	0.00	0.00	0.00	0.00	0.00	0.00	0.00
Mg	0.98	1.01	1.01	0.99	0.97	0.97	1.01	0.96
Ca	0.01	0.01	0.01	0.01	0.01	0.01	0.01	0.01
Mn	0.01	0.01	0.01	0.02	0.01	0.01	0.01	0.01
Fe^{2+}	0.96	0.98	0.98	0.96	0.99	0.96	0.98	0.95
Na	0.00	0.00	0.00	0.00	0.02	0.02	0.00	0.00
K	0.00	0.00	0.00	0.00	0.00	0.00	0.00	0.00
Total	4.01	4.03	4.03	4.02	4.04	4.01	4.03	4.00
Enstatite	50.16	50.68	50.68	50.53	49.25	50.13	50.68	50.12
Wollastonite	0.49	0.26	0.26	0.62	0.39	0.48	0.26	0.58
Ferrosillite	49.35	49.06	49.06	48.86	50.36	49.38	49.06	49.30
X_{Mg}	0.50	0.51	0.51	0.51	0.49	0.50	0.51	0.50

Rim	**Average (n=9)**
50.79	**49.92**
0.00	**0.03**
2.49	**2.40**
0.00	**0.00**
0.00	**0.00**
16.32	**17.03**
0.19	**0.20**
0.48	**0.37**
29.44	**29.86**
0.28	**0.11**
0.00	**0.01**
100.00	**99.92**
1.96	**1.93**
0.00	**0.00**
0.11	**0.11**
0.00	**0.00**
0.00	**0.00**
0.94	**0.98**
0.01	**0.01**
0.02	**0.01**
0.95	**0.97**
0.02	**0.01**
0.00	**0.00**
4.00	**4.02**
49.49	**50.19**
0.42	**0.42**
50.09	**49.39**
0.50	**0.50**

Plagioclase-EDS analyses-sample A106A					
Domain	**Mafic lens in nebulitic diatexite**				
Location	**Core**	**Core**	**Rim**	**Rim**	**Average (n=4)**
SiO_2	49.39	48.73	50.78	49.98	**49.72**
Al_2O_3	32.51	32.76	31.29	32.17	**32.18**
MgO	0.03	0.02	0.00	0.00	**0.01**
CaO	15.57	16.48	14.90	15.10	**15.51**
MnO	0.00	0.00	0.12	0.00	**0.03**
FeO	0.20	0.22	0.44	0.35	**0.30**
BaO	0.00	0.00	0.00	0.00	**0.00**
Na_2O	2.27	1.78	2.47	2.29	**2.20**
K_2O	0.04	0.01	0.00	0.11	**0.04**
Total	100.00	100.00	100.000	100.000	**100.00**
Cations based on 8 Oxygen atoms					
Si	2.25	2.23	2.31	2.28	**2.27**
Al	1.75	1.77	1.68	1.73	**1.73**
Mg	0.00	0.00	0.00	0.00	**0.00**
Ca	0.76	0.81	0.73	0.74	**0.76**
Mn	0.00	0.00	0.00	0.00	**0.00**
Fe	0.01	0.01	0.02	0.01	**0.01**
Ba	0.00	0.00	0.00	0.00	**0.00**
Na	0.20	0.16	0.22	0.20	**0.19**
K	0.00	0.00	0.00	0.01	**0.00**
Total	4.97	4.97	4.96	4.96	**4.97**
Or	0.24	0.05	0.00	0.66	**0.24**
An	78.96	83.60	76.95	77.95	**79.37**
Ab	20.80	16.35	23.05	21.39	**20.40**
A	50.07	49.58	49.40	50.30	**49.84**
C	49.32	49.83	49.15	48.82	**49.28**
F	0.62	0.59	1.45	0.88	**0.88**

Biotite-EDS analyses-sample A106A			
Domain	**Mafic lens in nebulitic diatexite**		
Location	**Core**	**Rim**	**Average (n=2)**
SiO_2	38.48	38.60	**38.54**
TiO_2	4.35	3.74	**4.04**
Al_2O_3	14.68	14.98	**14.83**
Cr_2O_3	0.14	0.00	**0.07**
MgO	12.57	13.45	**13.01**
CaO	0.00	0.18	**0.09**
MnO	0.00	0.15	**0.08**
FeO	20.86	21.71	**21.28**
BaO	0.10	0.08	**0.09**
Na_2O	0.06	0.16	**0.11**
K_2O	8.72	6.75	**7.73**
Dry	96.00	96.00	**96.00**
Total	99.96	99.80	**99.88**
Cations based on 24 Oxygen atoms			
Si	5.59	5.58	**5.58**
Ti	0.48	0.41	**0.44**
Al	2.51	2.55	**2.53**
Cr	0.02	0.00	**0.01**
Mg	2.72	2.90	**2.81**
Ca	0.00	0.03	**0.01**
Mn	0.00	0.02	**0.01**
Fe	2.53	2.62	**2.58**
Ba	0.01	0.00	**0.01**
Na	0.02	0.04	**0.03**
K	1.62	1.24	**1.43**
Total	15.49	15.39	**15.44**
X_{Mg}	0.52	0.52	**0.52**

	Pl-EDS Analyses						
Sample	**976A-mes**			**976B-mes**			
Domain	**Nebulitic mesosome**			**Nebulitic mesosome**			
Location	**Core**	**Rim**	**Average (n=2)**	**Core**	**Core**	**Rim**	**Rim**
SiO_2	57.93	57.84	**57.88**	47.04	46.62	46.98	46.09
Al_2O_3	26.37	26.56	**26.46**	33.68	33.85	33.51	34.28
MgO	0.00	0.07	**0.03**	0.03	0.00	0.00	0.00
CaO	9.21	8.87	**9.04**	17.50	18.15	17.73	18.29
MnO	0.00	0.00	**0.00**	0.01	0.00	0.06	0.00
FeO	0.13	0.24	**0.18**	0.43	0.52	0.40	0.43
BaO	0.14	0.04	**0.09**	0.00	0.00	0.00	0.00
Na_2O	5.85	5.21	**5.53**	1.29	0.84	1.26	0.90
K_2O	0.38	1.17	**0.77**	0.02	0.02	0.06	0.02
Total	100.00	100.00	**100.00**	100.00	100.00	100.00	100.00
Cations based on 8 Oxygen atoms							
Si	2.60	2.60	**2.60**	2.16	2.15	2.16	2.12
Al	1.39	1.40	**1.40**	1.82	1.84	1.82	1.86
Mg	0.00	0.00	**0.00**	0.00	0.00	0.00	0.00
Ca	0.44	0.43	**0.43**	0.86	0.90	0.87	0.90
Mn	0.00	0.00	**0.00**	0.00	0.00	0.00	0.00
Fe	0.00	0.01	**0.01**	0.02	0.02	0.02	0.02
Ba	0.00	0.00	**0.00**	0.00	0.00	0.00	0.00
Na	0.51	0.45	**0.48**	0.12	0.08	0.11	0.08
K	0.02	0.07	**0.04**	0.00	0.00	0.00	0.00
Total	4.97	4.96	**4.97**	4.98	4.97	4.99	4.99
Or	2	7	**5**	0	0	0	0
An	45	45	**45**	88	92	88	92
Ab	52	48	**50**	12	8	11	8
A	49.12	50.12	**49.62**	49.23	49.03	48.82	49.19
C	50.33	48.34	**49.33**	49.67	49.86	50.17	49.90
F	0.55	1.54	**1.05**	1.10	1.12	1.02	0.91

		Pl-EPMA Analyses				
	Sample	976B-mes				
	Domain	Nebulitic mesosome				
Average (n=4)	Location	Core	Core	Rim	Rim	Average (n=4)
46.68	**SiO_2**	43.81	43.73	43.19	43.97	**43.68**
33.83	**Al_2O_3**	35.93	35.82	36.75	36.16	**36.16**
0.01	**MgO**	0.00	0.00	0.00	0.00	**0.00**
17.92	**CaO**	18.11	17.84	18.39	18.05	**18.10**
0.02	**MnO**	0.00	0.00	0.00	0.00	**0.00**
0.45	**FeO**	0.00	0.00	0.00	0.00	**0.00**
0.00	**BaO**	0.00	0.00	0.00	0.00	**0.00**
1.07	**Na_2O**	1.16	1.20	0.85	1.16	**1.09**
0.03	**K_2O**	0.07	0.23	0.05	0.07	**0.10**
100.00	**Total**	99.08	98.822	99.213	99.421	**99.13**
	Cations based on 8 Oxygen atoms					
2.15	**Si**	2.04	2.04	2.01	2.04	**2.03**
1.83	**Al**	1.97	1.97	2.02	1.98	**1.98**
0.00	**Mg**	0.00	0.00	0.00	0.00	**0.00**
0.88	**Ca**	0.90	0.89	0.92	0.90	**0.90**
0.00	**Mn**	0.00	0.00	0.00	0.00	**0.00**
0.02	**Fe**	0.00	0.00	0.00	0.00	**0.00**
0.00	**Ba**	0.00	0.00	0.00	0.00	**0.00**
0.10	**Na**	0.11	0.11	0.08	0.10	**0.10**
0.00	**K**	0.00	0.01	0.00	0.00	**0.01**
4.98	**Total**	5.03	5.03	5.02	5.02	**5.03**
0	**Or**	0	1	0	0	**1**
90	**An**	89	88	92	89	**90**
10	**Ab**	10	11	8	10	**10**
49.07	**A**	50.77	50.87	51.37	51.00	**51.00**
49.90	**C**	49.23	49.13	48.63	49.00	**49.00**
1.04	**F**	0.00	0.00	0.00	0.00	**0.00**

	Pl-EDS Analyses						
Sample	**976A-L**						
Domain	**Leucocratic Pocket**						
Location	**Core**	**Core**	**Core**	**Rim**	**Rim**	**Rim**	**Average (n=6)**
SiO_2	57.05	57.19	56.81	57.44	56.58	57.11	**57.03**
Al_2O_3	27.13	26.74	27.23	27.14	27.43	27.23	**27.15**
MgO	0.00	0.00	0.00	0.00	0.00	0.00	**0.00**
CaO	9.94	9.60	9.91	9.12	10.11	9.67	**9.72**
MnO	0.00	0.00	0.03	0.00	0.00	0.00	**0.00**
FeO	0.05	0.14	0.13	0.06	0.23	0.23	**0.14**
BaO	0.00	0.26	0.00	0.05	0.02	0.00	**0.05**
Na_2O	5.62	5.80	5.67	5.81	5.38	5.45	**5.62**
K_2O	0.21	0.27	0.22	0.39	0.26	0.32	**0.28**
Total	100.00	100.00	100.00	100.00	100.00	100.00	**100.00**
Cations based on 8 Oxygen atoms							
Si	2.56	2.57	2.55	2.57	2.54	2.56	**2.56**
Al	1.43	1.42	1.44	1.43	1.45	1.44	**1.44**
Mg	0.00	0.00	0.00	0.00	0.00	0.00	**0.00**
Ca	0.48	0.46	0.48	0.44	0.49	0.46	**0.47**
Mn	0.00	0.00	0.00	0.00	0.00	0.00	**0.00**
Fe	0.00	0.01	0.00	0.00	0.01	0.01	**0.01**
Ba	0.00	0.00	0.00	0.00	0.00	0.00	**0.00**
Na	0.49	0.51	0.49	0.50	0.47	0.47	**0.49**
K	0.01	0.02	0.01	0.02	0.01	0.02	**0.02**
Total	4.97	4.98	4.98	4.97	4.97	4.97	**4.97**
Or	1	2	1	2	2	2	**2**
An	49	47	49	45	50	49	**48**
Ab	50	51	50	52	48	50	**50**
A	49.31	48.93	49.19	50.75	49.44	50.03	**49.61**
C	50.49	50.50	50.18	49.00	49.68	49.07	**49.82**
F	0.20	0.57	0.63	0.25	0.87	0.91	**0.57**

	Pl-EDS Analyses					
Sample	**976B-L**					
Domain	***In-situ* leucosome**					
Location	**Core**	**Core**	**Rim**	**Average (n=3)**	**Core**	**Rim**
SiO_2	47.17	47.73	47.08	**47.33**	43.92	44.00
Al_2O_3	33.56	33.18	33.65	**33.46**	36.03	35.74
MgO	0.00	0.00	0.00	**0.00**	0.00	0.00
CaO	17.53	17.32	17.65	**17.50**	17.85	17.75
MnO	0.06	0.04	0.02	**0.04**	0.00	0.00
FeO	0.41	0.30	0.27	**0.32**	0.00	0.00
BaO	0.00	0.07	0.13	**0.07**	0.00	0.00
Na_2O	1.22	1.35	1.21	**1.26**	1.34	1.38
K_2O	0.05	0.01	0.00	**0.02**	0.04	0.04
Total	100.00	100.00	100.00	**100.00**	99.186	98.907
Cations based on 8 Oxygen atoms						
Si	2.17	2.19	2.16	**2.17**	2.04	2.05
Al	1.82	1.79	1.82	**1.81**	1.98	1.96
Mg	0.00	0.00	0.00	**0.00**	0.00	0.00
Ca	0.86	0.85	0.87	**0.86**	0.89	0.89
Mn	0.00	0.00	0.00	**0.00**	0.00	0.00
Fe	0.02	0.01	0.01	**0.01**	0.00	0.00
Ba	0.00	0.00	0.00	**0.00**	0.00	0.00
Na	0.11	0.12	0.11	**0.11**	0.12	0.13
K	0.00	0.00	0.00	**0.00**	0.00	0.00
Total	4.98	4.97	4.98	**4.98**	5.03	5.03
Or	0	0	0	**0**	0	0
An	89	87	89	**88**	88	87
Ab	11	12	11	**12**	12	12
A	49.19	49.18	49.35	**49.24**	51.00	50.88
C	49.76	50.07	50.02	**49.95**	49.00	49.12
F	1.05	0.75	0.63	**0.81**	0.00	0.00

						Pl-EDS A
	Sample					**985A**
	Domain	**Mafic fragments**				
Average (n=3)	**Location**	**Core**	**Core**	**Rim**	**Rim**	**Average (n=4)**
43.96	**SiO_2**	59.17	58.71	59.14	58.76	**58.94**
35.89	**Al_2O_3**	25.80	26.11	25.80	26.01	**25.93**
0.00	**MgO**	0.00	0.00	0.00	0.00	**0.00**
17.80	**CaO**	8.36	8.57	8.25	8.36	**8.38**
0.00	**MnO**	0.00	0.00	0.00	0.00	**0.00**
0.00	**FeO**	0.00	0.00	0.00	0.00	**0.00**
0.00	**BaO**	0.00	0.00	0.00	0.00	**0.00**
1.36	**Na_2O**	6.51	6.46	6.54	6.64	**6.54**
0.04	**K_2O**	0.17	0.15	0.27	0.23	**0.20**
99.05	**Total**	100.00	100.00	100.00	100.00	**100.00**
						Cations based on 8 Oxy
2.05	**Si**	2.64	2.62	2.64	2.63	**2.63**
1.97	**Al**	1.36	1.37	1.36	1.37	**1.36**
0.00	**Mg**	0.00	0.00	0.00	0.00	**0.00**
0.89	**Ca**	0.40	0.41	0.39	0.40	**0.40**
0.00	**Mn**	0.00	0.00	0.00	0.00	**0.00**
0.00	**Fe**	0.00	0.00	0.00	0.00	**0.00**
0.00	**Ba**	0.00	0.00	0.00	0.00	**0.00**
0.12	**Na**	0.56	0.56	0.57	0.58	**0.57**
0.00	**K**	0.01	0.01	0.02	0.01	**0.01**
5.03	**Total**	4.97	4.97	4.97	4.98	**4.97**
0	**Or**	0	0	0	0	**0**
88	**An**	58	57	58	58	**58**
12	**Ab**	42	43	42	42	**42**
50.94	**A**	49.53	49.56	49.58	49.41	**49.52**
49.06	**C**	50.47	50.44	50.42	50.59	**50.48**
0.00	**F**	0.00	0.00	0.00	0.00	**0.00**

Analyses				
A-L				
Leucocratic Network				
Core	Core	Core	Rim	Average (n=4)
59.75	59.35	59.75	59.20	**59.51**
25.15	25.44	25.39	25.71	**25.42**
0.00	0.00	0.00	0.00	**0.00**
7.70	8.01	7.66	7.95	**7.83**
0.11	0.05	0.00	0.00	**0.04**
0.05	0.18	0.13	0.10	**0.11**
0.19	0.00	0.00	0.00	**0.05**
6.94	6.76	6.99	6.90	**6.90**
0.11	0.21	0.09	0.14	**0.14**
100.00	100.00	100.00	100.00	**100.00**
ygen atoms				
2.67	2.65	2.66	2.64	**2.66**
1.32	1.34	1.33	1.35	**1.34**
0.00	0.00	0.00	0.00	**0.00**
0.37	0.38	0.37	0.38	**0.37**
0.00	0.00	0.00	0.00	**0.00**
0.00	0.01	0.00	0.00	**0.00**
0.00	0.00	0.00	0.00	**0.00**
0.60	0.59	0.60	0.60	**0.60**
0.01	0.01	0.01	0.01	**0.01**
4.97	4.98	4.98	4.98	**4.98**
1	1	1	1	**1**
61	60	62	61	**61**
38	39	38	39	**38**
48.89	48.65	49.44	49.33	**49.08**
50.29	50.23	49.90	50.18	**50.15**
0.82	1.12	0.66	0.49	**0.77**

Sample		
Domain		L
Location	Core	Core
SiO_2	55.22	54.82
Al_2O_3	28.40	28.73
MgO	0.00	0.00
CaO	11.22	11.43
MnO	0.00	0.06
FeO	0.16	0.07
BaO	0.00	0.00
Na_2O	4.84	4.79
K_2O	0.16	0.11
Total	100.00	100.00
		Cations based
Si	2.49	2.47
Al	1.51	1.53
Mg	0.00	0.00
Ca	0.54	0.55
Mn	0.00	0.00
Fe	0.01	0.00
Ba	0.00	0.00
Na	0.42	0.42
K	0.01	0.01
Total	4.97	4.98
Or	1	1
An	56	57
Ab	43	43
A	49.56	49.72
C	49.89	49.84
F	0.55	0.44

Pl-EDS Analyses		
J10B-L		
eucocratic pocket		
Rim	Rim	Average (n=4)
56.89	53.99	**55.23**
27.42	29.25	**28.45**
0.00	0.00	**0.00**
10.06	12.08	**11.20**
0.02	0.02	**0.02**
0.02	0.23	**0.12**
0.00	0.00	**0.00**
5.45	4.38	**4.86**
0.15	0.05	**0.12**
100.00	100.00	**100.00**
on 8 Oxygen atoms		
2.55	2.44	**2.49**
1.45	1.56	**1.51**
0.00	0.00	**0.00**
0.48	0.58	**0.54**
0.00	0.00	**0.00**
0.00	0.01	**0.00**
0.00	0.00	**0.00**
0.47	0.38	**0.42**
0.01	0.00	**0.01**
4.97	4.98	**4.97**
1	0	**1**
50	60	**56**
49	39	**44**
49.92	49.62	**49.70**
49.92	49.58	**49.81**
0.16	0.80	**0.49**

	Alkali feldspar-EDS A			
Sample				**976B-L**
Domain				***In-situ* leucosom**
Location	**Core**	**Core**	**Core**	**Rim**
SiO_2	65.36	65.34	65.22	63.26
Al_2O_3	17.65	17.74	17.60	18.78
MgO	0.00	0.07	0.00	0.04
CaO	0.09	0.05	0.09	1.85
MnO	0.00	0.01	0.06	0.00
FeO	0.16	0.03	0.15	0.05
BaO	1.17	1.31	1.24	2.21
Na_2O	0.96	0.86	1.07	0.56
K_2O	14.60	14.59	14.57	13.26
Total	100.00	100.00	100.00	100.00
				Cations based on 8 Oxygen at
Si	3.02	3.02	3.02	2.95
Al	0.96	0.97	0.96	1.03
Mg	0.00	0.00	0.00	0.00
Ca	0.00	0.00	0.00	0.09
Mn	0.00	0.00	0.00	0.00
Fe	0.01	0.00	0.01	0.00
Ba	0.02	0.02	0.02	0.04
Na	0.09	0.08	0.10	0.05
K	0.86	0.86	0.86	0.79
Total	4.97	4.96	4.98	4.96
Or	90	92	90	85
An	0	0	0	10
Ab	9	8	10	5

nalyses	
ıe	
Rim	Average (n=5)
65.35	**64.90**
17.62	**17.88**
0.00	**0.02**
0.01	**0.42**
0.01	**0.02**
0.13	**0.10**
1.43	**1.47**
0.97	**0.88**
14.48	**14.30**
100.00	**100.00**
oms	
3.03	**3.01**
0.96	**0.98**
0.00	**0.00**
0.00	**0.02**
0.00	**0.00**
0.00	**0.00**
0.03	**0.03**
0.09	**0.08**
0.86	**0.85**
4.96	**4.96**
91	**89**
0	**2**
9	**8**

	Alkali feldspar-EDS Analyses				
Sample	**985A-L**				
Domain	**Leucocratic Network**				
Location	**Core**	**Core**	**Core**	**Rim**	**Rim**
SiO_2	65.81	65.68	65.56	65.62	65.32
Al_2O_3	17.63	17.84	17.83	17.87	17.94
MgO	0.00	0.00	0.00	0.00	0.00
CaO	0.13	0.00	0.23	0.11	0.06
MnO	0.03	0.02	0.01	0.09	0.00
FeO	0.00	0.18	0.02	0.00	0.07
BaO	0.76	0.75	0.86	0.93	1.16
Na_2O	1.09	0.86	1.21	0.90	1.16
K_2O	14.55	14.67	14.28	14.48	14.28
Total	100.00	100.00	100.00	100.00	100.00
	Cations based on 8 Oxygen atoms				
Si	3.03	3.03	3.02	3.03	3.02
Al	0.96	0.97	0.97	0.97	0.98
Mg	0.00	0.00	0.00	0.00	0.00
Ca	0.01	0.00	0.01	0.01	0.00
Mn	0.00	0.00	0.00	0.00	0.00
Fe	0.00	0.01	0.00	0.00	0.00
Ba	0.01	0.01	0.02	0.02	0.02
Na	0.10	0.08	0.11	0.08	0.10
K	0.86	0.86	0.84	0.85	0.84
Total	4.96	4.96	4.97	4.95	4.97
Or	89	92	88	91	89
An	1	0	1	1	0
Ab	10	8	11	9	11

		Alkali feldspar-EDS Analyses					
	Sample	J10B-L					
	Domain	Leucocratic Pocket					
Average (n=5)	Location	Core	Core	Core	Rim	Rim	Rim
65.60	SiO_2	65.86	65.75	65.94	66.02	65.84	65.85
17.82	Al_2O_3	17.50	17.59	17.85	17.58	17.91	17.80
0.00	MgO	0.00	0.00	0.00	0.00	0.00	0.00
0.11	CaO	0.07	0.04	0.04	0.06	0.03	0.07
0.03	MnO	0.04	0.00	0.00	0.03	0.00	0.00
0.05	FeO	0.00	0.14	0.00	0.09	0.07	0.09
0.89	BaO	0.41	0.37	0.36	0.30	0.44	0.39
1.05	Na_2O	0.38	0.39	0.71	0.80	0.88	0.91
14.46	K_2O	15.74	15.72	15.10	15.13	14.83	14.90
100.00	Total	100.00	100.00	100.00	100.00	100.00	100.00
		Cations based on 8 Oxygen atoms					
3.03	Si	3.04	3.04	3.03	3.04	3.03	3.03
0.97	Al	0.95	0.96	0.97	0.95	0.97	0.97
0.00	Mg	0.00	0.00	0.00	0.00	0.00	0.00
0.01	Ca	0.00	0.00	0.00	0.00	0.00	0.00
0.00	Mn	0.00	0.00	0.00	0.00	0.00	0.00
0.00	Fe	0.00	0.01	0.00	0.00	0.00	0.00
0.02	Ba	0.01	0.01	0.01	0.01	0.01	0.01
0.09	Na	0.03	0.03	0.06	0.07	0.08	0.08
0.85	K	0.93	0.93	0.89	0.89	0.87	0.87
4.96	Total	4.96	4.97	4.96	4.96	4.96	4.96
90	Or	96	96	93	92	92	91
1	Anc	0	0	0	0	0	0
10	Ab	4	4	7	7	8	8

Average (n=6)
65.88
17.70
0.00
0.05
0.01
0.06
0.38
0.68
15.24
100.00

3.03
0.96
0.00
0.00
0.00
0.00
0.01
0.06
0.90
4.96
93
0
6